THE UNIVERSITY
of EDINBURGH

Modelling and Optimisation of Solar Power Plants with Energy Storage Systems

Ruben Bravo

Doctor of Philosophy

THE UNIVERSITY OF EDINBURGH

2021

To my wife, Daniela, and to Ruben and Maite,

for their patience and support through this journey.

Abstract

To avoid driving climate change on a dangerous path, a substantial reduction in greenhouse gases emissions is required. Hence, a high penetration of renewable energy technologies is essential, but most renewables are either affordable or dispatchable but not both.

Energy storage systems integrated into concentrating solar power (CSP) plants can enhance dispatchability and solar-to-electricity efficiency. Besides, the combination of dispatchable CSP plants with lower cost photovoltaic (PV) plants exploits synergies between the reliability of CSP with energy storage and cost of PV. However, this integration leads to complex interactions between the different technologies and requires sophisticated design guidelines to achieve low costs and high dispatchability simultaneously.

In this thesis, a two-stage multi-objective optimisation framework for the design and operation of hybrid CSP-PV plants with energy storage is developed. The two-stage optimisation simultaneously optimises the design and operation of a hybrid solar power plant with respect to competing technical and financial performances.

The multi-objective operational optimisation stage finds the best operational strategy of a hybrid power plant with energy storage systems. The model, written in Python, uses a typical meteorological year to optimise one-year hourly operation. The results demonstrate that the integration of an energy storage system in a concentrating solar power plant provides dispatchability and, when hybridised with photovoltaic, enhances its competitiveness with current electricity prices. The low mismatch between supply and demand, even when a fixed commitment is required throughout the year, together with high overall efficiency, indicates that the integration of energy storage in hybrid solar power plants is an opportunity to increase the penetration of solar energy in the power sector.

The design of reliable and cost-competitive hybrid solar power plants requires the careful balancing of trade-offs between financial and technical performance. Hence, the design optimisation stage optimises the capacities of the main components of the hybrid power plant and handles financial and technical objectives.

Different configurations are analysed as case studies throughout the thesis to analyse the impacts, interactions, and synergies of technology integration. Three locations are investigated, which present different solar resource profiles: Seville (Spain), Tonopah (USA), and the Atacama Desert (Chile).

The optimisation results are used to develop some guidelines for the optimal design of dispatchable hybrid solar power plants with energy storage based on the given solar resource

and required dispatchability. These guidelines provide an initial design for affordable and dispatchable hybrid solar power plants and can enable their widespread deployment.

The model developed can be applied to other locations under different input parameters and demand profiles. Besides, the flexibility of the model allows it to be extended in order to evaluate different energy conversion and storage technologies to design hybrid power plants with energy storage under different configurations and requirements. Thus, the optimisation framework can provide valuable information for the integration of different technologies to support the affordable and sustainable transition to a clean energy system.

Lay Summary

A substantial reduction of greenhouses gas emissions is required in the power sector to prevent a significant rise in the global atmospheric temperature. Renewable power generation technologies are essential to achieve the required emissions reduction and to promote sustainable development. The development of affordable and reliable renewable power plants is essential to support the widespread deployment of sustainable energy technologies.

Current research on sustainable energy systems has shown that the integration of thermal energy storage in large scale concentrating solar power plants enhances the reliability and the solar-to-electricity efficiency of solar energy technologies. Besides, the hybridisation of concentrating solar power plant with solar photovoltaic plants improves the plant's affordability while maintaining the reliability. The intermittency of the solar resource and the integration of energy storage systems requires the use of sophisticated techniques for the optimal design of hybrid solar power plants.

This thesis focuses on the development of modelling and optimisation tools to optimise the design and operation of solar power plants with energy storage and to provide guidelines for the optimal development of sustainable energy systems under different conditions and requirements. Different configurations are analysed as case studies, to evaluate the impacts, interactions, and synergies of technology integration. Besides, three locations are studied, which cover a range of solar resource profiles, in order to evaluate opportunities in the integration of clean technologies in different places.

The tools developed provide essential information in the decision-making process for the design of reliable and affordable power plants, going beyond the often used manual design process. The optimisation provides key performance indicators such as affordability, reliability, capacity factor, and efficiencies, to compare the performance of different designs and locations.

The results confirm that the integration of an energy storage system increases the reliability of concentrating solar power plants and that the combination with photovoltaic plants is essential to achieve competitive energy costs. The results highlight the potential of the integration of different technologies in the design of affordable and reliable renewable power plants to support the transition to a sustainable energy system.

Acknowledgements

Firstly, I would like to thank my PhD supervisor, Dr Daniel Friedrich, for his support, guidance, knowledge, encouragement and inspiration throughout this fantastic PhD journey. From the first meeting I had during my PhD interview, I felt that I would enjoy this academic adventure, and I did. I enjoyed every step, stage, and new experience of this journey, even though the road was challenging, full of emotions, sometimes uncertain, and many ups and downs. Thank you, Daniel, for being the best supervisor.

I would like to thank Dr Harry Van Der Weijde for all the support and advice and Dr Aristides Kiprakis for every annual review, organising my viva and help me during this stage of my academic life. I am also grateful to Prof Gareth Harrison for the support and encouragement. I would also like to extend my thanks to all academics I worked as a teaching and demonstrator in Fluid Mechanics, Engineering Thermodynamics, and Thermofluids; I thank Prof Tom Bruce, Dr Matthew Borg, Prof Mark Linne, Dr Katherine Dunn, Dr Brian Petterson, and Dr Rohit Pillai.

Part of the research presented in this thesis was made possible by an international exchange at the University of Seville, Spain, during my third year. Thanks Dr Ricardo Chacartegui and Dr Carlos Ortiz, for all the discussion, the great experience, and the fantastic opportunity to apply my knowledge and skills working with a brilliant group of researchers.

A special thanks to Marcelo Barria for our friendship, deep conversations, and for teaching me how to enjoy and live life. Special thanks go to Serguey for all encouraging advice and engaging technical and personal discussions during our almost everyday lunches and coffee times (before the pandemic), and Renaldi for every piece of advice and inspiring conversations. Thank you to my old friends Luis Aguilera and Rodrigo Diaz for the friendship that transcends space and time, and for always having time to discuss anything; and Esteban Montero, for encouraging me to pursue my dreams and follow this path. Thank you, Ben McGilton, for all your help and advice in preparing my postdoctoral application. A special thank you to James Steer and Paul Bonar for the unforgettable West Coast trip and the 5k star hotel (camping on the beach) and that hillwalking with my son. I would also like to thank my friends, office-mates, and colleagues at the School of Engineering: Dan McKinley, Anup Nambiar, Jagadeesh Gunda, Naif Albagami, Duo Fang, Min Yao, Philip Machura, Kevin Kails, Alastair Heggie, Yvonne Baird, Jesus Lizana, Syahrul Nizam, Arturo Ortega, Thomas Spitz, Alfred Cotten, Wei Sun, Mbayer Abunku, Anna Garcia-Teruel, Eduardo Rosales, Aldo Eyres, Joe Burchell, Gerard Avellaneda, Monika Kreitmair, and Will Ubani for all support, fascinating moments, and exciting conversation during these years.

I am grateful to my dearest family. Thanks to my beloved wife, Daniela, for everything, for all

the love, support, and patience[3]. Thanks to my son Ruben and my daughter Maite for their love and for transmitting to me their enthusiasm, boundless energy and passion. I would like to thank my parents, Ruben and Carmen; my siblings Catalina, Tatiana and Felipe; and my godmothers Margarita and Violeta; thanks all of you for being my greatest teachers I can always count on. A special thanks to my dearest grandmother, Raquel, for being with me from my firsts days in this world.

My PhD and this project would not have been possible without the financial support of the National Research and Development Agency (ANID-Chile), Scholarship Program, Doctorado Becas Chile 2015, Folio 72160177. The international exchange in the University of Seville that allowed me to work on the research presented in Chapters 6 and 7 was funded by the Energy Technology Partnership (ETP), International Exchange Grants for Postgraduate and Early Career Researcher Exchanges (PECRE) 2018

Edinburgh, May 2021

Ruben Bravo

Declaration

I declare that this thesis was composed by myself, that the work contained herein is my own except where explicitly stated otherwise in the text, and that this work has not been submitted for any other degree or professional qualification except as specified.

Ruben Bravo

Contents

List of Figures

List of Tables

Abbreviations

CaL	Calcium-looping System
CaO	Oxide Calcium
$CaCO_3$	Calcium Carbonate
CO_2	Carbon Dioxide
CSP	Concentrated Solar Power
DNI	Direct Normal Irradiation
eff	Efficiency
GA	Genetic Algorithm
GHG	Greenhouse Gas
GTI	Global Tilted Irradiation
HPSC	High Pressure Storage Compressor
HPST	High Pressure Storage Turbine
HRSG	Heat Recovery Steam Generator
HX	Heat Exchanger
Inv	Investment Cost
LCOE	Levelised Cost of Energy
LH	Lock Hopper
LP	Linear Programming
LPS	Loss of Power Supply
LPSC	Loss of Power Supply Capacity
LPSP	Loss of Power Supply Probability
MC	Main Compressor
MT	Main Turbine
PV	Photovoltaic
PB	Power block
SoC	State of Charge
ST	Steam Turbine
TCES	Thermochemical Energy Storage
TES	Thermal Energy Storage
TMY	Typical Meteorological Year

List of Symbols

a. Subindexes

i	Period	h
k	Component (material)	-
q	Equipment	-
s	Process	-

b. Power plant design and operation

A^{CSP}	Heliostats solar-field aperture area	m^2
A^{PV}	Photovoltaic modules solar-field area	m^2
E^{net}	Net energy generated	MWh
P_i^{demand}	Power demand period i	MW
P_i^{net}	Net power period i	MW
P^{q}	Nominal capacity of equipment q	MW
STO^q	Maximum storage capacity of storage q	MWh

c. Thermodynamics

η^s	Efficiency of process s	-
h	Enthalpy	$kJ \cdot kg^{-1}$
$\hat{h}$	Molar enthalpy	$kJ \cdot mol^{-1}$
$\Delta\hat{h}^0_{f,k}$	Molar enthalpy of formation, component k	$kJ \cdot mol^{-1}$
$\dot{m}_i$	Mass flow rate at time step i	$kg \cdot s^{-1}$
$\hat{m}_i$	Molar flow rate at time step i	$kmol \cdot s^{-1}$
MW_k	Molecular weight, component k	$kg \cdot kmol^{-1}$
X	Carbonator, CaO conversion	%

Chapter 1

Introduction

1.1 Overview

One of the main challenges as scientists is to support sustainable development, i.e. meeting current needs of our society without compromising future generations to meet their own needs (Independent Group of Scientists appointed by the Secretary-General, 2019). Provide access to affordable, reliable, sustainable and modern energy is one of the goals defined by the United Nations (Independent Group of Scientists appointed by the Secretary-General, 2019). This goal not only focuses on eradicating energy poverty and indoor air pollution but also in preventing the adverse effects of climate change.

Energy systems have been defined as "the connected processes of acquiring and using energy in a given society or economy" (Jaccard, 2006). Three subsystems are usually applied to describe energy systems: primary energy, energy carriers or secondary energy, and energy end-use. Primary energy involves the natural form of energy, i.e. renewable resources (e.g. solar, wind, wave, geothermal, biomass), fossil fuels (e.g. coal, oil, natural gas), and nuclear fuels (e.g. uranium). Then, energy carriers involve transformation of primary energy and are useful forms to connect primary energy with end-users. Common energy carriers are electricity, fossil fuels products (e.g. diesel, gasoline, natural gas), heat, hydrogen. Finally, these secondary energy sources are used in different end-use applications and devices in the society, e.g. farm mechanisation, heating, lighting, transport, etc.

Fossil fuels are the basis of our current energy system. In 2018, 81% of the world's primary energy demand was supplied by fossil fuels (IEA, 2019c). From extraction to combustion, the use of fossil fuels generates many environmental and societal hazards. In the last stage of this chain, the burning of fossil fuels creates high quantities of CO_2, the most significant greenhouse gas (Everett *et al.*, 2012). Based on scientific evidence and research (Pachauri *et al.*, 2014), there is a high correlation between the increase in the atmospheric temperature with the concentration of greenhouse gases in the atmosphere. Furthermore, the atmosphere is just one of the GHG sinks. The oceans also capture large amounts of CO_2. This addition of CO_2 increases its acidity, which threatens life in the oceans.

According to IEA (2019b), global greenhouse gas emissions have significantly increased in

the recent past. Nevertheless, despite a substantial deployment of renewable power plants, the global emission trend has flattened during the last decade but remains high. The increase in global greenhouse gas emissions during the last years is the product of two important and interdependent factors: (i) the increase in electricity consumption per capita (i.e. from 2.1 MWh per capita in 1990 to 3.2 MWh per capita in 2017), and (ii) the increase in emission from economies under development (IEA, 2019b). Nevertheless, the high increase in the electricity generation from renewable technologies from 2010 to 2017, i.e.: (i) solar PV, 1380%; (ii) solar thermal, 660%; (iii) wind 330%; (iv) tide and wave 200%; (v) geothermal, 125%; and (vi) hydro, 120%, compared with the growth of electricity generation from fossil fuels (natural gas, oil, and coal), i.e. 115%, suggests that the transition to a clean energy system is encouraging (IEA, 2019b).

Despite the dominance of renewable sources in the growth in the power generation capacity (IEA, 2019a), more efforts still have to be pursued. A high deployment of intermittent renewable energy technologies led by solar PV, then wind and hydro has been seen in the last years. Nevertheless, the imbalance between anthropogenic emissions and natural sinks is still high. In this context, due to the extensive emissions from industrial revolution, the current level of CO_2 in the atmosphere (over 400 ppm), compared with the amount estimated before the industrial revolution (around 200 ppm) has had substantial effect in the atmosphere and the oceans that have started jeopardising the life of some societies. Renewable energy technologies are key to enhance the sustainable development, and larger and quicker deployment of clean technologies is crucial to reduce greenhouse gas emissions and reach a long-term balance between sources and sinks to avoid a rise in global temperature higher than 2 °C (IEA, 2019a; Gür, 2018).

Renewable power plants have low maintenance and operational costs (NREL, 2018), their carbon emissions and air pollution are substantially lower compared to fossil fuel power stations (Pehl *et al.*, 2017), and their development is key to energy independence. Nevertheless, renewable power plants can dispatch energy just when the natural resource is available. For instance, solar and wind resources are intermittent. Consequently, power plants based on solar and wind are not dispatchable. This means that the power supply from some renewable power plants depends on the variability of the resource, and sometimes it is not possible to match supply and demand profiles. Hence, the continuous growth in the penetration of renewable energy technologies in the power sector and the natural variability of the resource (e.g. solar, wind) adds large fluctuations in generation and significant mismatches with power demand (Denholm and Hand, 2011). To reduce variability and increase dispatchability of renewable power plants, the integration of energy storage allows having control in the power dispatch (Denholm *et al.*, 2015b). Therefore, renewable energy technologies are fundamental to decarbonise the power sector, but the integration of energy storage is crucial to provide dispatchable energy (Denholm *et al.*, 2015b; Jenkins *et al.*, 2018; Amy *et al.*, 2019; Bui *et al.*, 2018).

Solar photovoltaic (PV) is an excellent alternative to provide affordable but intermittent power

(Sampaio and González, 2017). Electrical energy storage (e.g. batteries) integrated into PV plants enhance its dispatchability. However, current costs of batteries (around 300 - 550 USD $\cdot kWh^{-1}$) and the scarcity of the raw materials used (e.g. lithium) compromise their viability for large scale applications (Fernández *et al.*, 2019b). On the other hand, thermal energy storage (TES) can be up to two orders of magnitude cheaper than electrical energy storage systems (Lund *et al.*, 2016). Current power plants in operation suggest that Concentrated Solar Power plants (CSP) combined with TES have the potential to provide dispatchable power at competitive costs (Liu *et al.*, 2016; SolarPACES, 2018; Maximov *et al.*, 2019; Peng *et al.*, 2017). Due to its high potential, many studies have focused on the analysis of the integration of TES into CSP plants (Zurita *et al.*, 2018; Ortiz *et al.*, 2019a). Consequently, the hybridisation of CSP-TES with affordable solar PV is gaining attention (Peng *et al.*, 2017; Ströhle *et al.*, 2016).

The combination of these technologies exploits synergies between dispatchability of CSP with energy storage and affordability of PV. However, this combination leads to complex interactions between the different plants and requires sophisticated techniques to simultaneously achieve low costs and high dispatchability. To design a dispatchable and also affordable energy system, a design optimisation stage is necessary to select the right size of the main components. On the one hand, if one component is undersized, there will be a bottleneck in the operation, that results in a reduction in the efficiency of the whole process. On the other hand, the oversizing of a component will result in an unnecessary high investment cost, increasing the cost of energy. In addition, the operation of renewable power plants integrated with energy storage leads to complex interactions between the different components of the power plant, the intermittent resource, and the power supply required. Hence, this research aims to develop a framework to optimise the design of a hybrid solar power plant with energy storage (i.e. the size of the main components) while simultaneously optimising the operational strategy with the aim of providing design guidelines for affordable and dispatchable sustainable energy systems under different conditions and configurations.

Current optimal operational studies of hybrid power plants with energy storage have been focused on the analysis of single objectives (Petrollese and Cocco, 2016), or the evaluation of a limited temporal resolution representing the analysis of a whole year (Salas *et al.*, 2018; Alovisio *et al.*, 2017). In this context, Ortiz *et al.* (2018a) conclude that hourly simulations considering variable solar irradiation need to be investigated to improve the analysis in the integration and design of CSP plants with thermal energy storage.

According to IEA (2014b), locations close to the Tropics (Capricorn and Cancer), with clear skies and high solar irradiation have the best condition to the development of CSP technologies. However, each location requires a bespoke design due to the complex interactions between the different parts of the system and the differences in solar resource profile. Hence, to analyse projects under development, and potential locations for further deployment of solar plants

with energy storage, the following locations which cover a range of different profiles will be evaluated in this research: Seville, Spain; Tonopah, Nevada, United States; and the Atacama Desert, Chile. While Northern Chile has one of the highest solar irradiations in the world, Nevada and Southern Spain are among the sunniest region in the United States and Europe respectively. Moreover, power tower CSP projects in operation or under construction can be found in these areas, for instance, Gemasolar Thermosolar Plant (Seville), Crescent Dunes Solar Energy Project (Tonopah), Atacama-1 (Chile) (NREL, 2017)

This research develops a multi-objective optimisation framework for the optimal design of hybrid CSP-PV plants integrated with energy storage systems. Chapter 2 gives a background of solar energy technologies and energy storage systems applied in solar power plants. In addition, a review of modelling and optimisation techniques is presented. In Chapter 3, a two-stage optimisation framework to optimise the design of a hybrid power plant by genetic algorithms, and the operation by linear programming is presented. The results conclude that the analysis of the trade-off between technical and economic performance is key to design an affordable and dispatchable power plant. Moreover, the direct link between the objectives of the design and operational optimisation routines is crucial to exploit the synergies of different technologies. In Chapters 4 to 7, this framework is applied to design and analyse the performance of different configurations of hybrid solar power plants with energy storage, considering different solar resource profiles covering the feasible conditions for solar power plants. The results are then used to develop guidelines for the optimal design of dispatchable solar power plants for locations with good solar resource.

1.2 Aims and objectives

This research will address the following question: Can solar power plants be affordable and dispatchable, and help us in the transition to a clean and sustainable energy system and avoid driving climate change on a dangerous path? In order to analyse different technologies and strategies, the research background focuses on the integration of hybrid solar power plants with thermal energy storage systems. Then, the hypothesis of this research can be defined as: The integration of different existing technologies for energy generation, conversion, and storage can provide affordable, sustainable, clean and reliable power.

Finally, to test the hypothesis, this research focuses on the development of mathematical and programming tools to model and optimise the design and operation of hybrid solar power plants with energy storage systems under multi-criteria analyses. The tools provide decision-makers and policy developers a range of choices of affordable and dispatchable power plants that can be used in initial phases to design the transition to a future sustainable energy system or to set targets for widespread deployment of renewable power technologies under different conditions and requirements.

The following objectives are pursued throughout the thesis:

1. To develop a multi-objective optimisation model for the operation of hybrid solar power plants with energy storage, taking into account the daily and seasonal variability of the solar resource.
2. To develop a two-stage multi-objective optimisation framework to simultaneously optimise the design and operation of a hybrid solar power plant integrated with energy storage.
3. To investigate the importance of multi-objective optimisation in exploiting synergies by the integration of dispatchable concentrating solar power systems with energy storage and low-cost photovoltaic technology.
4. To explore the role of the integration of different technologies in improving the performance of hybrid solar power plants, e.g. sensible heat thermal energy storage (two-tanks molten salts), thermochemical energy storage (calcium-looping), electrical energy storage (batteries).
5. To explore characteristics of dispatchable hybrid solar power plants under different solar conditions and operational requirements.
6. To examine flexibility approaches in increasing the performance of sustainable technologies to support the transition to an affordable and clean energy system.
7. To develop guidelines for the optimal design of hybrid solar power plants based on the solar resource and required dispatchability.

1.3 Contribution to knowledge

The research presented in this work integrates perspectives from energy systems, mechanical engineering, chemical processes, mathematical optimisation and computer programming. The main focus is to model, simulate, and optimise hybrid solar power plants with energy storage. The framework, methodologies, and tools presented can be applied to different energy systems by modifying the input parameters and configuration in the model. Original contribution to knowledge resulted from the present research can be attributed to the:

- Design and operational optimisation of a hybrid solar power plant integrated with molten salt as a sensible heat thermal energy storage.
- Flexibility analysis for the design of a dispatchable power plant to provide electricity and heat for an off-grid isolated consumer, e.g. a copper mine in Northern Chile.
- Operational optimisation of a calcium-looping system as a thermochemical energy storage integrated into a concentrating solar power plant.
- Multi-objective optimal design of dispatchable hybrid solar power plants with thermochemical energy storage.

1.4 List of Publications

Part of the work presented in this thesis has been published in journal articles and presented in conferences, as follows:

1.4.1 Journal articles

- R.Bravo, C.Ortiz, R.Chacartegui, and D.Friedrich (2020). Multi-objective optimisation and guidelines for the design of dispatchable hybrid solar power plants with thermochemical energy storage. Applied Energy, 282, PartB, 116257.
  DOI: 10.1016/j.apenergy.2020.116257
- R.Bravo, C.Ortiz, R.Chacartegui, and D.Friedrich (2019). Hybrid solar power plants with thermochemical energy storage: A multi-objective operational optimisation. Energy Conversion and Management, 205.
  DOI: 10.1016/j.enconman.2019.112421
- R.Bravo, and D.Friedrich (2018). Two-stage Optimisation of Hybrid Solar Power Plants. Solar energy, 164, 187-199.
  DOI: 10.1016/j.solener.2018.01.078.

1.4.2 Conference proceedings

- R.Bravo, and D.Friedrich (2019), Two-Stage, Multi-objective Optimisation Framework for an Efficient Pathway to Decarbonise the Power Sector. In: Rodrigues H. et al. (eds) EngOpt 2018 Proceedings of the 6th International Conference on Engineering Optimization. EngOpt 2018. Springer, Cham.
  DOI: 10.1007/978-3-319-97773-7_122.
- R.Bravo, and D.Friedrich (2018), Integration of energy storage with hybrid solar power plants, Energy Procedia, Volume 151, October 2018, Pages 182-186.
  DOI: 10.1016/j.egypro.2018.09.045

1.4.3 Conference presentations

- Design and operational optimisation of a hybrid solar power plant with thermochemical energy storage. Energy Technology Partnership 8th Annual Conference. November 2019, The University of Dundee, UK.
- Multi-objective operational optimisation of a thermochemical energy storage system. Maths - Energy Seminars. July 2019. School of Mathematics, The University of Edinburgh, UK.
- Two-Stage, multi-objective optimisation framework for an efficient pathway to decarbonise the power sector. EngOpt2018, 6th International Conference on Engineering Optimization. September 2018. Instituto Superior Tecnico Lisbon, Portugal.

- Integration of energy storage with hybrid solar power plants. 3rd Annual Conference in Energy Storage and Its Applications. September 2018. Centre for Doctoral Training in Energy, EPSRC. The University of Sheffield, UK.
- Two-stage Optimisation of Hybrid Solar Power Plants. Maths - Energy Seminars. August 2018. School of Mathematics, The University of Edinburgh, UK.
- Two-stage optimisation of hybrid solar power plants with energy storage. Carbon Capture and Storage & Energy Storage Working Group, Annual Meeting. June 2018. School of Engineering, The University of Edinburgh, UK.
- Optimisation of solar power plants for electricity generation in Northern Chile. Chile Global Seminars UK, Energy in Chile: Trends, Challenges and Solutions. December 2017. The University of Manchester, UK.

1.4.4 Poster presentations

- Planning the integration of electrical and thermal energy storage with solar power plants. UK Energy Storage Conference. March 2017. The University of Newcastle, UK.

1.4.5 Academic awards

- Award for best presentation: Integration of energy storage with hybrid solar power plants. 3rd Annual Conference in Energy Storage and Its Applications. September 2018. Centre for Doctoral Training in Energy, EPSRC. The University of Sheffield, UK.

1.5 Thesis structure

The thesis is divided in 8 chapters.

- Chapter 2 gives a background of solar energy technologies and energy storage systems applied in solar power plants. In addition, a review of simulation and optimisation techniques and tools is presented.
- Chapter 3 presents the optimisation method used in this thesis. A two-stage optimisation framework to simultaneously find the optimal design of hybrid solar power plants with energy storage while optimising its operation is developed. In this chapter, a complete analysis of the operation of each energy conversion and storage technology is studied. Moreover, the main equations used in the multi-objective optimisation, i.e. financial and technical performance, are detailed.
- Chapter 4 exposes the application of the framework for the optimal design of a hybrid solar power plant with two-tanks molten salt technology as a sensible thermal energy storage system. Here the model focuses on the improvement of the design of a power plant under development in the Atacama Desert in Northern Chile. The results of the

case study analysed in this chapter demonstrate the importance of balancing the trade-off between financial and technical performance in order to enhance the affordability of solar technologies.

- Chapter 5 illustrates different configurations to improve the performance of renewable power plants. In this chapter, the integration of batteries as electrical energy storage for the PV plant, as well as the integration of a fossil backup unit for the thermal energy storage of the CSP plants are studied. In addition, the analysis of the heat supply (from the heat rejection of the CSP plant) for low-temperature processes of a copper mine is developed. Finally, the integration of a wind farm, in order to decrease the joint variability of the renewable resource of a hybrid power plant is analysed and discussed.
- Chapter 6 focuses on the operational optimisation of a calcium-looping process as a thermochemical energy storage system integrated into a hybrid solar power plant. In this analysis, a one-year hourly time-step optimisation is performed in order to evaluate the daily and seasonal variability of the solar resource. Besides, different configurations are evaluated and a sensitivity analysis is carried out in order to evaluate the effects of technical and financial parameters in the affordability and dispatchability of hybrid solar power plants with thermochemical energy storage systems.
- Chapter 7 details the application of the two-stage multi-objective optimisation framework for the optimal design of a thermochemical energy storage system integrated into a hybrid solar power plant in three different locations, i.e. Seville, Tonopah, and the Atacama Desert. In addition, the results of the multi-objective optimisation are used to develop guidelines to use as an approximation to design affordable and dispatchable sustainable power plants under different solar resource and requirements.
- Chapter 8 summarises the results and conclusions presented in this thesis and discusses potential further research.

Chapter 2

Background

This chapter provides the background necessary to understand the main technologies studied in this research. Section 2.1 presents information of solar energy technologies. Here the main technologies analysed are solar photovoltaic and solar thermal. Then, concentrating solar power (CSP) plants are explained. Section 2.2 gives an overview of different energy storage technologies employed in power systems. After that, this section introduces different energy storage technologies suitable or under development for the integration into renewable power plants. Section 2.3 describes a hybrid solar power plant and its integration with energy storage systems. In this section, some synergies achieved with technology integration are illustrated. Section 2.4 exposes three conceptual levels that apply to energy systems optimisation. Then, a review of optimisation techniques is provided, and some examples found in the literature are presented. Finally, Section 2.5 exposes key knowledge gaps that will be addressed in this thesis.

2.1 Solar energy technologies

The conversion of solar energy into electricity is achieved by two types of technologies, i.e. solar thermal and solar photovoltaic (PV) power plants. Solar thermal uses solar irradiation to heat a fluid that can be used as a heat addition in a gas or a vapour power cycle to generate electricity by the use of a turbine and generator. Solar PV converts the sunlight directly into electricity by the photovoltaic effect employing semiconductor materials.

2.1.1 Solar Photovoltaic

The most deployed photovoltaic modules currently used in PV plants are made of silicon. Mono-crystalline silicon modules, with typical nominal efficiencies close to 20%, maximum power and voltages in the order of 300 W_{dc} and 50 V_{dc}, respectively, are usually employed in large scale solar power plants (NREL, 2018). In a typical array, solar panels are installed in series to produce the desired voltage. Exposed to sunlight, the characteristic of a semiconductive silicon cell allows the flow of electrons, creating an electrical current and voltage, this effect is known as the photovoltaic effect.

PV modules convert sunlight into direct current (dc) electricity. Then in order to dispatch power to the grid, an inverter is used to transform dc electricity into alternate current (ac) electricity. Other main components of a PV power plant are support structures, wires and control system. The characteristics of the photovoltaic modules are generally provided based on the peak output (kWp), which represents the power output of the module under reference conditions, i.e. total irradiance of 1000 $W \cdot m^{-2}$, and cell temperature of 25 °C (NREL, 2018).

Currently, according to NREL (2018), the total installed cost of a commercial PV plant, based on peak output, is lower than 2 $USD \cdot W_{dc}^{-1}$, and fixed annual operational and maintenance costs are around 16 $USD \cdot kW^{-1}$. Some benefits like the flexibility of solar PV to be installed in remote locations, the high drop in investment costs of modules, and the need to reduce carbon emissions, have allowed a high penetration of PV in the last decade. In this context, the global installed capacity of PV has increased from 22 GW in 2009 to 480 GW in 2018 (IRENA, 2018) where the leaders are China (175 GW), USA (50 GW) and Germany (46 GW). Figure 2.1 shows the potential of photovoltaic electricity in the world. Here kWh/kWp indicates the electricity generated by a solar PV array on average over a period of a day and a year. The figure highlights that Chile is one of the best places to develop PV projects. This country has seen an increase in the installed capacity of PV power plants from 2 MW at the end of 2012 (IRENA, 2018) to 2.7 GW in March 2020 (Energía Abierta, 2019).

The large-scale and quick penetration of intermittent PV presents essential challenges in the electrical grid (Sinsel *et al.*, 2020). Different alternatives are suggested to spread the integration of variable renewable resources in the power sector. For example, the combination of energy storage and grid reinforcement (Sinsel *et al.*, 2020), as well as a more extensive portfolio of generation technologies to reduce the total variability of the renewable resource (Carnegie Mellon University, 2013), are the most attractive options.

2.1.2 Solar thermal power

Solar thermal technologies capture the solar irradiation and convert it into heat. Then, depending on the application, the heat can be used to provide process heat or electricity. High-temperature heat is required to produce electricity. The most deployed technologies to generate electricity from sunlight are based on the concentration of irradiation by mirrors, producing superheated steam and running a turbine-generator in a conventional Rankine cycle. Concentrating solar power (CSP) plants use tracking mirrors to focus the sunlight on a small area (collector), where the solar irradiation is converted into heat and used to heat a fluid (Kalogirou, 2009). Hence, CSP plants need direct solar irradiation to operate. Then, the heat is used in the thermodynamic cycle to generate electricity, or, in the case that an energy storage system is integrated, stored to use when needed. Large scale commercial CSP plants have been operating in California since the 1980s, and some of these power plants are still in operation (IEA, 2014b). Four different CSP technologies have been under development and implemented from small

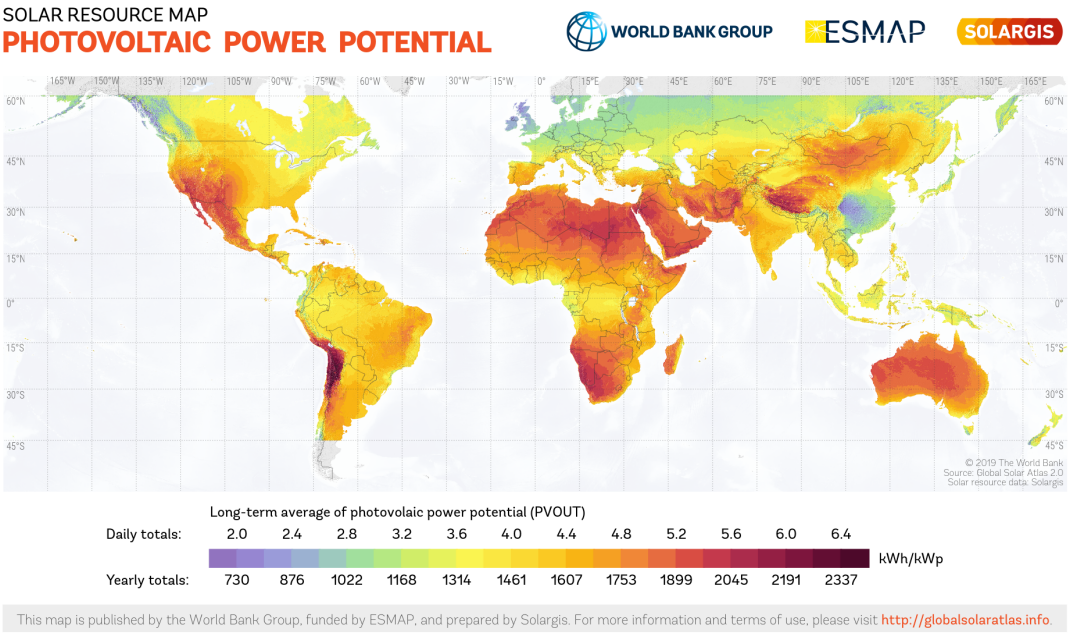

Figure 2.1: World map of photovoltaic electricity potential (The World Bank, 2019)

scale to utility-scale projects around the world, i.e. parabolic trough, linear Fresnel reflectors, dish or Stirling-engine systems, and heliostat field collectors or solar tower (SolarPACES, 2018). While parabolic trough and solar tower technologies are commercially available and have been implemented as large-scale projects, linear Fresnel collectors have not achieved commercial maturity, and parabolic dish configurations are generally applied in small-scale off-grid systems.

Parabolic trough and linear Fresnel reflectors are composed of single-axis mirrors that focus the solar irradiation onto a linear receiver tube. Dish and heliostats field technologies focus the sunlight in a focal point. Focal point CSP technologies reach higher temperatures and efficiencies. Nevertheless, focal point configurations require more advances 2-dimensional tracking mechanisms compared with 1-dimensional tracking mechanisms required in parabolic trough and linear Fresnel reflectors (Fernández *et al.*, 2019a).

Parabolic trough collectors track the sun in one direction focusing it along a focal line, as shown in Figure 2.2. This mature technology is commonly used to reach temperatures close to 400 °C (Duffie and Beckman, 2013). An example of a large-scale solar power plant based on this technology built during the last decade is the Mojave Solar Project, located in the Mojave Desert, California. With 250 MW net electricity generation capacity and an investment of approximately 1,600 MUSD, this power plant started its operation in 2014 (Abengoa Solar, 2016). Mojave Solar Project is composed of 2,200 parabolic trough collectors, with a total reflective area of $1.5{\cdot}10^6$ m^2. During the last four years (2016-2019), this solar power plant supplied an average of 584.6 GWh·$year^{-1}$ of electricity, achieving an average capacity factor

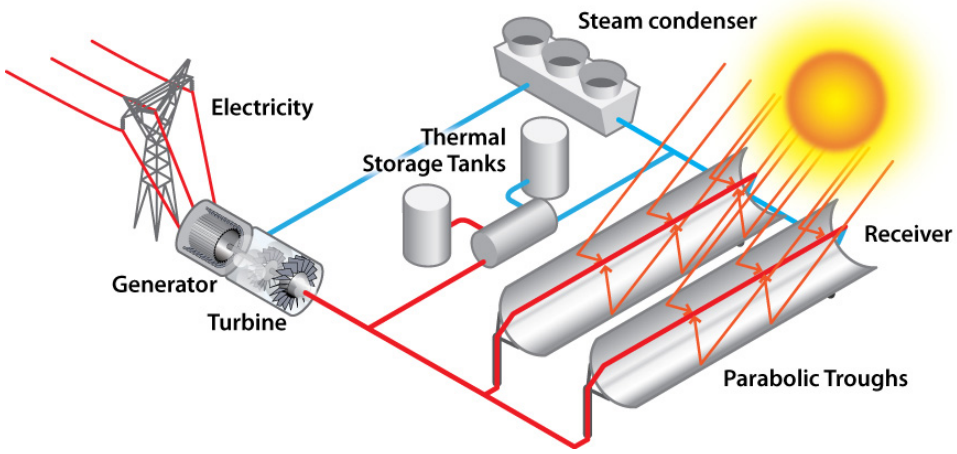

Figure 2.2: Parabolic trough CSP (Solar Energy Technologies office, 2013)

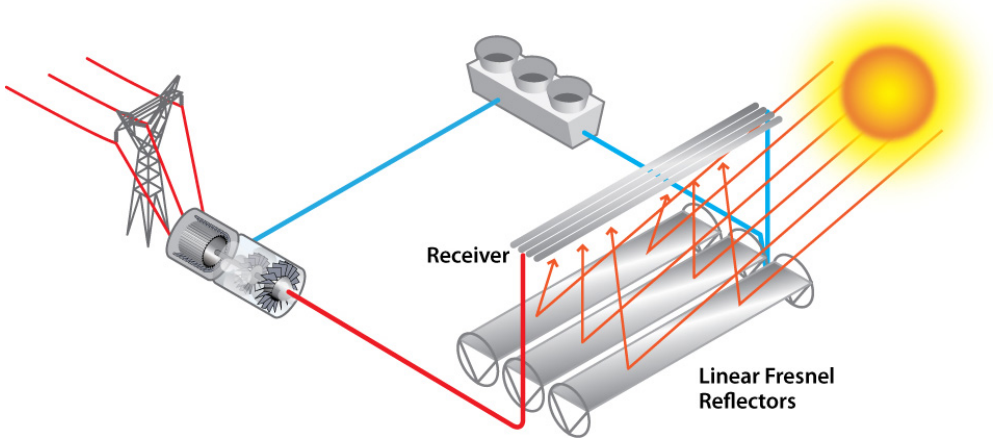

Figure 2.3: Linear Fresnel CSP (Solar Energy Technologies office, 2013)

of 27% (U.S. Energy Information Administration, 2020).

Linear Fresnel collectors are linear mirrors that concentrate the solar irradiation on a linear receiver. This technology, illustrated in Figure 2.3, has not achieved commercial maturity (Duffie and Beckman, 2013). Hence, only a limited number of projects have been developed. One of the largest power plants in operation is Puerto Errado 2, located in Murcia, Spain. With a 30 MW net capacity, this power plant started its operation in 2012 (SolarPACES, 2018). Puerto Errado 2 Thermosolar Power Plant is composed of 28 lines of 940 m linear Fresnel collectors, with a total reflective area of $3{\cdot}10^5$ m^2. This solar power plant generates annually approximately 49 GWh of electricity, resulting in a capacity factor of 19% (SolarPACES, 2018).

Parabolic dish reflector, as shown in Figure 2.4, is a two-axis collector that focuses the sunlight in the focal point of the dish. This system can reach temperatures larger than 1,500 °C. Each dish operates independently and has a capacity in the range of 5-25 kW (Duffie and Beckman, 2013). This technology is commonly used as a stand-alone off-grid system and used in small

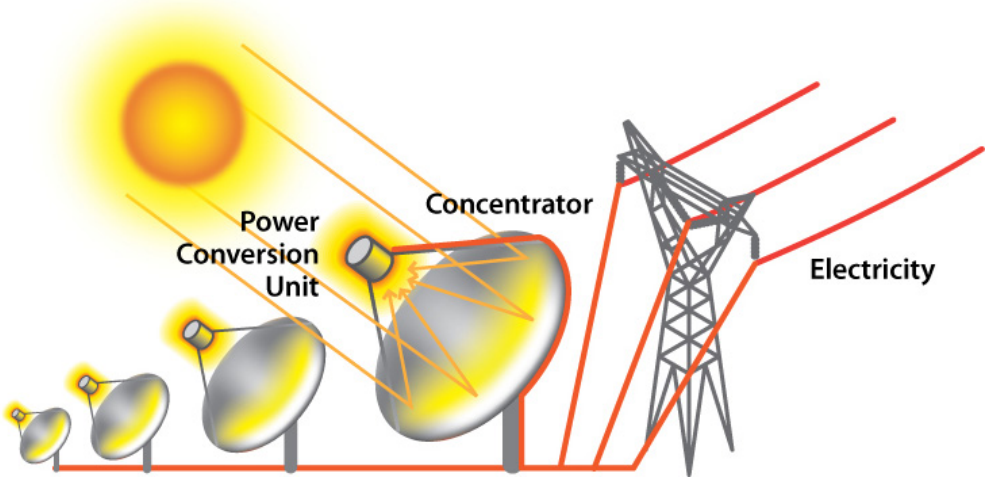

Figure 2.4: Dish/Engine CSP (Solar Energy Technologies office, 2013)

scale applications in the range 10-400 kW.

Finally, heliostat field collector (Figure 2.5), or solar tower technology, uses two-axis tracking mirrors (heliostats) to focus the solar irradiation into a chamber located at the top of a tower. More details on the solar tower technology are given in Section 3.3. This technology, also known as central receiver system, is typically used in large-scale configurations, with optimal capacities in the range of 50-400 MW (Duffie and Beckman, 2013). During recent years, solar tower systems have shown an interesting development, and the largest solar power plants in operation or under construction are based on this technology. For instance, the Crescent Dunes power plant, located in Nevada started its operation in 2015. This power plant is one of the first large-scale CSP plants to supply almost continuous electricity by using a single tower, a 110 MW power block, and energy storage system equivalent to 10 hours of full power (Solar Reserve LLC, 2012). Current solar tower power plants integrate molten salts as a thermal energy storage (TES) system, reaching capacity factors, based on the power block capacity, closer to 65% (Duffie and Beckman, 2013). For instance, Atacama-1, located in Northern Chile, is composed of a solar tower power plant that is expected to start its operation during this year (2020). With a 110 MW net capacity, Atacama-1 is composed of 10,600 heliostats, with a total solar field aperture area of $1.48{\cdot}10^6$ m^2. The integration of 17.5 hours of TES will allow a continuous operation (Cerro Dominador, 2019).

In order to reach the desired performance, CSP technologies need high values of direct normal irradiation. For instance, to produce more than 1 kWh_e per m^2 per day, the solar field of the CSP plant needs a direct normal irradiation (DNI) greater than 7 $kWh{\cdot}m^{-2}{\cdot}$ day^{-1} (IEA, 2014b). As shown in Figure 2.6 and according to IEA (2014b), areas with clear skies close to the Tropic of Capricorn and Cancer, between north or south latitudes of 15 and 40, present the best conditions for its operation. Currently, large power plants that are under study, development and construction are located in these zones, for example, the south-western United States

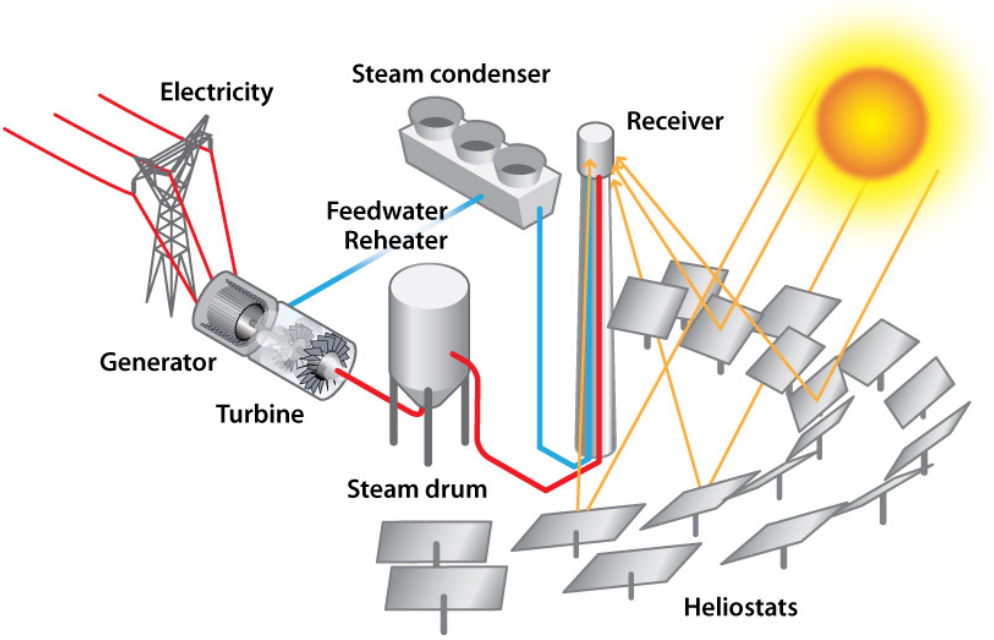

Figure 2.5: Solar tower CSP (Solar Energy Technologies office, 2013)

(California, Arizona), Southern Spain, Northern Chile, among others (Balghouthi *et al.*, 2016; SolarPACES, 2018; Parrado *et al.*, 2016b). In this context, the Atacama Desert is one of the most attractive places to develop CSP plants due to high levels of direct normal irradiation (Cáceres *et al.*, 2013; Starke *et al.*, 2016; Parrado *et al.*, 2016a). Other studies demonstrate the suitability of CSP with TES to work as baseload power plant (Grageda *et al.*, 2016; Starke *et al.*, 2018). Some of these projects integrate TES, while other designs consider hybridisation. For instance, Atacama-1 or Cerro Dominador Solar Power Plant, located in Northern Chile, will supply firm electricity by combining CSP with TES, capable of delivering energy at full working capacity for 17.5 hours during hours without solar irradiation. Besides, hybridisation was considered by integrating a PV plant (Abengoa Solar, 2016). While energy storage systems allow full dispatchability, hybridisation offers performance benefits and synergies. It improves both technical and financial performance by integrating a cheaper technology, e.g. solar PV, with more expensive but dispatchable technology, e.g. CSP with TES (Petrollese and Cocco, 2016; Pan and Dinter, 2017). In the long term, due to the cost reduction of batteries, the integration of electrical batteries as energy storage systems with solar PV could be key to develop dispatchable power plants with improved financial performance.

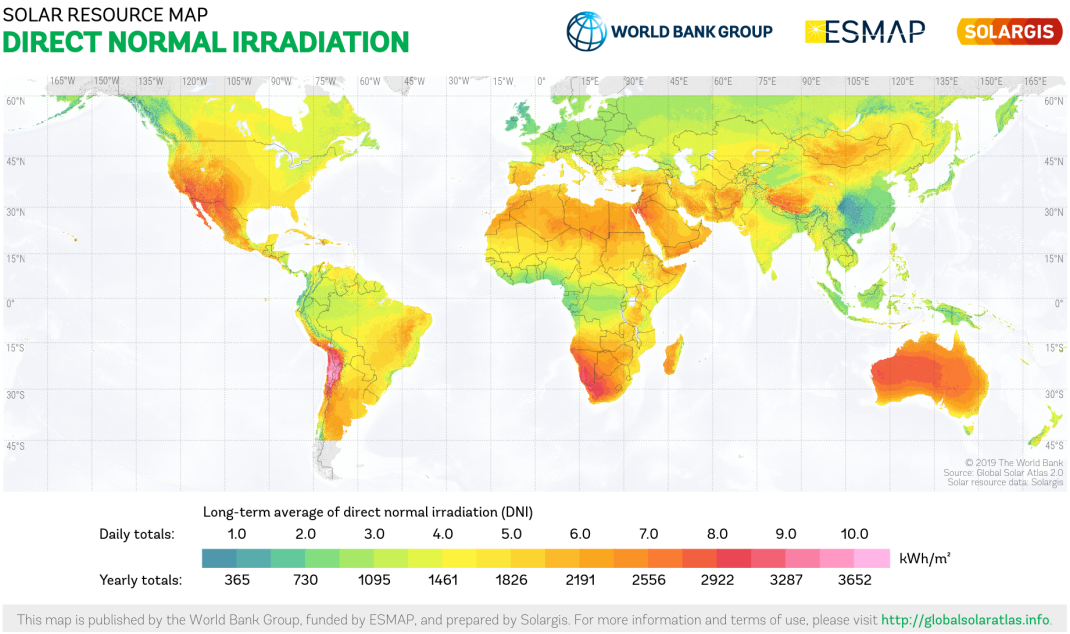

Figure 2.6: World map of direct normal irradiation (The World Bank, 2019)

2.2 Energy storage systems

Energy storage systems can store energy to change its temporal or even its geographical consumption (IEA, 2014a). Energy storage technologies can be deployed at a large or small scale at different locations in the energy system. According to the application, energy storage systems are commonly divided into electricity and thermal. Nowadays, the energy storage research community aims to improve the efficiency of the energy storage systems and its integration into intermittent renewable resources to increase the stability of the grid.

In power systems, energy can be stored in different forms: Mechanical, Electrochemical, Electrical, Chemical or Thermal (IEC, 2011). Currently, the most used technologies in the electrical grid, due to its technical and financial performance in large scale integration, are different kinds of mechanical energy storage (pumped hydro, compressed air energy storage) and chemical energy storage (hydrogen, synthetic natural gas) (Abbas *et al.*, 2013; IEC, 2011).

Moreover, depending on the required application, energy storage systems can be integrated into different areas of the electrical grid: generation, transmission, distribution, or the customer side (Abbas *et al.*, 2013). In renewable energy power plants, energy storage systems can be applied to the system under two objectives: injection profiling (time-shifting) or injection smoothing (capacity firming) (Zini, 2016). While injection profiling focus on storing energy to be used later, injection smoothing aims to provide a firm power supply over a period of time.

Energy storage technologies that are suitable or under development for the integration into renewable energy plants focusing on both time-shifting and injection smoothing are batteries

(Abbas *et al.*, 2013) and TES (Denholm *et al.*, 2015b). One of the prominent technologies that are plausible to be included in large scale power plants are batteries based on lithium-ion (Li-ion), sodium sulphur and lead-acid technologies (IEA, 2017). Large scale batteries are used in intermittent renewable power plants, such as wind farms or PV plants, to decrease the curtailment and increase the dispatchability (International Renewable Energy Agency, 2019). According to IRENA, around 90% of the battery system projects developed during 2017 were based on Li-ion technology.

However, a large scale battery infrastructure is at least one or two orders of magnitude more expensive than TES (NREL, 2018). TES is a key alternative that has been implemented in CSP plants to store heat and deliver energy in the form of heat or electricity, increasing the dispatchability of solar power plants and promoting the integration of renewable energy power plants (Dinter and Möller, 2016; Powell *et al.*, 2017). TES systems can be divided into three categories: sensible, latent, and thermochemical energy storage (TCES).

Sensible energy storage is currently developed in commercial CSP plants (Mohan *et al.*, 2019). In this context, molten-salt technologies are the most deployed technology (Fernández *et al.*, 2019a). More details on the two-tanks molten salts technology are given in Section 3.4.1. This system uses differences in the temperature of a substance to store energy (sensible heat). For instance, a typical molten-salt used in CSP plants is composed of $NaNO_3$/KNO_3 (i.e. sodium nitrate and potassium nitrate), with a heat capacity of 1.52 $kJ{\cdot}kg^{-1}{\cdot}{}^{\circ}C^{-1}$ (at 390 °C) (Fernández *et al.*, 2019a). In addition, costs reported for molten-salt thermal energy storage systems are around 25 $USD{\cdot}kWh_t^{-1}$ (Zurita *et al.*, 2018; NREL, 2018).

Latent heat storage systems use the enthalpy of phase change of a suitable material to store and release energy (Prieto and Cabeza, 2019). Usually, this process is based on the solid-liquid phase change (melting-solidification) (Cabeza *et al.*, 2015). Hence, this process occurs at a constant temperature (latent heat). Due to the complexity in the design and operation of these systems, currently, the integration of latent heat thermal energy storage systems into a CSP plant has not reached commercial maturity. Nevertheless, several studies have proposed different configurations and materials to demonstrate their technical feasibility (Prieto and Cabeza, 2019). Examples of components that have been proposed for the integration into CSP are $NaNO_3$ (specific heat 1.82 $kJ{\cdot}kg^{-1}{\cdot}{}^{\circ}C^{-1}$, cost 25.2 $USD{\cdot}kWh_t^{-1}$), NaCl-KCl-LiCl (1.34 $kJ{\cdot}kg^{-1}{\cdot}{}^{\circ}C^{-1}$, cost 36 $USD{\cdot}kWh_t^{-1}$), among others (Prieto and Cabeza, 2019).

Finally, TCES uses the enthalpy of a reversible chemical reaction. Materials based on chemical reactions with high energy storage density and reversibility are required. TCES is generally used in high-temperature processes, and usually, the enthalpy of reaction ($\Delta\hat{H}_r^{\circ}$) of the chemical process is between 80-180 $kJ{\cdot}mol^{-1}$ (Cabeza *et al.*, 2015). TCES is a promising technology with the potential for high energy storage densities and no storage losses beside the initial loss of the sensible heat (Ortiz *et al.*, 2018a). A reversible process that has received significant attention for the implementation into CSP plants is the calcination/carbonation of calcite,

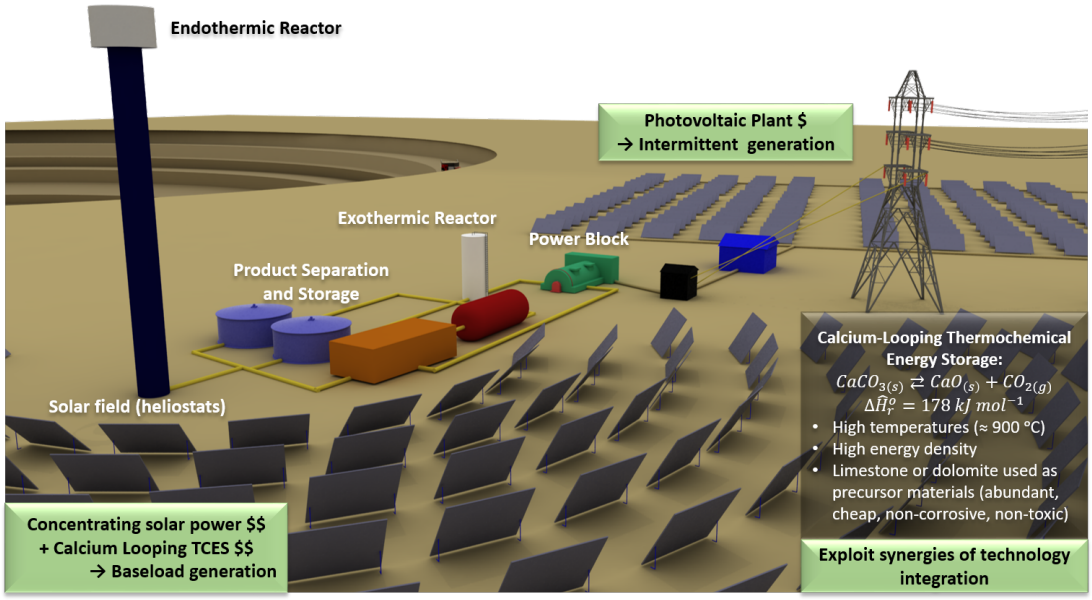

Figure 2.7: Hybrid solar power plant (CSP-PV) integrated with a thermochemical energy storage system

with a working temperature in the range of 700 - 1000 °C. This process, knows as calcium-looping (CaL) has important advantages that make it an attractive technology as a TCES system (Pardo *et al.*, 2014; Ortiz *et al.*, 2019a; Criado *et al.*, 2017; Bui *et al.*, 2018). For instance, the abundance and low price of the precursor materials (i.e. limestone or dolomite), the properties of the products (non-corrosive, non-toxic) (Müller *et al.*, 2011; Bui *et al.*, 2018), and its theoretical high energy density (4.4 GJ m^{-3}) (Gil *et al.*, 2010). More details on the calcium-looping technology are given in Section 6.2.

Due to its high potential, many studies have focused on the analysis of the integration of two-tank molten salt as TES or calcium-looping as a TCES process into CSP plants (Zurita *et al.*, 2018; Ortiz *et al.*, 2019a). For instance, Figure 2.7 shows a calcium-looping process integrated into a CSP plant and hybridised with solar PV. This configuration will be studied in depth in Chapters 6 and 7.

2.3 Hybrid solar power plants with energy storage systems

Some research demonstrates that hybrid systems integrating high-cost CSP with TES and low-cost PV power plants are one of the most suitable sustainable technologies to provide economical, reliable, and dispatchable power (Denholm *et al.*, 2015b), and that the hybridisation of such systems allows even greater performance (Petrollese and Cocco, 2016; Pan and Dinter, 2017; Srilakshmi *et al.*, 2017; Starke *et al.*, 2018). Moreover, the operational optimisation of a solar

tower system integrated with TES and hybridised with a PV plant allows reaching high capacity factors (Green *et al.*, 2015; Starke *et al.*, 2016). Hence, the hybridisation of firm generation from CSP plants with TES and lower cost generation from PV power plants enables excellent features like dispatchability, decreases the intermittent generation from renewables, it is able to match supply and demand, and reduce the levelised cost of electricity from solar power plants. Besides, as a pathway to cost-competitive decarbonisation for electricity generation, a co-firing option can be included into a CSP plant to get a firm power supply, working even with no solar irradiation, hence, increasing its dispatchability but at the cost of emissions.

In order to evaluate the dispatchability of renewable power plants integrated with energy storage, several studies focus on the simulation of a typical period to estimate the operation of a whole year (Ortiz *et al.*, 2018a; Fernández *et al.*, 2019b), for instance, one or two representative days with hourly time steps. Nevertheless, studies suggest that a one year with hourly time step simulation is crucial to evaluate the operation of a renewable power plant under variable energy sources, to consider daily and seasonal variability of the renewable resource (Ortiz *et al.*, 2018a). According to Renaldi and Friedrich (2017), to define the best operational strategy for a renewable energy system integrated with energy storage, an optimisation study is required; however, the storage system increase the complexity of the problem. Several studies exploit synergies between expensive and dispatchable power plants, such as CSP with TES, integrated with affordable and intermittent renewable technologies (Petrollese and Cocco, 2016). These studies, based on the application of optimisation techniques, focus on the development of operational strategies that minimise or maximise different performance metrics as objective functions.

Nevertheless, to design a dispatchable and also affordable energy system, the optimal design of its components is required. On the one hand, if one component is undersized, there will be a bottleneck in the operation, that results in a reduction in the efficiency of the whole process. On the other hand, the oversizing of a component will result in an unnecessary high investment cost, increasing the investment costs as well as the levelised cost of each energy unit produced during the lifetime of the power plant.

2.4 Optimisation of energy systems

The use of optimisation techniques has become an essential tool to find the best possible decision or a range of solutions for an engineering problem. The formulation of an optimisation problem requires an appropriate definition of system boundaries, decision variables, system constraints and objective functions (Dincer *et al.*, 2017). Modelling and simulation techniques are usually studied and applied in engineering to get relevant information about the behaviour of real problems and applications. Models are developed by mathematical formulation, identifying physical laws and principles, and considering assumptions and approximations (Dincer

et al., 2017).

According to Frangopoulos *et al.* (2002), three conceptual levels apply to energy systems optimisation:

- Synthesis optimisation, focusing on the optimal selection of components, processes or equipment and their interconnections, which define the superstructure of the energy system.
- Design optimisation, that focuses on the optimal design and specifications of the components, i.e. sizes, capacities.
- Operational optimisation, which finds the best strategy to operate as well as process parameters under specific requirements.

The optimisation problems analysed in this research consider that the superstructure is given in each case. Here, the superstructure is defined according to current projects under development, construction or operation. In some cases, the superstructure also considers the integration of other technologies that have been proposed in the literature to exploit synergies, or to improve the performance of existing renewable power plants. Hence, the two-stage multi-objective optimisation framework developed and explained in Chapter 3, focuses on the simultaneous optimisation of the design and operation of a given superstructure. Different configurations are studied in Chapters 4, 5, 6 and 7. These superstructures are based on the integration of different energy conversion and storage technologies into hybrid solar power plants composed of a solar tower and a PV plant. The energy conversion and storage technologies integrated and studied in this thesis are sensible heat TES, TCES, electrical batteries, fossil backup, heat integration, and wind power plants.

Optimisation problems can be defined as single objective or multi-objective. In decision-making processes, the analysis of multiple targets is essential to consider different approaches as well as trade-offs between various criteria. According to Dincer *et al.* (2017), optimisation techniques can be defined based on:

- the characteristics of the variables and objective functions, e.g. linear, integer, quadratic, non-linear, stochastic programming;
- the nature of the variables, e.g. deterministic, probabilistic; and
- the algorithm used to solve the optimisation problem, i.e. exact approaches (e.g. Branch and Bound), approximation strategies (e.g. sequential algorithms, local algorithms, random algorithms), and heuristic/metaheuristic approaches (e.g. evolutionary algorithms) (Festa, 2014).

In an energy system optimisation, the problem can be solved sequentially or simultaneously. While the sequential approach handles each level independently, simultaneous strategies optimise all levels together, increasing the complexity by generating a large size non-linear problem. Different energy systems optimisation studies applied a simultaneous approach to solving

a two-level optimisation problem using different techniques in each stage (Fazlollahi *et al.*, 2012).

In pursuance of reaching high dispatchability as well as low cost of energy generation, several studies focusing on the implementation of CSP with TES in different areas have been published in recent years. Some of them are focused on the optimisation of the design and its operation through various approaches, e.g. linear programming, neural networks, evolutionary algorithms, non-linear modelling. For instance, to optimise the design of a solar power plant by sizing its elements, Kalogirou (2004) employs artificial neural networks and a genetic algorithm approach to maximise the financial performance of the project.

In other study, Amusat *et al.* (2016) evaluated the capacity to supply electricity and heat in an off-grid scheme for a large scale copper mine, Collahuasi, one of the largest copper mines located in Chile (Mining Council Chile, 2015). This research was focused in the optimal selection of the best technology of a hybrid solar power plant (CSP and PV) with energy storage (pumped hydro energy storage, advanced adiabatic compressed air storage, and TES), minimising the investment cost of the complete system to ensure the supply of energy.

A multi-objective approach for the optimal size of a hybrid CSP-PV power plant integrated with TES has been implemented by Starke *et al.* (2018). In this study, the design optimisation focusing on the analysis of the trade-off between costs and capacity factor is developed by a genetic algorithm coupled with a surrogate model for each objective function. To built the surrogate model, an annual simulation of the operation estimates the thermal and economic performance of each power plant by a transient model.

2.5 Knowledge gaps

Previous studies do not exploit the synergies of large scale hybrid renewable power plant systems by simultaneously optimising financial and technical performance in both the design and the operational optimisation stages. While a small number of design variables enables the use of multi-objective non-linear optimisation techniques, the operational optimisation requires the use of linear programming methods. A large number of operational optimisation variables for a yearly operation profile with an hourly resolution, makes the problem intractable with optimisation methods for non-linear problems. However, the standard linear programming methods are only capable of single-objective optimisation, and thus previous studies typically consider a single objective. This research aims to fill this gap, by optimising at the same time the design and operation of hybrid solar power plants composed of a CSP and a PV plant, and the integration of other conversion and storage technologies, concerning multiple objectives.

In this thesis, a two-stage optimisation framework is developed to simultaneously optimise both stages (i.e. the design and operation). The structure is defined as a multi-objective operational

optimisation by linear programming nested in the fitness evaluation of the multi-objective design optimisation stage by an evolutionary algorithm. The results of both optimisation stages are Pareto frontiers (multi-dimensional, depending on the number of objectives) which show the trade-offs of different operation strategies and designs concerning technical, financial, and environmental performance metrics of solar power plants.

A scalarisation method to find the best operational strategy considering hourly time steps and one-year operation is designed to develop the multi-objective linear operation routine. The operational optimisation by linear programming allows analysing a considerable time frame, which is necessary to evaluate the long-term and seasonal behaviour of the system under variable solar resource. For instance, one of the goals when finding the best operational strategy of a renewable power plant is by maximising both the energy supplied and the dispatchability under a specific commitment, two goals that during some periods of the year are conflicting objectives. Consequently, a multi-objective optimisation technique to model a one-year hourly operation strategy of a hybrid solar power plant with energy storage is one of the aims of the present study. Here the capacity of linear programming to optimise the annual performance of the power plant, taking into account the daily and seasonal variability of the solar resource is exploited.

The parametric model developed in this study considers a typical meteorological year (TMY) with an hourly resolution to represent the long term solar resource performance of the location under consideration. According to Sengupta *et al.* (2015), designers and developers, to evaluate the feasibility of a solar power plant project in a particular location, usually use the TMY, which represents the condition of the site under analysis through an annual data set.

As indicated in Denholm *et al.* (2015a), the typical meteorological year (TMY) is used to estimate the probable annual performance of a proposed solar power plant for a specific location. The TMY data set provides 8760 hourly values detailing the meteorological conditions at a particular place and is based on several years of meteorological data. TMY data sets represent natural diurnal and seasonal variations of a year of typical climatic conditions. Hence, these are not created to provide meteorological extremes. A TMY data set is essentially the 50^{th} percentile of the full distribution of probabilities, then, it is the best estimate and most probable value. Other data set with more conservative estimations can also be created, such as P90. This means that the real values can exceed the data set with 90% probability, giving more confidence to investors that sufficient energy will be generated, allowing reduce financial risks of the project.

The TMY data sets used in this research are the following:

- Tonopah, United States, TMY3 data set, 15-year updated National Solar Radiation Database for 1991-2005. Source: National Renewable Energy Laboratory. (NREL, 2018)
- Seville, Spain, TMY data, the data set has been produced considering 10 years of data. Source: European Commission, Photovoltaic Geographical Information System, PVGIS

version 5. (European Commission, 2017)

- Atacama Desert, Chile. TMY Data set at one-hour interval for the years 2004 to 2016. Source: Ministry of Energy, Chilean Government, and Department of Geophysics, Universidad de Chile. (Ministry of Energy - University of Chile, 2016)

The design and operational optimisation of a renewable power plant integrated with energy storage, suggests that a multi-objective optimisation routine is crucial to estimate and analyse the trade-off between technical and financial performance to design an affordable and dispatchable power plant. Moreover, the direct link between the objectives of the design and operational optimisation routines is required to exploit the synergies of technology integration.

Throughout the thesis, the framework will be applied to different superstructures and used to design hybrid solar power plants for locations which have different solar resource profiles covering the feasible conditions for solar power plants. Hence, to analyse projects under development, and potential sites for further deployment of solar plants with energy storage, the following locations will be evaluated: Seville, Spain; Nevada, United States; and the Atacama Desert, Chile, where each location under study requires a bespoke design due to the complex interactions between the different parts of the system and the differences in solar resource profile. Finally, the results are used to develop guidelines for the optimal design of dispatchable solar power plants for locations with an excellent solar resource.

Chapter 3

Two-stage Design and Operational Optimisation Framework

The operation of renewable power plants integrated with energy storage leads to complex interactions between the different components and the intermittent resource, requiring sophisticated techniques to achieve high dispatchability and low cost simultaneously. Besides, the optimal design of these power plants requires the use of multi-objective optimisation tools to handle the trade-off between technical and financial performance (Tezer *et al.*, 2017). On the one hand, due to the variability of the renewable resource, these optimisation problems have to consider a more significant number of parameters compared with conventional power plants. On the other hand, the integration of energy storage, that allows to change the temporal consumption of energy, requires that the operation of every design has to be optimised in order to find the best operational strategy to accomplish different requirements. Hence, the optimal design of a hybrid renewable power plant with energy storage has to focus on both the optimisation of the size of the power plant (design) and the best strategy to operate (operation). In this chapter, a two-stage multi-objective optimisation problem is proposed and developed to simultaneously solve these problems. Here, the first stage of the framework corresponds to the operational optimisation, while the second stage to the design optimisation.

3.1 Overview

In this study, a hybrid solar power plant composed of two different solar technologies: a concentrating solar power (CSP) plant, and a photovoltaic power (PV) plant will be analysed. Currently, PV is the most cost-competitive technology to provide intermittent renewable energy, while CSP integrated with thermal energy storage can provide dispatchable energy but at higher costs (Liu *et al.*, 2016; SolarPACES, 2018; Maximov *et al.*, 2019; Peng *et al.*, 2017). Furthermore, the integration of a fossil backup unit into a CSP plant allows continuous operation even during long periods with no solar irradiation. However, this depends on the sizes of the fossil backup unit and the energy storage system.

The purpose of integrating different technologies is to exploit synergies by the combination of them, in this case, the affordability of PV and the dispatchability of CSP with energy storage. Moreover, it is possible to evaluate the value of flexibility by giving some degrees of freedom to the operation of renewable power plants. In this research, we study different flexibility options. One option is that the system does not need to fulfil all its commitment in every single time step; in other words, a mismatch between supply and demand is allowed. Another option analysed in this study, when looking for an optimal transition to a sustainable energy system, is the integration of a small fossil backup unit. In that case, the power plant can emit greenhouse gases, that makes the system not entirely renewable and sustainable, but this flexibility improves both technical and financial performance. Each option will be studied in this research under a proper definition of the variables, constraints and objectives of the optimisation.

The optimal design of an affordable and dispatchable renewable power plant has to examine and analyse its financial and technical performance carefully. For instance, to absorb some level of fluctuations, some power plants are oversized. This method is an excellent way to improve the ability to supply energy when it is needed (dispatchability), but in those cases, financial performance is negatively affected. On the contrary, if one of the main components is undersized, it produces a bottleneck that decreases the technical performance of the operation. Hence, the right selection of the size of the components is vital for an optimal design.

The analysis of the financial performance of a power plant is based on investment costs, as well as operational and maintenance costs. When comparing with other technologies, the Levelised Cost of Energy (LCOE) is a crucial indicator. The LCOE represents the present value of the total life cycle costs involved in the generation of each unit of energy during the lifetime of the power plant, according to equation 3.1 (Short *et al.*, 1995). Here C_t is the cost in year t (i.e. initial capital investment, annual operational and maintenance costs), and E_t is the energy dispatched in year t. Typical values for the annual interest rate and lifetime of r=7% and T=25 years, respectively, are used to be able to compare with other technologies and reports (IEA *et al.*, 2015).

$$\text{LCOE} = \frac{\sum_{t=0}^{T} \frac{C_t}{(1+r)^t}}{\sum_{t=1}^{T} \frac{E_t}{(1+r)^t}} \tag{3.1}$$

In this study, the technical performance is measured by the dispatchability and greenhouse gas emissions (in the case that the power plant is integrated with a fossil backup unit). In order to measure the dispatchability of a renewable power plant with energy storage, its operation has to be strategically defined according to the supply commitment. Renewable resources are intermittent as well as could be the demand. Nevertheless, supply and demand should match in each time step. Hence, the best operational strategy has to handle the complex interactions between a renewable supply, energy storage, and commitment that change every time-step.

In the next sections, the two-stage multi-objective optimisation framework is described. First, a fundamental background of energy system analysis is given in Section 3.2. Then, Section 3.3 exposes the simulation of the hybrid solar power plant based on the analysis previously detailed. Section 3.4 exposes the integration of thermal energy storage in the model. After that, the operational modelling and optimisation is explained, and an efficient method is exposed to deal with multi-objective linear programming in Section 3.5. Finally, Section 3.6 will focus on the multi-objective optimisation of the design of the power plant by genetic algorithms.

3.2 Fundamentals of energy system analysis

The operational modelling is performed by the simulation of energy conversion processes and energy and mass transfers for each process. Then, the operational optimisation will focus on objectives that enhance its performance from a holistic point of view.

The operation of the power plant is based on the fundamental study of thermodynamics. This section is a general analysis of the complete process based on the study of thermodynamics as presented in Cengel and Boles (2015) and lecture notes from the course Analysing Energy Systems of the Master in Energy Systems at the University of Melbourne (Webley, 2014). The study of thermodynamics allows us to analyse each process behind the conversion and energy transfers between different systems and technologies.

In the analysis of energy systems, the following statements for the conservation of matter (m) and energy (E), represent the balances of energy and mass entering and leaving a system:

$$m_{in} - m_{out} = \Delta m_{system} \tag{3.2}$$

$$E_{in} - E_{out} = \Delta E_{system} \tag{3.3}$$

Steady-flow conditions (i.e. the properties of the fluid at any fixed point do not change over time) are a very close approximation to model continuous operation devices like turbines, pumps, heat exchangers, power plants (Cengel and Boles, 2015). In the case of cyclic devices (e.g. compressors), steady-flow conditions can be applied using time-averaged values for the thermodynamic properties of the flow (Cengel and Boles, 2015). In modelling the operation of process units, i.e. systems defined by a control volume, in which mass can cross its boundaries (Dincer *et al.*, 2017), the present study considers hourly time-steps. Nevertheless, according the requirements of the problem under study, the code and algorithm developed in this research allow the analysis of different time-steps. Hence, each time-step (1 hour) will be simulated as a steady-flow process.

For a flowing fluid entering or leaving a control volume, the total energy (θ) on a unit-mass basis is defined by the sum of the flow energy ($P \cdot v$), the internal energy (u), the kinetic energy

(ke) and the potential energy ($g \cdot z$), according to:

$$\theta = P \cdot \nu + u + ke + pe = P \cdot \nu + u + \frac{v^2}{2} + g \cdot z \tag{3.4}$$

where P is the pressure, ν is the specific volume, V is the velocity, g is the acceleration of gravity, and z correspond to the elevation relative to a reference point. The terms: (i) work associated with a flowing fluid ($P \cdot \nu$) and (ii) internal energy, are combined in a property defined as enthalpy (h):

$$h = P \cdot \nu + u \tag{3.5}$$

In order to measure the enthalpy of a flowing fluid, the difference in enthalpy between the actual state and a reference state is used, this because it is not possible to calculate or measure absolute values for enthalpy. Hence, the enthalpy is defined as a function of the pressure and the temperature of the component. Besides, the specific heat at constant pressure, c_p is defined as the change in enthalpy of a substance per unit change in temperature at constant pressure. Then, the change in the enthalpy can be determined by:

$$\Delta h = h_2 - h_1 = \int_{T_1}^{T_2} c_p \, dT \tag{3.6}$$

As mentioned in Chapter 2, three different alternatives exist when working with thermal energy storage systems: latent heat, sensible heat, and thermochemical reaction. While latent heat is associated with a phase change (e.g. from gas to liquid), sensible heat is related with a temperature change of the material. When evaluating the difference in enthalpy between two stages, the analysis has to consider that c_p changes with temperature, and it is discontinuous at a phase change. Hence, the enthalpy of phase change has to be considered. Finally, to analyse a thermochemical reaction, the enthalpy of reaction is employed.

Now, the energy balance in a control volume involving a fluid stream, and the interaction with heat and work can be defined by:

$$\text{Accumulation} = \text{Input} - \text{Output} + \text{Generation} - \text{Consumption} \tag{3.7}$$

In this equation, accumulation is associated with the change in the energy within the boundaries of the system (e.g. energy storage tanks). Input and output energy are associated with: (i) energy accompanying a mass flow (internal, kinetic and potential energy); (ii) work associated with the mass flow (P·ν); (iii) work exchange (W_s) between the system and its surroundings (e.g. shaft work by a compressor); and (iv) heat transfer (Q) produced by a difference in temperature. Finally, the generation and consumption of energy are different from zero when a chemical or

nuclear reaction occurs. Therefore, the general energy balance equation can be defined by:

$$E_2 - E_1 = \left[\sum \left\{ m_i \cdot \left(u_i + \frac{v_i^2}{2} + z_i \cdot g \right) + m_i \cdot (P \cdot \hat{V})_i \right\} + Q + W_s \right]_{in} \tag{3.8}$$

$$- \left[\sum \left\{ m_i \cdot \left(u_i + \frac{v_i^2}{2} + z_i \cdot g \right) + m_i \cdot (P \cdot \hat{V})_i \right\} + Q + W_s \right]_{out} \tag{3.9}$$

In most of the cases when working with a fluid stream, the kinetic and potential energies are negligible (compared with the enthalpy), and when considering net quantities for Q and W_s (i.e. $Q = Q_{in} - Q_{out}$, and $W_s = W_{s,in} - W_{s,out}$, the last equation can be simplified to:

$$\Delta E = \sum_{\text{input}} (m \cdot h)_i - \sum_{\text{output}} (m \cdot h)_i + Q + W_s \tag{3.10}$$

For steady-flow systems (e.g. turbines, compressors, heat exchangers, coolers, reactors), the accumulation of mass and energy in the control volume per unit of time (i.e. $\dot{m}$ and $\dot{E}$) must be equal zero, hence the mass and energy balances are given by:

$$\sum \dot{m}_{in} = \sum \dot{m}_{out} \tag{3.11}$$

$$\left[\sum \left\{ \dot{m}_i \cdot h_i \right\} + \dot{Q} + \dot{W}_s \right]_{in} = \left[\sum \left\{ \dot{m}_i \cdot h_i \right\} + \dot{Q} + \dot{W}_s \right]_{out} \tag{3.12}$$

In this research, two of the main components of the thermochemical energy storage system are chemical reactors, detailed in Sections 3.4.2. These process units (calciner and carbonator), allow us to absorb/release heat by driving an endothermic/exothermic reaction, respectively. When modelling chemical reactors, in order to include the enthalpy of reaction, the energy balance equation can be written as:

$$\Delta E = - \left[\Delta \{ m_i \cdot h_i \} + \Delta h_r \right] + Q + W_s \tag{3.13}$$

where Δh_r is the enthalpy of reaction, defined as the difference between the enthalpy of the products and reactants (both at the same state, i.e. pressure and temperature) for a complete reaction. The enthalpy of reaction is evaluated at standard conditions. According to equation 3.13, Δh_r is negative for exothermic reactions (release of energy) and positive for endothermic reactions (absorption of energy). Moreover, the standard heat of reaction ($\Delta \hat{h}_r^{\circ}$) is specified considering that all reactants and products are at 298 K (25 °C) and 101.3 kPa (1 atm).

The following section describes the mass and energy balances used in the model for the operation of the main processes of the CSP plant with energy storage. The main components of the CSP plant are the solar field (heliostats), solar tower, and receiver. In the case of the sensible heat thermal energy storage system (i.e. molten salt), the principal components are the storage tanks, heat exchangers and power block. Finally, the thermochemical energy storage system

(i.e. calcium-looping) is composed of reactors (carbonator and calciner), heat exchangers, coolers, compressors, turbines, solids storage tanks, and gas storage vessels.

3.3 Hybrid solar power plant

The present research focuses on the design of power plants that provide dispatchable and affordable clean power. This is achieved by integrating a dispatchable but expensive technology (i.e. CSP with energy storage), with a non-dispatchable but relatively low-cost technology (solar PV). Hence, the optimisation handles technical and economic performance to design a dispatchable and cost-competitive power plant, exploiting synergies of technology integration. While the PV power plant does not directly interact with the energy storage system of the CSP, the net power dispatched from the hybrid plant to the grid is the result of the power generation from the CSP with energy storage plus the generation from the PV plant minus all own consumption of the hybrid power plant, i.e.:

$$P_i^{Net} = P_i^{Generated} - P_i^{Own\ consumption} \tag{3.14}$$

3.3.1 Concentrating solar power plant

The concentrating solar power (CSP) plant studied here is a solar tower. The energy conversion in a solar tower begins in the solar field, where a large number of strategically located heliostats (tracking mirrors) concentrate the solar irradiation into a receiver chamber located on the top of a tower. The heat flow transferred and used in the receiver at each time step ($\dot{Q}_i^{Receiver}$, kW) can be calculated using the following equation:

$$\dot{Q}_i^{Receiver} = DNI_i \cdot \eta_i^{opt,sf} \cdot \eta^{receiver} \cdot A^{CSP} - \dot{Q}_i^{CSP,Curtailment} \tag{3.15}$$

where: (i) DNI_i is the direct normal irradiation (kW·m^{-2}); (ii) $\eta_i^{opt,sf}$ is the optical efficiency of the solar field that varies every time-step in the model and depends on the relative position between the sun, the heliostats, and the tower, including losses related to blocking, soiling, reflectance, attenuation, interception and cosine effect (NREL, 2018); (iii) $\eta^{receiver}$ is the efficiency of the receiver, which is assumed in this work as 0.85 (NREL, 2018); (iv) A^{CSP} is the effective area covered by the heliostats (m^2); and (v) the curtailment ($\dot{Q}_i^{CSP,Curtailment}$, kW) is the thermal power that has to be curtailed when the power cycle is running at full capacity and the storage system is fully charged. Table 3.1 shows the description, nomenclature and units of the variables and parameters used in the model of a CSP plant.

Table 3.1: Variables and parameters of CSP plant

Description	Nomenclature	Unit
Thermal power receiver	$\dot{Q}^{Receiver}$	kW
Direct normal irradiation	DNI	kW m^{-2}
Optical efficiency heliostats field	$\eta^{opt,sf}$	-
Efficiency receiver	$\eta^{receiver}$	-
Area heliostats	A^{CSP}	m^2
Thermal power curtailed	$\dot{Q}^{CSP,Curtailment}$	kW

3.3.2 Photovoltaic power plant

The photovoltaic (PV) power plant directly produces electricity during sunshine hours. Here the use of mono-crystalline silicon modules is considered, as well as 61 kW_{ac} inverters (NREL, 2018). Table 3.2 shows the characteristics of the modules and inverters used in the analysis (NREL, 2018).

Table 3.2: Parameters of modules and inverters of PV plant

Module SunPower SPR-E19-310-COM			Inverter SMA America: STP 60-US-10		
Nominal efficiency	η^{nom}	0.192	Weighted efficiency	η^{inv}	0.982
Max power	$P^{max,\,dc}$	0.31 kW_{dc}	Max DC power	$P^{max,\,dc}$	61.131 kW_{dc}
Module area	A^{module}	1.631 m^2	Max Power AC	$P^{max,\,ac}$	59.860 kW_{ac}

The power generation from a photovoltaic solar field (P_i^{PV}, kW) can be estimated by:

$$P_i^{PV} = GTI_i \cdot A^{PV} \cdot \eta^{Subarray} \cdot \eta^{DC} \cdot \eta^{inv} \cdot \eta^{AC} - P_i^{PV,Curtailment} \tag{3.16}$$

where: (i) GTI_i is the global tilted irradiation, i.e. the sum of the direct and diffuse irradiation in an inclined plane (in this study the slope is approximated to the latitude of the place in order to maximise the annual power supply); (ii) $\eta^{Subarray}$ is the sub-array efficiency that varies every time-step and depends on the characteristics of the modules and the solar irradiation; (iii) η^{DC} considers the efficiency of the direct current circuits ($\eta^{DC} = 95.5\%$), here the losses are related with module mismatch, connections, and DC wiring (NREL, 2018); (iv) $\eta^{AC} = 99\%$ is associated with alternate current wiring losses; (v) A^{PV} is the total area covered by the photovoltaic modules (m^2); and (vi) $P_i^{PV,Curtailment}$ is the power that has to be curtailed when there is a constraint in the power dispatched due to the capacity of the transmission network. Table 3.3 shows the description, nomenclature and units of the variables and parameters used in the model of a PV plant.

Table 3.3: Variables and parameters of PV plant

Description	Nomenclature	Unit
Power array	P^{PV}	kW
Global tilted irradiation	GTI	kW m^{-2}
Area modules	A^{PV}	m^2
Nominal efficiency modules	η^{nom}	-
DC circuits efficiency	η^{DC}	-
Inverter efficiency	η^{inv}	-
AC circuits efficiency	η^{AC}	-
Power curtailed	$P^{PV,Curtailment}$	kWh

3.4 Hybrid solar power plant integrated with thermal energy storage system

3.4.1 Hybrid solar power plant with sensible heat thermal energy storage

The basic structure of a CSP plant integrated with a two-tank molten salt process as a sensible heat thermal energy storage system is shown in Figure 3.1. The intention here is to show a general methodology, which can be modified and used to model different configurations and to estimate the performances of a hybrid solar power plant integrated with an energy storage system under different conditions. In this system, the material (molten salt) is in a liquid state during the complete operation cycle. Hence, the thermal energy from the solar field is used to increase its temperature (sensible heat). Then, the hot stream can be used directly as a heat injection in a Rankine cycle trough heat exchangers to produce steam and then electrical power by a turbine and generator. Alternatively, the hot stream can be stored in the hot tank and used afterwards in the same thermodynamic cycle described before (Rankine cycle). The thermodynamic properties of the molten salt (related to the heat transferred in the receiver) can be calculated by using the specific heat of the storage material (c_p), according to equation 3.6. The main properties of a typical molten salt used in CSP plants are shown in table 3.4 (Peiró *et al.*, 2017). According to Ushak and Grageda (2015), some features of molten salts that make them useful for CSP plants are: a broad range of working temperature, thermal stability, low viscosity, low corrosion rates, high heat capacity per unit of volume, and low production costs. The mass and energy balances for each process can be estimated by applying the thermodynamic analysis described previously.

Table 3.4: Properties of molten salts used in CSP plants (Peiró *et al.*, 2017)

Properties	Values	Unit
Composition	$NaNO_3/KNO_3$	-
Melting point	$238-241$	$^{\circ}C$
Density (ρ)	$0.636 \cdot T(^{\circ}C) + 2089.905$	kg·m^{-3}
Specific heat (c_p)	$1.723 \cdot 10^{-4} \cdot T(^{\circ}C) + 1.443$	kJ·kg^{-1}·K^{-1}

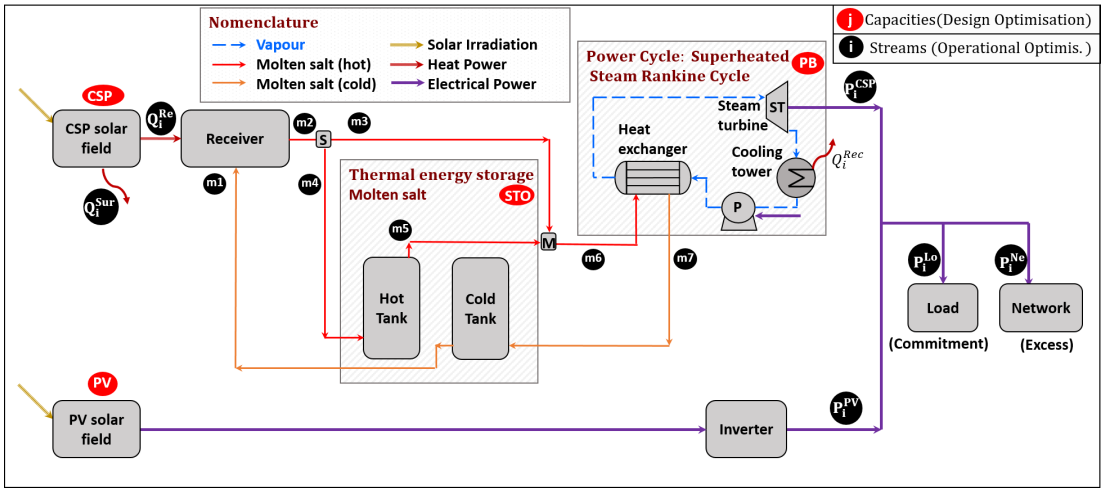

Figure 3.1: Energy and mass balances model of a hybrid solar plant with molten salt sensible heat thermal energy storage system

Previously, it was estimated that the thermal energy captured by the receiver is:

$$\dot{Q}_i^{Receiver} = DNI_i \cdot \eta_i^{opt,sf} \cdot \eta^{receiver} \cdot A^{CSP} - \dot{Q}_i^{CSP,Curtailment}$$

Then, this heat is used to increase the temperature of the molten salt according to:

$$\dot{Q}_i^{Receiver} = \dot{m}_i \cdot \int_{T_1}^{T_2} c_p \, dT \tag{3.17}$$

In this case, there is a non-linear expression that combines the heat available in the receiver with the energy absorbed by the molten salt as a function of the mass flow rate, the inlet and outlet temperature of the material, and its heat capacity. A power flow model will be employed to linearise the system. This simplified model is shown in Figure 3.2. Here the system is divided into four main components: (i) CSP, the solar field area which represents the effective area of heliostats A^{CSP}, m^2; (ii) TES, the thermal energy storage system, with a capacity $Q^{TES,Max}$, MWh; (iii) Power Block, involving the whole Rankine cycle to generate power from heat, where the capacity of the steam turbine generator block is $P^{PB,Max}$, MW; and (iv) PV, the solar photovoltaic plant, including the total area covered by the PV modules, A^{PV}, m^2 and the inverters. The input data required here correspond to efficiencies of each process, thermal efficiencies of pipelines, and efficiencies of electrical circuits. To get an estimation of the efficiencies between each component, the System Advisor Model (NREL, 2018) was used to model different power plants under different conditions. The values calculated will be exposed in each application that will be studied in detail in Chapters 4, 5, 6 and 7.

The linear equations that model the system are shown in Figure 3.2 where the sub-index i denoted the time steps, in this case with hourly resolution. Besides, these equations are outlined below:

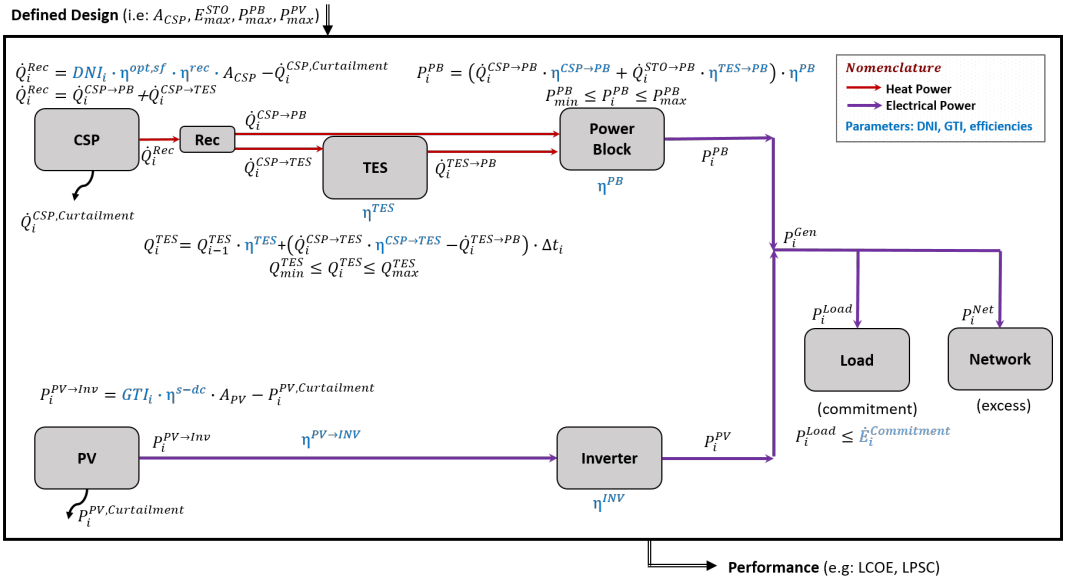

Figure 3.2: Power flow model of a hybrid solar plant with two-tanks molten salt energy storage system

$$\dot{Q}_i^{Receiver} = DNI_i \cdot \eta_i^{opt,sf} \cdot \eta^{receiver} \cdot A^{CSP} - \dot{Q}_i^{CSP,Curtailment} \tag{3.18}$$

$$\dot{Q}_i^{Receiver} = \dot{Q}_i^{CSP \mapsto PB} + \dot{Q}_i^{CSP \mapsto TES} \tag{3.19}$$

$$Q_0^{TES} = 0 \tag{3.20}$$

$$Q_i^{TES} = Q_{i-1}^{TES} \cdot \eta^{TES} + (\dot{Q}_i^{CSP \mapsto TES} \cdot \eta^{CSP \mapsto TES} - \dot{Q}_i^{TES \mapsto PB}) \cdot \Delta t_i \tag{3.21}$$

$$Q^{TES,min} \le Q_i^{TES} \le Q^{TES,Max} \tag{3.22}$$

$$P_i^{PB} = (\dot{Q}_i^{CSP \mapsto PB} \cdot \eta^{CSP \mapsto PB} + \dot{Q}_i^{TES \mapsto PB} \cdot \eta^{TES \mapsto PB}) \cdot \eta^{PB,cycle} \tag{3.23}$$

$$P_i^{PB} \le P^{PB,Max} \tag{3.24}$$

$$P_i^{PV} = GTI_i \cdot \eta^{nom} \cdot \eta^{DC} \cdot \eta^{inverter} \cdot \eta^{AC} A^{PV} - P_i^{PV,Curtailment} \tag{3.25}$$

$$P_i^{Net} = P_i^{PB} + P_i^{PV} \tag{3.26}$$

$$P_i^{Net} \le P^{Transmission,Max} \tag{3.27}$$

$$P_i^{Net} = P_i^{Load} + P_i^{Network} \tag{3.28}$$

$$P_i^{Load} \le P_i^{Commitment} \tag{3.29}$$

where: $\eta^{A \mapsto B}$ is the thermal efficiency associated with thermal losses in the pipe and applied to the stream flowing from A to B; Q_i^{TES} is the energy stored in the system in period i, where the energy stored at the beginning of the operational year is defined as Q_0^{TES}; η^{TES} is the thermal efficiency of the storage tank, associated with the self-discharge; $Q^{TES,min}$ and $Q^{TES,max}$ are the minimum and maximum capacities of the energy storage system used as constraints in the model. P_i^{PB} is the power generated by the Rankine cycle, considering a maximum power

production of $P^{PB,max}$, and total efficiency of $\eta^{PB,cycle}$. This efficiency considers the thermal energy transferred by the molten salts in the heat exchangers to produce superheated steam and the conversion to electricity in the turbine-generator unit. Then, the net power dispatched from the hybrid power plant will be supplied to satisfy the commitment, and any surplus will be dispatched to the network (if possible according to the transmission constraint $P^{Transmission,Max}$).

In order to evaluate the dispatchability of the power plant, the mismatch between the supply and a given commitment will be calculated by using the loss of power supply (LPS). The LPS is defined as 0 when generation exceeds demand, and by the difference between the commitment that should be dispatched in period i ($P_i^{\text{Commitment}}$) and the power supplied in the same period (P_i^{Net}) when commitment exceeds generation. In other words, LPS measures the ability to supply energy when it is needed (dispatchability), according to:

$$\text{LPS}_i = \begin{cases} P_i^{\text{Commitment}} - P_i^{Net} & , P_i^{\text{Commitment}} > P_i^{Net}, \\ 0 & , \text{otherwise.} \end{cases} \tag{3.30}$$

3.4.2 Hybrid solar power plant with thermochemical energy storage

Thermochemical energy storage (TCES) systems operate with a reversible chemical reaction, allowing to control the absorption and release of energy. Different TCES systems integrated with CSP plants are summarised by Pardo *et al.* (2014). While some TCES systems work at high temperature, hence, high efficiency when integrated into CSP plants (e.g. calcite calcination/carbonation) (Müller *et al.*, 2011), other processes work at lower temperature and are more suitable for industrial waste heat applications (e.g. magnesium oxide, 350 to 400 °C) (Knoll *et al.*, 2019). A reversible process that has received significant attention for the implementation into CSP plants is the calcination/carbonation of calcite, with a working temperature in the range of 700 - 1000 °C (Pardo *et al.*, 2014; Chacartegui *et al.*, 2016).

This process, knows as calcium-looping (CaL), involves calcium carbonate ($CaCO_3$), calcium oxide (CaO) and carbon dioxide (CO_2). The CaL process has important advantages that make it an attractive and promising technology as a TCES system (Pardo *et al.*, 2014; Ortiz *et al.*, 2019a; Criado *et al.*, 2017; Bui *et al.*, 2018). For instance, the abundance and low price of the precursor materials (i.e. limestone or dolomite), the properties of the products (non-corrosive, non-toxic) (Müller *et al.*, 2011; Bui *et al.*, 2018), and its theoretical high energy density (4.4 GJ m^{-3}) (Gil *et al.*, 2010). Current studies focus on the development of improved materials and process conditions to decrease the deactivation due to the multi-cyclic operation requirements (Obermeier *et al.*, 2017; Sánchez Jiménez *et al.*, 2019). Moreover, the high-temperature energy released in the CaL process allows the integration of high-efficiency power cycles (Ortiz *et al.*, 2017). Therefore, the CaL process integrated into CSP plants has the potential to supply dispatchable and affordable power.

Figure 3.3 shows the mass and energy flow diagram of hybrid CSP-PV plant integrated with CaL. The figure illustrates with different colours three operational modes (day, night and 24 h); with solid colour lines the solar irradiation, heat and electrical power; with dashed, solid, and dash-dotted line styles the streams of $CaCO_3$+CaO, CaO and CO_2 respectively; and with a long dashed line the steam of the Rankine cycle. During sunshine hours, illustrated by blue lines in the diagram, the solar irradiation from the CSP is concentrated and used as a heat input at the receiver to carry out the calcination of $CaCO_3$ (solid) to CaO (solid) and CO_2 (gas) (Ortiz *et al.*, 2018a). Short residence times and complete calcination are considered in this research when the reaction takes place at atmospheric pressure and a temperature of around 900 $^{\circ}C$ (Obermeier *et al.*, 2017; Hanak *et al.*, 2015). CaO and CO_2 streams at high temperature (900 $^{\circ}C$) leave the calciner to be stored in different tanks at ground level. Conveyors, equipped with lock hoppers to balance the pressure differences, are used to transport the CaO from the calciner to the CaO storage tank. This insulated tank works at high temperature and atmospheric pressure. The CO_2 stream is stored in a high-pressure tank at atmospheric temperature (CO_2 vessel) by using compressors and heat exchangers. To increase the efficiency of the power plant, part of the heat released by the CO_2 before compression is used as a heat input in a small-size Rankine cycle. When energy is needed, the carbonator drives the exothermic reaction, which releases heat by mixing CaO and CO_2, generating $CaCO_3$. While the CaO comes from the CaO storage tank, the CO_2 fed to the carbonator has two possibilities: (i) from the calciner during sunshine hours; (ii) from the CO_2 vessel during night operation, as shown with green lines in the figure. The carbonator works at 3 bar, and a CaO molar conversion of $X = 0.15$ is assumed (Ortiz *et al.*, 2019a). The heat released during the reaction is used to increase the temperature of the CO_2 stream (here well in excess), and then, this stream runs a gas turbine. After that, heat exchangers are used as a regenerative system to increase the efficiency of the process. The cyclic calcination-carbonation of calcium carbonate and calcium oxide is given by equation 3.31.

$$CaCO_{3(s)} \rightleftarrows CaO_{(s)} + CO_{2(g)} \qquad \Delta\hat{H}_r^{\circ} = 178\ kJ \cdot mol^{-1} \tag{3.31}$$

where $\Delta\hat{H}_r^{\circ}$ is the enthalpy of reaction, here in units kJ·mol^{-1}, defined previously as the difference between the enthalpy of the products and reactants (both at the same state, i.e. pressure and temperature) for a complete reaction.

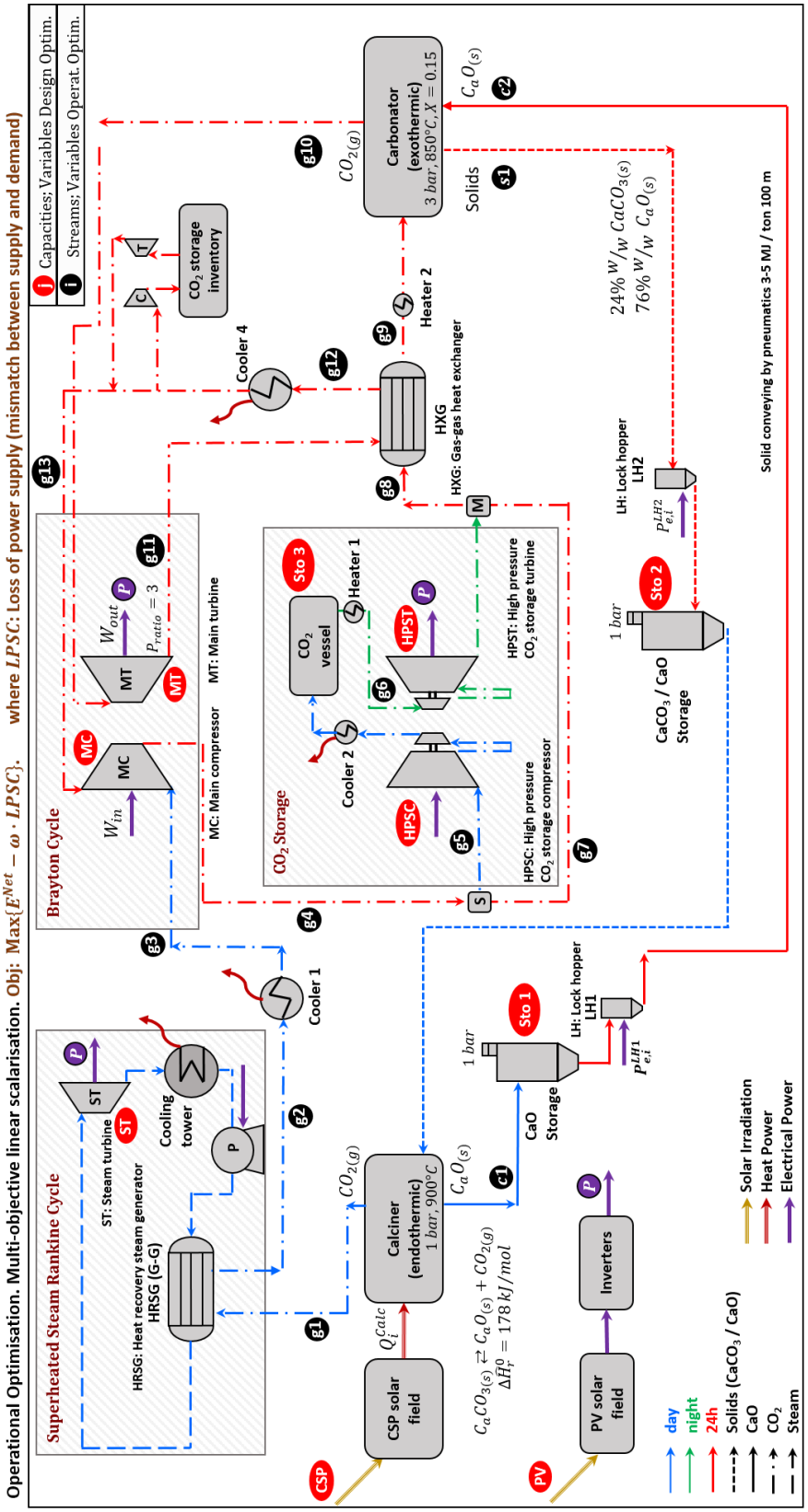

Figure 3.3: Mass and energy balances model of a hybrid solar power plant (CSP-PV) integrated with calcium-looping thermochemical energy storage (TCES) system

Calciner

The endothermic calcination reaction occurs within the calciner, which in this case coincides with the receiver chamber located at the top of the tower, i.e. $\dot{Q}_i^{Receiver} = \dot{Q}_i^{Calciner}$. In this reactor, the inlet stream, which contains calcium carbonate and calcium oxide, is heated to drive the calcination. Main properties for $CaCO_3$, CaO and CO_2 are summarised in table 3.5, based on Jaffe and Washington (2018) and Perry *et al.* (1997). As previously indicated, complete calcination is assumed (Obermeier *et al.*, 2017). As shown in Figure 3.4, there is no accumulation of energy in the system, nor shaft work, then all the heat from the solar field is used to heat the input stream and complete the reaction, according to:

$$\dot{Q}_i^{Calciner} = \Delta(\hat{m}_{k,i} \cdot \hat{h}_{k,i}) + \Delta\hat{h}_{r,i} \tag{3.32}$$

with,

$$\Delta(\hat{m}_{k,i} \cdot \hat{h}_{k,i}) = \hat{m}_{g1,i} \cdot \hat{h}_{g1,i} + \hat{m}_{c1,i} \cdot \hat{h}_{c1,i} - \hat{m}_{s1,i} \cdot \hat{h}_{s1,i} \tag{3.33}$$

$$\Delta\hat{h}_{r,i} = \hat{m}_{s1,i} \cdot \Delta\hat{H}_r^{\circ} \tag{3.34}$$

where $\hat{m}$ is the molar flow rate, $\hat{h}$ is the enthalpy, and the subscripts correspond to the streams of $CaCO_3$+CaO, CaO and CO_2 (s1, c1, g1 respectively), as shown in Figure 3.3. In the calcination process, the molar flow rate of CO_2 (stream $g1$) is equal to the molar flow rate of CO_2 produced in the reaction, and the CaO molar flow rate (stream $c1$) is equal to the molar flow rate of CaO in stream $s1$ plus the molar flow rate of CaO produced in the reaction.

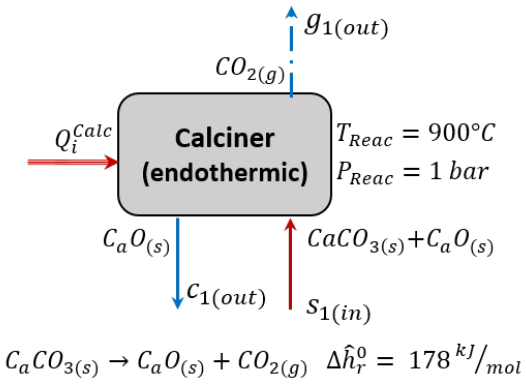

Figure 3.4: Mass and energy balances model of Calciner (calcium-looping TCES system)

Table 3.5: Properties of main components calcium-looping TCES system

	$\Delta\hat{h}_f^0$ (kJ·mol^{-1})	Cp (cal·mol^{-1}·K^{-1})	MW (kg·kmol^{-1})
$CaCO_3$	-1207	$19.68+0.01189\cdot T-307600\cdot T^{-2}$	100.09
CaO	-635	$10.00+0.00484\cdot T-108000\cdot T^{-2}$	56.08
CO_2	-394	$10.34+0.00274\cdot T-195500\cdot T^{-2}$	44.01

Heat exchangers, and coolers:

In a heat exchanger (Figure 3.5), there is no energy accumulation ($\Delta E = 0$), no shaft work ($W_s = 0$) and if considered as adiabatic ($Q = 0$), the mass and energy balance equations that represent the amount of heat transferred from the hot fluid (h) to the cold fluid (c) for each time step (i), are (Dincer *et al.*, 2017):

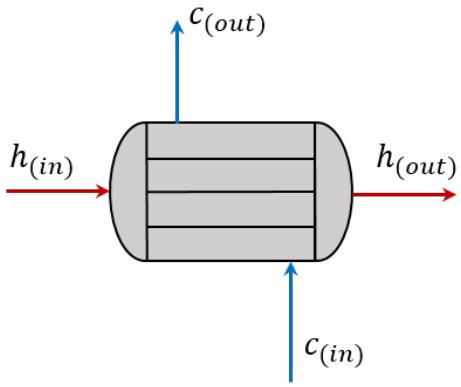

Figure 3.5: Mass and energy balances model of Heat exchangers (calcium-looping TCES system)

$$\dot{m}_{h_{in},i} = \dot{m}_{h_{out},i} \tag{3.35}$$

$$\dot{m}_{c_{in},i} = \dot{m}_{c_{out},i} \tag{3.36}$$

$$\sum_{\text{input}} (\dot{m}\cdot h)_i = \sum_{\text{output}} (\dot{m}\cdot h)_i \tag{3.37}$$

$$\implies \dot{m}_{h_{in},i}\cdot h_{h_{in},i} - \dot{m}_{h_{out},i}\cdot h_{h_{out},i} = \dot{m}_{c_{out},i}\cdot h_{c_{out},i} - \dot{m}_{c_{in},i}\cdot h_{c_{in},i} \tag{3.38}$$

Coolers are modelled similarly to heat exchangers (no energy accumulation, no shaft work, adiabatic), the difference here is that the working fluid cools (h) while a refrigerant (r) is heating (air or water are typically used). The energy balance for coolers is described as:

$$\dot{m}_{r,i}\cdot c_{p_r}\cdot \Delta T_{r,i} = \dot{m}_{h_{in},i}\cdot (h_{h_{out},i} - h_{h_{in},i}) \tag{3.39}$$

where c_{p_r} is the specific heat capacity of the refrigerant, e.g. $c_{p,air\ (23\ ^\circ C,41\%\ rel.\ humidity)} = 1.012$ kJ $\cdot$kg$^{-1}\cdot$K^{-1} (Jaffe and Washington, 2018)

Superheated steam Rankine cycle:

The turbine power output (ST) of the Rankine cycle is simulated as a linear relation with the heat absorbed in the heat recovery steam generator (HRSG) according to:

$$P_i^{ST} = \dot{Q}_i^{HRSG} \cdot \eta^{SSRC} \tag{3.40}$$

where η^{SSRC} is the global efficiency from thermal to electrical power. Based on the model and results published by Ortiz *et al.* (2018a), estimated by using the commercial software ASPEN PLUS, an efficiency $\eta^{SSRC} = 0.268$ will be considered in this study.

Compressors and turbines:

Figure 3.6 shows the relations used to estimate the total work in turbines and compressors according to Dick (2015):

$$\Delta(\dot{m}_i h_{turb,i}) = \dot{m}_i \frac{\gamma_i}{\gamma_i - 1} \frac{P_{in,i}}{\rho_{in,i}} \left\{ 1 - \left(\frac{P_{out,i}}{P_{in,i}} \right)^{\frac{\gamma_i - 1}{\gamma_i}} \right\} \eta_s \tag{3.41}$$

$$\Delta(\dot{m}_i h_{comp}) = \dot{m}_i \frac{\gamma_i}{\gamma_i - 1} \frac{P_{in,i}}{\rho_{in,i}} \left\{ \left(\frac{P_{out,i}}{P_{in,i}} \right)^{\frac{\gamma_i - 1}{\gamma_i}} - 1 \right\} \eta_s \tag{3.42}$$

where γ is the heat capacity ratio, used here as the isentropic expansion factor, and η_s is the isentropic efficiency of the turbine or compressor.

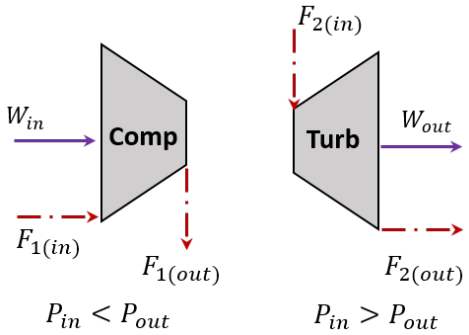

Figure 3.6: Mass and energy balances model of Compressors and Turbines (calcium-looping TCES system)

Carbonator:

In the carbonator, the reverse reaction of the calciner occurs. In this reactor, pure CaO from the CaO storage tank is combined with CO_2 from the CO_2 storage cycle to produce $CaCO_3$ and heat (with a molar conversion of 15%). After the carbonator, while the resulting solid stream ($CaCO_3$+CaO) is stored in the solid storage tank, the CO_2 stream (presented here in excess to absorb the heat released in the reaction) is first conducted to a turbine to produce electricity, after that to a heat exchanger to use part of the heat available in a regenerative system, and finally to a cooler and compressor to close the cycle.

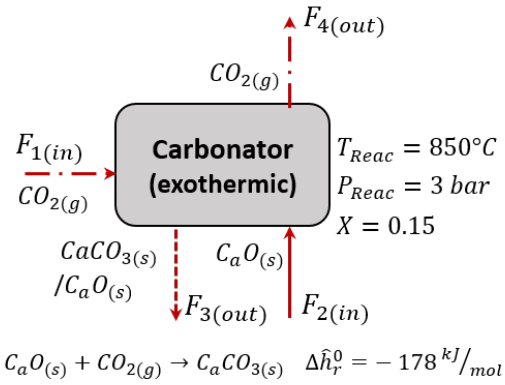

Figure 3.7: Mass and energy balances model of Carbonator (calcium-looping TCES system)

Storage tanks:

The three storage tanks, i.e. CaO storage tank, $CaCO_3$+CaO storage tank, and CO_2 storage vessel, are modelled by mass balances. In the CaO and $CaCO_3$+CaO tanks, the density under storage conditions considers internal porosity and particle packing density of the material, as described in Ortiz *et al.* (2018a). Here the state of charge (SoC_i in m^3) is defined as the volume of material that is presented in the tank in period i, which is equal to the state of charge of the previous period plus the input minus the output flows during the current period (in m^3), according to the following expressions:

$$SoC_i(m^3) = \begin{cases} SoC_{i=0}(\%) \cdot STO^{capacity}(m^3), & \text{if } i = 0 \\ SoC_{i-1} + (\dot{m}_{in} - \dot{m}_{out}) \cdot \Delta t \cdot \frac{1}{\rho_i}, & i \geq 1 \end{cases} \tag{3.43}$$

In this model, the state of charge (in percentage) for each tank at the start of the operation (i=0) is defined as:

$$SoC_{i=0} = \begin{cases} 100\% & CaO \text{ tank} \\ 0\% & CaO + CaCO_3 \text{ tank} \\ 100\% & CO_2 \text{ vessel} \end{cases} \tag{3.44}$$

This means that during the operation of the first hours, the storage tanks of the thermochemical energy storage system are fully charged, which allows the power plant to dispatch energy even without solar irradiation. This is just a criterion for the simulations, which has insignificant influence in the yearly results. However, in the operational optimisation routine, to calculate the actual net energy dispatched, it is necessary to estimate the difference between the available energy in the initial and final periods of the annual operation. To estimate this value, an average energy density factor (ξ) is calculated as the rate between net power dispatched and the mass flow rate of CaO that feeds the carbonator:

$$\xi_i \left(\frac{MWh}{ton_{CaO}} \right) = \frac{P_i^{net}(MW)}{\dot{m}_{c2}(\frac{kg_{CaO}}{s}) \cdot 3600(\frac{s}{h}) \cdot \frac{1}{1000}(\frac{ton}{kg})} \tag{3.45}$$

The results of the model were analysed for one year to estimate this rate and a specific power production value of $\xi_i \approx 0.053$ MWh·ton$_{CaO}^{-1}$ was calculated.

3.5 Multi-objective operational optimisation by linear programming

This section presents a multi-objective linear scalarisation method to optimise the operation of the power plant considering hourly time steps and one-year operation. This technique allows analysing a large time frame, which is necessary to evaluate the long-term and seasonal behaviour of the system under variable solar resource.

In addition, multi-objective optimisation techniques allow to handle different objective simultaneously. For instance, as shown in Figure 3.8, the multi-objective optimisation allows to maximise the energy dispatched while maximising the dispatchability, which is not possible to perform by a single objective optimisation. Figure 3.8 shows an example of single and multi-objective optimisation considering the maximisation of the energy dispatched and the minimisation of the loss of power supply. In a single-objective optimisation the objective reaches the best value while degrading other competing key performance indicators. By a multi-objective optimisation a set of non-dominated solutions that simultaneously optimise both objectives is achieved (Pareto optimal solutions).

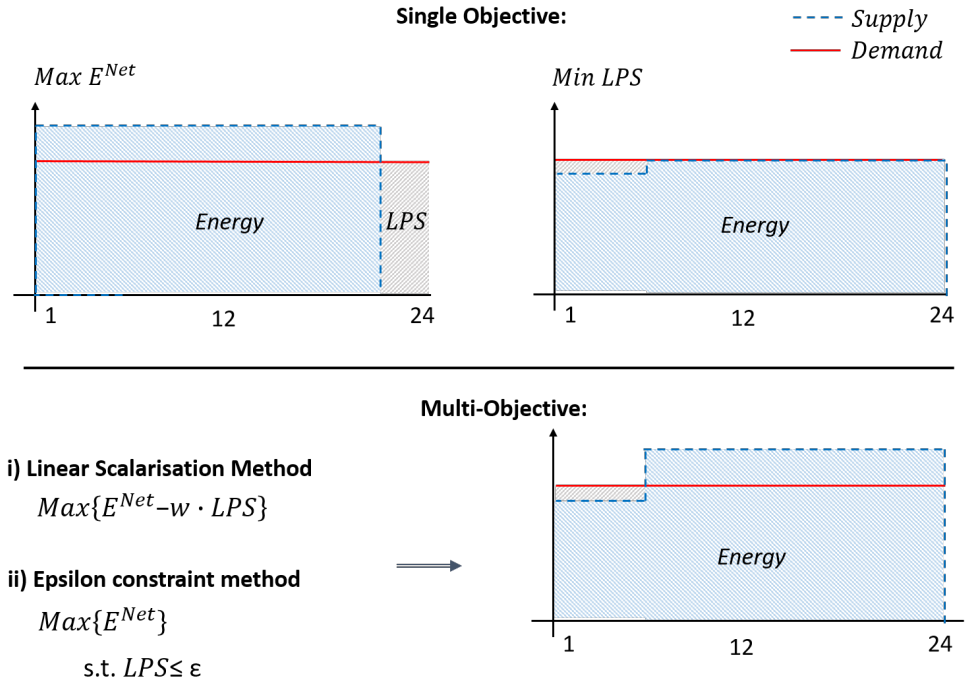

Figure 3.8: Comparison between single and multi-objective optimisation

3.5.1 Linear programming modelling

The main objective of the operational optimisation is to find the best strategy to operate taking into account the daily and seasonal variability of the solar resource. Hence, the model needs to analyse one year of operation (8760 time steps), considering the hourly solar resource of a typical meteorological year. The simplification of this complex problem by using linear programming allows us to run the model with high speed and to analyse a power plant with energy storage under a long term evaluation. There are two simplifications that will be developed throughout this research to simplify the system by a linear programming model. The first approximation will be applied to the model of a hybrid solar power plant with molten salt as a sensible heat thermal energy storage system. In this case, the system is modelled as power flows between the main components, considering efficiencies of power plants in operation found in the literature, e.g. SolarPACES (2018).

The second approximation by linear programming will be elaborated in the integration of a thermochemical energy storage system. In this case, the model will be developed using the non-linear equations presented previously. Then, the temperatures of the processes will be fixed, according to the results presented in current non-linear models developed with commercial software, e.g. the results presented by Ortiz *et al.* (2018a) in which the authors simulate the operation of a CSP plant with calcium-looping under different solar irradiation levels. In a real power plant, this may be achievable by the instrumentation engineering, through the definition and control of the temperatures of each process. Hence, the operational optimisation stage

optimises the mass flow rate of some streams and calculate those that are dependent (because there are direct relationships between some streams) in order to optimise the hourly operation.

3.5.2 Variables

Depending on the model used to approximate the problem by linear programming, in the operational optimisation routine, the variables are defined as power flow or mass flow rates between each subsystem. According to the equations previously detailed to analyse energy conversion and storage systems, some of the variables defined are independent, and they will be optimised. In contrast, other variables will be calculated by energy balances and the capacity of the components as constraints.

3.5.3 Input parameters

According to the equations previously described, that are used to simulate each process, the input parameters required are:

1. Direct normal irradiation (DNI_i).
2. Global tilted irradiation (GTI_i).
3. Demand that the power plants should dispatch: $P_i^{\text{Commitment}}$.
4. Efficiencies (process, pipelines, circuits, etc.).
5. Operational and network constraints (e.g., capacity of the transmission network).
6. Financial parameters (investment costs, operational and maintenance costs).

Here the DNI is the solar irradiation captured by the heliostats of the CSP that track the sun. The GTI is the irradiation in a fixed plane, converted into electricity by the PV plant in which each PV module is non-tracking. The demand that the power plant should dispatch is used in the optimisation to estimate its dispatchability.

3.5.4 Objectives

The objectives defined in the model depend on the target pursued by the user. For instance, the objectives can be focused just on a financial perspective by selling the maximum quantity of energy, thus, reaching the lowest LCOE. Alternatively, in the case that the user is a large consumer, its objectives might be focused on both financial and technical performance (reliability). Nevertheless, these objectives should be different for grid connected or off-grid power plants. Finally, the electricity market operator should be focused on both, a low price of the electricity, as well as a firm electricity supply, which can be evaluated through the mismatch between supply and demand.

Hence, depending on the user of the model, and the feature of the power plant, the objectives can be related with financial, technical, environmental, or societal performance. The flexibility of the model allows to include any objective or combination of them. The only requirement is

that the objectives have to be quantitative and related to the operation. The following are some key performance indicators for technical and financial performance that can be analysed:

- E^{net}, is the total net electricity dispatched by the power plant in one year of operation.

$$E^{Net} = \sum_{i=1}^{8760} P_i^{Net} \tag{3.46}$$

- $\bar{P}^{Net}$ is the average power dispatched in one year, according to:

$$\bar{P}^{Net} = \frac{E^{Net}}{8760\ h} \tag{3.47}$$

- P^{Max} is the maximum power dispatched during at least one hour, over one year of operation.
- $E^{Commitment}$ is the electricity dispatched to fulfil the commitment .
- E^{Excess} is the electricity dispatched when the net energy exceeds the commitment.
- $E^{Curtailed}$ is the amount of thermal energy available in the heliostat solar field that has to be curtailed when the power plant is running at full capacity and the storage system is fully charged.
- ΔE_{f-i} is the energy difference between the last hour and the first hour of operation. This difference is used to calculate the net electricity dispatched during one year of operation.
- LPSC and LPSP (loss of power supply capacity and loss of power supply probability, respectively), are used to estimate the total loss of power during one year of operation, according to:

$$LPSC = \sum_{i=1}^{8760} LPS_i \tag{3.48}$$

$$LPSP = \frac{LPSC}{P_i^{Commitment} \cdot 8760} \tag{3.49}$$

- CF^{CSP} is the capacity factor of the power cycle. For the CaL system, the CO_2 Brayton cycle is normally considered (Ortiz *et al.*, 2019b).

Useful estimations of efficiencies are:

- $\eta^{CSP,Rec}$ is the efficiency of the solar tower power plant considering the energy available and used in the receiver:

$$\eta^{CSP,Rec} = \frac{E^{Net,CSP}}{E^{\text{Total, receiver}}} \tag{3.50}$$

- $\eta^{CSP,DNI}$ is the overall efficiency of the solar power plant considering the solar energy available in the solar field:

$$\eta^{CSP,DNI} = \frac{E^{Net,CSP}}{E^{\text{Total, solar field}}} \tag{3.51}$$

Finally, other indicators that can be useful depending on the case study are:

- Greenhouse gas emissions (total emissions), in the case that a fossil backup unit is used as heat injection for the TES.
- Water consumption during the operation of the power plant (total consumption), that is key in locations with restricted water availability.

Any of these key performance indicators, or the combination of them, can be defined as objectives, for instance:

$$Max\ E^{net} \tag{3.52}$$

$$Min\ LPSC \tag{3.53}$$

$$Min\ GHG \tag{3.54}$$

$$Min\ Q_{water} \tag{3.55}$$

The operational optimisation developed in this model will focus on the first two objectives, i.e. the maximisation of the energy supplied (to minimise the levelised cost of electricity) and the minimisation of the loss of power supply (to maximise the dispatchability).

The use of linear programming ensures a proper approximation of the best operational strategy for one year of operation, considering variable solar resource, in a reasonable computational time. The operational optimisation routine analyses 8760 optimisation variables for each power flow or mass flow rate in Figures 3.2 and 3.3. However, linear programming solvers can only handle a single objective so that multiple objectives can only be added as a constraint or through a weighting process.

3.5.5 Multi-objective linear optimisation

The multi-objective operation optimisation produces a range of Pareto optimal solutions, representing the trade-off between objectives. Each point in the Pareto set is a non-dominated solution or potential candidate. Hence, an a-posteriori analysis should be carried out to select the best result under a trade-off between the objectives. Two techniques have been applied to solve multi-objective optimisation problems in linear programming (Gebreslassie *et al.*, 2009): the weighted-sum or scalarisation method, and the ε-constraint method. These methods, which are modelled and applied to the hybrid power plant, are described below.

Scalarisation method

In the scalarisation method, the multi-objective optimisation problem is transformed to a single objective optimisation by combining and weighting both objectives (Nguyen *et al.*, 2014). The following function describes the new single objective optimisation problem:

$$\text{maximise} \sum_{i=1}^{I} \{P_i^{Net} - \omega \cdot LPS_i\} \tag{3.56}$$

where the positive parameter ω is the scaling factor applied to the second objective.

Epsilon constraint method

In the ε-constraint method, one objective is considered as a constraint in the formulation of the optimisation problem (Fazlollahi *et al.*, 2012), here the optimisation problem is formulated as:

$$\begin{aligned} &\text{maximise} \sum_{i=1}^{I} P_i^{Net} \\ &\text{subject to} \sum_{i=1}^{I} LPS_i \leq \varepsilon \end{aligned} \tag{3.57}$$

An essential challenge of these methods is to define a suitable value of the scaling or constraint parameters in order to get a proper solution. Figure 3.9 shows an example of the Pareto frontier reached when working with both objectives. Points I_1 and I_2 are achieved when the optimisation is done by single objectives, i.e. I_1 corresponds to the $Max\ E^{net}$, and I_2 when $Min\ LPSC$. Then, the dashed line shows the Pareto frontier for both the linear scalarisation and the ε-constraint methods, obtained by varying the scaling and constraint value, respectively. Because the purpose of the model is focused on the design of an affordable and dispatchable power plant, the objective of the operational optimisation will focus on the optimal combination of both objectives. Thus, the target of the optimisation is to be in the top left of the figure. Both the $Max\ E^{net}$ and the $Min\ LPSC$ methods do not reach this zone. On the contrary, the scalarisation and the ε-constraint method, with a good definition of values of ω and ε, respectively, are able to reach values close to this area (i.e. the zone highlighted with an ellipse). The main difference between the scalarisation and the ε-constraint methods is that each iteration of the scalarisation method takes a few seconds to calculate, compared with each iteration of the ε-constraint method which takes almost 10 minutes to be processed. Hence, the scalarisation method is analysed in detail, and is automated to ensure that an optimal value of ω is chosen.

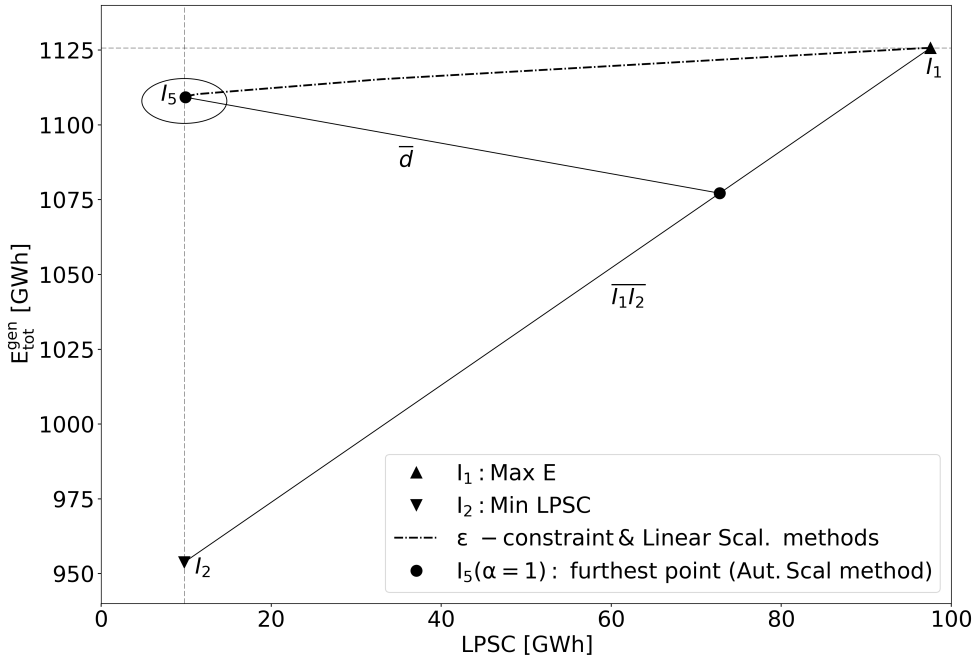

Figure 3.9: Numerical example of single and multi-objective linear optimisation methods applied in the operation of a hybrid solar power plant with thermal energy storage

Automated scalarisation method

In order to have an automated decision process to ensure that the solution of the operational optimisation is in the desired zone, an automated scalarisation method was developed and applied. This autonomous algorithm requires 7 iterations for the case with two objectives. The first iteration is a single objective optimisation of $Max\ E^{net}$ and it gives the point $I_1 = (E_{max}, \mathrm{LPSC}_{max})$ in Figure 3.9. Then, the second iteration is a single objective optimisation of *Min LPSC* which produces the point $I_2 = (E_{min}, \mathrm{LPSC}_{min})$. The purpose of these first two iterations is to get an estimation of ω and the line $\overline{I_1 I_2}$. Then, to standarise and give the same relative weight to both objectives, an initial value of ω is calculated by:

$$\omega_0 = \frac{E_{max} - E_{min}}{\mathrm{LPSC}_{max} - \mathrm{LPSC}_{min}} \tag{3.58}$$

After that, 5 iterations are carried out to get an improved ω ($\omega = \alpha \cdot \omega_0$) which is used as input to the automated selection. This last step, the automated selection can be modelled by different methods depending on the purpose of the user. In this case, it is done by selecting the α-value for which the result ($I_i = (E_i, \mathrm{LPSC}_i)$) of the i^{th} iteration is furthest from the line $\overline{I_1 I_2}$. This is calculated by finding the maximum distance d_i which is the perpendicular line that connects I_i

with $\overline{I_1 I_2}$). The algorithm shown in Figure 3.10 describes this procedure.

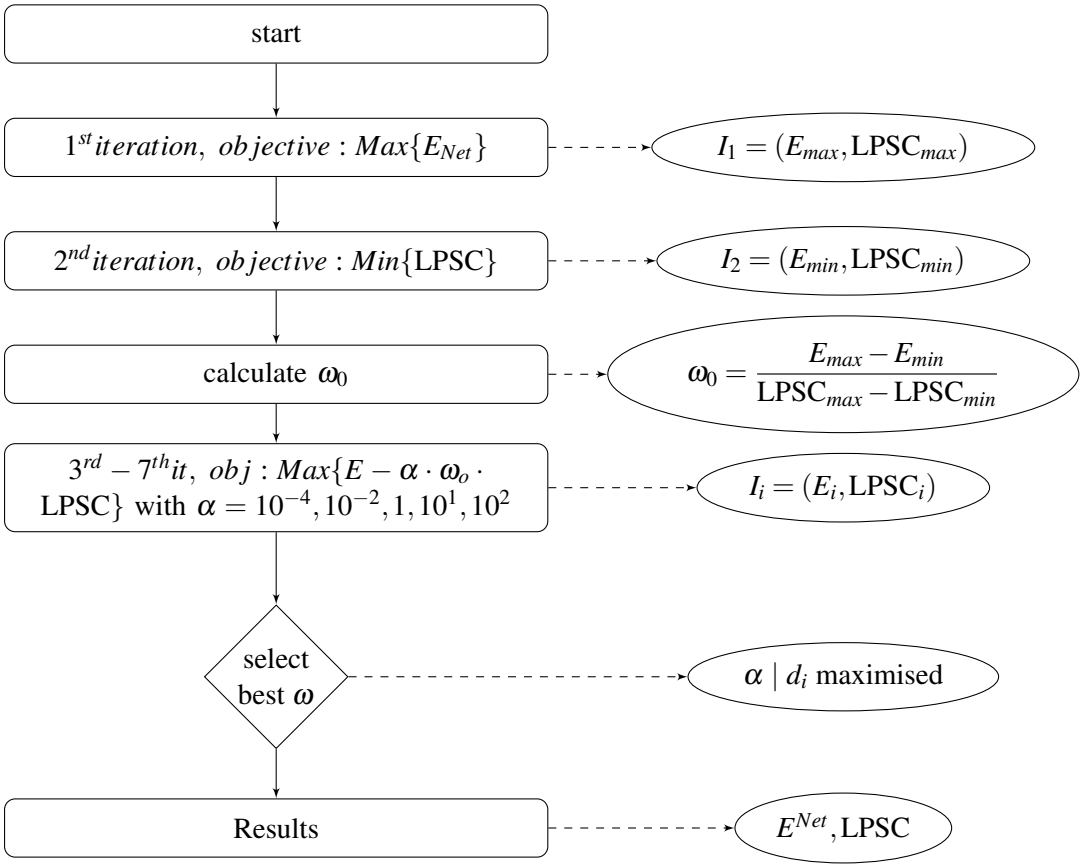

Figure 3.10: Automated linear scalarisation algorithm

3.6 Multi-objective design optimisation by genetic algorithms

As previously mentioned, in order to design an affordable and dispatchable solar power plant, the trade-off between financial and technical performances has to be examined. While an oversized CSP plant can give us full dispatchability at a high LCOE, a PV plant will be more affordable, but not dispatchable. These conflicting objectives are handled by a multi-objective optimisation method which produces a range of non-dominated or Pareto optimal solutions. For optimal design of a hybrid power plant with energy storage, a two-stage optimisation framework is proposed. This framework uses a genetic algorithm to optimise the design of the power plant under techno-economic objectives. The use of genetic algorithms allows us to handle non-convex objectives and several variables. Then, nested as a fitness function, the operational optimisation stage is incorporated in the design optimisation routine.

This genetic algorithm process is shown in Figure 3.11, explaining a two-stage mathematical optimisation model of the design by genetic algorithms and of the operation of the power plant

by linear programming. The optimisation starts generating a random population of a defined number of individuals. This means that each individual is a solar power plant with a defined size or capacities of components. After that, the algorithm finds the best operational strategy during a one-year operation with hourly time-steps. The results of the operational optimisation are all hourly power flows, and these are used to calculate crucial indicators that are employed in the fitness evaluation. Then, the genetic algorithm defines the best offspring by crossing and mutating the population in which power plants with better performance have higher chance to evolve. Finally, the stopping criterion is defined by a given number of generations.

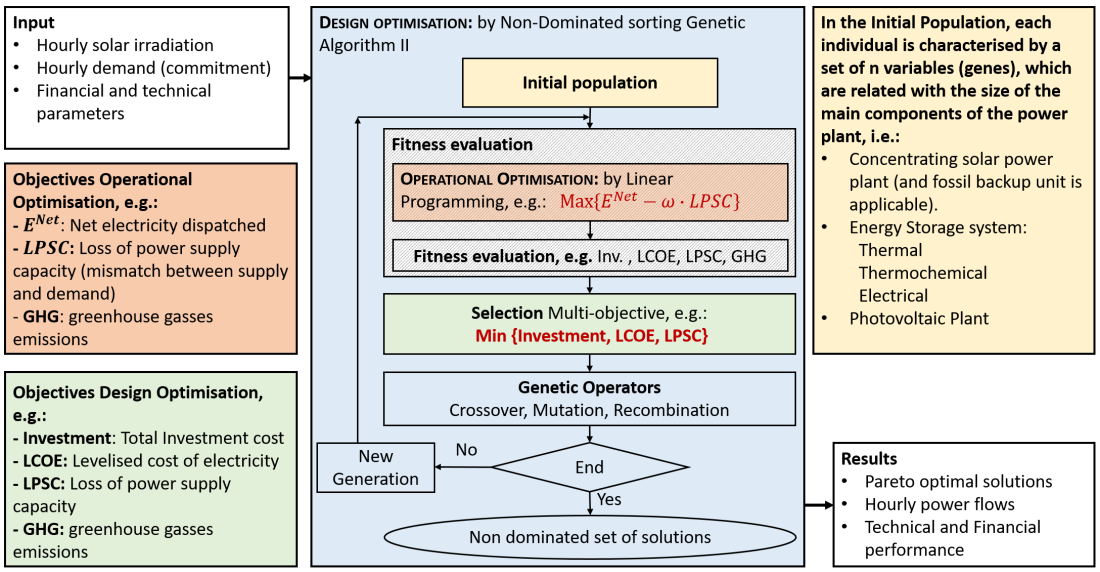

Figure 3.11: Two-stage multi-objective design and operational optimisation framework

3.6.1 Variables

The design of the power plant is given by the size of the main components of each technology considered, which are defined as variables in the design optimisation stage. Different configurations integrating the technologies previously defined will be developed throughout the case studies. These technologies and design variables considered are:

- CSP with molten salt as a sensible TES system
  1. Heliostats field area, tower and receiver: A^{CSP} (m^2)
  2. Molten salt tanks: $\mathrm{STO}^{\mathrm{TES}}$ (MWh)
  3. Steam Turbine: P^{ST} (MW)
  4. Fossil backup unit P^{FBU} (MW) (the integration of this technology is analysed Section 5.3)
- CSP with calcium-looping TCES
  1. Heliostats field area, tower: A^{CSP} (m^2)
  2. Steam Turbine: P^{ST} (MW)

3. Main CO_2 Compressor: P^{MC} (MW)
4. Main CO_2 Turbine: P^{MT} (MW)
5. High Pressure CO_2 Compressor: P^{HPSC} (MW)
6. High Pressure CO_2 Turbine: P^{HPST} (MW)
7. CO_2 Storage Vessel: STO^{CO_2} (m^3)
8. CaO Storage Tank: STO^{CaO} (m^3)
9. $CaCO_3$+CaO Storage Tank: $STO^{CaO+CaCO_3}$ (m^3)

- Photovoltaic power plant
  1. PV modules area and inverters: A^{CSP} (m^2)
  2. Electrical energy storage STO^{EES} (MWh) (the integration of batteries is analysed in Chapter 5)
- Wind farm (the integration of a wind farm is analysed in a case study presented in Section 5.5)

For instance, the design variables are shown in the red ovals in Figure 3.3. The combination of these variables will result in a power plant with known capacities. Then, the initial investment is calculated. Next, the operational optimisation by linear programming nested as a fitness function in the genetic algorithm defines the best operational strategy, e.g. maximising the net energy dispatched and minimising the mismatch between supply and commitment. Finally, three indicators (detailed in section 3.6.3) are considered as objectives for the design optimisation stage and used by the genetic operators.

The integration of different technologies are analysed and presented as cases studies in the remainder of this thesis.

Chapter 4

- CSP-TES & PV.
- Location: Atacama Desert, Chile.
- Aim: Improvement of a hybrid solar power plant under construction.

Chapter 5.2

- CSP-TES & PV-EES.
- Location: Spence copper mine, Atacama Desert, Chile.
- Aim: Long-term analysis of technology costs and integration.

Chapter 5.3

- CSP-TES-FBU (Fossil Backup unit) & PV-EES.
- Location: Spence copper mine, Atacama Desert, Chile.
- Aim: Integration of a fossil backup unit to increase the dispatchability of CSP plants.

Chapter 5.4

- CSP-TES-FBU & PV-EES.
- Electricity and heat supply
- Location: Spence copper mine, Atacama Desert, Chile.
- Aim: Heat supply for low-temperature heating process in copper mines.

Chapter 5.5

- CSP-TES-FBU & PV & Wind farm-EES
- Location: El Abra copper mine, Atacama Desert, Chile.
- Aim: Integration of a wind farm into a hybrid solar power plant.

Chapter 6

- CSP-TCES & PV.
- Location: Seville, Spain.
- Aim: Multi-objective operational optimisation of a TCES integrated into a hybrid solar power plant.

Chapter 7

- CSP-TCES & PV.
- Location: Seville, Spain; Tonopah, USA; Atacama Desert, Chile.
- Aim: Design of dispatchable hybrid solar power plants with TCES.

3.6.2 Fitness evaluation

The multi-objective linear scalarisation model for the operational optimisation presented previously is nested here as a fitness evaluation, linking the objectives of both levels. The operational optimisation routine simultaneously optimises the objectives considered in the problem (e.g. maximises the energy dispatched, minimises the mismatch between supply and demand, minimises the greenhouse gas emissions). Hence, the operation of each design of the genetic algorithm stage is optimised, considering one-year hourly solar irradiation.

3.6.3 Objectives

As stated previously, the design optimisation aims to select the optimal sizes of the components to design an affordable and dispatchable power plant. In this study, the investment cost and the LCOE are employed to measure the affordability. The LCOE is a crucial indicator that represents the cost of each electricity unit generated over the lifetime of the power plant considering the total life cycle costs, while the investment cost is essential when defining a limiting initial budget for the feasibility of a project. In regard to the technical performance, the loss of power supply capacity is used to measure the dispatchability, that is the quantification of the mismatch between supply and the commitment. Besides, the emission of greenhouse gases is considered as a technical objective in configurations that integrate a fossil backup unit to increase the performance of the CSP plant. Hence, the objectives of the design optimisation routine will be divided into financial and technical performance, according to:

- Financial performance:
  - Total investment cost (MUSD)
  - Levelised cost of electricity (USD·MWh^{-1})
- Technical performance:
  - Loss of power supply probability (%)
  - Greenhouse gas emissions (tCO_{2eq})

References and procedures to estimate total investment cost as well as operational and maintenance cost (used to calculate the LCOE), are summarised bellow. To convert estimated cost from some references expressed in Euros, an average exchange rate of $r_{exch} = 1.18$ (EUR to USD, 2018) was considered here (Cherowbrier, 2019).

Investment costs: Concentrating solar power plant

The data required to estimate the investment cost of a concentrated solar power plant, i.e. the heliostat field and the solar tower were obtained using the System Advisor Model (SAM) (NREL, 2018). Here, the cost of the solar field (including the solar tower), in thousands of USD, was estimated as a function of the heliostats field (A^{CSP}, in m^2).

$$IC_{\text{heliostats field \& tower}} = 0.175 \cdot A^{CSP} + 3460 \tag{3.59}$$

$$IC_{\text{receiver}} = 0.055 \cdot A^{CSP} + 12540 \tag{3.60}$$

$$Land\ use_{\text{ CSP}}\ (m^2) = 5.96 \cdot A^{CSP} \tag{3.61}$$

$$Water\ usage\ (m^3\ year^{-1}) = 0.07 \cdot A^{CSP} \tag{3.62}$$

$$O\&M_{\text{CSP, fixed}} = 66\ USD\ kW^{-1} year^{-1} \tag{3.63}$$

$$O\&M_{\text{CSP, variable}} = 3.5\ USD\ MWh^{-1} \tag{3.64}$$

Investment costs: Photovoltaic power plant

The investment and operational cost of the solar PV plant were obtained using the modelling tools presented in SAM (NREL, 2018). The direct investment costs (direct costs) are calculated by adding the direct cost of the PV modules, inverters, balance of system (BoS), installation and contingency, according to:

$$IC_{direct\ costs} = IC_{PV\ modules} + IC_{inverters} + IC_{BoS} + IC_{installation} \tag{3.65}$$

According SAM, these costs (in thousands of USD) can be approximated based on the capacity of the PV plant (PV^{dc}, in kW_{dc}), according to:

$$IC_{PV\ modules} = 0.35 \cdot PV^{dc} \tag{3.66}$$

$$IC_{inverters} = 0.1 \cdot PV^{dc} \tag{3.67}$$

$$IC_{BoS} = 0.3 \cdot PV^{dc} \tag{3.68}$$

$$IC_{installation} = 0.84 \cdot PV^{dc} \tag{3.69}$$

In the case that the area of the PV plant is defined as a variable in the optimisation, the power capacity of the PV plant (in kW_{dc}) can be estimated using the data presented in Table 3.2 and the following relations:

$$PV^{dc}(kW_{dc}) = \frac{A^{PV}(m^2) \cdot P^{max\ module}(kW_{dc})}{A^{module}(m^2)} \tag{3.70}$$

If the power capacity of the PV plant (PV^{ac} in kW_{ac}) is defined as a variable, the power capacity in kW_{dc} can be estimated by:

$$PV^{dc}(kW_{dc}) = \frac{PV^{ac}}{PV^{\text{DC to AC ratio}}} \tag{3.71}$$

where the $PV^{\text{DC to AC ratio}}$ is defined in this study as 1.2 (NREL, 2018). Finally, the land use and operational and maintenance cost are given by:

$$Land\ use_{\text{PV}}\ (m^2) = 3.3 \cdot A^{PV} \tag{3.72}$$

$$O\&M_{\text{PV, fixed}} = 13\ USD\ kW^{-1} year^{-1} \tag{3.73}$$

Investment costs: Molten salts sensible thermal energy storage system

- The investment cost, in thousands of USD, of the thermal energy storage system (two-tanks molten salts), as a function of the capacity of storage (STO^{TES}, in MWh_t)) can be estimated by (NREL, 2018):

$$IC_{TES} = 22 \cdot STO^{TES} \tag{3.74}$$

- Then, the power block and balance of plant (BoP) costs (in thousands of USD), as a function of the power block capacity (P^{ST}, in MW) are defined by NREL (2018) as:

$$IC_{PB} = 1040 \cdot P^{ST} \tag{3.75}$$

$$IC_{BoP} = 290 \cdot P^{ST} \tag{3.76}$$

Investment costs: Calcium-looping thermochemical energy storage system

In the case of the CSP with TCES, the investment cost of the solar tower (in thousands of USD) was incremented by 10% to consider the installation and connections of the calciner located inside the receiver chamber.

$$IC_{\text{heliostats field \& tower}} = (0.175 \cdot A^{CSP} + 3460) \cdot 1.1 \tag{3.77}$$

$$\tag{3.78}$$

Other costs associated to the CSP plant are the same than described in the case of CSP with TES (land use, water usage, and operational and maintenance costs). Then, the cost of the thermochemical energy storage system is defined by the following components:

- Calciner, as a function of the thermal capacity of the reactor (Michalski *et al.*, 2019):

$$IC_{Calciner} = (13140 \cdot Q_{calc}^{0.67} \cdot 10^{-6}) \cdot r_{exch} \tag{3.79}$$

- Carbonator, as a function of the thermal capacity of the reactor (Michalski *et al.*, 2019)

$$IC_{Carbonator} = (16591 \cdot Q_{carb}^{0.67} \cdot 10^{-6}) \cdot r_{exch} \tag{3.80}$$

- Heat exchangers, as a function of the total exchange area and the working pressure (Michalski *et al.*, 2019):

$$IC_{HX} = (2546.9 \cdot A_{HE}^{0.67} \cdot P_{HE}^{0.28} \cdot 10^{-6}) \cdot r_{exch} \tag{3.81}$$

- Cooling towers, as a function of its cooling capacity (Michalski *et al.*, 2019)

$$IC_{CT} = (32.3 \cdot Q_{cool} \cdot 10^{-3}) \cdot r_{exch} \tag{3.82}$$

- CO_2 compressors & turbines, as a function of the power capacity (Carlson *et al.*, 2017):

$$IC_{Compressor} = 7331 \cdot W_{comp}^{0.7865} \tag{3.83}$$

$$IC_{Turbine} = 8279 \cdot W_{turb}^{0.6842} \tag{3.84}$$

- The investment cost of CO_2 storage tank, is calculated by using the relations presented by Bayon *et al.* (2018):

$$V_{material} = \pi(d_{out}^2 - d_{in}^2) \cdot (l_{out} + s \cdot \delta_{vessel}) + \frac{1}{6}\pi(d_{out}^3 - d_{in}^3) \tag{3.85}$$

$$\delta_{vessel} = \frac{P_{design} \cdot {}^{d_{in}}/_{2}}{2SE - 0.2P_{design}} \tag{3.86}$$

$$l_{in} = \sqrt[3]{\frac{V_{storage}}{\pi(\frac{0.22}{2})^2 + \frac{4}{3}\pi(\frac{0.22}{2})^3}} \tag{3.87}$$

$$d_{in} = 0.22 \cdot l_{in} \tag{3.88}$$

$$l_{out} = l_{in} + 2\cdot \tag{3.89}$$

where P_{design} is the design pressure (75 bar), S is the allowance stress defined as 90% of the yield stress (Y). The material suggested by Bayon *et al.* (2018) is SSCrMo (chromium molybdenum steel), with Y =962 MPa (Health and Safety Executive, 1992). Besides, E is the joint efficiency defined as 0.9 by Bayon *et al.* (2018), and a safety factor of 1.5 is suggested. The unitary cost of the materials used are given in table 3.6 (Jonemann, 2013).

- The solid-particle storage tank cost is estimated by using the relations presented by Bayon *et al.* (2018). Here the total cost is the cost of the fire brick (brick), carbon steel (steel), ceramic insulation (ins) and concrete foundations (concrete), according to:

$$V_{steel} = \frac{\pi}{4}(d_{steel}^2 - d_{ins}^2) \cdot H_{ins} + \frac{\pi}{6}(d_{steel}^2 - d_{ins}^2) \cdot H_{elip} \tag{3.90}$$

$$V_{ins} = \frac{\pi}{4}(d_{ins}^2 - d_{brick}^2) \cdot H_{brick} + \frac{\pi}{4} d_{ins}^2 \delta_{ins,bot} + \frac{\pi}{4} d_{ins}^2 \delta_{ins,top} \tag{3.91}$$

$$V_{brick} = \frac{\pi}{4}(d_{brick}^2 - d_{material}^2) \cdot 1.2 H_{material} + \frac{\pi}{2} d_{brick}^2 \delta_{brick} \tag{3.92}$$

$$V_{concrete} = \frac{\pi}{4} d_{concrete}^2 \delta_{concrete} \tag{3.93}$$

$$d_{material} = 2.714 \cdot H_{material} \tag{3.94}$$

$$\delta_{steel} = 0.00133 \cdot H_{material} \tag{3.95}$$

$$H_{elip} = 0.25 \cdot H_{steel} \tag{3.96}$$

$$H_{material} = \sqrt[3]{\frac{V_{storage}}{\pi \cdot 1.357^2}} \tag{3.97}$$

Typical insulation thickness (for a heat flux in the order of 150 $W \cdot m^{-2}$) are estimated by Jonemann (2013):

$$\delta_{\text{refractory, brick}} = 17.5\ in \tag{3.98}$$

$$\delta_{\text{ceramic, blanket}} = 12\ in \tag{3.99}$$

Finally, the unitary prices are given by Jonemann (2013) and shown in table 3.6

Table 3.6: Unitary cost of materials to estimate investment cost of storage tank

material	unit cost $USD \cdot ton^{-1}$	density $ton \cdot m^{-3}$
Stainless steel	3,000	8.03
Carbon steel	800	7.75
Refractory brick	2,000	4.315
Ceramic insulation	1,500	0.128

Contingency and indirect capital costs

The following values were considered for all case studies, according to financial estimations from SAM (NREL, 2018): (i) Contingency = 7%; (ii) Land cost = 25 $USD \cdot m^{-2}$; (iii) EPC (engineering, procurement and construction) cost = 13%; (iv) Balance of plant = 10% (to include all other components and auxiliary systems). (v) Sales taxes basis: 80% of direct costs and sales tax rate 5%.

3.7 Implementation

In summary, the number of variables of the design optimisation depends on the case study that will be described in details in the next chapters. The genetic algorithm (GA) method will be used to optimise the three objectives, producing several solutions in a three-dimensional space which form a Pareto surface. As can be seen in Figure 3.11, GA starts with an initial population, where each individual represents a power plant with given capacities. Then, each design in the population is optimised by using the operational optimisation by linear programming to find the best strategy to operate.

For the present research, a model written in Python was developed to optimise the design optimisation of the hybrid solar power plant with energy storage. DEAP (Distributed evolutionary Algorithms in Python) was employed inside the code to carry out the genetic algorithm routine (Fortin *et al.*, 2012). Here, the fitness evaluation of each individual is performed by solving the operational optimisation stage using Pyomo (Hart *et al.*, 2017) with Gurobi as solver (Gurobi Optimization, 2019). In addition, real solar irradiation data is used as input, and it can be easily modified to evaluate any location. In summary, the hardware and software used to solve the two-stage multi-objective optimisation framework presented in this chapter are reported below:

- PC: Intel Core i7-6700 CPU @ 3.4 GHz, 16 GB RAM.
- Operating system: 64-bits Windows 10 Education.
- Programming language: Python 3.5.3 (Python Software Foundation, 2017).
- Optimisation packages: Pyomo 5.6.1 (Hart *et al.*, 2017, 2011), DEAP 1.3.0 (Fortin *et al.*, 2012)
- Solver: Gurobi 8.1.1 (Gurobi Optimization, 2019)

3.8 Uncertainties, model limitations and advantages

Simulations of the energy system presented in this research will unavoidably give forecasts that deviate from a real operation. These differences result from the limitations of the model to correctly simulate a real system. These uncertainties can be listed into three groups:

- Model uncertainty. When using mathematical approximations to simulate a system and simplifications to make the problem flexible and tractable from a computational perspective. In this research, an example of a model error is the use of linear or bilinear efficiencies in the power block, and not consider the turbine-generation operation under full or part load.
- Numerical uncertainty. To solve the mathematical optimisations and simulations, the equations were discretised and resolved in time steps. This approximation of a continuous function using a discrete approximation can be improved by using higher resolutions or time steps in the input data (e.g. 15 min instead of 60 min), which increase the computational time.

- Data uncertainty. To evaluate the performance of the solar power plant integrated with energy storage, different locations were considered. The mathematical model requires input data such as solar irradiation, cost of components, technical parameters, etc. In the present research, these parameters were collected using different sources such as technical reports and scientific publications. Depending on the case study, difficulties in the acquisition of such parameters can be found. For instance, information on the technology readiness level in the location depends on the experience that a particular site has in developing such systems. In this context, Atacama-1 is the first large scale concentrating solar power plant in South America; hence, the investment costs and operational costs were difficult to estimate. The other essential input data that has a considerable impact in the uncertainty of the results is the typical meteorological year used to estimate the long-term operation of the solar plant. The typical meteorological year (TMY) is highly accepted and used by the scientific community to assess a proposed solar power plant's probable annual performance for a specific location. TMY selects individual historic months to represent climate conditions for a location. Nevertheless, TMY usually exclude extreme conditions. In order to solve this problem, some researchers suggest combining the use of the TMY to represent typical conditions with an extreme meteorological year data set to capture a range of power plant performance. A similar approach, by estimating the performance of a power plant during the 12 years is shown in Figure 9. The details of this case study is included in section 5.3 in the thesis document.

To evaluate these three types of uncertainty, sensitivity analyses are performed to assess the power plant's financial and technical performance indicators by changing the value of different input parameters. In addition, long-time evaluations are performed to analyse worst-case scenarios when analysing a small number of designs.

The main objective of this research is to optimise the annual performance of a hybrid solar power plant with energy storage, taking into account the daily and seasonal variability of the solar resource. Then, the model employed a typical meteorological year with hourly resolution (8760 time steps). In the next sections, mass and energy balances are modelled by using non-linear equations. Nevertheless, the computational cost by using non-linear formulation is excessively high; then, the operational optimisation routine could become a computational bottleneck when considering complex systems. Therefore, nonlinearities were reformulated as linear constraints in the design of the mathematical programming problems. In the CSP-TCES model, in order to linearize the non-linear equations that simulates the mass and energy balances of each process, the temperatures of the processes are fixed, according to the parameters and results published, were non-linear models are used to simulate the operation of the CSP plant with TCES. In a power plant, this may be possible by the instrumentation engineering, through the definition and control of the temperatures of each process. Hence, the operational optimisation routine optimises the mass flow rate of some streams and calculate those that are

dependent (because there are direct relationships between some streams) in order to optimise the hourly operation. Consequently, this model exploits the capacity of linear programming to optimise the annual performance of the power plant, taking into account the daily and seasonal variability or the renewable resource, giving a sufficiently accurate solution with significantly faster computational time compared with non-linear formulation.

In addition to decrease the computational time compared with non-linear models, crucial to optimise the annual performance with hourly time steps, other advantages of the model developed in this research compared with available tools can be listed by:

- The model can integrate different energy conversion and energy storage technologies.
- The model can optimise the power operation of the power plant under different objectives that can be easily defined.
- The model can consider any time step and data horizon. For instance, 10 min time steps, 25 years of input data, etc. Moreover, in the case that an in-depth analysis is required to address the impact of climate change in the operation of solar power technologies, different scenarios can be created and used as input data. Then, the model results can give a set of opportunities for adaptation by designing a more resilient power network.
- The model can be easily modified to consider annual changes in input parameters that depend on the technology readiness level and location. These parameters can be related with efficiencies, investment costs of different components (heliostat field, tower, receiver, photovoltaic modules, inverters, thermal energy storage, chemical reactors, turbines, compressors, and heat exchangers), contingencies, discount rates, taxes, price of land, annual degradation rate, operational and maintenance costs, etc.
- The model, written in python, can be integrated with machine learning tools that would give substantial advantages, like data clustering, emulators, big data analyses, neural network and deep learning, etc.

Chapter 4

Atacama-1: Improvement of a hybrid solar power plant with thermal energy storage

The work presented in this chapter is based on an article published in the Journal Solar Energy (Bravo and Friedrich, 2018)

4.1 Introduction

In this chapter, the two-stage optimisation framework presented in Chapter 3 is applied for the optimal design of a hybrid solar power plant with thermal energy storage. Here, the integration of a two-tank molten salt technology as a sensible heat thermal energy storage system is studied. The operational optimisation is performed by linear programming, and the automated linear scalarisation method is analysed in order to develop guidelines for future applications. The dispatchability and affordability of the system are studied, and the trade-off between financial and technical performance is analysed. The optimisation framework is applied to analyse and improve the design of a power plant under construction in Northern Chile, known as Atacama-1 or Cerro Dominador solar power plant. Through the analysis of the results presented, it is demonstrated that balancing the trade-off between financial and technical performance is crucial to increase the affordability of solar technologies. Moreover, the direct link between the objectives of the design and operational optimisation routines is crucial to exploit the synergies of technology integration.

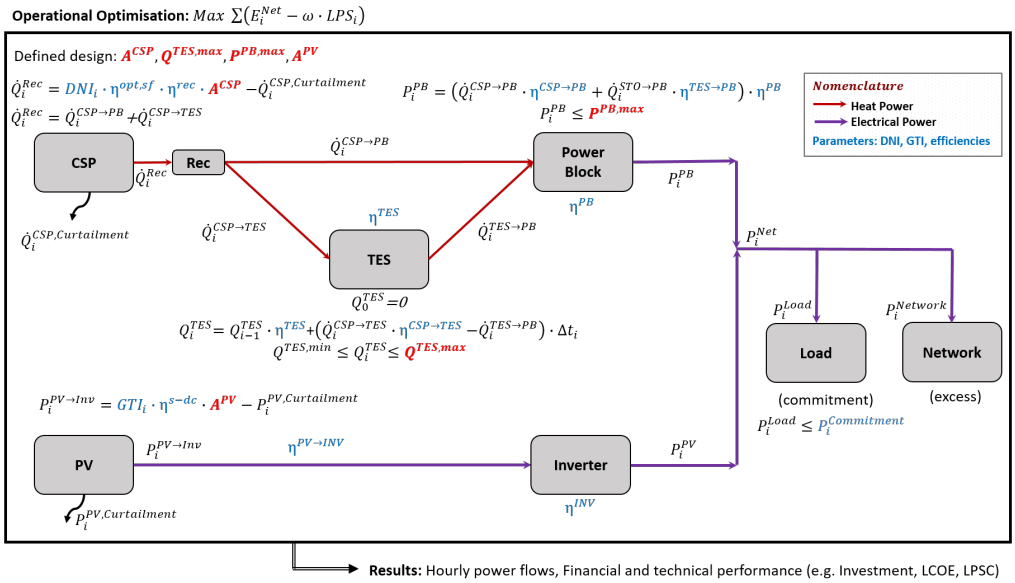

Figure 4.1: Power flow model of Atacama-1 hybrid solar power plant

4.2 Plant modelling

In order to simulate and optimise the operation of the hybrid solar power plant, the application of the energy system analysis presented in Chapter 3 is carried out. The power flow model used to analyse the operation of the power plant is shown in Figure 4.1. This figure illustrates the power flows between subsystems with solid lines, which are the variables of the operational optimisation. In addition, with red letters, the capacities of the mains components are shown, that correspond to the variables of the design optimisation.

The power flow model exposes the processes involved in the operation of the hybrid power plant in terms of power flows, energy balances, energy losses, and capacities of components. In the power flow model, every block is one of the main subsystems of the power plant: solar field of the CSP, thermal energy storage system, power block (PB), PV power plant, inverter, and network. Every line that connects two subsystems represents heat or electricity transfer. Constraints are related to the capacities of different subsystems or components. The following heat flows $\dot{Q}_i^{CSP\mapsto PB}$ (heat flow from the receiver to the power block); $\dot{Q}_i^{CSP\mapsto TES}$ (heat flow from the receiver to the thermal energy storage system); $\dot{Q}_i^{TES\mapsto PB}$ (heat flow from the thermal energy storage system to the power block), are optimisation variables which are optimised concerning the objectives of the operational optimisation. Energy balances calculate other variables like the amount of curtailed energy, thermal losses and the energy dispatched by the PV power plant according to the results of the optimisation. The variables of the design optimisation are the capacities of four subsystems: solar field area of the CSP (A^{CSP}), the capacity of the storage system ($Q^{TES,max}$), capacity of the power block $P^{PB,max}$, and solar PV area (A^{PV}), which are

shown with red letters in the figure. The model focuses to supply energy to a given commitment; moreover, the excess of generation has no penalty and can be delivered to the network. Finally, parameters are given by blue letters, and these are associated with:

- DNI data of the location.
- GTI data of the location for a defined slope.
- The efficiencies of each component.
- Demand that the power plants should dispatch: P_i^{demand} (in order to calculate LPS_i).
- Operational and local limits, e.g., capacity of the network.

The power flow model is used in the operation optimisation and nested in the design optimisation of the hybrid solar power plant. The optimal plant is reached by selecting the best sizes of each subsystem, i.e. solar field area, thermal energy storage, power block, and a photovoltaic array. Therefore, the two-stage optimisation model simultaneously optimises the operation and the design of the hybrid solar power plant. A schematic of the framework is shown in Figure 3.11.

4.2.1 Operational optimisation

The operational optimisation aims to find the specific operation at each time step that enhances the performance of a hybrid solar power plant for a given design. As shown in Figure 4.1, the results of the operational optimisation are related to power flows. Then, different financial and technical indicators can be calculated. In order to link financial performance in the design optimisation, the operational optimisation aims to maximise the energy supplied (to minimise the LCOE), and to minimise the loss of power supply. Hence, the objectives of the operational optimisation are:

$$Max \sum E_i^{Net} \tag{4.1}$$

$$Min \sum LPS_i \tag{4.2}$$

The one-year, hourly operational optimisation is performed by linear programming due to the large number of optimisation variables, i.e. 8760 optimisation variables for each connection shown in Figure 4.1. Moreover, in order to handle both objectives, the automated scalarisation method presented in Chapter 3 is applied.

4.2.2 Design plus operational optimisation

The aim of the design optimisation, defined as a two-stage optimisation problem, is to have the best or a range of designs of hybrid solar power plants that optimise the pursued objectives. The design optimisation needs to simultaneously optimise the operation of each candidate and focus on the selection of the best designs. This process is done by the operational optimisation described above, and its results are the input data to select the best range of designs. In other words, the operation of each configuration of the design optimisation is optimised by the operational optimisation.

Depending on the number of objectives, the design plus operational optimisation can be modelled as single or multi-objective optimisation. While the single objective optimisation gives the best design that optimises the objective; the multi-objective optimisation reaches a range of non-dominated or Pareto optimal solutions, which represent the best design showing the trade-off between objectives. Therefore, every point on the Pareto frontier is valuable and a potential candidate and a-posteriori process to select the best design regarding the desired target has to be done by the user of the model.

Objectives

The objectives of the design optimisation can be related to technical (described for the operational optimisation), financial, environmental or societal performance metrics. Because the present model is a numerical approximation of the best design, each objective should be quantitative. This study is focused on minimising the financial costs and maximising the dispatchability of the power plant, according to:

- Minimisation of Investment cost.
- Minimisation of LCOE.
- Minimisation of LPSC, i.e. maximise dispatchability.

Decision Variables

The decision variables of the design optimisation are:

- Solar field area of CSP plant: A^{CSP}, m^2.
- Storage capacity: $Q^{\mathrm{STO,max}}$, MWh.
- Power block capacity: $P^{\mathrm{PB,max}}$, MW.
- Solar PV area: A^{PV}, m^2.

Some of these variables are related to each other under the following indicators, which can be crucial to understand and define guidelines for optimised plants:

- SM, Solar multiple. Defined as the relation between the design capacity of the solar field and the power block (Denholm *et al.*, 2015b).

- StH, hours of storage. Is the ratio between the total capacity of the storage system (MWh) and the power block capacity (MW).

4.3 Case study

In order to set a case study, the Atacama Desert will be considered. This arid region which covers around 300,000 km^2 is located in Northern Chile. It is one of the sunniest places on Earth (Cordero *et al.*, 2016), wherein a typical year, the annual Direct Normal Irradiation (DNI) is near or more than 3,500 $kWh \cdot m^{-2}$ (Ministry of Energy - University of Chile, 2016; Parrado *et al.*, 2016b). This zone contains 23 of the 30 largest copper mines of the Chilean copper industry (Mining Council Chile, 2015), which produce approximately 73% of the copper in Chile. This Chilean industry contributes more than 30% of the total copper production of the world (Northey *et al.*, 2013). The copper industry is a continuous and energy-intensive process, in fact, during 2015, Chilean copper mines used around 23,600 GWh of electricity and additionally around 2,700 GWh of fossil fuel was burned for low-temperature heating operations mainly in copper refining and hydrometallurgical processes (Comisión Chilena del Cobre, 2016). Because the mining industry leads the electricity consumption in Northern Chile, the demand is quite flat, with no significant variations between day and night. Hence, the Northern Chile electricity market needs to supply a steady energy demand 24 hours and seven days per week. Regarding the Chilean Centre for Economic Load Dispatch (CDEC) of the Northern Interconnected System (SING), 75.4% of the electricity generated during 2015 was generated in coal-fueled power plants, 21% from other fossil-fuelled power plants (Natural gas, Diesel, Fuel Oil), and just 3.6% from renewable resources (solar, wind, hydro) (CDEC-SING, 2015). According to these numbers, the Chilean Ministry of Energy reported that the carbon intensity of SING in 2015 was 0.764 $tCO_{2eq} \cdot MWh^{-1}$ (Ministry of Energy - Chilean Government, 2017). On the other hand, one of the biggest challenges of the Chilean mining industry is to get economical, reliable, and sustainable energy resources, as well as the efficient use of them (Mining Council Chile, 2015). To apply and prove the model, the Atacama-1 or Cerro Dominador Solar Power Plant, a hybrid solar power plant under construction in the Atacama Desert in Chile has been studied. Regarding the published information by the engineering and construction company (Abengoa Solar, 2016) and by the Chilean Ministry of Environment (Servicio de Evaluación Ambiental, 2014), some features of the project are:

- **Location:** Antofagasta Region, Chile $\approx$ S 22° W 69°
- **CSP Plant**
  - Heliostats: 10,600 $\approx 148.4 \cdot 10^4 m^2$
  - StH: 17.5 h
  - Power Block Capacity: 110 MW
- **PV Plant:** Capacity: 100 MW

- **GHG emissions avoided:** 870,000 $tCO_{2eq}\cdot$ $year^{-1}$
- **Total Investment:** between 1,300 and 1,500 MUSD

4.3.1 Solar irradiation, data quality control and preparation

The DNI and the GTI (for a panel slope $\approx$ latitude) data in the location of the project was obtained from the Chilean Ministry of Energy and University of Chile solar resource data centre (Ministry of Energy - University of Chile, 2016). This open-source information includes weather and irradiation data of the Chilean territory.

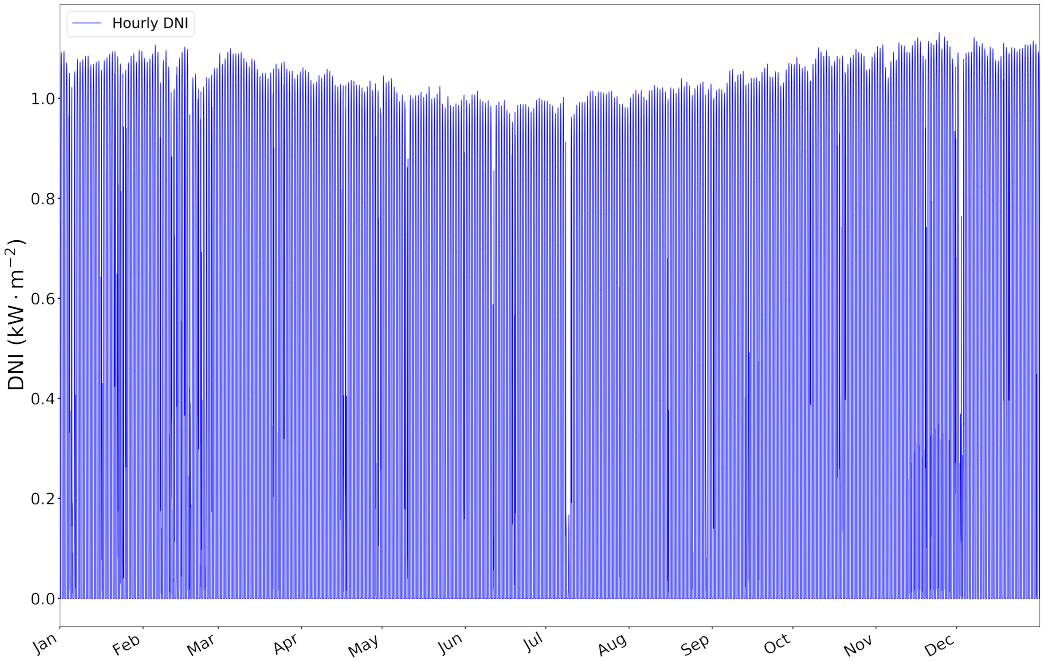

Figure 4.2: Typical meteorological year, Direct normal irradiation, hourly time-steps at the Atacama-1 location

Figure 4.2 shows the direct normal irradiation with hourly resolution, of the typical meteorological year in the location under analysis. It is important to note that all simulations and optimisations carried out in this research use the typical meteorological year with hourly time-steps. To present the same data in a more comprehensible perspective, Figure 4.3 shows the 1-day and 2-day moving average, and the annual average for the DNI. In both cases, the 5^{th} percentile is around 330 W·m^{-2}, this means that 95% of the time the DNI is at least 330 W·m^{-2}, in other words, the daily DNI has no considerable variation during the year. The present study considers the typical meteorological year, hence, the results represent the long time performance of the project. Nevertheless, the irradiation variability in the Atacama Desert is influenced by El Niño-Southern Oscillation (ENSO). While La Niña (occurring at irregular intervals of around six years) has a high correlation with high precipitations during summer (Dec-Jan-Feb-March) of the Southern Hemisphere in the Atacama Desert, high rainfalls during

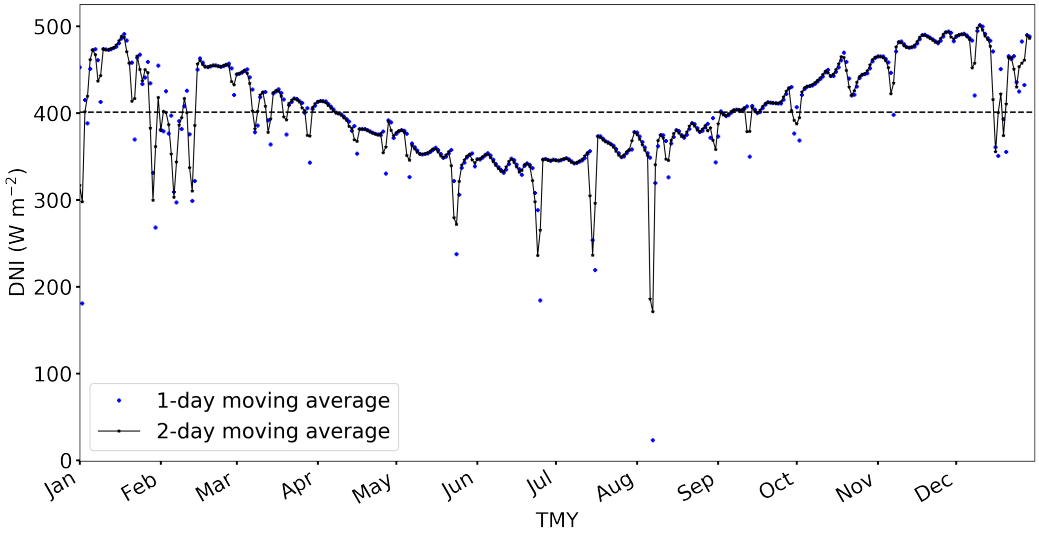

Figure 4.3: Moving average of the solar irradiation for the typical meteorological year at the Atacama-1 location

winter are associated with El Niño (Houston, 2006). These phenomena will result in years with solar irradiation significantly different from TMY. This effects should be analysed in further research.

4.3.2 Solar power plant simulation conditions

As explained previously, technical and financial information of solar power plants in operation and under construction is necessary as input to the model. The System Advisor Model (SAM) (NREL, 2018) was used to get financial (unitary costs) and technical (efficiencies) data. The investment cost is calculated by scaling the unitary cost detailed in Chapter 3 (section 3.6.3) of the components of the CSP and the PV power plants, e.g. USD·m^{-2} for the solar field, USD·MWh^{-1} for the thermal energy storage system, USD·MW^{-1} for the power block.

According to the solar irradiation, for around 70% of the total annual daytime hours the DNI is higher than 800 Wh·m^{-2}. Moreover, the operational optimisation is focused on maximising the use of the power plant. Hence the power block will work near full capacity most of the time. For these reasons, and in order to simplify the model, the efficiencies used for each subsystem are constant for every hour and every design and are shown in Table 4.1. These efficiencies are used to estimate the sizes of the components and the operational performance of the system. In order to validate the model, results of the model were compared with both, the System Advisor Model and information published by the IEA in the report: Projected Cost of Generating Electricity 2015 edition (IEA *et al.*, 2015).

Table 4.1: Parameters used in the power flow model of the hybrid solar power plant with two-tanks energy molten salts energy storage system

CSP Plant			PV Plant		
Description	Name	Value	Description	Name	Value
Solar field eff.	$\eta^{\text{solar field}}$	0.487	PV array efficiency	η^{PV}	0.192
Pipelines thermal eff.	$\eta^{\text{pipelines}}$	0.99	PV mod. to inverter eff.	$\eta^{PV \rightarrow inv}$	0.85
TES eff.	η^{TES}	0.99	Inverter to network eff.	$\eta^{inv \rightarrow netw}$	0.973
Power block eff.	η^{PB}	0.371			

4.3.3 Validation of simulation results

In order to validate the model, the configuration of Atacama-1 was simulated using SAM, and compared with the result of achieved by the python model. As can be seen in the table, the results indicate that differences between the values obtained through the Python and SAM models are in the order of 1% and lower.

Table 4.2: Validation with SAM (NREL)

System	Variable	Unit	Python model	SAM model
Solar tower + Molten salt energy storage	Energy	$GWh/year$	863.9	864.3
	CF	%	89.8	89.7
Photovoltaic plant	Energy	$GWh/year$	258.7	261.4
	CF	%	22.2	22.4

4.3.4 Operational optimisation methodology

Table 4.3: Single and multi-objective operational optimisation results for Atacama-1

		CSP	PV	Hybrid		
				$Max\{E^{Net}\}$	$Min\{\text{LPSC}\}$	Automated
KPI	unit					Scalarisation
E^{Net}	GWh·year^{-1}	864.3	261.4	1,125.7	953.8	1,109
LPSC	GWh·year^{-1}	99.3	615.9	97.5	9.8	9.9
LPSP	%	10.30	72.30	10.12	1.016	1.02
CF_{CSP}	%	89.69	-	89.69	71.85	87.98
CF_{PV}	%	-	27.12	27.12	27.12	27.12
Investment	MUSD	1,192	262	1,455	1,455	1,455
LCOE	USD·MWh^{-1}	132.06	92.40	122.85	144.04	124,60

The operational optimisation model was applied to Atacama-1 and run a series of times to compare different operational strategies, as shown in Table 4.3. First, the CSP and PV plants were optimised independently. Hence, the values shown in the columns "CSP" and "PV" represent the multi-objective optimisation by the application of the method to single technologies.

When analysing the CSP plant, the commitment was defined as constant and equal to 110 MW, which corresponds to the maximum capacity of the power block. Hence, 110 MW is the power that can be dispatched during hours with no solar irradiation. In the case of the PV plant of Atacama-1, a constant supply of 100 MW, which is the maximum capacity of the plant, was defined as a constant commitment. These results are shown in the columns CSP and PV in Table 4.3. The results indicate that a CSP with TES has a higher LCOE but lower LPSC than a PV plant (due to the ability of the CSP to store energy during the day and to dispatch power during the night). The values show that the maximum energy dispatched is 864 GWh·year^{-1} and the minimum LPSP is 10.3 %, both achieved by the use of an expensive CSP with energy storage. On the contrary, the PV plant, with considerable lower investment, reaches an LCOE of 92.4 USD·MWh^{-1} compared to 132.06 USD·MWh^{-1} for the CSP plant. By the combination of these two solar power plants, the synergy of technology integration could be exploited, meaning an improvement on both financial and technical performances. Consequently, a decrease in both LCOE and LPSC is expected by the hybridisation.

Then, the hybrid solar power plant was studied under single and multi-objective operational optimisation. In this case, the model was run twice with two different objectives: $Max\{E^{Net}\}$ and $Min\{\text{LPSC}\}$. Nevertheless, as previously explained, the objectives defined in the model depend on the goal pursued by the user of the model and can be easily modified. The objectives can be focused on a financial perspective by selling the maximum quantity of energy, thus, reaching the lowest LCOE, and on a technical perspective, e.g. a firm electricity supply.

In order to estimate the dispatchability of the hybrid solar power plant, the commitment was defined fixed and constant at every hour and equal to the maximum capacity of the CSP power plant (110 MW), this because unlike PV, CSP with TES can deliver energy during the night. Results summarised in table 4.3 shown that both methods: $Max\{E^{Net}\}$ and $Min\{\text{LPSC}\}$ get different results.

First, the $Max\{E^{Net}\}$ method achieves the highest total energy generated (1,125.7 GWh·year^{-1}), consequently, the minimum LCOE, but the LPSP is high (10.12 %). Second, the $Min\{\text{LPSC}\}$ results in a very low value in both LPSP (1.016 %), and E^{Net} (953.8 GWh·year^{-1}), hence, a higher LCOE. Consequently, the hybridisation of the power plant can improve the performance of solar technologies. However, the right operational strategy of the hybrid solar power plant is essential in order to simultaneously maximise the energy delivered to the network (which influences the LCOE) and minimise the LPSC. Therefore, the next step is to find the best operational strategy under a multi-objective optimisation.

The two techniques described in Section 3.5.5 to solve multi-objective optimisation problems in linear programming are analysed here. In the scalarisation method, the multi-objective optimisation problem is transformed into a single objective optimisation problem by combining and weighting both objectives. While in the ε-constraint method, one objective is considered as a constraint in the formulation of the optimisation problem. The challenge here is to define

a proper value of the scaling or constraint.

Scalarisation method

As described in Chapter 3, the following function represents the new single objective optimisation problem:

$$\text{maximise} \sum_{i=1}^{I} \{P_i^{Net} - \omega \cdot LPS_i\} \tag{4.3}$$

where the positive parameter ω is the scaling factor applied to the second objective. Regarding the results shown in Table 4.3, the scaling factor that balances the second objective (LPS_i) with respect to the first one (P_i^{gen}) can be approximated by

$$\frac{E_{max}^{Net} - E_{min}^{Net}}{\text{LPSC}_{max} - \text{LPSC}_{min}} = \frac{1,125.5 - 953.8}{97.5 - 9.8} = 1.96 \tag{4.4}$$

Then, in order to build the Pareto frontier, and compare the solutions of this method with the previous results of the single objective optimisations, ω was evaluated in the range $\omega \in [0, 100]$, which is large enough to cover the range between the two single objective optimisations. The Pareto frontier generated from this method is presented in Figure 4.4 and some solutions are shown in Table 4.4.

Table 4.4: Multi-objective linear optimisation results of ε constraint and linear scalarisation methods

ε constraint method		Linear scalarisation method		
ε: LPSC GWh	Objective: E^{Net} GWh	ω -	1^{st} Obj: E^{Net} GWh	2^{nd} Obj: LPSC GWh
97.5	1125.7	0	1125.7	97.5
88.1	1124.6	0.1	1125.6	96.4
78.3	1123.2	0.2	1115.3	32.9
68.5	1121.7	0.4	1110.2	11.1
58.7	1120.1	0.6	1109.9	10.4
48.9	1118.4	1.0	1109.6	10.2
39.1	1116.5	1.5	1109.4	10.0
29.4	1114.5	2.0	1109.2	9.9
19.6	1112.3	5.0	1109.0	9.8
9.8	1108.1	10.0	1108.8	9.8

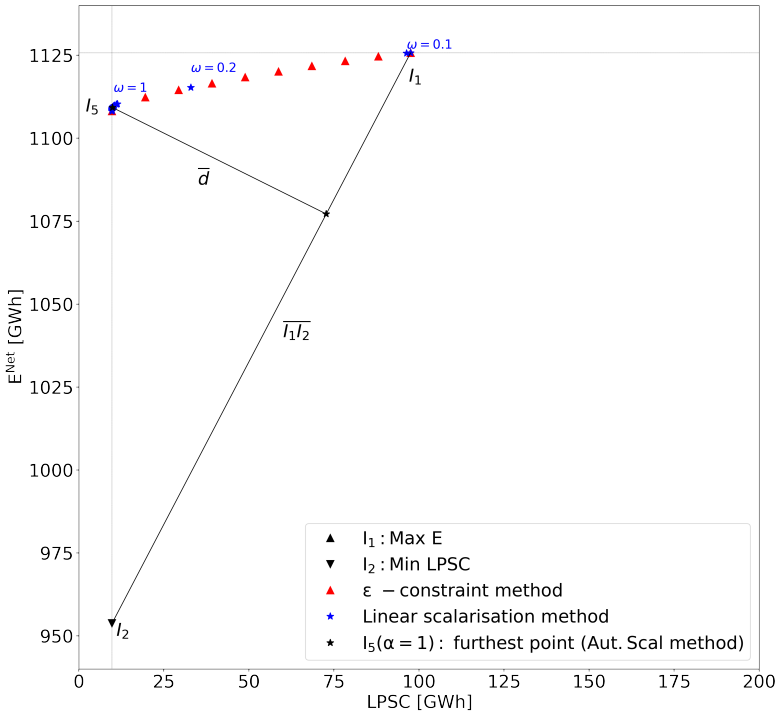

Figure 4.4: Summary of single and multi-objective optimisation methods for the optimal operation of Atacama-1

Epsilon constraint method

In this method the optimisation problem is formulated as:

$$\begin{aligned} &\text{maximise} \sum_{i=1}^{I} P_i^{Net} \\ &\text{subject to} \sum_{i=1}^{I} LPS_i \leq \varepsilon \end{aligned} \tag{4.5}$$

where ε varies between the values of the LPSC given by both previous single objective optimisations shown in Table 4.3: $\varepsilon \in [9.8, 97.5]\,\text{GWh}\cdot\text{year}^{-1}$. The Pareto optimal values generated from this method are also shown in Figure 4.4 and solution points are presented in Table 4.4. The diagram and table show that a similar Pareto frontier is achieved in both methods.

From Figure 4.4 it is possible to appreciate the behaviour of each of the four different methods studied: First, the $Max\{E^{Net}\}$ method maximises the energy delivered, getting the lowest LCOE (122.85 USD·MWh^{-1}). Nevertheless, it presents the highest LPSP 10.12%, which is not an attractive value for the reliability of the system. Second, the $Min\{\text{LPSC}\}$ method is

outside of the Pareto frontier, and it presents a very low value of the total energy delivered to the network. Consequently, the LCOE associated with this method is high and not attractive for the financial optimisation of the system. Finally, both the scalarisation and the ε-constraint methods show similar Pareto optimal solutions.

The purpose of the model is to design an affordable and dispatchable power plant. Thus, the target of the optimisation should reach the zone highlighted with an ellipse in Figure 4.4. Both the scalarisation and the ε-constraint methods, with a good definition of values of ω and ε, respectively, reach this area. Nevertheless, while the scalarisation method takes around 10 seconds to be processed, the ε-constraint takes almost 10 minutes. Hence, the next step is to apply the automated scalarisation method proposed in Chapter 3.

Automated scalarisation method

The automated scalarisation method was applied to find the best operational profile for Atacama-1. Figure 4.4 and Table 4.3 summarise the result of this technique. Figure 4.4 shows that the maximum value of the segment d was found for $\alpha = 1$. This value suggests that the relation presented in Eq. 4.4, that weights both objectives, is a simple and suitable estimation for ω.

The results of the automated scalarisation are shown in Table 4.3. These results, compared with the method in which the objective is $Max\{E^{Net}\}$ means an increase in 1.4% in the LCOE. Nevertheless, the LPSP is just 10% of the original (1.02% instead of 10.12%). As expected, comparing the CSP plant with the hybrid plant, the LCOE decreases from 139.06 to 124.6 USD·MWh^{-1} and the LPSP decreased from 10.30% to 1.02%. The improvement on both indicators confirms the synergies of technology integration for hybrid power plants.

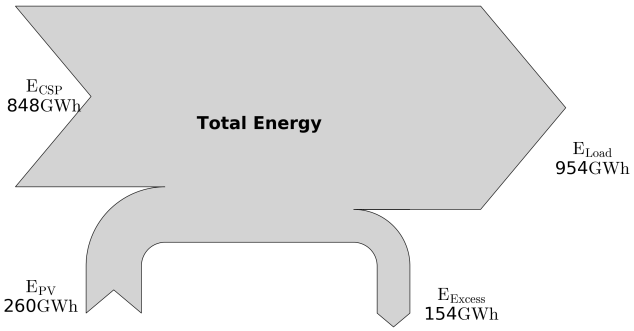

Figure 4.5: Sankey diagram of the annual energy flows

The main results of the operational optimisation are the hourly power flows, as well as losses or curtailments. For instance, Figure 4.5 shows the total flows from both technologies and the supply to the commitment as well the excess energy dispatched to the network. Figure 4.6 illustrates the state of charge (SoC) of the thermal energy storage system over one year. The

storage system of Atacama-1 has an StH of 17.5 h. This value means that when the storage is fully charged (100%), the power plant can work at full capacity for 17.5 h with no solar irradiation. However, regarding Figure 4.6, the maximum state of charge of the TES system is 83%, with a mean of 36.3%. This value suggests that the TES system of Atacama-1 may be oversized. Hence, its capacity could be reduced in order to reduce investment costs in the design stage. This idea opens the possibility to improve the design of Atacama-1.

According to the features of the thermal energy storage system (Section 3.4), there is a lower limit of temperature below that molten salts solidified. Hence, as shown in Figure 4.6, special attention has to be put on the operational control of the plant when the SoC is 0 to avoid possible solidification.

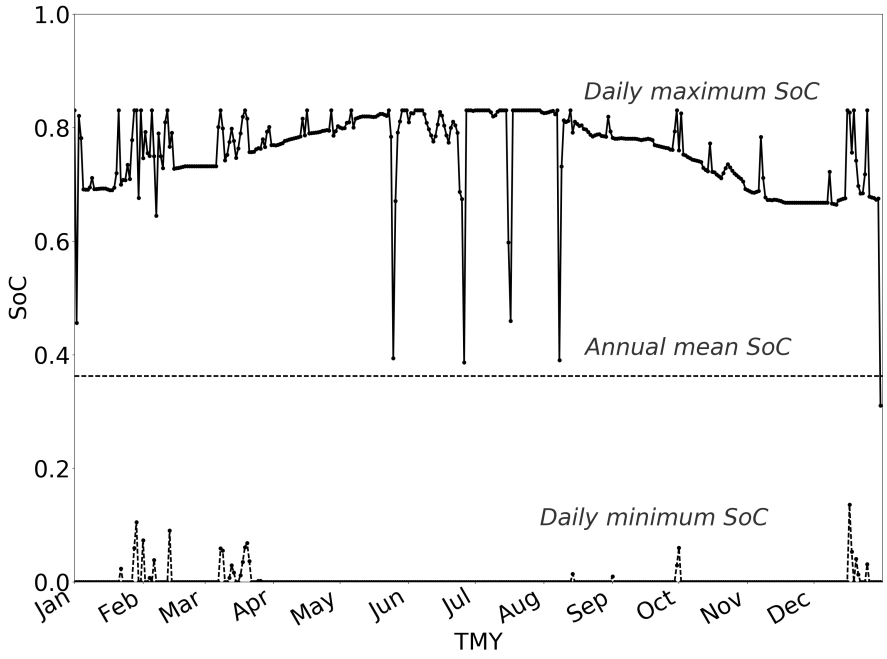

Figure 4.6: State of charge of the thermal energy storage system

4.4 Optimisation techniques implementation, results and comparison

The design optimisation method was applied and run for the same location as Atacama-1. The main purpose is to improve the design of the hybrid solar power plant. Table 4.5 summarises the elements considered in the optimisation. First, the parameters are related with the solar resource of the location, the efficiencies and unitary investment cost of the components given by data from power plants under construction and in operation, as well as other financial parameters like the lifetime and the discount rate, among others. Second, the constraints are associated with energy balances and capacities of the systems. Third, the objectives are defined as financial and technical performance metrics. Finally, the variables are the capacities of the main components of the power plant.

Table 4.5: Design optimisation model, list of parameters, constraints, objectives, and variables considered

Parameters	Constraints	Objectives	Variables
DNI	Energy balances	LCOE	A^{CSP}
GTI	Capacities	Investment	$Q^{\mathrm{STO,max}}$
Efficiencies		LPSC	$P^{\mathrm{PB,max}}$
Unitary investment costs			$A^{\mathrm{PV,max}}$

The following sections outline different strategies to handle the design optimisation. These approaches are related to the number of objectives and the number of variables. First, the number of variables considered in the optimisation can be from one variable up to four variables. When one variable is studied in the optimisation, it can be analysed as an upgrade to the existing power plant in order to improve its performance. On the other hand, four variables can be considered in order to develop a brand new power plant defined by the given parameters. Then, the number of objectives considered are crucial in the complexity of the problem. For instance, a generator company might want to increase the revenues of the existing power plant by reaching the lowest LCOE. Other users could be the market operator or a large consumer, which could be interested not just in the financial performance but in the dispatchability as well. The most complicated situation is a multi-objective optimisation, in which different conflicting objectives are pursued.

The aim of considering different approaches is to demonstrate the importance of a multi-objective optimisation method for the design of dispatchable power plants. This optimal design is crucial to support an affordable transition to a sustainable energy system.

Table 4.6: Single variable and single objective (LCOE) design optimisation results

Indicator	unit	Atac-1	CSP	Storage	PB
New value		-	$161.4 \cdot 10^4 m^2$	3503 MWh	108.3 MW
SM	-	2.59	2.82	2.59	2.63
StH	h	17.5	17.5	11.68	17.8
E^{Net}	GWh·year^{-1}	1,109	1,157	1,110	1,105
LPSC	GWh·year^{-1}	9.9	6.3	69.1	16.1
LPSP	%	1.02	0.65	7.17	1.67
CF_{CSP}	%	87.98	93.0	88.1	88.9
CF_{PV}	%	27.1	27.1	27.1	27.1
Investment	MUSD	1,455	1,513	1,381	1,450
LCOE (objective)	USD·MWh^{-1}	124.6	123.95	118.78	124.57

4.4.1 Single variable, single objective

As a first approximation, a single-variable single-objective design optimisation was developed and applied to the CSP plant of Atacama-1, in order to analyse the dispatchability of the hybrid power plant. In this case the affordability is improved by the PV plant that is fixed in the following evaluations. In this model just one of the main components is considered as a variable and the other three are considered parameters (fixed). This problem was developed as a deterministic global optimisation problem, and an improved design was reached. Table 4.6 shows the results achieved by the design optimisation focusing on the minimisation of the LCOE. Here the operation of each iteration (which correspond to a different CSP plant design) was optimised by the automated scalarisation method described previously.

Variable: Solar field area

Keeping TES, PB, and PV capacities fixed, the deterministic global optimisation was run, and an improved design was achieved. In this case, a solar field area of $161.4 \cdot 10^4 m^2$, is the optimal value. This means 930 more heliostats than the original design (11,530 instead of 10,600), hence, a larger SM. As a result, despite the investment increase, more energy can be delivered, and more energy is available during the night. Thus, both LCOE and LPSC decrease.

Variable: Thermal energy storage capacity

Holding the solar field area, the PB and the PV capacities fixed, the best design of the plant is given by a decrease of the TES capacity from 5243 MWh (StH of 17.5 h) to 3503 MWh (StH 11.7 h), achieving an LCOE of 118.78 USD·MWh^{-1}. This result agrees with the previous analysis of the state of charge of the TES system. The reduction in TES capacity directly reduces the investment costs and thus has a positive impact on the LCOE. Moreover, the lower TES capacity produces two effects: (i) a decrease in the energy losses in the storage system

(because less energy is stored), as a result more energy can be delivered (which has a positive effect on the LCOE), (ii) because less energy is available during night hours, less energy is delivered during this time (which has a negative effect on the LPSC), therefore, LPSC increases. The combination of all these interactions results in a small increase on the energy delivered during the day, a decrease in the energy available during night, and a considerable decrease on the investment, as a result, LCOE decreases and LPSC increases.

Variable: Power block capacity

It is necessary to point out that the focus of these sections is to analyse and to show the importance of considering multiple optimisation variables and objectives. Hence, the study considers the decision variable with continuous values. Then, by keeping the solar field area, TES and PV capacities fixed, the best design of the plant is reached by a power block very close to the nominal 110 MW. Hence, in the next sections the power block is fixed at 110 MW.

In summary, all the iterations of the optimisation for the three cases are shown in the sensitivity analysis in Figure 4.7, which shows the convexity of the model for single-variable and single-objective optimisation. This diagram illustrates the best options to improve the design of the project to reduce LCOE. Nevertheless, as shown in Table 4.6, while the LCOE improves, the dispatchability declines. Therefore, the development of a multi-objective optimisation technique allows us to handle this trade-off.

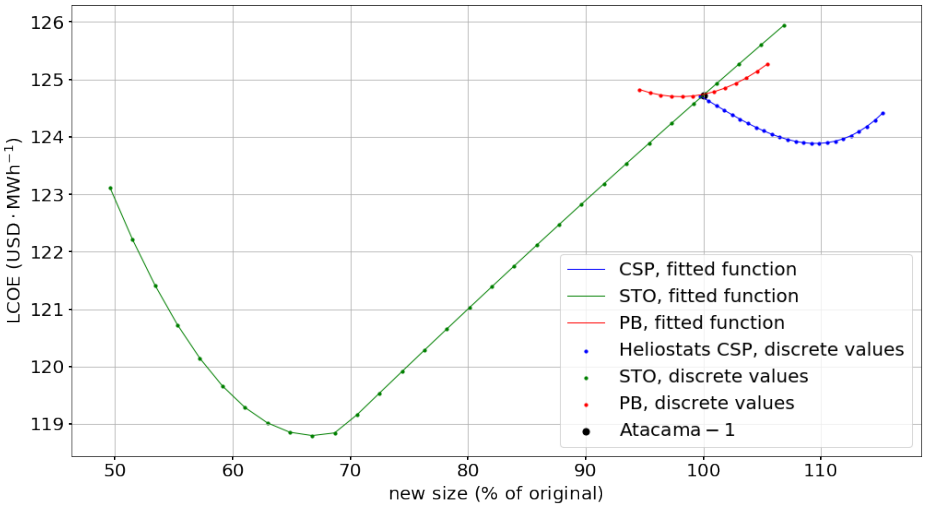

Figure 4.7: Single-variable, single-objective (LCOE) design optimisation model, discrete values

4.4.2 Multi-variable, multi-objective optimisation

The two-stage design and operational optimisation framework by genetic algorithms is applied in this section. This heuristic optimisation method applies the NSGA-II algorithm, which has been used in several multi-objective optimisation problems in energy systems (Starke *et al.*, 2018; Amusat *et al.*, 2017). The algorithm starts with a random population. In order to have a detailed first population, here 200 individuals are defined to cover a large range of combinations of the variables under analysis. In this case, three design variables, i.e. A^{CSP}, $Q^{\mathrm{STO,max}}$, and $A^{\mathrm{PV,max}}$, as shown in Table 4.5, are considered. Hence, every individual is composed of 3 variables, corresponding to a defined design. In the genetic algorithm, the total investment cost of each design is calculated. Then its optimal operational performance is achieved by applying the automated scalarisation method described previously. This technique links the LCOE and LPSC in both stages. The genetic algorithm executes the selection of the best individuals under two or three objectives: Min LCOE, Min Investment and Min LPSC. This loop repeats until the criterion is reached. Here the stopping criteria was defined as 80 generations, in order to exploit the capacity of the computer exposed in Section 3.7, during 2.5 days.

In order to calculate the dispatchability, and to get results comparable with Atacama-1, the power commitment is defined as $P_i^{\mathrm{Commitment}} = 110$ MW for all time-steps. For this reason, and because only the CSP plant can deliver energy during the night, the power block capacity was fixed and equal to the commitment, $P^{\mathrm{PB,max}} = 110$ MW.

The optimisation produces a range of different points that represent different options of the optimal design of the hybrid solar power plant and the respective performance during its lifetime (based on the TMY). Each design on this Pareto frontier represents a potential solution, and the final choice will depend on the aims of the developer.

Three variables, two objectives:

First, the design optimisation is extended with three variables (A_{CSP}, E_{max}^{STO}, P_{max}^{PV}) and two objectives (LCOE and Investment cost). Figure 4.8 shows the results of the optimisation, the Pareto frontier and the performance of Atacama-1 in order to make a quick comparison between the results. For instance, Figure 4.8 highlights two points (A and B) belonging to the non-dominated solutions. These solutions are detailed in Table 4.7, including the performance of Atacama-1. These points are related to the best performance that can be reached with similar investment or similar LCOE achieved by Atacama-1. The first point, A, shows a design with a decrease of the LCOE and Investment; nevertheless, its LPSP is 22%. The second point, B, displays that a similar LCOE can be reached with just 65% of the original investment, but the LPSP is 37%, a very high value compared with Atacama-1.

Figure 4.9 shows every design on the Pareto frontier with LPSP$<$ 30%. On the horizontal axis are shown the 4 components of the design (P_{max}^{PB}, A_{CSP}, E_{max}^{STO}, and the capacity of the PV

plant in MW P_{max}^{PV}), the two objectives of the design optimisation (LCOE, investment cost), and the LPSP which is calculated from the operational optimisation. The vertical axis shows the normalised value of the variables, where the minimum and maximum values are shown. This figure explains that the model can reach simultaneously better LCOE and Investment cost for a design similar to Atacama-1. Nevertheless, because the technical performance (represented by the LPSP) is not included in the design optimisation stage, the values of the LPSP are very high. As a consequence of these results, in order to reach better financial (LCOE, Investment) and technical (LPSP) performances, the LPSP has to be incorporated as a third objective.

Table 4.7: Three variables and two objectives (LCOE, Investment) design optimisation results

item	unit	Atac-1	A	B
A^{CSP}	ha	148.4	115.3	92.2
$Q^{STO,max}$	MWh	5243	2314	1230
$P^{PV,max}$	MW	100	164	69
SM	–	2.59	2.01	1.61
StH	h	17.5	7.72	4.1
E^{Net}	GWh·year^{-1}	1,109	1,119	742
LPSC	GWh·year^{-1}	9.9	215	363
LPSP	%	1.02	22	37
CF_{CSP}	%	87.98	71.4	58.28
CF_{PV}	%	27.1	27.1	27.1
Investment	MUSD	1,455	1,353	951
LCOE	USD·MWh^{-1}	124.6	115.9	125.3

Three variables, three objectives:

In this step, the complexity of the model is increased through a third objective. Here the aim is to examine the benefits in the integration of the dispatchability as another objective. Figure 4.10 shows the Pareto surface and the performance of Atacama-1. Here, the 3D Pareto surface is represented in a 2D diagram (LCOE, Investment), in which the third objective (LPSP) is illustrated through different ranges and symbols. Near to the centre is Atacama-1, which divides the plane into four quadrants. The crosses and the stars have a LPSP lower than Atacama-1. Therefore, any of these points located in Quadrant I have both better financial and technical performance than Atacama-1. Second, all points in Quadrant I have better financial performance than Atacama-1, but their LPSP varies between 0.65% to 3%. Third, in order to reach lower values of LPSP (shown by crosses and stars in the diagram), similar or higher investments are needed. Nevertheless, lower values of LCOE can be reached simultaneously. Fourth, while lower values of LCOE (Quadrants I and II) are possible with similar investments than Atacama-1, their LPSP can even be near 0.285%. Five of these points are summarised in Table 4.8 and shown in Figure 4.10 bounded in a circle and defined by the letters A, B, C, D and

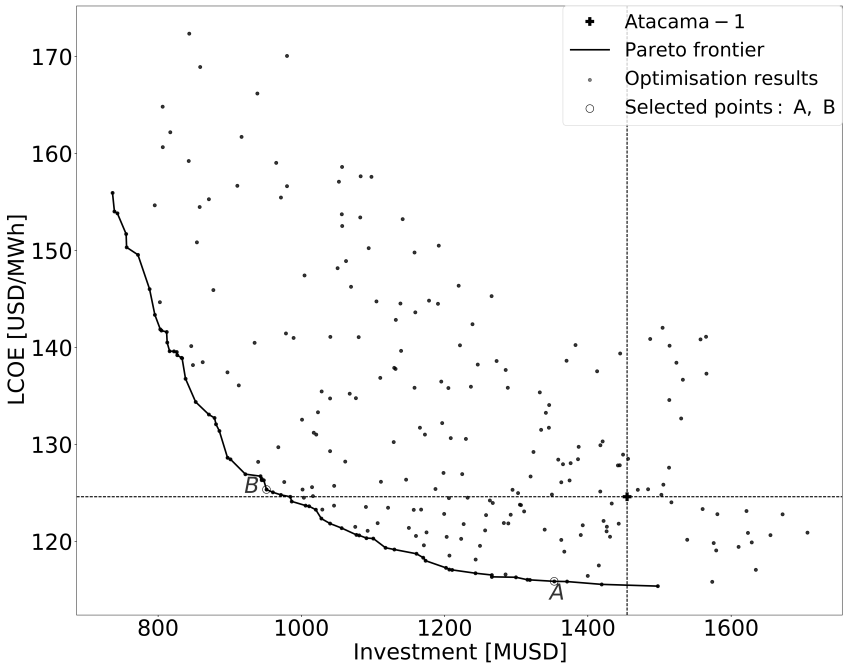

Figure 4.8: Pareto optimal solutions considering three variables and two objectives (LCOE, Investment). Here the best solution is located at the bottom left of the diagram.

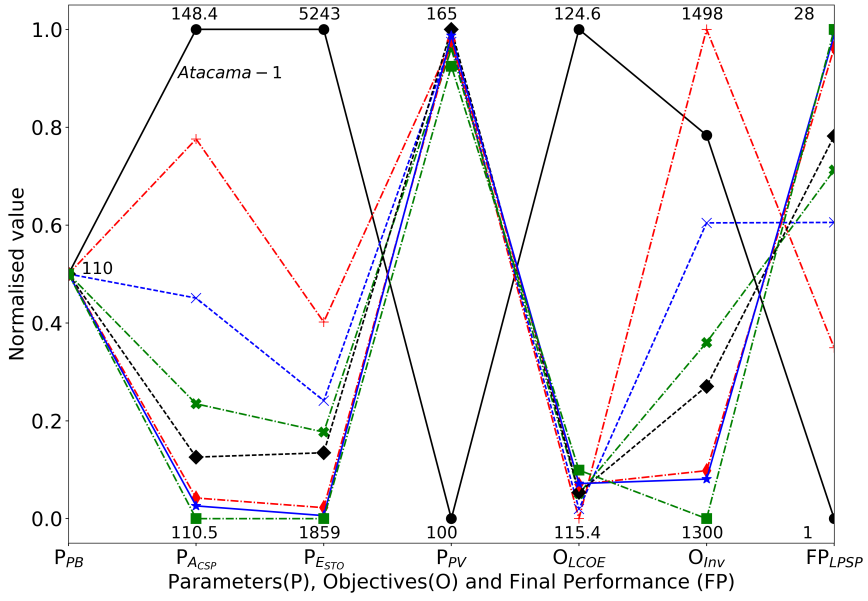

Figure 4.9: Key performance indicators of designs with LPSP<30% (three variables and two objectives)

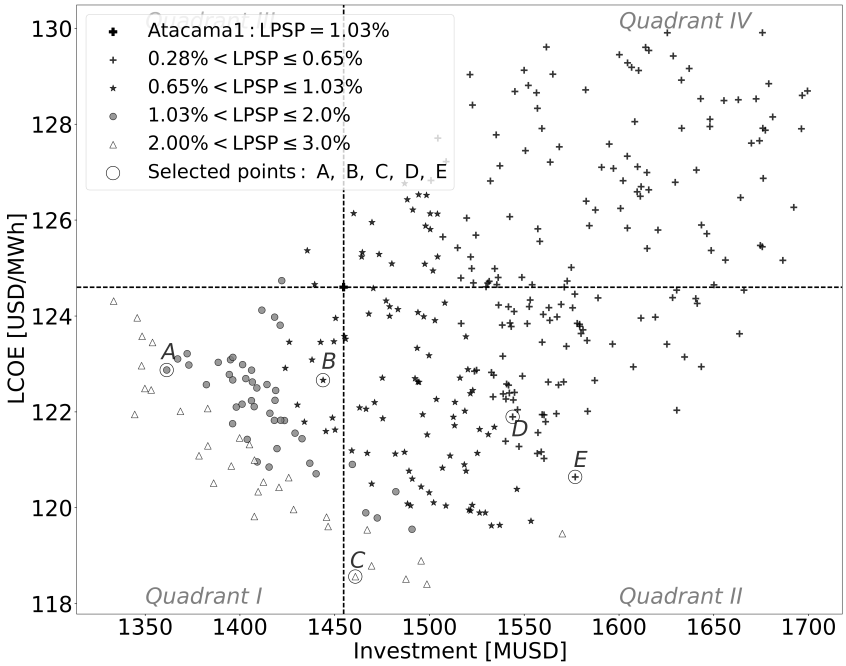

Figure 4.10: Pareto optimal solutions considering three variables and three objectives (LCOE, Investment, LPSP)

E. Designs A and B reach a lower LCOE than Atacama-1. Design C represents a power plant with similar investment but a lower LCOE than Atacama-1. Designs D and E are examples of more reliable power plants, which can be developed with low LCOE, however high investment is necessary.

In addition, the 12 stars located in Quadrant I in Figure 4.10, with all three objectives improved compared with Atacama-1, are detailed in Figure 4.11. This figure shows the design parameters, the results of the three objectives and some key design indicators (SM, StH, and CF_{CSP}) as well as its comparison with Atacama-1. Moreover, for these 12 individuals, a correlation matrix between each objective and the indicators mentioned (SM and StH) is shown below:

$$corr(X,Y) = \begin{array}{c} \\ \text{LCOE} \\ \text{INV} \\ \text{LPSP} \\ \text{SM} \\ \text{StH} \end{array} \begin{array}{c} \begin{array}{ccc} \text{LPSP} & \text{SM} & \text{StH} \end{array} \\ \begin{bmatrix} -0.635 & 0.468 & 0.791 \\ -0.629 & -0.29 & 0.42 \\ 1 & -0.236 & -0.76 \\ -0.236 & 1 & -0.073 \\ -0.76 & -0.073 & 1 \end{bmatrix} \end{array} \tag{4.6}$$

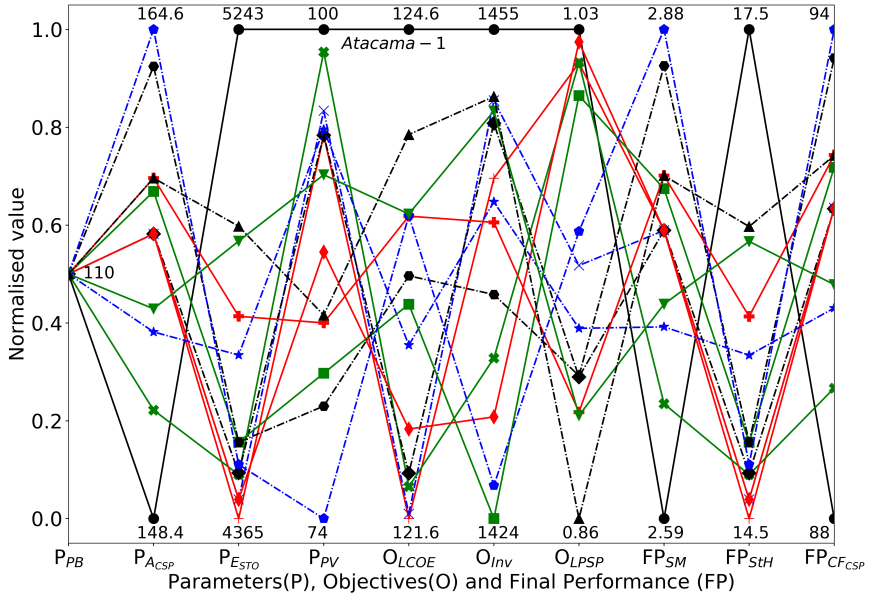

Figure 4.11: Key performance indicators of 12 designs with better performance than Atacama-1 (three variables and three objectives)

These results provide us with an understanding of the design of the power plant. Moreover, some of them are key to define some guidelines. For instance, because SM and StH are related to the installed capacities of the solar field and the storage system, both have a positive correlation with the LCOE. As expected, the LPSP has a negative correlation with both LCOE and Investment. Consequently, to increase the dispatchability, a decrease in financial performance is expected. This concept can also be explained by the negative correlation between LPSP and both SM and StH, suggesting that lower LPSP is reached in oversized power plants. For that reason, the trade-off between technical and financial performance is essential. Another interesting point is the correlation between SM and StH, which suggest that there is a positive correlation between the solar field capacity and the storage capacity observed in optimised designs.

Finally, Figure 4.10, that represents all non-dominated solutions, and Table 4.8 can be combined to make a better a-posteriori decision to select the best design under optimised objectives and other key performance indicators. For instance, if the user is looking for a low LCOE, quadrants I and II should be considered. Then, if high dispatchability is pursued, points D and E should be analysed in more detail. Table 4.8 shows that the capacity factor of the CSP of design E is better than the capacity factor of design D. Hence, if the budget allows, design E could be selected. Finally, the solar multiple and storage hours presented in optimised designs shown in Table 4.8 provide us with guidelines for the development of CSP plants with energy

storage.

Table 4.8: Multi-variables and multi-objectives (LCOE, Investment, LPSP) design optimisation results

item	unit	Atac-1	A	B	C	D	E
A^{CSP}	ha	148.4	151.5	154.6	146.6	157.5	164.7
$Q^{\mathrm{STO,max}}$	MWh	5243	4276	4658	3956	5040	4717
$P^{\mathrm{PV,max}}$	MW	100	75	95	125	121	126
SM	–	2.59	2.64	2.7	2.56	2.75	2.88
StH	h	17.5	14.27	15.55	13.2	16.81	15.74
E^{Net}	GWh·year^{-1}	1,109	1,057	1,120	1,173	1,201	1,239
LPSC	GWh·year^{-1}	9.9	19	8.9	27.5	6	5.8
LPSP	%	1.02	2.0	0.9	2.86	0.6	0.6
$\mathrm{CF_{CSP}}$	%	87.98	89.44	90.51	87.58	91.64	94.06
$\mathrm{CF_{PV}}$	%	27.1	27.1	27.1	27.1	27.1	27.1
Investment	MUSD	1,455	1,361	1443	1,461	1,544	1,577
LCOE	USD·MWh^{-1}	124.6	122.87	122.66	118.57	121.89	120.6

4.5 Result analysis and Conclusions

In order to make renewable energy systems economical and reliable, the design and operation of hybrid renewable energy systems have to consider the trade-off between financial and technical performance of the system and the synergies of technology integration.

The design optimisation needs an internal routine which optimises the operational profile for multiple and often conflicting objectives. However, the operational optimisation is usually performed with single objective linear programming methods. The two-stage optimisation framework applied here to improve the design of Atacama-1, simultaneously optimise the design and operation of a hybrid solar power plant under multiple objectives. While the design optimisation focuses on the selection of the best configuration for the hybrid solar power plant, the operational optimisation finds the best strategy to operate. The latter can be used to analyse the hourly power flows between each component as well as the estimated losses in each subsystem.

Two methods for the operational optimisation were evaluated and it was found that the linear scalarisation method achieves the same results but is much faster than the ε-constraint method. Then, the automated linear scalarisation method was implemented by valuing the trade-off between the two objectives. This enabled the integration of the multi-objective linear optimisation in the two-stage multi-objective optimisation framework.

The optimisation framework was applied to analyse and improve the design of the hybrid solar power plant Atacama-1. The results show that both the financial and technical performance

can be optimised. First, it was shown that the hybrid CSP-PV plant could improve both the affordability and the dispatchability.

By varying a single design variable from Atacama-1 it was shown that the energy storage system could be reduced by 33% (from 17.5 to 11.7 h), whereby the LCOE decreases by almost 5% (from 124.6 to 118.78 USD·MWh^{-1}). However, the LPSP increased from 1.02% to 7.17%. Then, a two-objective optimisation showed that both the LCOE and investment cost could be reduced simultaneously. However, its reliability was considerably degraded because it was not considered as an objective in the design optimisation.

Finally, a three-objective optimisation (LCOE, investment cost and LPSP) was analysed. This method shows that the technical and financial performances of Atacama-1 can be simultaneously improved. For example, with an investment of 1443 MUSD (lower than Atacama-1) a decrease in the LCOE from 124.6 to 122.66 USD·MWh^{-1} and a decrease in the LPSP from 1.02% to 0.9% can be reached. Moreover, the optimisation produces a Pareto frontier of non-dominated solutions outlining the trade-off between different objectives. Consequently, the specific design needs to be selected by the developer based on further criteria.

A large number of potential solutions enabled the development of correlations between the different design parameters (e.g. SM, StH) and objectives (LCOE, investment cost, LPSP) of optimised plants. These correlations can be used to propose guidelines for the optimal design of hybrid solar power plants with energy storage. For instance, a SM of 2.6 and a StH of 15 h can be used as guidelines to develop affordable and dispatchable hybrid solar power plants with energy storage in the Atacama Desert. In addition, the negative correlation between LPSP with LCOE and Investment indicates the trade-off between technical and financial performance. Besides, the negative correlation between LPSP with SM and StH suggests that oversized power plants improve the dispatchability.

Chapter 5

Technology integration analysis and optimal design of dispatchable power plants in Northern Chile

5.1 Introduction

The present chapter investigates the synergies of technology integration. Different configurations will be described and analysed through four case studies. The location that will be considered, due to its high potential to develop solar power plants, is the Atacama Desert in Northern Chile. Figure 5.1 shows the region of Antofagasta in the Atacama Desert. As illustrated in the figure, the Antofagasta region is one of the sunniest places on Earth. In this context, Figure 5.2 shows the daily average of the direct normal irradiation (DNI) and the global tilted irradiation (GTI) of the location highlighted with a green circle in Figure 5.1. All case studies analysed are shown in Table 5.1. Some configurations described here are based on the design of an off-grid hybrid power plant to supply energy to an isolated copper mine. An off-grid power plant is not connected to the grid; hence it is not possible to dispatch energy when the supply exceeds the demand of the copper mine. Moreover, the operation of the copper mine will be restricted to the power supply of the power plant. Consequently, dispatchability becomes crucial.

First, due to the low cost of solar PV, and the expected reduction in the cost of batteries, Section 5.2 analyses the combination of a solar power plant with thermal and electrical energy storage, and a long-term cost analysis is addressed. Second, some studies suggest that the integration of a fossil backup unit is key to increase the dispatchability and affordability of solar power technologies; hence, an essential aspect in an economical pathway to decarbonise the power sector. This configuration is analysed in Section 5.3. Then, Section 5.4 evaluates the heat supply for low-temperature mining processes from the heat rejection of the Rankine cycle of the CSP plant. Despite that the technical feasibility of this project depends on the location of the power plant and the mining processes that require heat, the high cost of diesel in the Atacama Region could be a transcendental variable. Finally, due to CSP and PV plants work

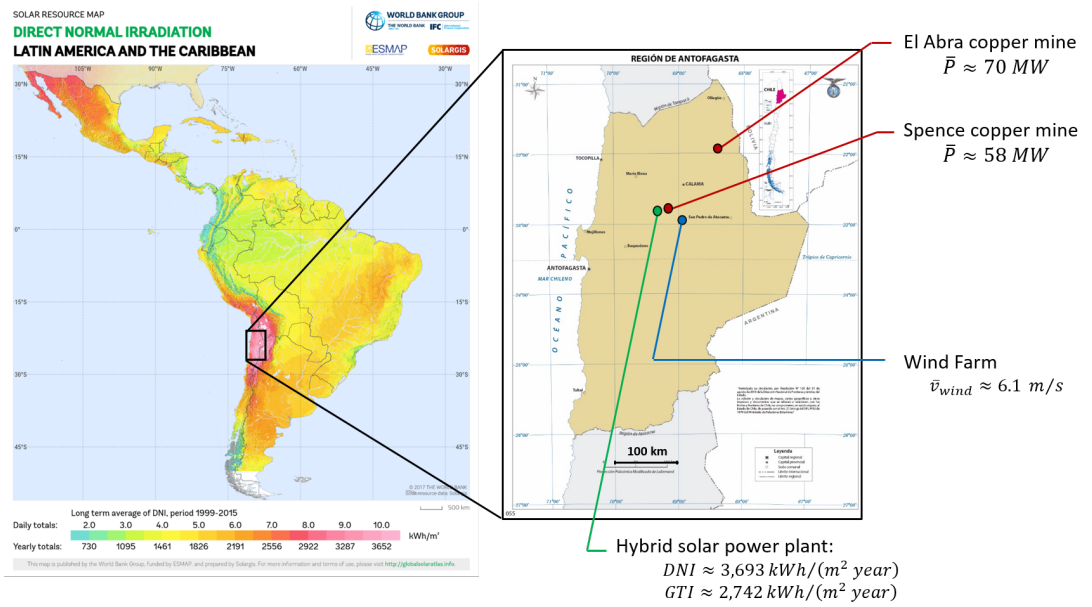

Figure 5.1: Location and details of four case studies analysed in Chapter 5

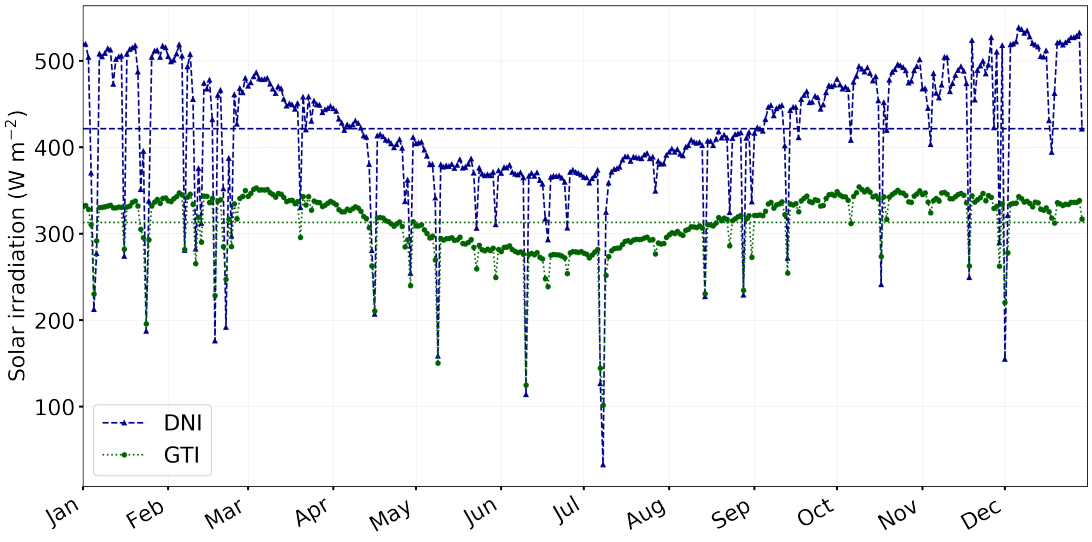

Figure 5.2: Daily average of solar irradiation (DNI, GTI), Atacama Desert

Table 5.1: Summary of case studies based on technologies integrated into hybrid solar power plants. TES: thermal energy storage, FBU: fossil backup unit, EES: electrical energy storage

Section	Technology	Details	Copper Mine	Configuration
5.2	TES +EES	Long-term analysis	Spence	Grid connected
5.3	TES+FBU+EES	Fossil backup integration	Spence	Off-grid
5.4	TES+FBU+EES	Low-temp. heat supply	Spence	Off-grid
5.5	TES+FBU+Wind+EES	Wind power integration	El Abra	Grid connected

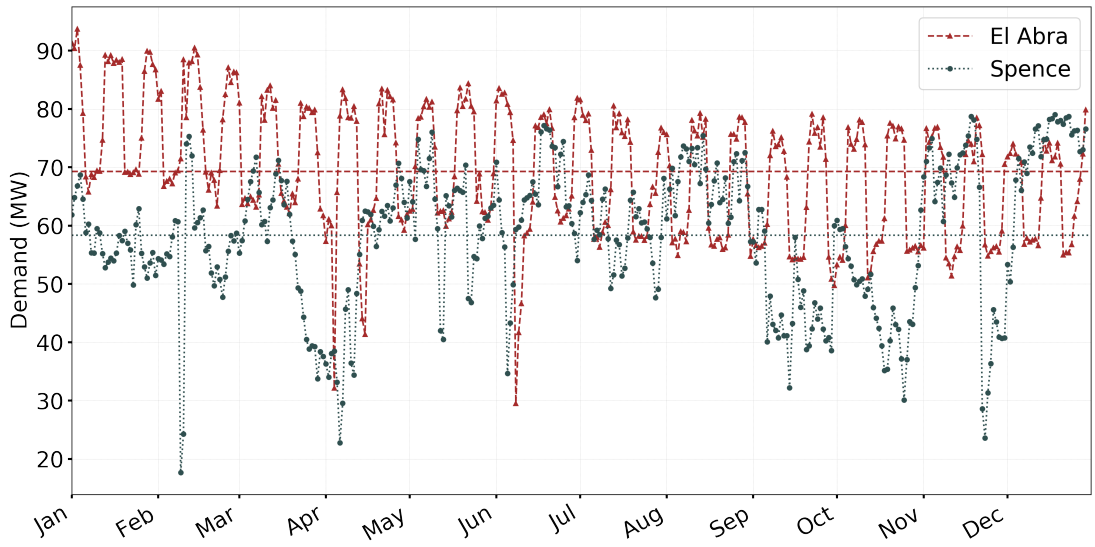

Figure 5.3: Daily average of power demand for El Abra and Spence copper mines, Atacama Desert

with solar irradiation, the integration of a Windfarm, analysed in Section 5.5, decreases the variability of the renewable resource used in the hybrid power plant. Hence, the deployment of hybrid power plants considering three (or more) different renewable technologies enhance the competitivity of distributed sustainable power plants.

The location of the hybrid solar power plant, the wind farm, and the two copper mines examined in the case studies are shown in Figure 5.1. Figure 5.3 presents the daily average power demand of the two copper mines analysed in the case studies: El Abra copper mine (Freeport-McMoRan, Codelco), and Spence copper mine (BHP) (Chilean Center for Economic Load Dispatch, 2016). In this study, the fluctuating hourly power demand of these copper mines is used as a commitment for the operational optimisation of the power plant.

The base model applied in this chapter is exposed in Figure 5.4. The diagram represents the mass and energy flows of the concentrating solar power plant and the photovoltaic power plant that will be integrated and analysed in the case studies detailed in the following sections.

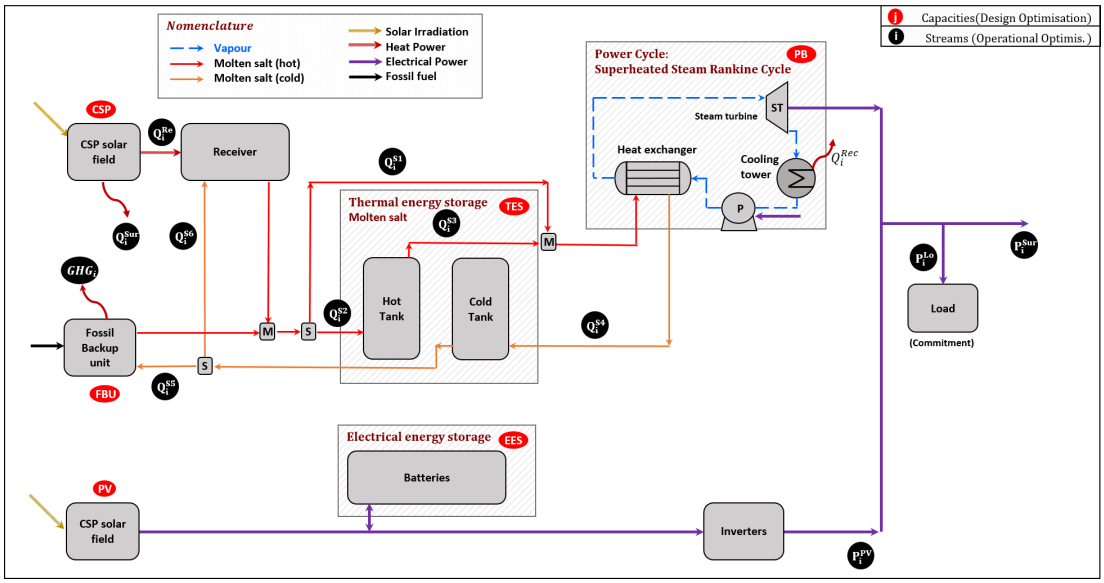

Figure 5.4: Mass and energy balances model of the hybrid solar power plant with energy storage system

5.2 Long-term analysis of electrical and thermal energy storage integration

The work presented in this section is based on a published conference paper, Bravo R, Friedrich D. Integration of energy storage with hybrid solar power plants. 3rd Annual Conference in Energy Storage and its Applications: Energy Procedia; 2018

5.2.1 Introduction

The integration of energy storage can reduce the large fluctuations of electricity supplied from the intermittent resource in renewable power plants. While electrical energy storage is suitable for the integration with PV plants, thermal energy storage is valuable for CSP plants.

PV systems are one of the more affordable technologies to provide electricity, and further reductions are expected (Fraunhofer ISE, 2015). According to the results of Chapter 4, the levelised cost of energy (LCOE) of a PV plant located in Northern Chile, without storage is around 90 USD·MWh^{-1}. On the contrary, the LCOE is close to 130 USD·MWh^{-1} for a CSP plant with 17.5 h of two-tank molten salt energy storage and a solar multiple of 2.6 (i.e. the design capacity of the solar field is 2.6 times the capacity of the power block). In terms of the storage system, investment costs of TES are approximately 25 USD·kWh^{-1} (molten salts), and electrical energy storage (EES) system costs are around 600 USD·kWh^{-1} (DC batteries) (NREL, 2017). Then, if we include the efficiencies to transform both stored thermal energy and energy stored in batteries to electrical AC, TES systems are around ten times cheaper than EES. Thus, CSP systems integrated with TES are currently one of the most cost-competitive

technologies to provide reliable and baseload power, and it becomes more affordable when it is hybridised with PV. However, in the medium-term, EES systems are expected to have an extreme cost reduction, and then PV with EES could be the best alternative.

According to published projections, cost reductions depend on the learning rate of each technology. In the case of PV and battery systems, Fraunhofer ISE (2015) analyses the projections of costs for the modules, inverter and balance of the system as well as the improvement in efficiencies, and concluded that, considered 2015 as baseline, the total investment cost of a PV system would decrease between 40% and 70% by 2050. In another study, Joint Research Centre (2014) reported that the expected reduction in PV costs without tracking system could be in the range of 50% to 60%. Besides, some publications estimate that costs of EES systems could be closer to 100 USD·kWh^{-1} by 2050 (Schmidt *et al.*, 2017; Worley Parsons, 2012). Otherwise, the expected reduction for CSP and TES systems are in the range of 20% to 30% (Joint Research Centre, 2014; IEA *et al.*, 2015). Finally, based on the projections of Joint Research Centre (2014), a reduction between 20% and 40% in the fixed and variable operational and maintenance costs (O&M) for both technologies are considered in this study.

In this study, these estimations are used to define different scenarios of cost reduction, based on 2016 costs, where each scenario represents a particular level of learning rate reached for each technology by 2050. These levels will be interpreted as the investment and O&M costs and used as parameters in the two-stage multi-objective optimisation framework developed in Chapter 3. Finally, the results of each scenario will be analysed to find the features of the dominant technology in a hybrid solar power plant that provides dispatchable energy.

5.2.2 Optimisation Implementation

As a case study, the design of an off-grid power plant that delivers energy to Spence copper mine (Figure 5.1) is examined. As reported before, hourly power demand was obtained from Chilean Center for Economic Load Dispatch (2016) (Figure 5.3), and solar irradiation information for the typical meteorological year from Ministry of Energy - University of Chile (2016) (Figure 5.2). Technical and financial performance of CSP and PV power plants, i.e. efficiencies, capacities, investment costs, operational and maintenance cost are estimated by using SAM (NREL, 2017).

Figure 5.5 shows the hourly power demand for Spence, the direct normal irradiation (DNI) and the global tilted irradiation (GTI) during one week in summer (January) and one week in winter (July) for the year 2016. The diagram reflects, among others, the profile of the demand required to be met, and the mismatch between power commitment and solar resource availability. The maximum power demand of Spence during the year of analysis (2016) was 83 MW, and its average power consumption was 58 MW. In addition, the reported solar irradiation for that year was: DNI$\approx$ 3500 kWh·m^{-2}, and GTI$\approx$2630 kWh·m^{-2}.

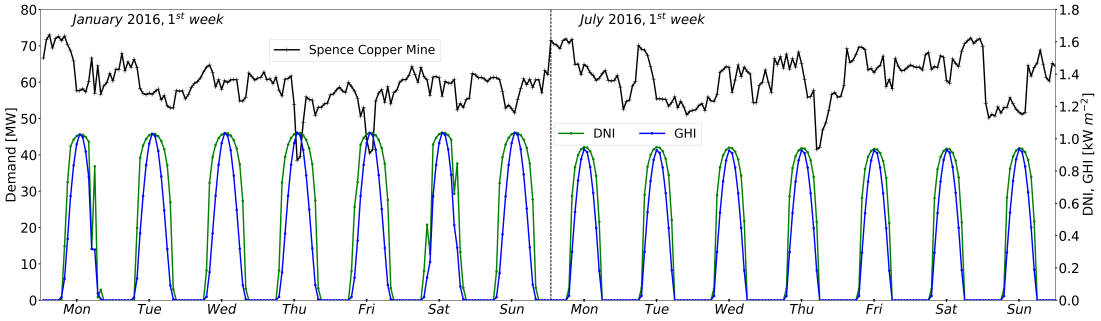

Figure 5.5: Electricity demand of Spence copper mine and solar resource in Northern Chile

Table 5.2: Variables and parameters used in the power flow model of a CSP plant with TES.

Description	Name	type
Thermal power receiver	$\dot{Q}^{Rec}$	variable
Thermal power receiver to PB	$\dot{Q}^{Rec \to PB}$	variable
Thermal power receiver to TES	$\dot{Q}^{Rec \to TES}$	variable
Thermal power curtailment	$\dot{Q}^{CSP,Curt.}$	variable
Energy stored in TES	Q^{TES}	variable
Thermal power TES to PB	$\dot{Q}^{TES \to PB}$	variable
Electrical power CSP to Network	$P^{PB \to Netw}$	variable
Pipelines thermal efficiency	$\eta^{\text{pipelines}}$	0.99
TES efficiency	η^{TES}	0.99
Power block efficiency	η^{PB}	0.371

Figure 5.6 details the power flow model of the hybrid solar power plant with thermal energy storage (molten salt) and electrical energy storage (batteries). Here the capacity of the battery system is included as a variable in the design optimisation. Tables 5.2 and 5.3 enumerate all variables and parameters used in the model. For instance, in the battery system, the charging power ($P_i^{PV \mapsto EES}$), discharging power ($P_i^{EES \mapsto Inv}$), as well as the energy stored in the battery system (E_i^{EES}) are variables in the operational optimisation model. The energy stored in the battery is calculated based on an energy balance analysis, according to:

$$E_0^{EES} = 0 \tag{5.1}$$

$$E_i^{EES} = E_{i-1}^{EES} \cdot \eta^{EES} + (P_i^{PV \mapsto EES} \cdot \eta^{PV \mapsto EES} - P_i^{EES \mapsto Inv}) \cdot \Delta t_i \tag{5.2}$$

$$E_i^{EES} \leq E^{EES,Max} \tag{5.3}$$

Then, the net power dispatched by the hybrid power plant is the sum of the power supplied from both solar power plants, and the commitment constrains the maximum power dispatched. In this case, because the analysis is for an off-grid power plant, any extra power that could be generated that exceeds commitment has to be curtailed in the solar fields.

Table 5.3: Variables and parameters used in the power flow model of a PV plant with EES.

Description	Name	type
Electrical power PV array	P^{PV}	variable
Electrical power PV array to Inv	$P^{PV \to Inv}$	variable
Electrical power PV array to EES	$P^{PV \to EES}$	variable
Electrical power curtailment	$P^{PV,Curt.}$	variable
Energy stored EES	E^{EES}	variable
Electrical power EES to Inv	$P^{PV \to Inv}$	variable
Electrical power power PV to Network	$P^{PV \to Netw}$	variable
PV array efficiency	η^{PV}	0.192
EES efficiency	η^{EES}	0.99
PV array to inverter efficiency	$\eta^{PV \to inv}$	0.85
Inverter to network efficiency	$\eta^{inv \to Netw}$	0.973

$$P_i^{Net} = P_i^{CSP \mapsto Netw} + P_i^{PV \mapsto Netw} \tag{5.4}$$

$$P_i^{Net} = P_i^{Load} + P_i^{Surplus} \tag{5.5}$$

$$P_i^{Load} \leq P_i^{Commitment} \tag{5.6}$$

5.2.3 Results analysis

Different scenarios are considered and compared. Each case combines a particular expected level of investment cost (IC) reduction, by technology in the year 2050. Table 5.4 shows five scenarios examined, based on 2016 costs and combining different reductions by 2050 between CSP-TES and PV-EES technologies. As an example, Scenario 1 (S1: Lr_{CSP} & Lr_{PV}) considers a low reduction in CSP technology costs (Lr_{CSP}), i.e. 20% reduction in both investment and O&M costs, and a low reduction in PV system costs (Lr_{PV}), i.e. 40% reduction in investment costs for the PV plant, 60% drop in investment costs for the EES system, and 20% reduction in O&M costs of the photovoltaic power plant.

Then, the two-stage multi-objective optimisation framework was applied for each scenario. For each case, the results create a three-dimensional Pareto surface, illustrated in Figure 5.7. These optimal set of solutions summarise the three objectives chosen in the design optimisation stage (LCOE, LPSP, and Investment), highlighting current and future configurations of hybrid power plants to provide affordable and reliable energy from solar technologies. From all solutions, just those that meet the following criteria are displayed in Figure 5.7: $LPSP \leq 8$ %; $LCOE \leq$ 130 USD·MWh^{-1}; Investment $\leq$ 700 MUSD. Each point represents an optimal design for a hybrid solar power plant. Here, the line connecting the solutions is used to facilitate the reading, showing the two-dimensional Pareto front between LCOE and LPSP.

Figure 5.7 exposes that for all scenarios, a substantial reduction in LCOE and investment costs

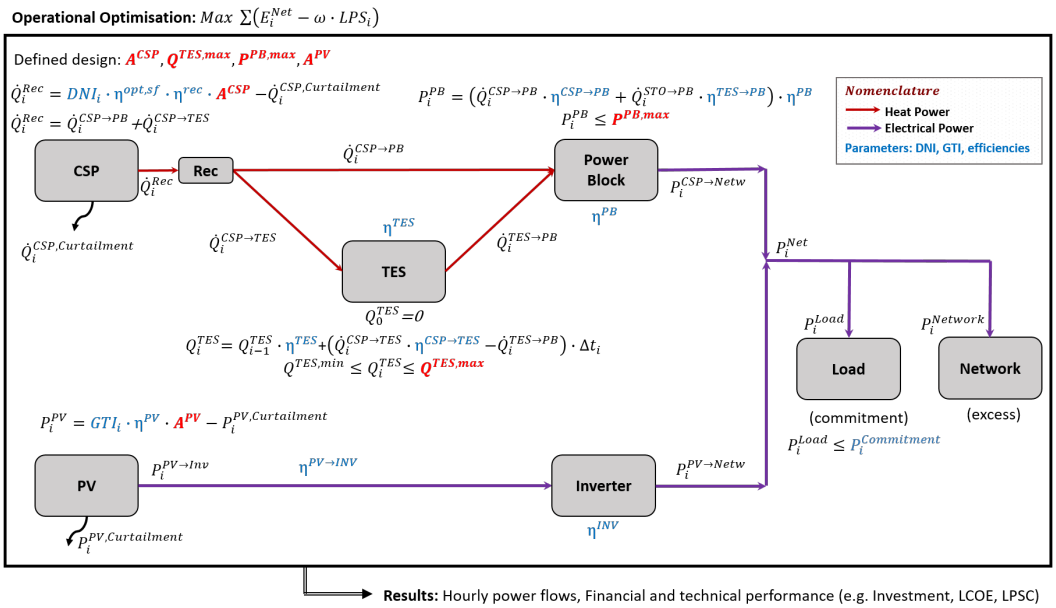

Figure 5.6: Power flow model of a hybrid solar power plant with thermal and electrical energy storage systems

Table 5.4: Descriptions of scenarios of technology cost reduction by 2050 considered in the long-term analysis of energy storage integration

Scenario		$IC_{CSP-TES}$	IC_{PV}	IC_{EES}	$OM_{CSP-TES}$	OM_{PV-EES}
S1	Lr_{CSP} & Lr_{PV}	20%	40%	60%	20%	20%
S2	Lr_{CSP} & Hr_{PV}	20%	60%	80%	20%	40%
S3	Mr_{CSP} & Mr_{PV}	30%	50%	70%	30%	30%
S4	Hr_{CSP} & Lr_{PV}	40%	40%	60%	40%	20%
S5	Hr_{CSP} & Hr_{PV}	40%	60%	80%	40%	40%

are expected. For instance, a high dispatchability, accounted for a hybrid solar plant with a $LPSP \approx 1\%$ (follow the vertical line in LPSP = 1%) is reached in 2016 with an LCOE close to 130 USD·MWh^{-1}, and an investment cost close to 700 MUSD. Even in the most conservative scenario (S1), the same level of dispatchability is achieved with an $LCOE \approx 100$ USD·MWh^{-1} and an investment close to 500 MUSD. On the other hand, a power plant designed under the most optimistic scenario (S5) attains the same level of dispatchability with an LCOE of around 65 USD·MWh^{-1} and an investment around 350 MUSD.

Figure 5.8 presents the optimal design of a power plant with a LPSP$\approx$ 1% for each scenario (including 2016). This diagram displays the normalised value of the three objectives considered in the design optimisation. Then three features of the design for optimised power plants are expanded. These characteristics are defined by: (i) A_{SF}, the fraction between the solar field area (m^2) of the CSP plant and the total solar field area (CSP+PV); (ii) E_{STO}: the capacity based on

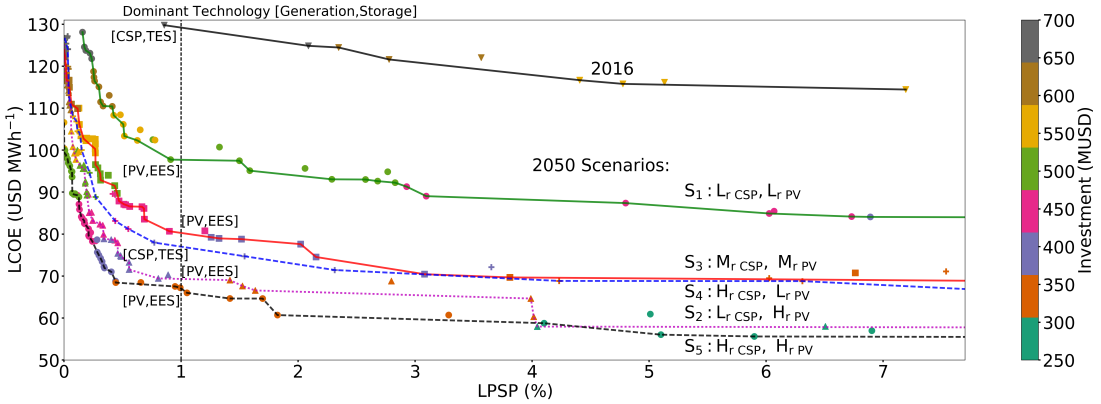

Figure 5.7: Design optimisation results for all scenarios considered in the long-term analysis of TES and EES integration

electrical energy (MWh_e) of the thermal energy storage as a fraction of the total energy storage capacity (TES+EES); and (iii) E^{Supply}: the electricity supplied by the CSP plant divided by the total energy supplied from the hybrid power plant.

Interestingly, in terms of the dominant technology, CSP with TES is currently the best option and the dominant technology for an affordable and dispatchable hybrid solar power plant. This trend will continue just in scenario 4 (i.e. Hr_{CSP} & Lr_{PV}) that considers a high reduction in CSP-TES and a low reduction in PV-EES system costs. In all other cases, a shift to PV with EES as a dominant technology is expected.

Hence, the design of hybrid solar power plants for scenarios 2016 and S4 are dominated by CSP-TES. For all other scenarios (S1, S2, S3 and S5) the optimal design of dispatchable power plants is dominated by a great PV solar field area, a similar or larger capacity of the EES system compared with the TES. Finally, in these last cases, the PV plant supplies more than 80% of the total energy dispatched.

As anticipated, these values satisfactorily support the idea that in the medium term, the integration of solar photovoltaics and battery systems may be the most affordable technology to provide dispatchable energy. The optimisation framework can be extended to incorporate other strategies or technologies which could improve both technical and financial performance.

5.2.4 Discussion

This study outlines a valuable approach to design optimised hybrid solar power plants under different assumptions. The findings confirm that currently, CSP with TES is the most competitive technology to provide affordable and dispatchable power. However, due to the extreme reduction expected in the cost of EES systems, a shift to PV with EES is anticipated. Furthermore, in future scenarios, a considerable improvement in the financial performance of solar hybrid power plants is expected. This method represents a valuable blueprint for

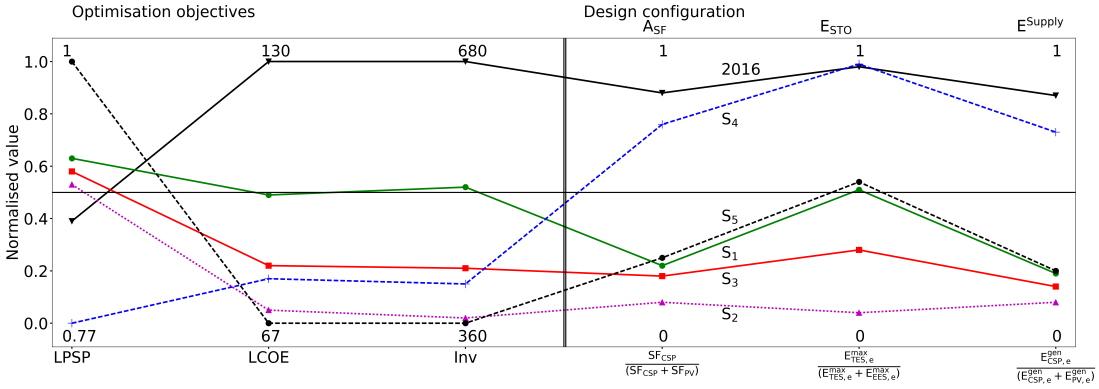

Figure 5.8: Performance of selected designs by scenario in the long-term analysis of TES and EES integration

current and future researches in order to have a broader range of cost-competitive, reliable and sustainable technologies. This procedure can be extended to investigate diverse configurations in order to combine different energy conversion and energy storage technologies as a single technology as well as hybrid power plants. Moreover, to design a practical and economic pathway to decarbonise the power sector gradually, the model could analyse the construction of PV plants in the short term, and the integration of batteries in the medium term. However, some constraints that have a large influence in the design, like the availability of materials for batteries, are not considered in this study. The analysis of objectives related not only to financial and technical parameters but also societal or environmental indicators can be useful to improve the strategies of decision and policy-making.

The following sections investigates heat demand analysis and fossil backup. In addition, the flexibility of the model allows us to study other techniques that could be crucial to design an economical pathway to a sustainable energy development, for instance, demand-side management, the study of a variable demand, among others.

5.3 Integration of a fossil backup unit to increase the dispatchability of CSP plants

The work presented in this section is based on a published conference paper: R.Bravo and D.Friedrich, Two-stage multi-objective optimisation framework for an efficient pathway to decarbonise the power sector. EngOpt 2018 Proceedings of the 6th International Conference on Engineering Optimization Cham: Springer International Publishing; 2018

5.3.1 Introduction

Hybrid renewable power plants that integrate renewable energy technologies with energy storage have the potential to provide sustainable, cost-competitive and dispatchable electricity supply. Moreover, solar thermal technologies, e.g. concentrating solar power plants, can be integrated with a fossil backup unit in order to work continuously, as a baseload, even during long periods with no solar irradiation available (IEA, 2014b). However, its ability depends on the size of the fossil backup unit and the storage system. In these cases, despite the power plant emitting some quantities of greenhouse gases, its operation can be improved, resulting in enhanced technical and financial performances. As a result, the use of energy storage and fossil-fuelled backup units increases the dispatchability and decreases the integration costs of hybrid solar power plants.

Hence, in this study, two flexibility strategies are investigated. As in previous analysis, the first flexibility is that a mismatch between supply and commitment is allowed. The second strategy is that the system can emit greenhouse gases by the integration of a fossil backup unit which makes the system not entirely renewable and sustainable. However, this flexibility improves both technical and financial performances.

5.3.2 Optimisation Implementation

A hybrid power plant integrated with energy storage and a fossil backup unit that supplies energy to Spence copper mine is analysed as a case study. Figure 5.4 shows the mass and energy flow model considering a fossil backup unit (FBU), while Figure 5.9 illustrates the power flow model in an off grid configuration, used in this study to simplify the analysis of energy conversion and storage systems. Here the capacity of the FBU is considered a variable of the design optimisation stage, and the heat power supplied as a heat injection process for the thermal energy storage system ($\dot{Q}_i^{FBU \mapsto TES}$) is a variable in the operational optimisation model. To calculate the heat injection from the fossil backup unit, a heating value 10.63 $\mathrm{MWh \cdot m^{-3}}$, a diesel cost of 54 $\mathrm{USD \cdot MWh_{th}^{-1}}$ in Northern Chile, and a heater efficiency of 78% were considered (Quiñones *et al.*, 2020).

The following modified equations represent the energy balances of the thermal energy storage system under the integration of the FBU:

$$Q_0^{TES} = 0 \tag{5.7}$$

$$Q_i^{TES} = Q_{i-1}^{TES} \cdot \eta^{TES} + (\dot{Q}_i^{CSP \mapsto TES} \cdot \eta^{CSP \mapsto TES} + \dot{Q}_i^{FBU \mapsto TES} \cdot \eta^{FBU \mapsto TES} - \dot{Q}_i^{TES \mapsto PB}) \cdot \Delta t_i \tag{5.8}$$

$$\dot{Q}_i^{FBU} \leq \dot{Q}^{FBU,Max} \tag{5.9}$$

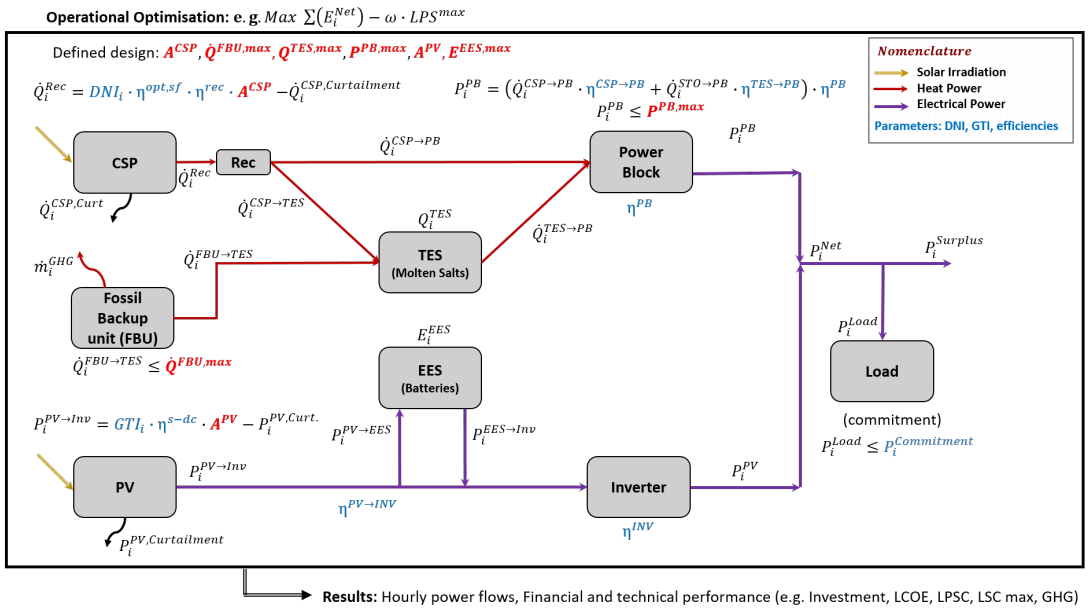

Figure 5.9: Power flow model of a hybrid solar power plant with TES, fossil backup, and EES

In the model, the power commitment, i.e. the power that the power plant needs to dispatch, corresponds to the power demand of Spence copper mine, as shown in Figure 5.3. For the year considered in this study (2016), the total electricity demand of Spence was approximately 511.3 GWh.

In this case study, the operational optimisation focuses on two objectives. First, the maximisation of the energy supply:

$$Max E^{Net} = Max \sum_{i=0}^{T} P_i^{Net} \cdot \Delta t_i \tag{5.10}$$

In the case of an off-grid configuration, the maximisation of the energy supplied, at the same time minimises the mismatch between supply and demand.

As a second objective, here, the focus is to minimise the maximum value of the loss of power over the entire evaluation period:

$$Min\ LPS^{Max} \tag{5.11}$$

This variable represents the maximum power shortage for a given configuration. This variable depends on the design, the commitment, and the operational strategy for every time step. In contrast with the LPSP, the LPS^{max} can be useful to know the maximum power that the power plant is not able to supply in order to evaluate further steps to define a fully dispatchable system, for instance, to evaluate the minimum capacity for an alternative electric generator system or

the integration of demand side management techniques.

Therefore, the multi-objective optimisation by linear programming will be developed by the linear scalarisation method presented in Chapter 3, according to:

$$Max\, E^{Net} - \omega \cdot LPS^{Max} \tag{5.12}$$

Here, in order to automate the linear scalarisation method (i.e. automatically choose just one result from the Pareto optimal solutions), the operation optimisation is performed three times. The first two iterations ($j = 1, 2$) are developed as single objective linear optimisation routines, considering the single objectives mentioned previously: $j = 1,\ MaxE^{Net}$; $j = 2,\ MinLPS^{Max}$. In each iteration the energy supplied (E_j^{Net}) and the maximum LPS (LPS_j^{Max}) is recorded. Finally, the linear scalarisation technique is performed with the following ω:

$$\omega = \begin{cases} 1 & , LPS_{j=1}^{Max} = LPS_{j=2}^{Max} \\ \dfrac{E_{j=1}^{Net} - E_{j=2}^{Net}}{LPS_{j=1}^{Max} - LPS_{j=2}^{Max}} & , \text{otherwise.} \end{cases} \tag{5.13}$$

Then, the design optimisation stage is carried out by the two-stage optimisation framework using genetic algorithms. Table 5.5 shows the variables of the design optimisation. In order to link both stages, the genetic algorithm performs the optimisation of the design of the power plant analysing three objectives: (i) levelised cost of energy; (ii) investment, and (iii) maximum power shortage. Then, as a second stage (as the fitness function), the operational optimisation is calculated by the automated linear scalarisation method. As a result, the model optimises the operation simultaneously by maximising the energy delivered to the copper mine, and minimising both the total and the maximum power shortage.

Table 5.5: Variable of the design optimisation for a hybrid solar power plant with TES, FBU and EES

CSP Plant			PV Plant		
Description	Variable	Unit	Description	Variable	Unit
Area solar field	$A^{CSP,SF}$	m^2	Area solar field	$A^{PV,SF}$	m^2
Capacity TES	$Q^{TES,Max}$	MWh	Battery capacity	$E^{EES,Max}$	MWh
Capacity Power block	$P^{PB,Max}$	MW			
Capacity fossil backup unit	$Q^{FBU,Max}$	MW			

Table 5.6: Selected variable ranges for the design optimisation model with fossil backup integration

Variable	Unit	Initial ranges	Improved ranges
$A^{CSP,SF}$	$\cdot 10^4\ m^2$	0 - 150	60 - 100
$Q^{TES,Max}$	MWh	10 - 10,000	5,000 - 7,300
$P^{PB,Max}$	MW	10 - 90	45 - 77
$Q^{FBU,Max}$	MW	0 - 5	0 - 5
$A^{PV,SF}$	$\cdot 10^4\ m^2$	10 - 150	10 - 70
$E^{EES,Max}$	MWh	10 - 1,000	10 - 135

5.3.3 Results analysis

In order to set the limits of each variable of the design optimisation, the model was run with a broad range for every component in a first approach, considering the power commitment and the solar irradiation. Then, the best cost-competitive and dispatchable power plants were selected, considering an LCOE $\leq$ 150 USD·MWh^{-1} and a $LPSP \leq 15\%$, and used to define smaller ranges. Table 5.6 shows the initial range used to run the model and the improved range by filtering the results.

After that, the improved ranges were used in the model, and the solutions were added to the initial results. Figure 5.10 illustrates the Pareto optimal solutions for both cases. This plot contains the LPS^{Max} in the abscissa, the LCOE in the ordinate, and the Investment is represented by a sequential colour-map. Pareto optimal or non-dominated solutions represent designs that are optimised under the three objectives defined. Therefore, every point can be selected as an optimised design for a suitable hybrid power plant in the decision-making process. The diagram shows the trade-off between technical (LPS^{Max}) and financial performances (LCOE, Investment) which must be analysed to make a final decision.

In order to improve the decision-making process, a post-optimisation analysis should be carried out to have more valuable information and reduce the number of solutions. For instance, it is possible to analyse the behaviour of different non-dominated solution under other key performance indicators, like the greenhouse gas emissions, the annual loss of power supply, the total curtailment when generation exceeds demand, among others.

First, it was found that power plants that can reach a $LPSP \leq 10\%$ have a $LPS^{Max} \leq 29$ MW. Nevertheless, in order to have a range of solutions, considering dispatchable and also affordable power plants, four designs are selected and represented in the diagram with the letters A, B, C and D. Design A has a $LPS^{Max} = 0$, but the highest LCOE and investment. B is the point with the lowest LCOE, and $LPSP \leq 10\%$ and C has the lowest investment in the Pareto surface, but a high LCOE and LPS^{Max}. Finally, D is the point with the minimum LCOE between all the solutions.

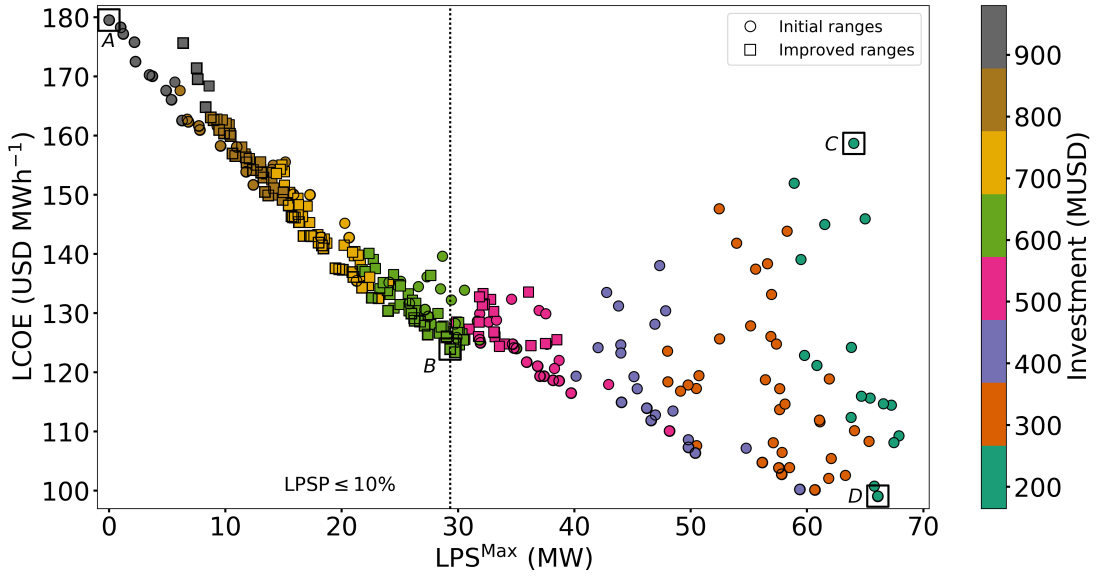

Figure 5.10: Design optimisation results of a hybrid solar power plant with TES, FBU and EES

Table 5.7 shows key performance indicators of these four designs. The first three rows are the objectives of the design optimisation. Then, the following four values (E^{Dem}, $E^{Surplus}$, LPSP, GHG) are shown. These variables are not considered as objectives (hence not optimised); however, they are useful for the decision-making process. Finally, the size of each component (variables of the design optimisation) is summarised for each solution. A post-optimisation analysis could be done by analysing this table, and any indicator here described. For instance, the decision could be made by considering the loss of power supply probability (LPS), or the greenhouse gas emissions (GHG). An important finding revealed in Table 5.7 is that the design of highly dispatchable power plants (e.g. A or B) consider a small fossil backup unit (10 kW and 110 kW, respectively). Hence, the integration of a fossil backup unit to improve the technical and financial performance is not relevant in the design of a hybrid solar power plant that dispatch energy to Spence copper mine, this is mainly due to the high levels of solar irradiation, stable power demand, high costs of diesel in the Atacama Desert, among others.

In addition, Figure 5.11 details the annual operational optimisation of configuration B, considering the hourly solar irradiation from 2004 to 2015, as well as the typical meteorological year (TMY), published for the years 2016 and 2018. This analysis is crucial to analyse different configurations under the solar resource of different years and evaluate worst-case scenarios. In terms of the LCOE, while the best-case scenario for configuration B was 2006, with an LCOE $\approx$ 122.4 USD·MWh^{-1}, the most unfavourable year was 2015, when the LCOE reached $\approx$ 124.7 USD·MWh^{-1}. A similar analysis for the LPS^{Max} shows that the highest value was reached in 2007 (43.7 MW), while the best scenario was achieved in 2010 (21.8 MW).

Table 5.7: Post-optimisation analysis of selected optimal designs integrating a fossil backup unit

Description	Variable	unit	A	B	C	D
Max. power shortage	LPS^{Max}	MW	0	29.3	64.3	66
Levelised cost of energy	LCOE	$USD\ MWh^{-1}$	179	124	159	99
Investment	Inv.	MUSD	972	613	165	253
Energy supplied to demand	E^{Dem}	GWh_e	511.3	471	129	277
Energy surplus	$E^{Gen,Surplus}$	GWh_e	121.2	0.2	0	14
Loss of power supply prob.	LPSP	%	0	7.8	75	46
GHG emissions	GHG	tCO_{2eq}	18	224	11,850	6,713
Area solar field, CSP	$A^{CSP,SF}$	$\cdot 10^4\ m^2$	111	85	10	21
Capacity TES	$E^{TES,Max}$	MWh	8,500	5,215	907	624
Capacity power block	$P^{PB,Max}$	MW	78	58	22	22
Capacity fossil backup	$P^{FBU,Max}$	MW	0.01	0.11	5	3
Area solar field, PV	$A^{PV,SF}$	$\cdot 10^4\ m^2$	67	17	12	38
Capacity battery system	$E^{EES,Max}$	MWh	40	18	27	11

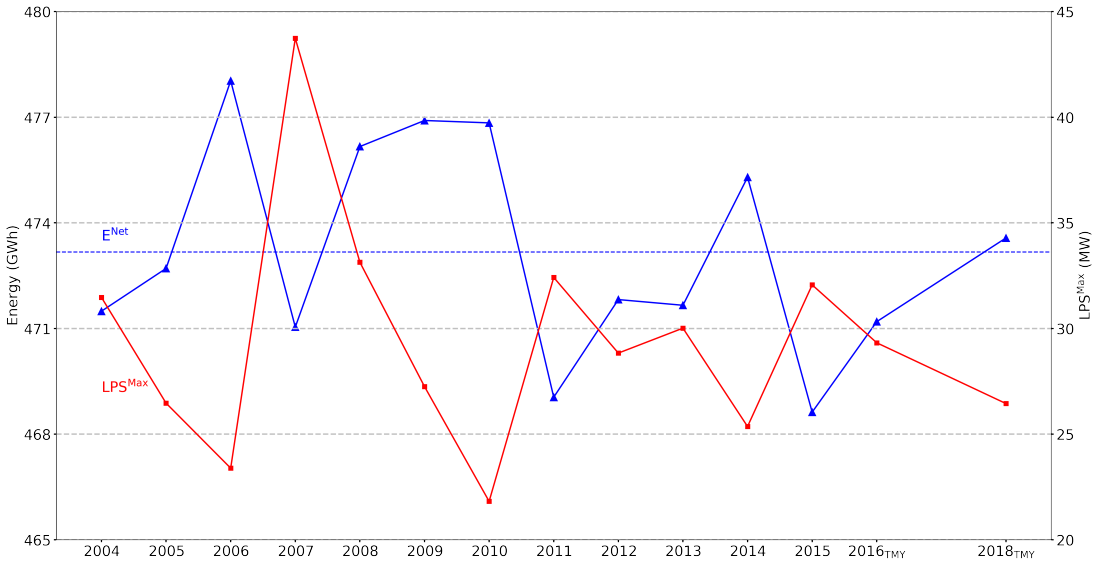

Figure 5.11: Annual performance from 2004 to 2015, and TMY for the selected design (B)

5.3.4 Discussion

The integration of different renewable technologies, energy storage, and flexibility are essential for the design of cost-competitive and dispatchable sustainable power plants. The design of renewable power plants has to handle a large number of parameters, and the integration of energy storage requires an operational strategy for every design. Here the two-stage multi-objective optimisation framework is used to optimise the design of an off-grid hybrid power plant considering two different solar technologies (CSP and PV), thermal and electrical energy storage, and incorporates two flexibility strategies (mismatch between supply and demand, and greenhouse gas emissions).

The optimisation framework was applied to supply energy to Spence, a copper mine located in Northern Chile. The results illustrate that an LCOE close to 100 USD·MWh^{-1} can be reached but with a significant mismatch between supply and demand. Here, a fully dispatchable system can be achieved with an LCOE close to 180 USD·MWh^{-1}. A key finding in this study is that a small fossil backup unit is selected in the optimal design of the hybrid solar power plant, mainly due to the relationships between high solar resource available, the stable demand profile, and the cost of diesel. Consequently, a post-optimisation analysis has to be done to select the most suitable design according to the user's requirements. In this last step, a set of optimal solutions can be analysed with more details in order to examine other key performance indicators not considered as objectives, but essential for the decision making.

5.4 Heat supply for low-temperature heating processes in copper mines

5.4.1 Introduction

According to Comisión Chilena del Cobre (2016), approximately 10% of the total energy used in a copper mine is to supply heat (typically by the combustion of fossil fuels in a heater) for low-temperature heating processes. In addition, according to (Quiñones *et al.*, 2020), the annual heat demand of Spence is around 80 GWh. These systems belong to copper refining and hydro-metallurgical processes. Figure 5.12 shows the power flow model with processes that require heat supply. Here, the primary heat consumer is the solvent extraction and electrowinning process, where water heaters are used to maintain a process stream between 45 °C and 60 °C (Quiñones *et al.*, 2020).

5.4.2 Optimisation Implementation

In order to supply the required heat, the heat rejection process of the power block of the CSP can be employed. The power block works with a Rankine cycle, as shown in Figure 5.13. This thermodynamic cycle is composed of four main components: (i) a pump, used to increase the pressure of the water; (ii) a heat exchanger, which uses the sensible heat of the molten salts as a heat injection to the water to produce superheated steam; (iii) a turbine-generator, that produces power from the pressure drop of the superheated steam to saturated vapour; and finally (iv) a cooling system, that condenses the stream and closes the cycle. Figure 5.13 shows the heat injection Q_{in}, the power generation W_{out}, and the heat rejection Q_{out}. Consequently, the condensation process could be coupled with a heat exchanger in order to supply the heat required to supply low-temperature heat for the hydro-metallurgical process.

5.4.3 Results analysis

The heat supply analysis from a CSP plant for the mining process that uses low-temperature heat was carried out considering the operational costs. To secure the dispatchability of heat, hot water storage tanks must be employed. Here the main difference is the primary source of energy used to generate heat. The analysis focuses on comparing the excess heat that needs to be released in the condensation process of the power block of the CSP plant, with the use of imported crude oil or diesel from China, Canada, U.S.A, Colombia, Ecuador, Brazil, Peru or Argentina, with fluctuating prices, expensive cost, highly contaminant, and a complex logistic chain, that is typically used for these applications in copper mines in Northern Chile. Nevertheless, both systems use components that can be similar, like hot water storage tanks. Then, a more detailed analysis is required to be carried out for each application. As a simple exploration, the main components for both systems are:

- Heat from diesel heaters:
  - Ships to transport crude oil or diesel from abroad to a refinery in Chile, and ships and/or trucks to transport the diesel from refineries or ports to the copper mines in Northern Chile.
  - Diesel storage tanks.
  - Heaters that burn diesel to heat water to around 90°C.
  - Hot water storage tanks and pipelines.
- Heat from excess heat from CSP plant:
  - Large pipelines to pump hot water from the CSP plant to the mining operation (the length will depend on the location of both plants).
  - Hot water storage tanks and pipelines.

Figure 5.13 represent the thermodynamic cycle to generate power through the turbine of the concentrating solar power plant. In this case, point 4 represent the thermodynamic state after the turbine and before the condenser. This saturated stream (with a steam quality close to 95%)

could be used in a heat exchanger as a heat injection for the electrowinning process. In addition, the diagram shows the enthalpies of points 3 and 4, corresponding to the input and output of the turbine. Then, the difference between points 4 and 3 represents the power that can be generated by the turbine in kJ per kg, i.e. $w_{out} = h_4 - h_3 \approx 823$ kJ·kg^{-1}. Next, if the power block produces 60 MW (1 MW = 10^3 kJ·s^{-1}), the mass flow rate required is $\dot{m} \approx 73$ kg·s^{-1}. Here we consider a heat supply to the electrowinning process of $Q_{EW} = 15$ MW$_{th}$, then, point 5 in the diagram can be calculated by $Q_{EW} = \dot{m} \cdot (h_4 - h_5)$.

Finally, the levelised cost of the thermal energy supplied to the system can be estimated by calculating the investment (IC_{HX}) of the heat exchanger unit required (as a function of the total exchange area in m^2 and the working pressure in bar) (Michalski *et al.*, 2019), and the operational and maintenance costs ($O\&M_{HX}$).

$$IC_{HX} = (2546.9 \cdot A_{HE}^{0.67} \cdot P_{HE}^{0.28} \cdot 10^{-6}) \cdot 1.18(USD) \tag{5.14}$$

$$O\&M_{HX} = 10\% \cdot IC_{HX} \tag{5.15}$$

Then, the present value of the total life cycle costs involved in the generation of each unit of thermal energy during the lifetime, considering an annual interest rate r=7%, and a lifetime T=25 years, is:

$$LCOE_{th} \approx 1.1 \frac{USD}{MWh} \tag{5.16}$$

5.4.4 Discussion

To compare with the current situation, where the heat is supplied by the combustion of diesel, considering the following parameters reported by Quiñones *et al.* (2020): lower heating value 10.63 MWh·m^{-3}, diesel cost of 54 USD·MWh$_{th}^{-1}$ in Northern Chile, heater efficiency of 78%, then, the operational cost per MWh of heat produced from the combustion of diesel is close to 70 USD·MWh^{-1}. Hence, the heat supply for low-temperature heating processes from the heat rejection of the CSP plant is highly recommended in order to reduce total operating costs. In addition, the use of solar energy to supply the heat required for low-temperature processes in Spence can avoid the emissions of approximately 40 kton CO_{2e} per year (Quiñones *et al.*, 2020). Finally, the correct design of the process needs to consider the location where the heat is available in the CSP plant, and where the heat is needed in the copper mine. Then, the pipeline and pumping systems have to be considered in a more detailed evaluation.

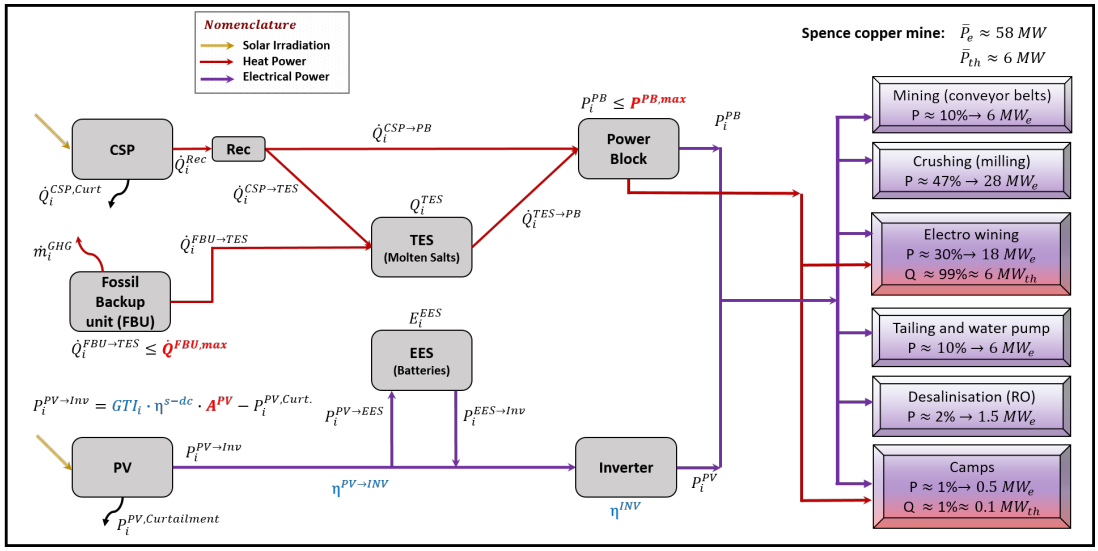

Figure 5.12: Electricity and heat demand for Spence copper mine, Atacama Desert

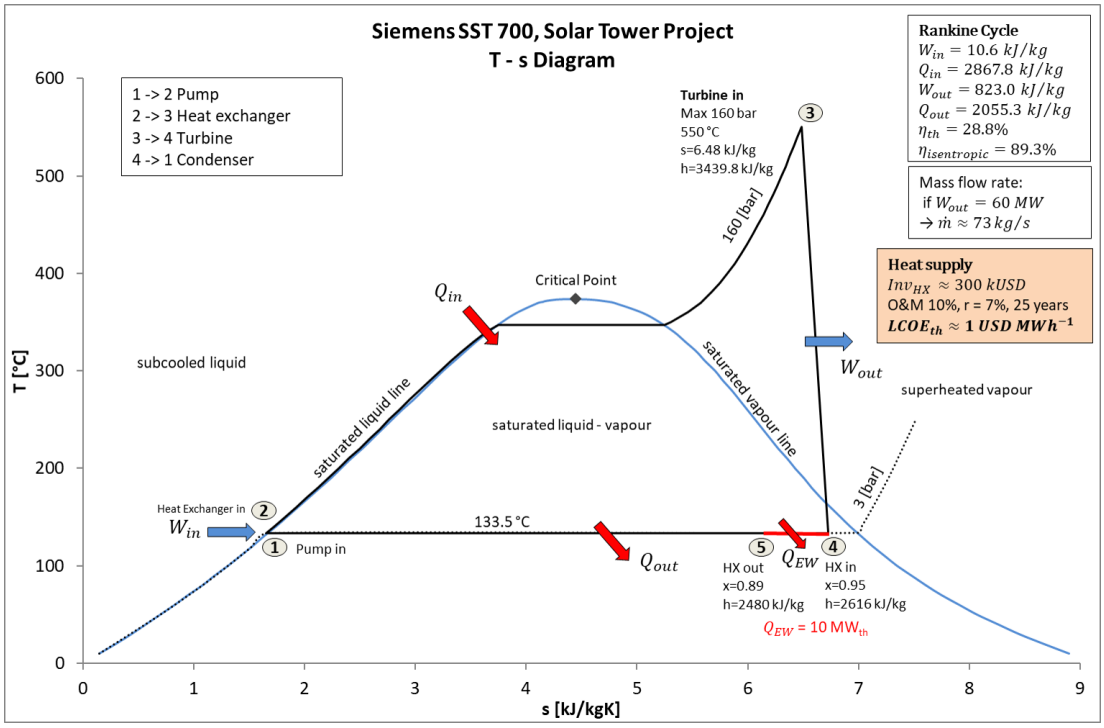

Figure 5.13: Rankine cycle representing the power block of the CSP plant

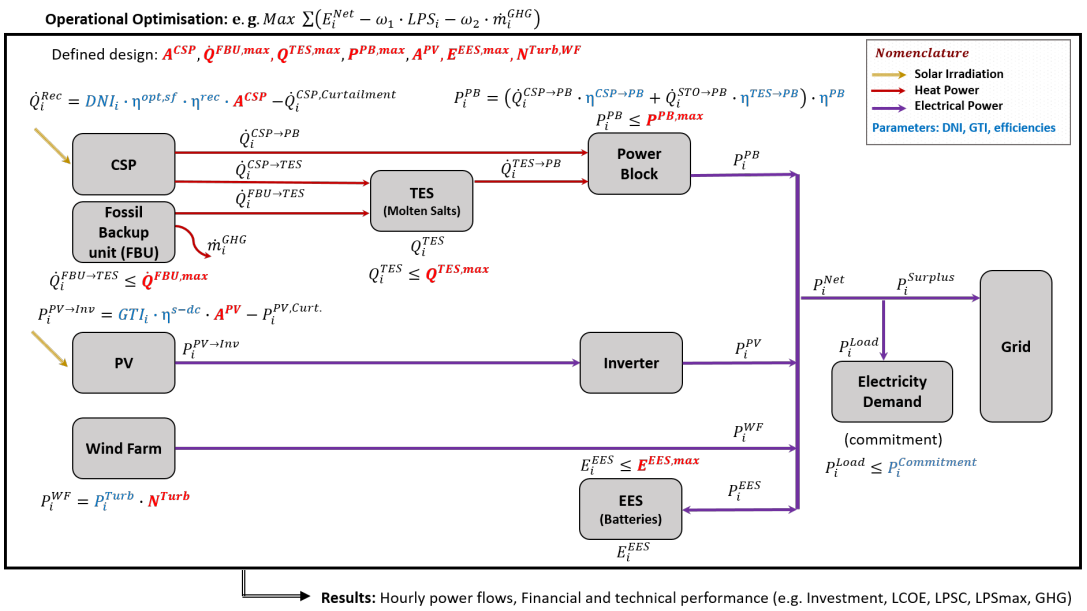

Figure 5.14: Power flow model of a hybrid solar power plant with energy storage and a wind farm

5.5 Integration of a wind farm into a hybrid solar power plant

5.5.1 Introduction

In this study, the analysis of a grid connected hybrid power plant that supplies energy to El Abra copper mine will be analysed. El Abra copper mine is a large scale copper mine located in the Atacama Desert (Figure 5.1) with an annual average power consumption close to 70 MW (Figure 5.3).

Here, the integration of a wind farm into a hybrid solar power plant is examined. The combination of wind and solar technologies reduces the variability of the natural resources used in the energy conversion process. Figure 5.14 shows the new configuration analysed in this study. The diagram represents a grid-connected power plant that integrates a CSP plant with TES, a solar PV and a wind farm. In addition, electrical batteries are employed as an electrical energy storage system to increase the dispatchability. Hence, the new design variables in this configuration are the number of turbines in the wind park (N^{Turb}), and the capacity of the battery system ($E^{EES,max}$). In terms of the operational optimisation variables, these are related to the power flows between each subsystem.

5.5.2 Optimisation Implementation

The information used to model the wind farm in the Python code for the design and operational optimisation stages was obtained from a wind park in operation located in the Atacama Desert. This wind farm is known as Sierra Gorda wind farm, and its location is shown in Figure 5.1. The following is a summary of the main data:

- Sierra Gorda Wind Farm
- Location: Antofagasta Region, Chile $\approx$ S 22° W 69°
- Wind Resource (Ministerio de Energia and Universidad de Chile, 2016)
  - Average density air: 0.91 $kg\ m^{-3}$
  - Average wind speed: 6.1 $m\ s^{-1}$
- Wind Farm (Servicio de Evaluación Ambiental, 2014)
  - 56 wind turbines
  - Gamesa G114-STD, 2 MW nominal power
  - Total investment: 260 MUSD

Figure 5.15 displays the daily average wind speed in the location under consideration. The figure illustrates a more abundant wind resource during winter months (July-September), compared with the solar irradiation that is more abundant during summer. It is expected that this difference is beneficial in the integration of wind with solar technologies. The Matrix 5.17 represents the correlation matrix between the solar resource (DNI and GTI) and the wind resource. Here, a high correlation between DNI and GTI represents the availability of solar resource during the day and the direct relationship between DNI and GTI. On the contrary, the low correlation between solar and wind resources represents the independent relationship between the energy conversion capacities of both technologies. In the case that a permanent power supply is required, a low correlation between the natural resources means that the synergies between the technologies could play an essential role in the optimal operation and affordability of the power plant.

$$corr(X,Y) = \begin{array}{c} \\ \text{DNI} \\ \text{GTI} \\ \text{Wind} \end{array} \begin{array}{c} \begin{array}{ccc} \text{DNI} & \text{GTI} & \text{Wind} \end{array} \\ \begin{bmatrix} 1 & 0.912 & -0.004 \\ 0.912 & 1 & -0.056 \\ -0.004 & -0.056 & 1 \end{bmatrix} \end{array} \tag{5.17}$$

The power curve shown in Figure 5.16 was created by using the data available from the manufacturer (Siemens, 2018), and integrated into the operational optimisation model. The polynomial function presented in the figure relates the output power of the turbine to the wind speed. Thus, this function is used in the model to estimate the power generated by each turbine based on wind speed.

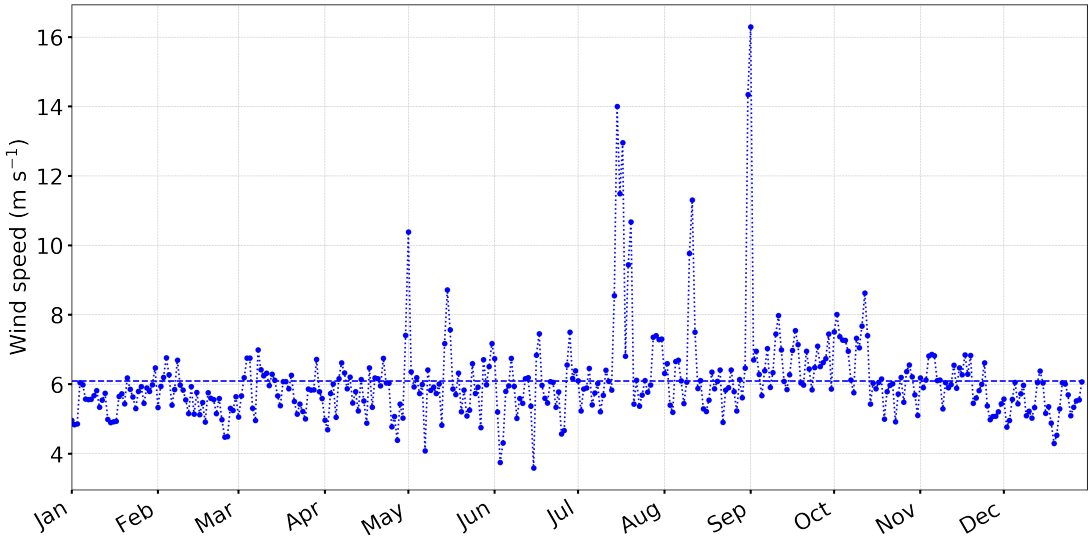

Figure 5.15: Wind speed Atacama Desert (at 91 m height), daily average

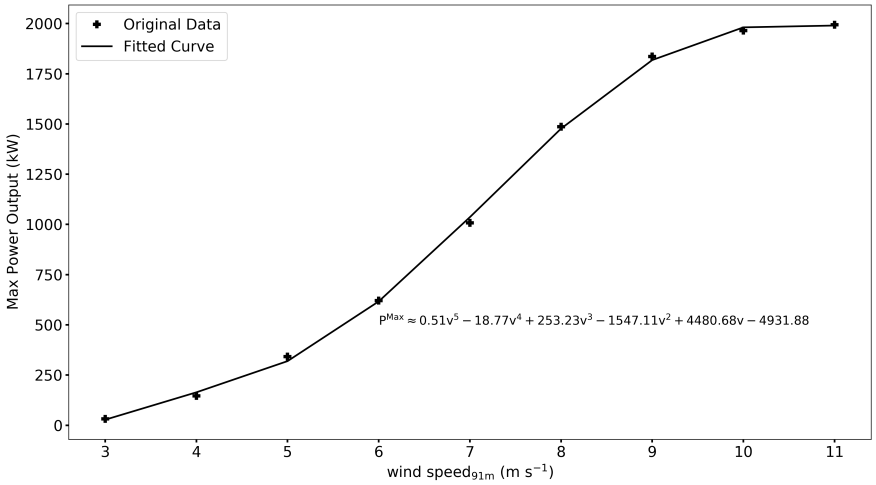

Figure 5.16: Power curve of a Siemens Gamesa Turbine, 2 MW, 90 m

Table 5.8: Variables of the design optimisation model of a hybrid solar power plant with a wind farm

Solar Power Plant			Wind Farm		
Description	Variable	Unit	Description	Variable	Unit
Area solar field, CSP	$A^{CSP,SF}$	m^2	Number of turbines	N^{Turb}	units
Capacity TES	$Q^{TES,Max}$	MWh	Capacity battery system	$E^{EES,Max}$	MWh
Capacity Power block	$P^{PB,Max}$	MW			
Capacity FBU	$Q^{FBU,Max}$	MW			
Area solar field	$A^{PV,SF}$	m^2			

Table 5.8 shows the variables considered in the design optimisation stage. Here, the multi-objective design optimisation stage optimises the following objectives: (i) levelised cost of energy; (ii) greenhouse gas emissions; and (iii) loss of power supply capacity. Finally, in order to link both stages, the multi-objective operational optimisation by linear programming will be developed by the linear scalarisation method, according to:

$$Max \quad E_i^{Net} - \omega_1 \cdot LPS_i - \omega_2 \cdot GHG_i^{FBU} \tag{5.18}$$

In this case, a third objective is added to the analysis. The incorporation of a third objective increases the complexity of the selection of the best point in the Pareto optimal solutions. In order to simplify this decision, a number of designs were evaluated, considering different combinations of ω_1 and ω_2. The results concluded that $\omega_1 = 1$ and $\omega_2 = 1$ are suitable scaling factors that simultaneously select an operational strategy that maximise the energy dispatched, minimise the loss of power supply, and minimise the greenhouse gas emissions.

5.5.3 Results analysis and discussion

In order to calculate the benefits in the integration of wind with solar technologies, two different case studies were evaluated. The first case study corresponds to a hybrid solar power plant with TES, fossil backup and EES. Then, the second configuration considers the integration of a wind farm. Figure 5.17 displays the three-dimensional Pareto non-dominated solutions. As can be observed, the integration of a wind farm allows an improvement of both technical and financial performance. This enhancement can be assessed by the displacement of the points and curve towards the bottom left corner of the diagram, which is the desirable zone. To have a more accurate comprehension and contrast, Figure 5.18 exposes the performance (using normalised values) of 4 different designs. Two of them are hybrid solar technologies, and two integrate also a wind farm with the solar power plant. These four designs are shown in Figure 5.17 highlighted with red circles, corresponding to designs with LPSP close to 0.5 and 1%. First, for the same level of dispatchability, the integration of wind allows a decrease in the LCOE of almost 10 USD·MWh^{-1}. This reduction is achieved by the integration of 28 or 29 wind turbines, and a decrease in most of the components of the hybrid solar power plant (the number

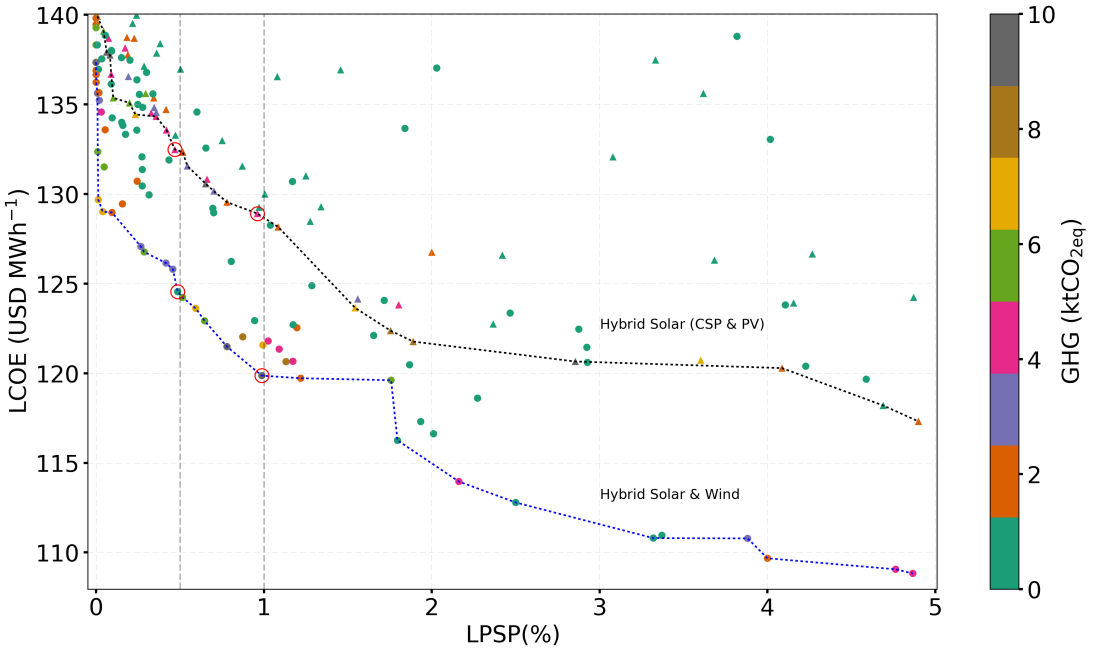

Figure 5.17: Design optimisation results of a hybrid solar power plant with a wind farm

of heliostats, the capacity of the power block, the capacity of the fossil backup unit, and the number of PV modules). The results also show that a small battery system is suggested in both configurations. For example, a 38 MWh battery system (as illustrated in the figure) can supply power for about 32 minutes in case a power of 70 MW is required (equivalent to El Abra's average power consumption). Finally, despite that the investment is not considered as an objective in the design optimisation stage, it is comparable for both alternatives.

It is worth to mention that each Pareto optimal set of solutions is achieved in around 40 h (using the computer detailed in Section 3.7). Thus, in order to reduce the computational time required to perform the design optimisation by genetic algorithms, a data clustering technique is proposed and studied in Appendix A. Then, the data clustering framework developed will be evaluated and compared with the results presented in this section.

5.6 Conclusions

This chapter investigates synergies of technology integration by the analysis of different case studies. The configurations studied were located in the Atacama Desert in Northern Chile. Here, off-grid and grid connected power configurations that supply energy to two large-scale mining operations were investigated.

First, due to the low cost of solar PV, and the expected reduction in the cost of batteries, Section 5.2 analysed the combination of a solar power plant with thermal and electrical energy storage,

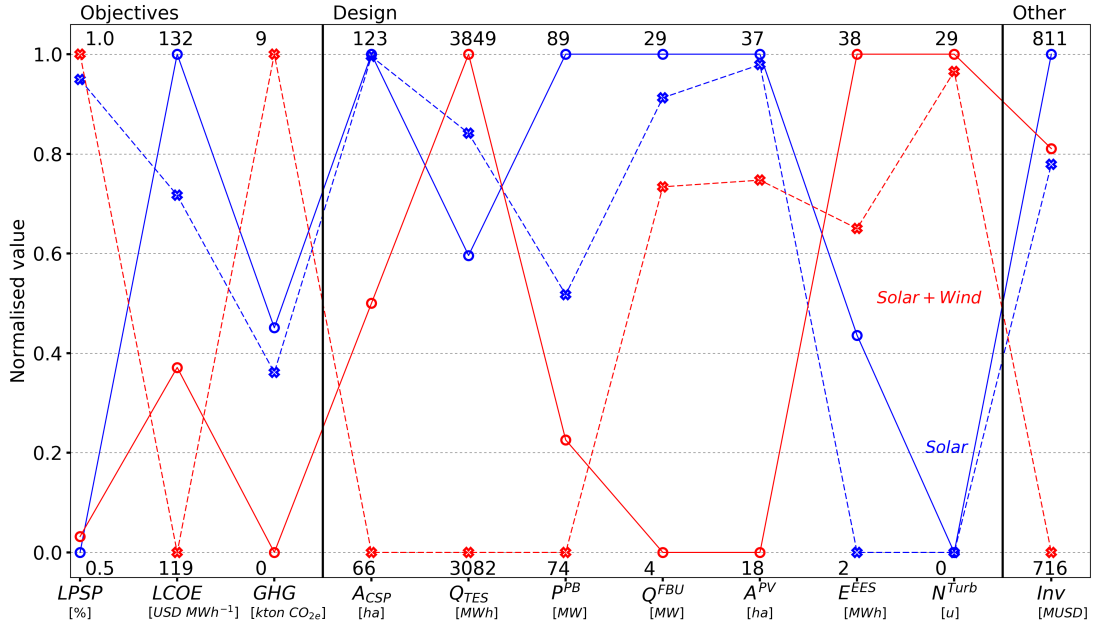

Figure 5.18: Performance of selected optimal designs of a hybrid solar power plant with a wind farm

and a long-term cost analysis was addressed. The results confirm that currently, CSP with TES is the most competitive technology to provide affordable and dispatchable power. However, due to the extreme reduction expected in the cost of EES systems, a shift to PV with EES is anticipated.

Second, some studies suggest that the integration of a fossil backup unit is key to increase the dispatchability and affordability of solar power technologies. Section 5.3 analysed the integration of a fossil backup unit to supply heat to the thermal energy storage system of the CSP plant. In this study, an off-grid configuration was considered; hence, the dispatchability becomes a crucial variable. An important finding revealed in this analysis is that the optimal design of dispatchable hybrid solar power plants considers a small fossil backup unit. This outcome can be related to the high levels of solar irradiation, the constant power demand, and the high costs of diesel in the Atacama Desert.

Section 5.4 evaluated the heat supply for low-temperature mining processes from the heat rejection of the Rankine cycle of the CSP plant. The technical feasibility of this project depends on the location of the power plant and the mining processes that require heat. Nevertheless, the high cost of diesel in the Atacama Region is a fundamental variable. The results suggest that the heat supply for low-temperature heating processes from the heat rejection of the CSP plant is highly recommended to reduce operational costs of mining processes.

Finally, due to CSP and PV plants work with solar irradiation, the integration of a Wind farm is analysed in Section 5.5. The combination of these technologies decrease the variability of the

renewable resource used in the hybrid power plant. The results confirmed that the deployment of hybrid power plants considering three (or more) different renewable technologies enhance the competitivity of distributed sustainable power plants.

Chapter 6

Multi-objective operational optimisation of a hybrid solar power plant with thermochemical energy storage

The work presented in this chapter is based on an article published in the Journal Energy Conversion and Management (Bravo, Ortiz, Chacartegui, and Friedrich, 2019)

In this work, C.Ortiz provided details and results of Aspen simulations, and all authors co-operated with the analysis.

6.1 Introduction

To increase the penetration of solar technologies in the power sector, the integration of energy storage is essential. Concentrated solar power technologies (CSP) integrated with energy storage are key systems that could provide clean and dispatchable energy (Ortiz *et al.*, 2017). Thermochemical energy storage (TCES) integrated with concentrated solar and photovoltaic power plants, has the potential to provide dispatchable and competitive energy. Hence, in this chapter, the integration of TCES into CSP plants is analysed and optimised. Here the multi-objective operational optimisation method is applied to find the best operational strategy of a hybrid solar power plant with a TCES system. The model uses the typical meteorological year to optimise one-year hourly operation.

The results demonstrate that the integration of a calcium-looping process as TCES in a concentrated solar power plant provides dispatchability and, when hybridised with PV, enhances its competitiveness with current electricity prices. The low mismatch between supply and demand, even when a fixed commitment is required throughout the year, together with high overall efficiency, indicate that the integration of calcium-looping in hybrid solar power plants

is an opportunity to increase the penetration of solar energy in the power sector. Through the optimisation framework presented, a seasonal energy storage analysis could be developed.

TCES uses the heat of reaction of a reversible chemical reaction that absorbs and rejects energy depending on the operation (Pardo *et al.*, 2014). Calcium-Looping (CaL) is a promising TCES technology that can be integrated into concentrated solar power plants. CaL is based on the calcination/carbonation of calcite, and it works at high temperatures. Hence, it is an attractive and efficient technology to integrate into CSP plants (Ortiz *et al.*, 2019a). This process is based on the following reaction that involves calcium carbonate ($CaCO_3$), calcium oxide (CaO) and carbon dioxide (CO_2):

$$CaCO_{3(s)} \rightleftarrows CaO_{(s)} + CO_{2(g)} \qquad \Delta\hat{H}_r^{\circ} = 178\ kJ\ mol^{-1} \tag{6.1}$$

The integration of CaL as an energy storage system into CSP plants has several benefits. For instance, because of its high energy density, a relatively small storage volume has the potential to operate as long-term energy storage. Besides, the precursor materials used in the process, such as limestone or dolomite, are an abundant, non-corrosive, non-toxic and cheap (Chacartegui *et al.*, 2016). In order to decrease the deactivation of the material due to a multi-cyclic operation, modified materials can be used in the process (Obermeier *et al.*, 2017). In this context, Ortiz *et al.* (2019a) compares different materials and conditions to enhance the multicycle CaO conversion. Hence, the integration of a CaL in CSP plants is a suitable sustainable alternative to provide dispatchable power.

In order to evaluate the dispatchability of solar power plants integrated with CaL as a TCES, current studies focus on the simulation of the operation using a typical period to estimate the operation of a whole year (Ortiz *et al.*, 2018a; Fernández *et al.*, 2019b), e.g. one or two representative days with hourly time steps. Nevertheless, these studies suggest that, in order to consider daily and seasonal variability of the solar resource, a one year with hourly time steps simulation is crucial to evaluate the operation of the solar power plant under variable solar irradiation (Ortiz *et al.*, 2018a).

Consequently, the multi-objective operational optimisation of the hybrid power plant with CaL considering one-year hourly time-steps is the main focus of the present chapter. Here the operational optimisation aims to find the best operational strategy by maximising both the energy supplied and the dispatchability, two goals that during some periods of the year are conflicting objectives.

6.2 Methodology, plant modelling

This study exploits the capacity of linear programming to optimise the annual performance of the power plant, taking into account the daily and seasonal variability of the solar resource. The CaL process is modelled as mass and energy balances as a function of the mass flow rate and temperature, as explained in Chapter 3. Besides, the thermodynamic properties also depend on the temperature. Then, the temperature of each process is fixed and defined according to a non-linear study published by Ortiz *et al.* (2018a). The Pareto frontier resulting from the multi-objective optimisation method represents the trade-off between the net energy dispatched ($GWh{\cdot}year^{-1}$) (that influences the levelised cost of the electricity), and the mismatch between supply and demand, estimated here through the loss of power supply capacity ($GWh{\cdot}year^{-1}$). Finally, to handle both objectives, the linear scalarisation method is applied.

Figure 6.1 represents the process involved in the generation of electricity through the use of a CaL process integrated with a CSP and hybridised with a PV plant. The CSP-CaL scheme (and nomenclature) is taken from the base case proposed by Ortiz *et al.* (2018a). Each stream is represented by a letter and a number, where the letter defines the type of substance (g: CO_2; c: CaO; s: solids CaO+$CaCO_3$), and the number indicates the position of the stream in the diagram. In addition, the diagram shows the temperature of each process according to the non-linear analysis (Ortiz *et al.*, 2018a). The Python model developed uses real solar irradiation as input, and by linear programming, optimises the annual hourly operation of a defined power plant (CSP with CaL plus PV). In this study, the algorithm optimises the operation, while the optimal design or sizing of the components is performed in Chapter 7. Consequently, the capacity of each component (shown in the black ovals in the figure) is an input to the model.

In the model, the CSP is a solar tower technology that provides heat to carry out the endothermic reaction that splits $CaCO_3$ into CaO and CO_2 at 900 $^{\circ}C$, according to equation 6.1. The location where this reaction takes place is known as calciner and coincides with the solar receiver. Full calcination is assumed in the model (Meier *et al.*, 2005). CaO exiting the calciner is stored at atmospheric pressure and high temperature in an insulated tank. The atmosphere inside the CaO tank is regulated by injecting an inert gas such as N_2 or He, in order to reduce the presence of CO_2 and avoid partial carbonation (Ortiz *et al.*, 2019a). Moreover, it must be highlighted that the CaO tank is maintained at 900 $^{\circ}C$ and the kinetics of carbonation near to the equilibrium is notably slow, which reduces the likelihood to have partial carbonation inside the CaO tank (Ortiz *et al.*, 2018c; Kyaw *et al.*, 1998). The second stream that exits the calciner, consisting of pure CO_2 at 900 $^{\circ}C$, first exchanges heat in a Heat Recovery Steam Generator (HRSG) to produce electricity. Next, the CO_2 leaves the heat exchanger and it cooled to approximately 40 $^{\circ}$C to improve the efficiency of the compression process that is occurring afterwards. After the main compressor, this stream (now with a pressure of approximately 3 bar) has two possibilities: (i) it can be used in the carbonator to produce the reversible exothermic reaction (carbonation) where it reacts with CaO from the CaO storage tank forming

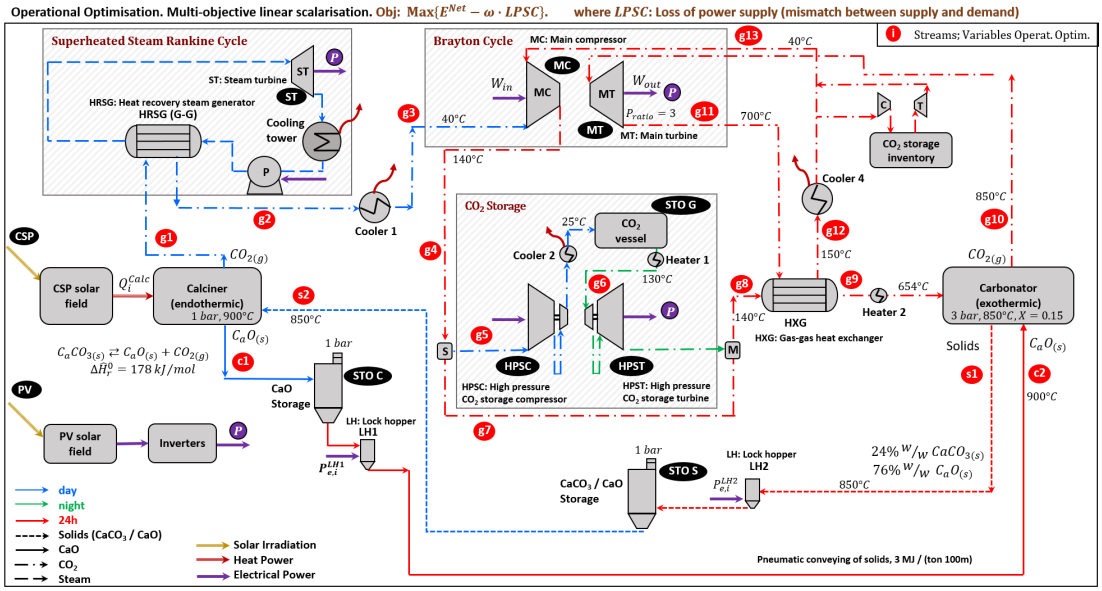

Figure 6.1: Mass and energy flows model of a hybrid solar power plant with calcium-looping TCES system

$CaCO_3$ and releasing heat according to the previous reaction; (ii) it can be stored at high pressure in a 75 bar vessel, by using a multi-stage compressor. Then, when power needs to be dispatched, this high-pressure stream first drives a turbine to generate electricity and then mixes with the stream flowing from the power loop. This flow is heated in a regenerative system, which reaches around 654 °C and is then sent to the carbonator to drive the exothermic reaction described above. The storage of solids is carried out under atmospheric pressure. A mechanical conveyor system is considered here to transport the material. Hence, in order to decouple the pressure between solids storage tanks (1 bar) and carbonator (3 bar), lock hoppers are used in the conveyor system (Ortiz *et al.*, 2018a).

The CaO conversion (X) in the carbonator is highly dependent on the reactor conditions (pressure, temperature, CO_2 volume fraction) and the CaO precursor used (Ortiz *et al.*, 2019a). In this work, a conservative value of X=0.15 is assumed. The heat released from the reaction is taken by the CO_2 that is present in excess in the carbonator. After that, this pure CO_2 stream runs a gas turbine (main turbine) to produce electricity that is used to drive the main compressor, and the surplus is dispatched to the network. The CO_2 leaves the turbine at 1 bar and approximately 700 $^{\circ}C$ and then it exchanges heat in the regenerative system to increase the temperature of the CO_2 stream before entering the carbonator. Then, the CO_2 flow described above is cooled to 40 $^{\circ}C$ to be compressed in the main compressor, closing the cycle (see Figure 6.1).

6.2.1 Operational optimisation by linear programming

The mass and energy balances presented in Chapter 3 were used here to model the operation of the main processes of the power plant. The main components are the solar field (heliostats and receiver), reactors (carbonator and calciner), heat exchangers, coolers, compressors and turbines.

The main objective of this research is to model the operation of one year (8760 time-steps), considering the hourly solar resource of a typical meteorological year. To linearise the equations presented above, the temperatures of the processes are fixed, according to the parameters and results presented in (Ortiz *et al.*, 2018a), were non-linear models are used to simulate the operation of the CSP plant with CaL. In a power plant, this may be possible by the instrumentation engineering, through the definition and control of the temperatures of each process. Hence, the operational optimisation routine optimises the mass flow rate of some streams and calculate those that are dependent (because there are direct relationships between some streams), in order to optimise the hourly operation.

The optimisation objectives can be defined according to user preferences. In this study, for a fixed power plant, the objectives of the operational optimisation are defined by:

- Maximisation of the net energy supplied during one year of operation (typical year), where the hourly net power dispatched is defined by:

$$P_i^{Net} = P_i^{Generated} - P_i^{Own\ consumption} \tag{6.2}$$

- Minimisation of the loss of power supply (LPS), which estimates the mismatch between the energy supplied and the commitment, i.e. the net power to be dispatched by the power plant, according to the following equation:

$$LPS_i = \begin{cases} P_i^{\text{Commitment}} - P_i^{Net} & , P_i^{\text{Commitment}} > P_i^{Net} \\ 0 & , \text{otherwise.} \end{cases} \tag{6.3}$$

6.2.2 Scalarisation method

In order to handle both objectives, and according to the results presented in Chapter 4, here, a linear scalarisation method is implemented. In Chapter 4, it was found that the linear scalarisation method works faster than the epsilon (ε) constrain method, obtaining the same Pareto frontier. The only precaution is to choose a suitable scaling factor (ω) to scale the second objective. Therefore, the function that describes the multi-objective optimisation problem in the present study is:

$$\text{maximize} \quad \sum_{i=1}^{I} \{P_i^{Net} \cdot \Delta t_i - \omega \cdot LPS_i \cdot \Delta t_i\} \tag{6.4}$$

6.3 Case Study

To compare the results from the evaluation of the model with Aspen simulations available and published for Seville, in addition to that a prototype is currently being built in the University of Seville, the power plant under analysis will be located in Seville, Spain ($\approx$ N 37.4 °, W 6.2 °, elevation 72 m). Public data available in the "Photovoltaic Geographical information system" (PVGIS project) of the European Commission Joint Research Centre (European Commission, 2017) is used in this study.

6.3.1 Input data, data quality and preparation

To run the model, the following hourly annual input data is required:

- Direct normal irradiation (DNI)
- Optical efficiency solar field (η^{opt})
- Global tilted irradiation (GTI)

In the present study, the typical meteorological year (TMY) is used as a representative year. Then, the direct normal irradiation is used to model a solar tower plant in SAM 2019 (NREL, 2018) to estimate the hourly optical efficiency of the heliostat field of the solar tower system. While values of hourly optical efficiency during summer days are from 0.42 to 0.6, winter day values are between 0.3 to 0.55, and the annual average value ($\bar{\eta}^{opt}$) is around 0.53.

According to the previous equations and relations, the model also needs a series of technical and financial parameters. Among the technical parameters necessary to run the model are: efficiencies of each component from NREL (2018), thermodynamic properties of the elements (as presented in Chapter 3), and operational temperatures and pressures of each process from Ortiz *et al.* (2018b). In addition, the model considers thermal efficiencies and heat losses in the carbonator and heat exchangers. Storage tanks are modelled by mass balances, and heat losses are considered according to the design of the tanks. Here, the insulation of the storage tanks is designed to achieve a heat transfer coefficient in the order of 150 $\mathrm{W{\cdot}m^{-2}}$, and its thermal losses are included as electrical consumption of the power plant, in order to consider the energy needed if heat injection is required.

Financial parameters used in the model are investment costs (IC) and operational and maintenance costs (O&MC) of the solar tower, the CaL system and the photovoltaic system. The relations used to calculate the IC and O&M costs are summarised in Section 3.6.3.

Finally, the hourly power that the power plant has to dispatch (P_i^{demand}) is required to evaluate the dispatchability.

Table 6.1: Cases analysed for the validation with Aspen Plus^{TM}

	$\dot{Q}^{calciner}$	Solar multiple	CaO carbonation conversion
Case A	100 MWh_{th}	3	0.15
Case B	33 MWh_{th}	1	0.15
Case A	100 MWh_{th}	3	0.3

6.3.2 Validation of simulation methodologies and results

In order to validate the model, different configurations based on Ortiz *et al.* (2018a), were evaluated using Aspen Plus^{TM} and optimised by the model written in Python. Table 6.1 defines three different cases studied. The results are exposed in Table 6.2, these correspond to mass flow rate of different streams ($kg \cdot s^{-1}$) and the energy conversion in turbines, compressors, and heat exchangers (MW). As can be seen in the table, the results presented indicate that differences between the values obtained through the Python and Aspen models are less than 1%.

Table 6.2: Validation with Aspen Plus^{TM}

		Case A		Case B		Case C	
item	unit	Aspen	Python	Aspen	Python	Aspen	Python
s2	$^{kg}/_{s}$	216.6	215.8	72.2	71.6	125.6	125.2
c2	$^{kg}/_{s}$	64.6	64.3	64.6	64	33.9	33.8
g9	$^{kg}/_{s}$	133.9	134	133.8	134.4	132.6	132.7
g13	$^{kg}/_{s}$	126.2	126.5	126.2	126.8	124.6	124.7
ST	MW	5.8	5.8	1.9	1.9	6.1	6.1
MC	MW	12.9	12.8	12.9	11.5	12.8	12.7
MT	MW	23.9	24	23.9	24	23.6	23.6
HPSC	MW	5.3	5.3	0	0	5.6	5.6
HPST	MW	0	0	0	0	0	0
HXG	MW	75.9	75.8	75.9	76	75	74.8
P^{Net}	MW	8.2	8.2	11.3	12.5	9.3	9.3

6.3.3 Linear scalarisation method, definition of ω

In the present study, as shown in Table 6.3, different optimisation routines with different ω were evaluated (according to Section 6.2.2). According to equation 6.4, ω =0 correspond to the maximisation of the energy delivered as a single objective. On the other extreme, when $\omega \to \infty$ the optimisation focuses on the minimisation of the loss of power supply. Table 6.3 shows that $\omega = 1$ is a suitable scaling factor, that gives the same weight to both objectives, allowing a simultaneous optimisation of total energy supply and dispatchability. This result can be explained because both objectives have the same units and the same order of magnitude in each time step. In the model, there are no penalties or costs for energy not served. In other cases, for instance, when the cost associated with unserved energy is greater than the cost of

Table 6.3: Results of the multi-objective linear scalarisation method

Objective	unit	$\omega = 0$	$\omega = 1$	$\omega \to \infty$
E^{Net}	GWh·year^{-1}	118.2	117.6	115.6
$LPSC$	GWh·year^{-1}	24.6	21.0	18.9

energy generation, a large scaling factor may be more appropriate.

6.3.4 Simulation conditions

According to Figure 6.1, to optimise the annual operation of the power plant, the equipment sizes have to be known. This section presents a process to estimate the capacities of each main component using the equations and relationships described in Chapter 3. In Chapter 7, this method will be improved by applying the two-stage optimisation framework.

To establish a case study it is necessary to define the capacities of the main components of the solar power plant. The process starts with the definition of the expected average power dispatched by the CSP+CaL system. In this case, a capacity of 15 MW is defined. Then, according to the estimated global efficiency value reported in Ortiz *et al.* (2018a) ($\eta_{CSP,Rec} = 0.321$), it is possible to estimate the average power needed in the calciner: $\bar{Q}^{Calciner} \approx 47\ \mathrm{MW}_{th}$. Next, using equation 6.5 modified to take into account the average thermal power available in the calciner ($\bar{q}^{Calciner}$) per square meter of the heliostat field, it is possible to have an estimated value for the heliostat aperture area (A^{CSP}), as shown in equation 6.6:

$$Q_i^{Calciner} = DNI_i \cdot \eta_i^{opt,sf} \cdot \eta^{receiver} \cdot A^{CSP} - Q_i^{Curtailment} \tag{6.5}$$

$$\bar{Q}^{Calciner} = A^{CSP} \cdot \bar{q}^{Calciner} = 47{,}000\ kW \tag{6.6}$$

where

$$\bar{q}^{Calciner} = \frac{\sum_1^{8760} \eta_i^{opt,sf} \cdot \eta^{receiver} \cdot DNI_i}{8760} \approx 0.1089\ \frac{kW}{m^2} \tag{6.7}$$

By using SAM (NREL, 2018) for the simulation of a solar tower located in Seville, the average thermal power in the receiver per square meter of heliostat reflective area is approximately 0.1032 kW·m^{-2}. Hence,

$$A^{CSP} \approx 430{,}000\ m^2 \tag{6.8}$$

Then, with this solar field aperture area, the design capacity of the calciner is calculated considering the equation given above (with optical efficiency of the solar field: $\eta^{opt,sf} \approx 0.53$,

Table 6.4: Capacities of the main components of the CSP with CaL obtained by Aspen

Name	Nomenclature	Value	unit
Capacity steam turbine	P^{ST}	10	MW
Capacity main CO_2 compressor	P^{MC}	23	MW
Capacity main CO_2 turbine	P^{MT}	43	MW
Capacity high pressure CO_2 compressor	P^{HPSC}	10	MW
Capacity high pressure CO_2 turbine	P^{HPST}	2	MW

receiver efficiency: $\eta^{receiver} = 0.85$, and direct normal irradiation design: DNI_{design} =0.95):

$$Q^{Calciner,design} \approx 180\ MW_{th} \tag{6.9}$$

After that, in order to find the capacities of each component mentioned in section 6.3.4, this thermal power is used as input in the Aspen model ($Q^{Calciner} = 180\ \mathrm{MW}_{th}$). Then, the capacities for each component were obtained and these are shown in table 6.4.

Then, a number of storage hours can be defined to combine with the specific power production (ξ) defined in Chapter 3, to estimate the capacity of the CaO storage tank (with $\rho_{CaO} \approx 3370$ kg·m^3 (Valverde *et al.*, 2015), and values of porosity and packing density of solids equals to 0.5 and 0.6 respectively). For instance, with 20 hours of storage:

$$\xi_{i,P} = 0.053\ \frac{MWh}{ton_{CaO}} = \frac{15\ MW \cdot 20\ h}{STO^{CaO} \cdot \rho_{CaO}} \tag{6.10}$$

$$\rightarrow STO^{CaO} \approx 5650\ m^3 \tag{6.11}$$

Now, considering the following properties in the storage tanks: $\rho_{CaCO_3} \approx 2700$ kg·m^3 (porosity = 0.5) (Valverde *et al.*, 2015), $\rho_{CO_2} \approx 762$ kg·m^3, and a CaO conversion X=0.15, an estimation of the capacity in m^3 of the two other tanks can be calculated as a ratio of STO^{CaO}, where $V_{m,i}$ is the molar volume of substance i, defined as the volume occupied by one mole of component i in the storage tank, by the following relationships:

$$V_{m,i} = \frac{MW_i}{\rho_i} \tag{6.12}$$

$$STO^{Solids} = STO^{CaO} \cdot \left(x \cdot \frac{V_{m,CaCO_3}}{V_{m,CaO}} + (1-x) \right) \approx 5735\ m^3$$

$$STO^{CO_2} = STO^{CaO} \cdot \left(x \cdot \frac{V_{m,CO_2}}{V_{m,CaO}} \right) \approx 875\ m^3 \tag{6.13}$$

As detailed in Section 3.4.2, the storage tanks of the thermochemical energy storage system

are initially fully charge. This means that during first hours of operation, the power plant can dispatch energy even without solar irradiation. Then, to calculate the actual net energy dispatched, the difference between the available energy in the initial and final periods of the annual operation is calculated. Hence, the state of charge for each tank at the start of the operation (i=0) is defined as:

$$SoC_{i=0} = \begin{cases} 100\% & CaO \text{ tank} \\ 0\% & \text{Solids } (CaO + CaCO_3) \text{ tank} \\ 100\% & CO_2 \text{ vessel} \end{cases} \tag{6.14}$$

To calculate this difference, an average energy density factor (ξ) is used, defined as the rate between net power dispatched and CaO mass flow rate that feeds the carbonator:

$$\xi_i \left(\frac{MWh}{ton_{CaO}} \right) = \frac{P_i^{net}(MW)}{\dot{m}_{c2}(\frac{kg_{CaO}}{s}) \cdot 3600(\frac{s}{h}) \cdot \frac{1}{1000}(\frac{ton}{kg})} \tag{6.15}$$

From the analysis of the results of different optimised designs, $\xi_i \approx 0.053$ MWh·ton$_{\text{CaO}}^{-1}$ was estimated.

Finally, as explained in section 6.2.2, the model was evaluated with $\omega = 0$ to maximise the energy dispatched and the capacities of all components indicated above. By the operational optimisation routine, it was calculated that the net energy delivered in one year is 118.4 GWh, and the average power dispatched is 13.5 MW. Therefore, for the following calculations, the power commitment will be defined as P_i^{commit} =13.5 MW for all hours of the year.

6.4 Optimisation results and analysis

Nine configurations were analysed to compare the results of different designs, which are summarised in Table 6.5. All configurations are initially composed of a 430,000 m^2 of heliostats field area. The first estimated capacities calculated above are shown as "BC" (base case) configuration. The columns of Table 6.5 show the name given to the configuration (Base Case, A to H). Then, the power capacity of the steam turbine, the main compressor and turbine capacities, next, the capacities of the high-pressure compressor and turbine, columns 8 to 10 show the capacities of the storage tanks, and finally, the photovoltaic solar field area.

In each row, different designs are presented, which are related to the Base Case, and all the configurations have the same aperture area of the heliostat field. For example, in configuration A the capacity of each component was increased by 20%, while in configuration B by 50%. Compressors and turbines of configuration C increase by 50%, and storage remains the same. Capacities of the storage systems in configuration D were multiplied by 3. Configuration E, F,

Table 6.5: Configurations analysed in the operational optimisation analysis of a hybrid solar power plant with CaL TCES. All configurations consider a CSP plant composed of 430,000 m^2 of heliostats field area

Conf. name	P^{ST} MW	P^{MC} MW	P^{MT} MW	P^{HPSC} MW	P^{HPST} MW	STO^{CaO} m^3	STO^{Solids} m^3	STO^{CO_2} m^3	A^{PV} 10^4 m^2
BC	10	23	43	10	2	5650	5735	875	0
A	12	28	52	12	2.5	6780	6880	1050	0
B	15	35	65	15	3	8475	8600	1310	0
C	15	35	65	15	3	5650	5735	875	0
D	10	23	43	10	2	16950	17200	2625	0
E	15	35	65	15	3	8475	8600	1310	10
F	15	35	65	15	3	8475	8600	1310	20
G	15	35	65	15	3	8475	8600	1310	30
H	15	35	65	15	3	8475	8600	1310	40

G and H are similar to B (50% increase in the capacity of each component), but now integrated with 10,000, 20,000, 30,000 and 40,000 m^2 of a photovoltaic solar field area.

The results of the operational optimisation for all configurations described in Table 6.5 are presented in Table 6.6. This table shows all configurations and key performance indicators proposed in Section 3.5.4.

First, the Base Case: according to Table 6.6, for this configuration and considering the typical meteorological year, the total net energy delivered to the network reaches 118 GWh (97 GWh dispatched to the commitment and 20 GWh are sent to the grid), and 18% of the commitment is not supplied. 52 GWh_{th} have to be curtailed in the solar field, and the difference between the initial and the final hour of operation was 220 MWh (equivalent to approximately 16 hours fulfilling the 13.5 MW commitment). The average net power was 13.4 MW, while the maximum power dispatched by the system was 22 MW. The capacity factor is 65%, and it is highly dependent on the capacity of the main components. As a comparison, a capacity factor of 58% was estimated by Ortiz *et al.* (2019b) for a CSP with 16 hours of TCES. In Chapter 7, the capacity factor of this hybrid solar power plant could be improved by the optimisation of the size of the units. The efficiency based on the energy used in the receiver is 32.8% (compared with 32.1 estimated by Ortiz *et al.* (2018a)), and the efficiency based on direct normal irradiation falls to 12.2%. Finally, the estimated investment is 323 MUSD, and the operational and maintenance costs are 1.9 MUSD per year, resulting in a levelised cost of energy of 252 $USD \cdot MWh^{-1}$.

Comparing the Base Case with configuration A, the results indicate that by increasing the capacities of all components by 20%, the net energy increases by 11% and the curtailment is reduced by 76%, improving the global efficiency based on the DNI. The LPSP still exceeds 15%, and although the investment increases by 2%, the LCOE is reduced by 7%. Then, configuration B (which increases all capacities by 50%), resulted in zero curtailments, which means that in

Table 6.6: Optimal operation results for configurations presented in Table 6.5

KPI	Description	unit	BC	A	B	C	D	E	F	**G**	H
E^{Net}	Net energy dispatched	GWh·year^{-1}	118	131	137	134	124	169	202	235	268
$E^{commitment}$	Energy dispatched to fulfil commitment	GWh·year^{-1}	97	100	101	98	103	107	110	111	112
E^{excess}	Energy dispatched when exceed the commitm.	GWh·year^{-1}	20	32	35	37	21	62	92	124	156
$LPSP$	Loss of power supply probability	%	18	16	14	17	13	9	7	6	5
$E^{curtailed}$	Energy curtailed	$GWh_{th}\ year^{-1}$	52	13	0	9	33	0	0	0	0
ΔE_{f-i}	Energy dif. last and first hour of operation	MWh	220	330	420	270	820	420	420	420	420
$\bar{P}^{net}$	Average net power dispatched	MW	13.4	15.0	15.6	15.3	14.1	19.3	23.1	26.8	30.6
P_{CSP}^{max}	Max. power dispatched from the CSP-CaL plant	MW	22.0	26.6	33.2	33.2	22.0	33.2	33.2	33.2	33.2
CF_{CSP}	Capacity factor CSP (CO_2Brayton cycle)	%	65	60	50	48	69	50	50	50	50
$\eta_{CSP,Rec}$	Eff. CSP considering energy in the receiver	%	33.8	33.0	33.3	33.4	32.7	33.1	33.1	33.2	33.2
$\eta_{CSP,DNI}$	Eff. CSP considering energy in the solar field	%	12.2	13.6	14.2	13.9	12.8	14.1	14.1	14.1	14.1
P_{hybrid}^{max}	Max. power dispatched from the hybrid plant	MW	22.0	26.6	33.2	33.2	22.0	44.8	58.9	74.9	91.3
Investment	Investment	MUSD	323	331	341	336	341	384	427	470	513
O&M	Operational and Maintenance costs	MUSD $year^{-1}$	1.9	2.2	2.7	2.7	1.9	2.8	3.0	3.1	3.3
$LCOE$	Levelised cost of energy	USD·MWh^{-1}	252	233	233	235	252	212	196	185	176

this configuration, the design of the CSP-CaL is oversized. These results show the importance of selecting the right equipment size for the plant efficiency, which will be addressed in Chapter 7.

When comparing configurations B, C and D, it is possible to note that, starting with the Base Case, an increase in the capacity of compressors and turbines results in more energy dispatched but a lower dispatchability and capacity factor compared with increasing the storage tank capacities. Nevertheless, a better approximation to an optimal design would be by appropriate and independent sizing of all units. Therefore, this enhances the importance of including a second optimisation stage in order to find the best design based on technical and financial performances.

Finally, configurations E, F, G and H show that the integration of a photovoltaic system is essential to reduce the levelised cost of energy, by including intermittent (non-dispatchable) but less expensive power generation. In these cases, the LCOE becomes less than 200 USD·MWh^{-1}. However, the integration of PV without a reduction in the capacities of the CSP-CaL system means a large energy generation and a large surplus that have to be dispatched to the network. For instance, in configuration G, which includes 30 hectares of PV modules, the energy dispatched to fulfil the commitment is 111 GWh (47% of total). In contrast, the excess of energy that has to be sent to the grid reaches 124 GWh (53% of total). In this case, it is possible that the dispatch of the surplus has adverse effects on the local market, and that, depending on the mechanisms of the market, the energy may not be sold at a competitive price. Nevertheless, variable electricity prices could easily be added to the model to study the interactions with the market.

In order to know the power flow profiles of a hybrid solar power plant with thermochemical energy storage, Figure 6.2 illustrates the time series of power production. The diagram shows the high amount of electricity generation during summer and the low power dispatch during cloudy days in winter. As can be seen in the diagram, during some days, the total daily dispatch is not able to cover the demand required. In addition, Figures 6.3 and 6.4 show two weeks of operation of configuration G, one week in summer and another in winter along with the solar resource. The green and orange bars of the diagrams represent the power dispatched by the PV system and the CSP-CaL, respectively. The continuous purple line and the dashed black line show the solar irradiation (direct normal and global tilted respectively), for the location under study. These results highlight that the strategy suggested by the optimisation routine is that the photovoltaic system delivers energy during the day, while the CSP-CaL stores energy to be dispatched during the night unless there is large solar irradiation available that allows the CSP-CaL to dispatch energy during day and night (in the case of summer). Besides, these results demonstrate the importance of the multi-objective optimisation technique presented. The diagram confirms that the optimised operational strategy simultaneously maximises the energy delivered and fulfil the commitment. Another crucial finding, shown in the diagram as

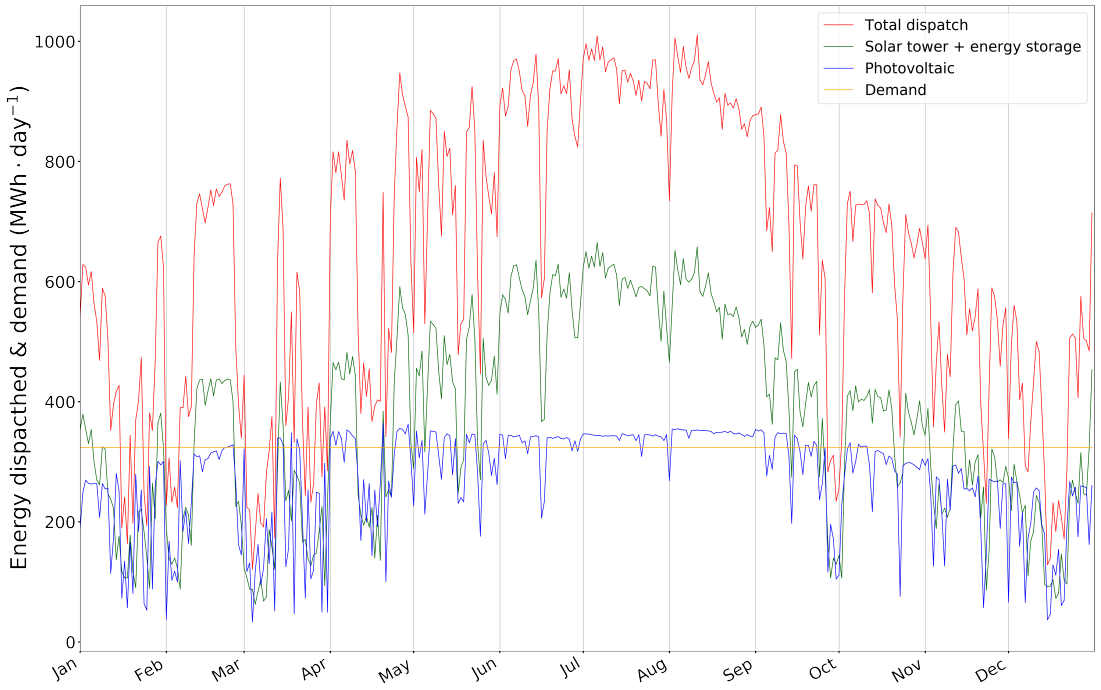

Figure 6.2: Time-series for optimal operation of the hybrid solar power plant, configuration G

Table 6.7: Financial and technical parameters considered in the sensitivity analysis

Variable	Description	Base value	Unit
$\eta^{receiver}$	Receiver-calciner efficiency	85	%
r	Annual interest rate	7	%
A^{PV}	Area photovoltaic field	30,000	m^2
κ^{Sto}	Multiplier capacities storage tanks	1	-
$\kappa^{T\&C}$	Multiplier capacities turbines and compressors	1	-
$\zeta^{Reactors}$	Multiplier investment carbonator and calciner	1	-

a dashed red line, is the state of charge of the CaO storage tank. Because the state of charge of the storage never reaches 0% during the week presented for the summer, and despite that, there is no restriction in the maximum capacity that can be dispatched, it could be inferred that the storage system is oversized compared with the capacities of compressor and turbines. Besides, the operation profile during winter suggests that some capacities could be increased in the CSP-CaL system in order to increase the dispatchability of the hybrid plant.

6.4.1 Sensitivity analysis

In this section, a sensitivity analysis will be carried out by varying different financial and technical parameters, as well as the design of some of the components of configuration G presented in Table 6.6. The parameters selected for the sensitivity analysis and its original values are shown in table 6.7.

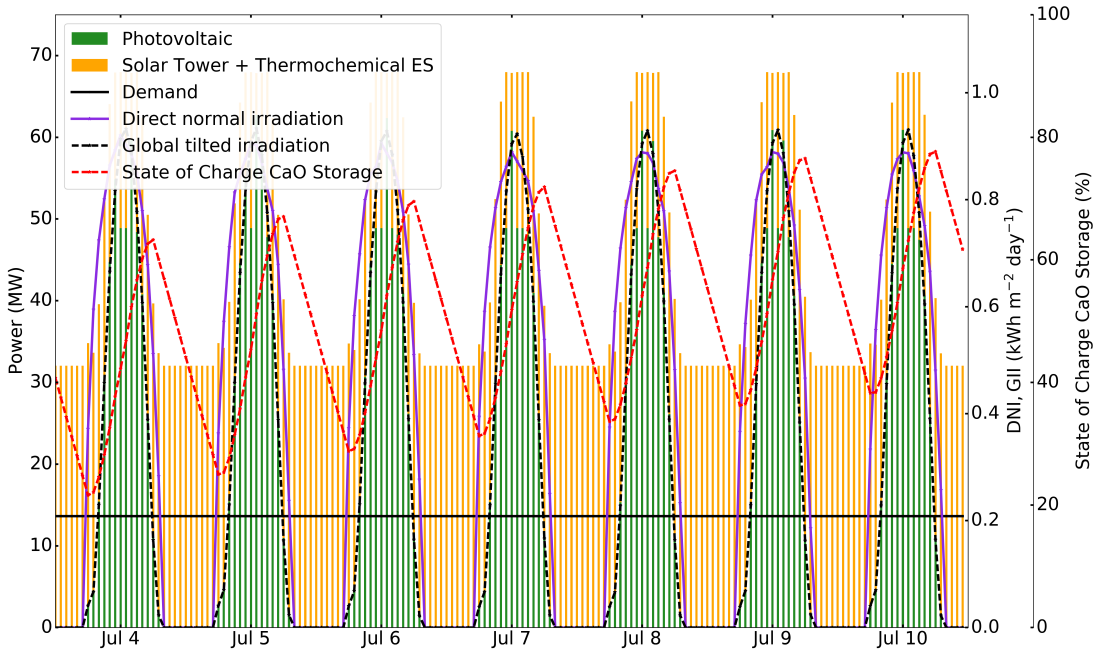

Figure 6.3: Optimal operation of the hybrid solar power plant, configuration G, plus solar resource and commitment for one week during summer

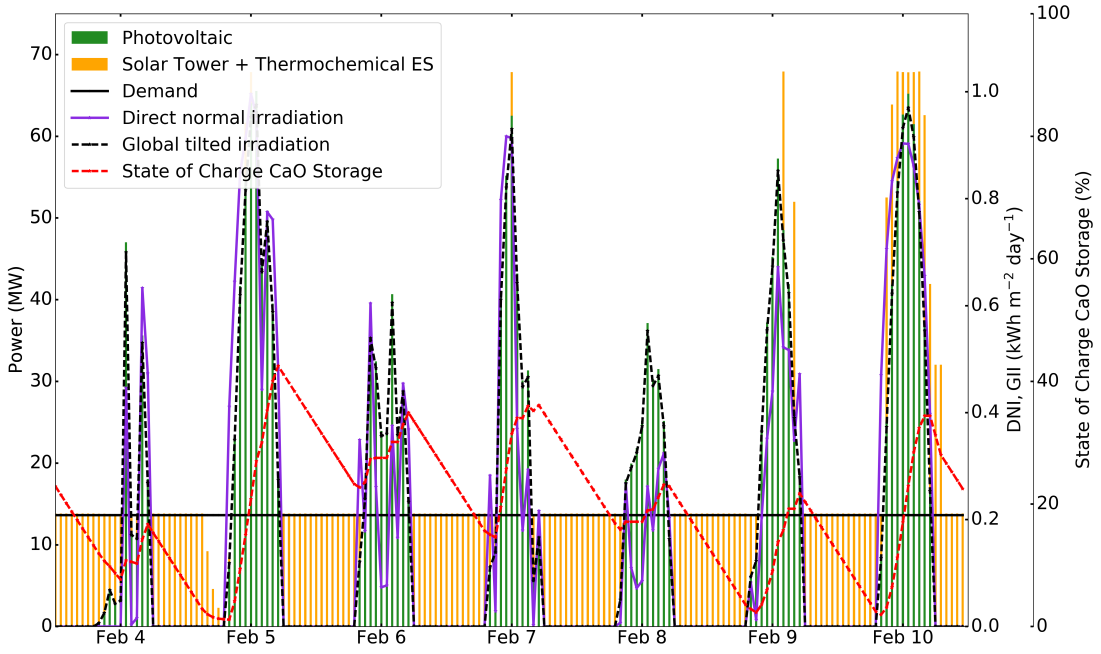

Figure 6.4: Optimal operation of the hybrid solar power plant, configuration G, plus solar resource and commitment for one week during winter

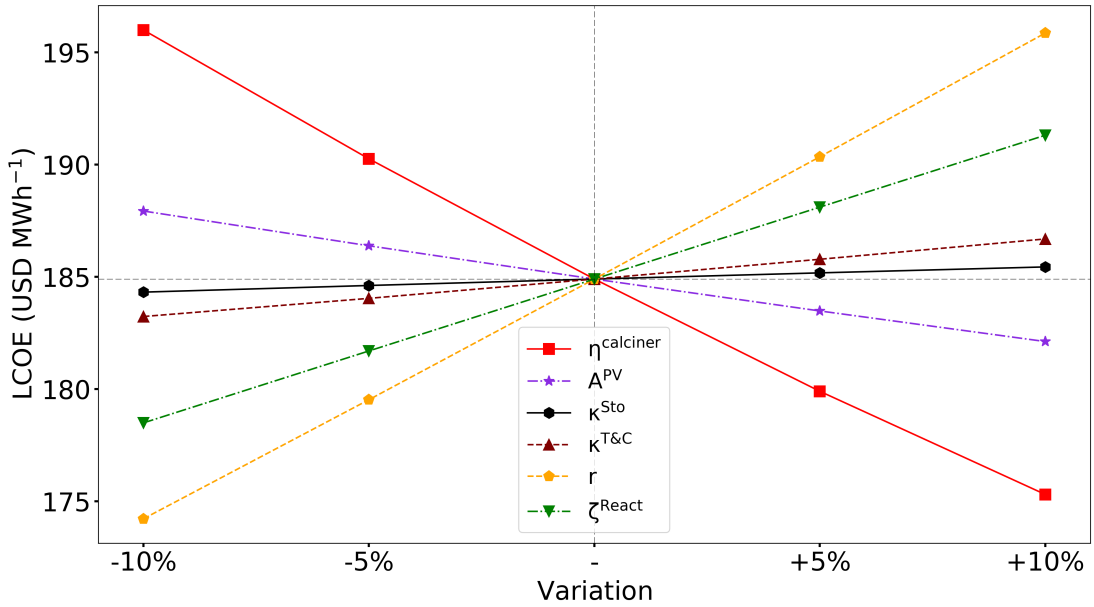

Figure 6.5: Sensitivity analysis for the LCOE by varying technical and financial parameters

In this case, because the analysis covers financial and technical parameters, appropriate key performance indicators are the levelised cost of energy (LCOE) and the loss of power supply probability (LPSP). Figures 6.5 and 6.6 show the sensitivity analysis for the LCOE and LPSP by varying the parameters described above by minus-plus 10% from the original value reported.

Figure 6.5 indicates that the parameters that have the most significant influence on the LCOE are the efficiency of the calciner, the interest rate, and the investment cost of reactors. The efficiency of the calciner increases the thermal energy available in the endothermic reaction, and the total energy dispatched. For instance, if $\eta^{receiver}$ is increased by 5% ($\eta^{receiver} \approx 0.89$), the LCOE decreases by 3%. Next, the interest rate also has a significant influence in the estimation of the LCOE, for example, if the project can be financed with $r \approx 6.3\%$ (instead of 7%), the LCOE falls by 6%. Finally, a reduction in 10% in the capital cost of the reactors (calciner and carbonator) decreases the LCOE by 4%. This reduction is very likely to be achieved because this technology is at an early stage of maturity.

Furthermore, the LCOE is highly dependent on the location of the power plant. In Chapter 7, different regions are analysed in order to compare key performance indicators under different solar resource and market features. For instance, if configuration G (with modifications in the solar field to keep the total energy available fixed) is analysed under the solar irradiation data of Atacama-1, a hybrid solar power plant located in Northern Chile, the LCOE drops to 138 USD·MWh^{-1} and the LPSP reaches 0.1%.

For the LPSP, by increasing any of the parameters shown in Figure 6.6, the energy dispatched to fulfil the commitment increases (and the LPSP decreases). Figure 6.6 shows that increasing

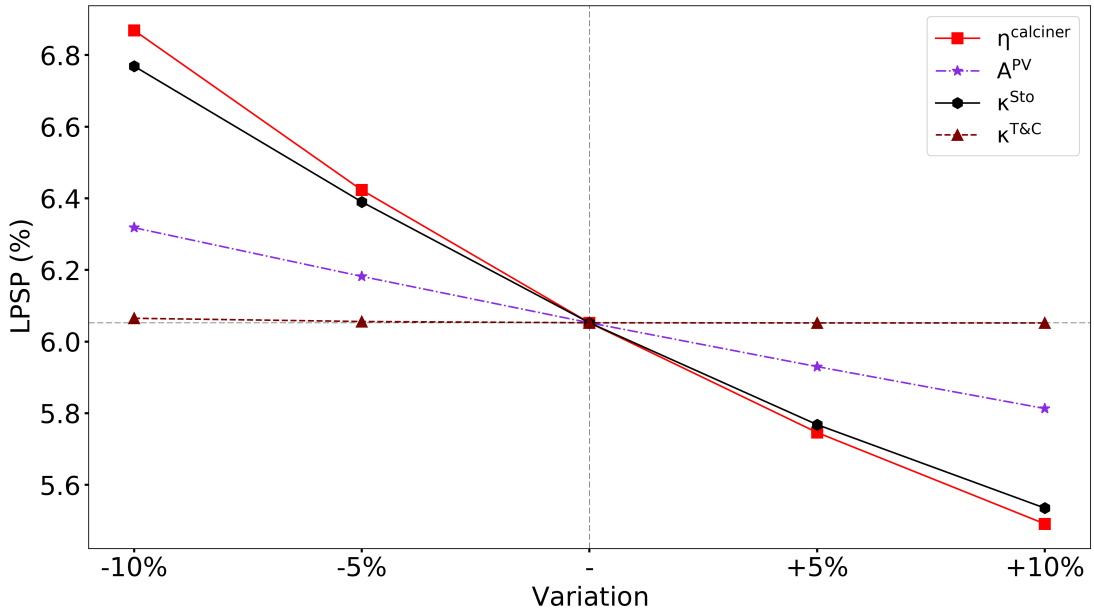

Figure 6.6: Sensitivity analysis for the LPSP by varying technical parameters

the efficiency of the calciner or the capacity of the storage is indispensable to increase the dispatchability. Finally, the results and diagrams suggest that by increasing the storage capacities, it is possible to dispatch a similar amount of energy. When large storage capacity is available, it is possible to manage the time when energy is dispatched, increasing the dispatchability of the power plant, allowing a long-term energy storage capacity.

6.5 Conclusions

In this chapter, the operation of a concentrated solar power plant integrated with a calcium-looping (CaL) process as a thermochemical energy storage system is analysed and optimised. Here, the linear programming model of the operation of the power plant is validated against the software Aspen Plus. Different designs and the hybridisation with a photovoltaic system were evaluated. This contribution provides relevant information to make renewable energy systems affordable and reliable. Besides, this framework enables long-term studies for the optimisation of the operation of solar power plants with thermochemical energy storage and their integration into energy systems.

The results summarise key indicators obtained by optimising the operation of a power plant located in Seville, Spain, using the solar irradiation data of the typical meteorological year as an input. Besides, by changing the input data, it is possible to find the best strategy to operate similar solar power plants in any location.

The findings of this study indicate that the use of a thermochemical energy storage system

in concentrated solar power plants increases the dispatchability, and by hybridising with a photovoltaic system, it can become cost-competitive. However, the significant differences in the solar irradiation in Seville between summer and winter could have a negative effect on the power system during summer by dispatching a large amount of power during the day.

The research highlights the importance of the multi-objective optimisation of the operation of a renewable power plant to reduce the fluctuations and maximise the energy delivered, which also influences the levelised cost of energy. When the design of the main components of the CaL is oversized (keeping the solar field fixed), less energy has to be curtailed, and more energy can be dispatched. However, this requires larger investments and results in lower capacity factors. Therefore a proper balance between capacities and curtailed energy should be pursued. Besides, it was found that the integration of a large CaL system, which can store a more substantial amount of energy, results in a significant increase in the dispatchability and the capacity factor. This means that a large storage system can work as a medium-term or even long-term energy storage system. Similar to the previous point, higher energy storage capacity requires more considerable investment.

The hybridisation with a photovoltaic system has beneficial effects. Because a larger solar field area is available, there is an improvement in both the energy dispatched and dispatchability. Besides, the operational strategy allows that during the day the PV dispatches power while the CSP stores energy, and during the night the CSP could dispatch, reducing the mismatch between supply and demand when no solar irradiation is available. Because PV is cheaper compared with CSP, the hybridisation results in a global reduction in the levelised cost of energy.

This study is the first step to improve the modelling and optimisation of the integration of CaL as a thermochemical energy storage system in hybrid solar power plants. In the next chapter, the design optimisation is developed in order to define the best capacities of the main components of the power plant. This second stage allows us to exploit synergies related to the dispatchability of CSP-CaL and affordability of PV systems.

Chapter 7

Multi-objective optimisation for the design of dispatchable hybrid solar power plants with thermochemical energy storage

The work presented in this chapter is based on an article published in the Journal Applied Energy (Bravo, Ortiz, Chacartegui, and Friedrich, 2021).

In this work, all authors collaborated with the analysis.

7.1 Introduction

As concluded in Chapter 6, thermochemical energy storage (TCES) integrated into concentrating solar power (CSP) plants can enhance dispatchability and solar-to-electricity efficiency. Combining these technologies with lower cost photovoltaic (PV) plants exploits synergies between dispatchability of CSP with TCES and cost of PV. However, this combination leads to complex interactions between the different plants and requires sophisticated design guidelines to simultaneously achieve low costs and high dispatchability.

In this chapter, the two-stage multi-objective optimisation framework is applied for the optimal design of hybrid CSP-PV plants with Calcium-Looping (CaL) TCES with respect to competing technical and financial performances. The first stage, design optimisation stage evaluates ten design variables and three objectives. The second stage, applied and analysed in detail in Chapter 6, finds the best one-year hourly operational strategy for each design defined in the first stage.

The design and operational optimisations consider technical and economic performance to design a dispatchable and cost-competitive power plant, exploiting synergies of CSP with CaL (dispatchability) and PV (affordability). The proposed framework provides a systematic

methodology and guidelines for the design of dispatchable power plants which takes the yearly operation into account and goes beyond a manual design process.

To analyse potential locations for further deployment of solar plants with TCES, the following locations which cover a range of different profiles will be evaluated: Seville, Spain; Tonopah, Nevada, United States; and the Atacama Desert, Chile. According to Figure 7.1, that shows the direct normal irradiation world map, Northern Chile has one of the highest solar irradiations in the world. Besides, Nevada and Southern Spain are among the sunniest region in the United States and Europe respectively.

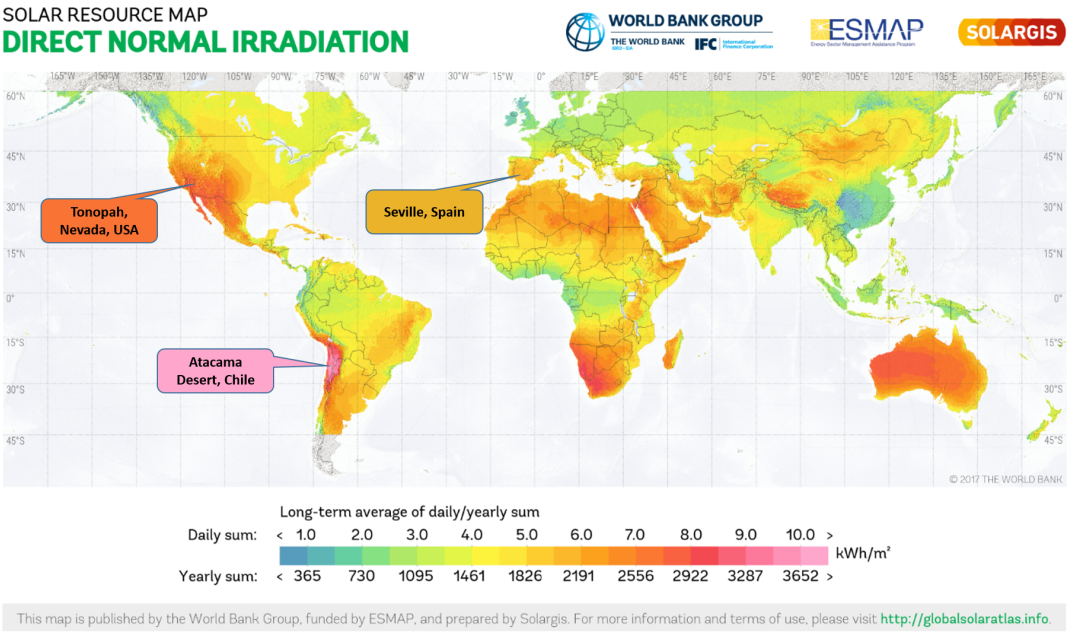

Figure 7.1: World map of direct normal irradiation and three locations studied in Chapter 7

The best dispatchable hybrid solar power plant with an LCOE of 123 USD·MWh^{-1} and a capacity factor of 73% is reached for the Atacama Desert, which has the best solar resource. The optimisation results are used to develop guidelines for the optimal design of dispatchable hybrid solar power plants with TCES based on the given solar resource and required dispatchability. These guidelines provide an initial design for affordable and dispatchable hybrid solar power plants and can enable their widespread deployment.

7.2 Methodology, plant modelling

In order to design an affordable and dispatchable solar power plant, the trade-off between financial and technical performances has to be examined. While an oversized CSP plant can give us full dispatchability at a high LCOE, a PV plant will be more affordable, but not dispatchable. These conflicting objectives are handled by a multi-objective optimisation method which produces a range of non-dominated or Pareto optimal solutions. To carry out the design optimisation stage, the two-stage optimisation framework developed is extended for the hybrid CSP-PV with TCES plant. Figure 7.2 shows the procedure adapted for the present research.

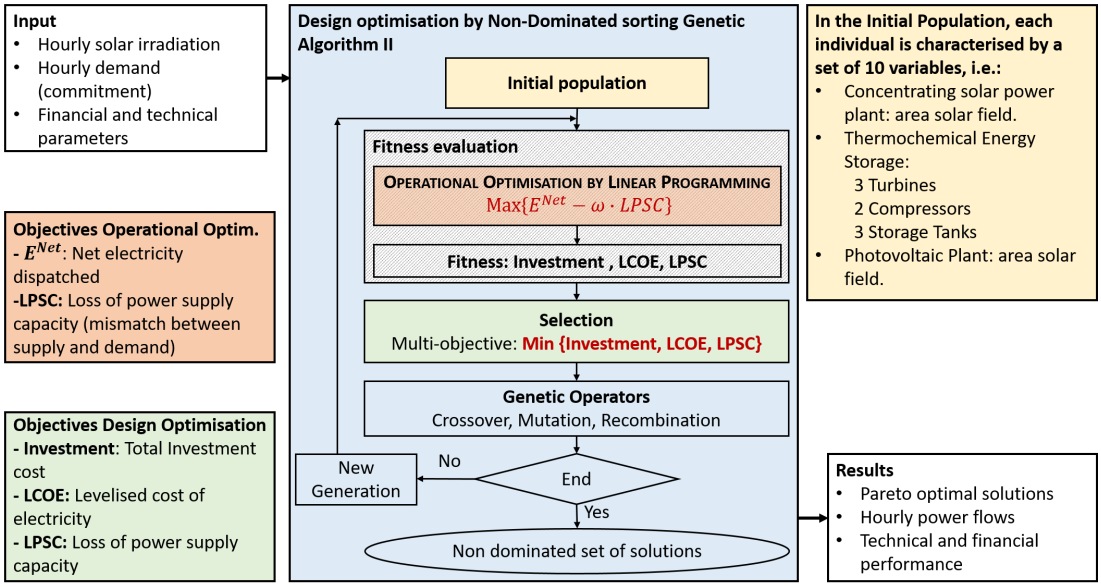

Figure 7.2: Schematic of the two-stage optimisation applied for the optimal design and operation of a hybrid CSP-PV with TCES system

This framework uses a genetic algorithm (GA) to optimise the design of the power plant under techno-economic objectives. The use of genetic algorithms allows us to handle non-convex objectives and several variables. As can be seen in Figure 7.2, GA starts with an initial population, where each individual represents a power plant with given capacities. Then, each individual design in the population is optimised by using the operational optimisation by linear programming presented in Chapter 6. After the operational optimisation is performed, the investment cost, LCOE, and LPSC are calculated and used by the GA to perform the fitness evaluation. After that, the genetic operators work to define the best offspring and then a new generation is produced. Finally, the stopping criteria used in our model is when the number of generations reaches a defined value. For the present research, real solar irradiation data is used as input, and it can be easily modified to evaluate any location. The multi-objective design optimisation produces a range of Pareto optimal solutions, representing the trade-off between objectives.

Table 7.1: Variables of the design optimisation model of a hybrid solar plant with CaL TCES

Variable	Description	Unit
A^{CSP}	Heliostats field area	m^2
P^{ST}	Capacity steam turbine	MW
P^{MC}	Capacity main CO_2 compressor	MW
P^{MT}	Capacity main CO_2 turbine	MW
P^{HPSC}	Capacity high pressure CO_2 compressor	MW
P^{HPST}	Capacity high pressure CO_2 turbine	MW
STO^{CO_2}	Capacity CO_2 storage tank	m^3
STO^{CaO}	Capacity CaO storage tank	m^3
STO^{Solids}	Capacity CaO+$CaCO_3$ storage tank	m^3
A^{PV}	Photovoltaic field area	m^2

7.2.1 Simulation conditions

The design of the power plant is given by the size of the components shown in Table 7.1, which are defined as variables in the design optimisation routine.

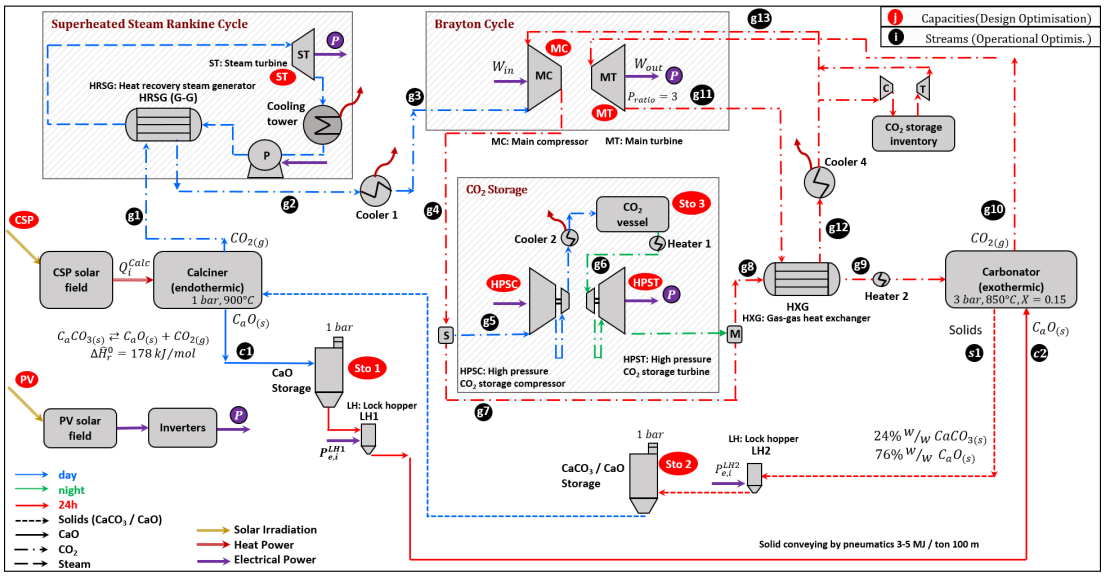

Figure 7.3: Mass and energy balances model of the hybrid solar power plant with CaL as TCES

The design variables are shown in the red ovals in Figure 7.3. The combination of these variables will result in a power plant with known capacities. Then, the initial investment is calculated with the relations presented in Chapter 3. Next, the operational optimisation by linear programming and nested as a fitness function in the genetic algorithm defines the best operational strategy, maximising the net energy dispatched and minimising the mismatch between generation and commitment. Finally, three indicators (detailed in Section 7.2.2) are considered as objectives of the design optimisation stage and used by the genetic operators.

7.2.2 Construction of indicators to characterise financial and technical performance

As stated previously, the design optimisation aims to select the optimal sizes of the components to design an affordable and dispatchable power plant. In this study, the investment cost and the LCOE are employed to measure the affordability while the loss of power supply capacity (LPSC) is used to measure the dispatchability. The LCOE is a crucial indicator that represents the cost of each electricity unit generated over the lifetime of the power plant considering the total life cycle costs, while the investment cost is essential when defining a limiting initial budget for the feasibility of a project. The LPSC measures the mismatch between the net electricity supply and a constant demand (details on the demand are given below at the end of this section).

The total investment cost is estimated using the references summarised in Section 3.6.3. The LCOE is calculated by Equation 3.1, where values for the annual interest rate and a lifetime of r=7% and T=25 years are used. To measure the ability to supply energy when it is needed (dispatchability), the loss of power supply (LPS), that measures the mismatch between supply and commitment as defined in Equation 3.30, is used.

To compare the results with the non-optimised hybrid solar power plants presented in Chapter 6, here, a permanent power commitment is defined. Moreover, to avoid an oversize PV plant, and hence, a significant difference in the dispatch between day and night, the operational optimisation model was constrained by defining a maximum power dispatch five times the commitment.

$$P_i^{\text{commitment}} = 13.5\ MW,\ \forall i \tag{7.1}$$

$$P_i^{net} \leq 67.5 MW,\ \forall i \tag{7.2}$$

Nevertheless, these capacities can be defined by the user according to the objectives pursued and the transmission constraints of the power plant.

The LPS is summed to the loss of power supply capacity (LPSC) which is used in the optimisation framework. To facilitate the final analysis, the LPSC value is reported as a percentage of the annual commitment which is given by the loss of power supply probability (LPSP, Equation 7.4).

$$LPSC = \sum_{i=1}^{8760} LPS_i \tag{7.3}$$

$$LPSP = \frac{LPSC}{P_i^{Commitment} \cdot 8760} \tag{7.4}$$

According to Equation 3.1, the LCOE is directly related to the investment, and more significant investment should result in a larger LCOE. Nevertheless, power plants with different designs

but similar investments can dispatch different amounts of energy. Hence, a direct correlation between investment and LCOE is not always guaranteed.

7.2.3 Fitness function for the design optimisation

The multi-objective linear scalarisation model for the operational optimisation exposed in Chapter 6 is nested as a fitness function, linking the objectives of both levels. The operational optimisation routine simultaneously maximises the energy dispatched and minimises the mismatch between supply and demand. The use of linear programming ensures a good approximation of the best operational strategy for one year of operation, considering variable solar resource, in a reasonable computational time. Hence, the operation of each individual design of the genetic algorithm stage is optimised, considering one-year hourly solar irradiation.

7.3 Case studies

To analyse and compare the performance of hybrid solar power plants with calcium-looping thermochemical energy storage, and to evaluate the opportunities in the integration of clean technologies to support the transition to a sustainable energy system under different conditions, the model will be evaluated in three locations:

- Seville, Spain, $\approx 37.4°N, 6.3°W$
- Tonopah, Nevada, United States, $\approx 38°N, 117°W$
- Atacama Desert, Chile, $\approx 22°N, 69°W$

The evaluation in each location will result in a distinctive 3-D Pareto surface illustrating the performance expected of an optimised set of different designs in each area. Each point in the Pareto set is a non-dominated solution or potential candidate. Hence, an a-posteriori evaluation of optimised designs for each location should be carried out by the user to select the best hybrid power plant under a trade-off between the objectives or considering other key performance indicators.

7.3.1 Data quality control and preparation

In the present study, the solar irradiation data was collected using three different open data sources: (i) Seville, the "Photovoltaic Geographical information system" (PVGIS project) of the European Commission Joint Research Centre (European Commission, 2017); (ii) Tonopah, System Advisor Model software (SAM-NREL) (NREL, 2018); (iii) the Atacama Desert, Chilean Ministry of Energy and University of Chile solar resource data centre (Ministerio de Energia and Universidad de Chile, 2016).

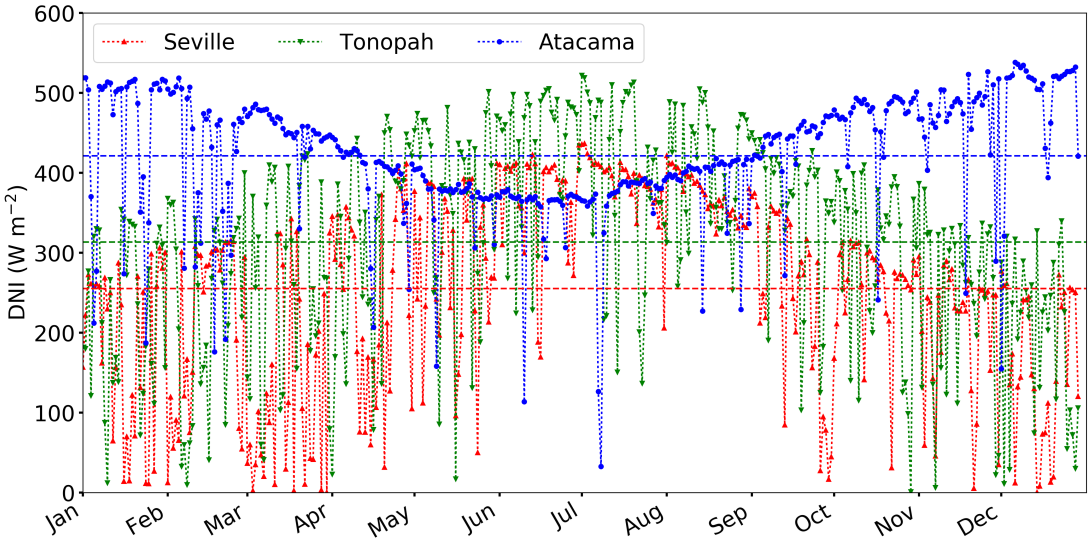

Figure 7.4: Daily and annual average DNI in Seville, Tonopah, and Atacama Desert

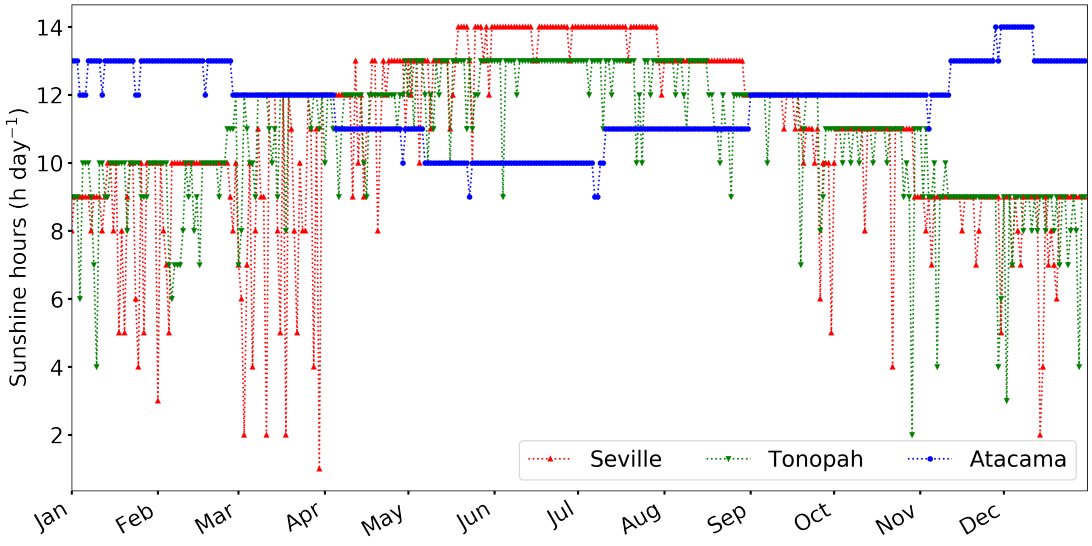

Figure 7.5: Sunshine hours (hours with $DNI > 0$) in Seville, Tonopah, and Atacama Desert

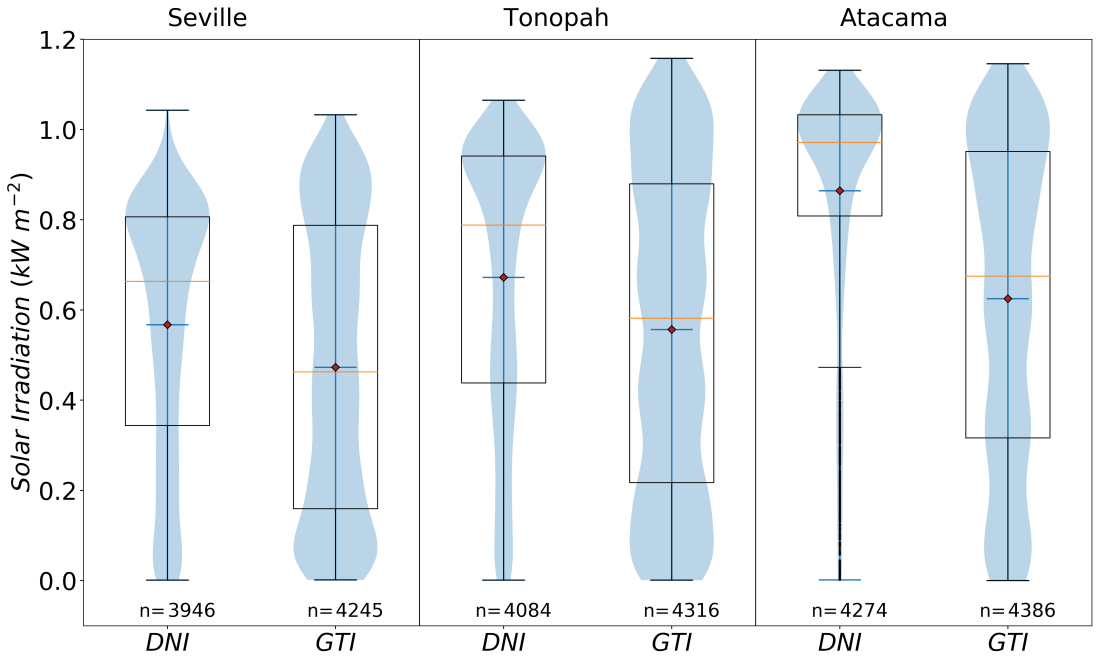

Figure 7.6: Box and violin plots for DNI and GTI in Seville, Tonopah, and Atacama Desert

To estimate the potential and to compare the solar resource in the three locations, Figure 7.4 highlights the direct normal irradiation (DNI) and the global tilted irradiation (GTI) in each area.

The DNI is the solar irradiation captured by the heliostats of the CSP that track the sun. The GTI is the irradiation converted into electricity by the PV plant in which each PV module is non-tracking. Table 7.2 shows the accumulated annual DNI and GTI considering the typical meteorological year.

Table 7.2: Solar irradiation (TMY) in Seville, Tonopah, and Atacama Desert

Location	DNI $kWh \cdot m^{-2} \cdot year^{-1}$	GTI $kWh \cdot m^{-2} \cdot year^{-1}$
Seville	2,238	2,006
Tonopah	2,745	2,403
Atacama	3,693	2,742

Figure 7.4 presents the DNI daily and annual averages, revealing the difference between each location. Moreover, it can be noted that the variability in the daily DNI of the Atacama Desert is lower than for the other two locations. To support this statement, the standard deviation (σ) of the daily average calculated for Seville, Tonopah, and the Atacama Desert is 120, 130 and 78 $W \cdot m^{-2}$ respectively. This variability should affect the dispatchability of a CSP plant with TCES if a fixed commitment is required throughout the year.

The variability is also illustrated in Figure 7.5, that shows the total number of sunshine hours

per day with a $DNI > 0$. While the average ($\bar{h}$) is similar for the three locations ($\bar{h}_{\text{Seville}} = 10.8$ h·day^{-1}, $\bar{h}_{\text{Tonopah}} = 10.8$ h·day^{-1}, $\bar{h}_{\text{Atacama}} = 11.7$ h·day^{-1}), Figure 7.5 highlights the stable solar resource of the Atacama Desert, i.e. $\sigma_{h,\text{Atacama}} \approx 1$ h·day^{-1}. In the case of Seville, the higher standard deviation ($\sigma_{h,\text{Seville}} \approx 3$ h·day^{-1}) shows that there is significantly more variation in the number of sunshine which is due to larger seasonal variations and more cloudy days in winter. A similar trend can be identified for Tonopah, with $\sigma_{h,\text{Tonopah}} \approx 2$ h·day^{-1}

All these characteristics for the DNI of each location are highlighted in Figure 7.6. This figure shows a box plot and a violin plot for the $DNI > 0$ and $GTI > 0$ for the selected locations. The central box in each set of data represents quartiles Q_1 and Q_3 (percentiles 25^{th} and 75^{th}), and the variability of the data set can be estimated by the height of the central box, i.e. the interquartile range or difference between Q_3 and Q_1. Then, the central orange line of each box represents the median of the population, or second quartile (Q_2, i.e. 50^{th} percentile). Next, the whiskers show the extreme values, and some outliers in the case of the DNI of the Atacama Desert can be seen. Besides, the red point located close to the median represents the mean, and at the bottom can be found the total number of samples greater than 0 (from a total of 8760 hours). In addition, the violin plot represented by the light blue area shows the probability density of the samples. For instances, in the case of the DNI of the Atacama Desert, the violin plot shows that the population is concentrated in the top, corroborating the small variability of the direct normal irradiation in the Atacama Desert. The same analysis can be done for the GTI, in this case, the plots show that the means of the GTI follow the same trend than the means of the DNI ($\overline{GTI}_{\text{Atacama}} > \overline{GTI}_{\text{Tonopah}} > \overline{GTI}_{\text{Seville}}$), and the variability can be estimated by the size of the box, or by the distribution of the sample by analysing the violin plots. It can be seen that the variability of the GTI is larger, because, as contrary to the DNI, the GTI is the irradiation in a fixed plane, and even in locations with high solar irradiation, the irradiation in a fixed plane has a large variability throughout the day.

This detailed analysis gives us an idea of the difference in the design of a dispatchable hybrid solar power plant with TCES in each location. For instance, it could be inferred that a smaller CSP-TCES system is required in the Atacama Desert to supply the same energy during the year. Hence, lower investment and lower LCOE is expected for optimised power plants with a similar level of dispatchability in the Atacama Desert, then Tonopah, and finally, Seville should be the most expensive. Moreover, as outlined before, the high variability in the irradiation in Seville and Tonopah should have a negative effect on the performance of the hybrid solar power plant.

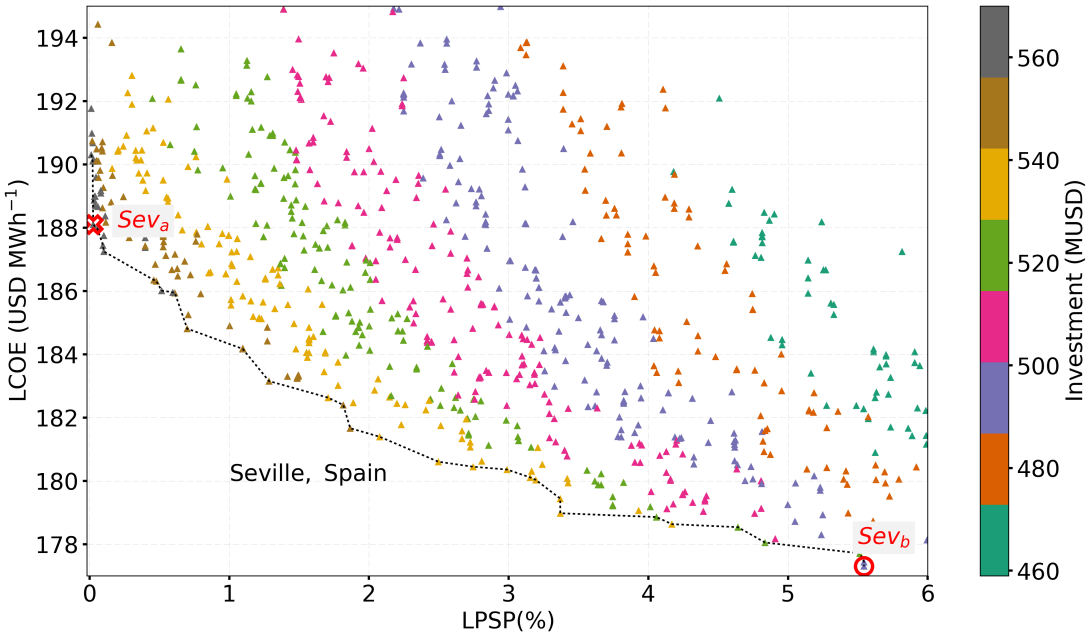

Figure 7.7: Pareto optimal solutions of the design optimisation for a hybrid solar power plant with TCES in Seville. The dashed line is an estimation of the Pareto frontier between LCOE and LPSP

7.4 Optimisation results and analysis

The two-stage optimisation framework was used to optimise a hybrid solar power plant with TCES in the selected locations. Here 100 individuals for the initial population are defined (100 combinations of independent design variables) and 100 generations are used as stopping criteria. Figures 7.7, 7.8, and 7.9 illustrate the 3-D non-dominated set of solutions at the end of the process.

In each diagram, the x-axis represents the LPSP, the LCOE is shown in the y-axis, and the third objective, the investment cost, is illustrated using different colours. The objective of the design optimisation is to provide affordable and reliable power, so, the goal is to be located in the bottom left corner in the diagram with low investments. Hence, the diagrams reveal the trade-off between technical (LPSP) and financial (LCOE and Investment) performances. It should be noted that 1% in the LPSP is equivalent to 1,182.6 MWh of energy not supplied, or 87.6 hours where the power plant was not able to dispatch electricity.

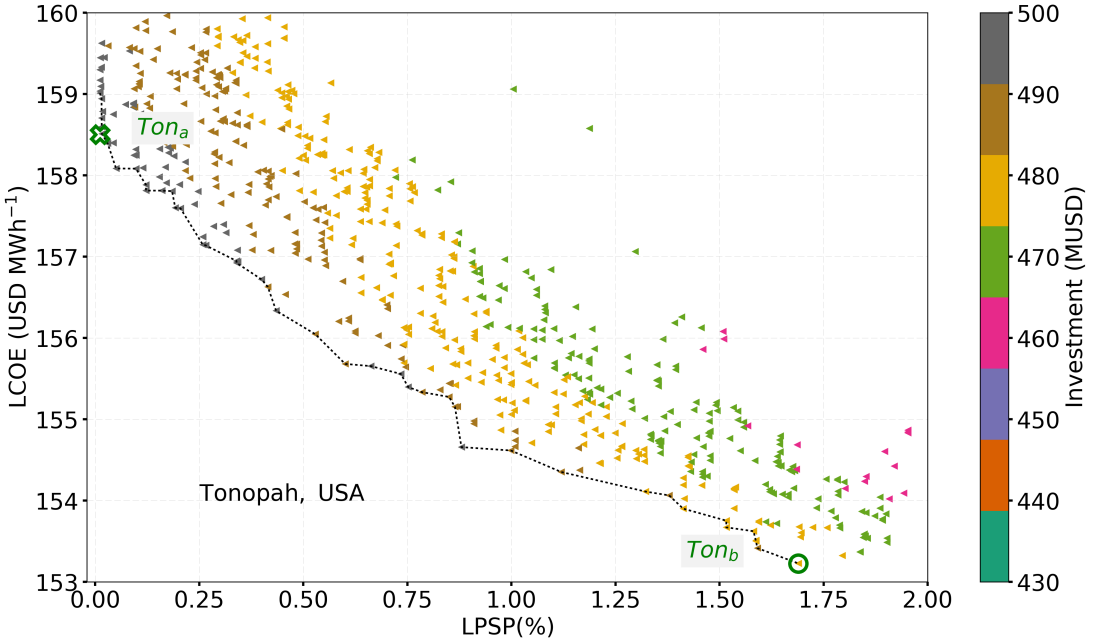

Figure 7.8: Pareto optimal solutions of the design optimisation for a hybrid solar power plant with TCES in Tonopah

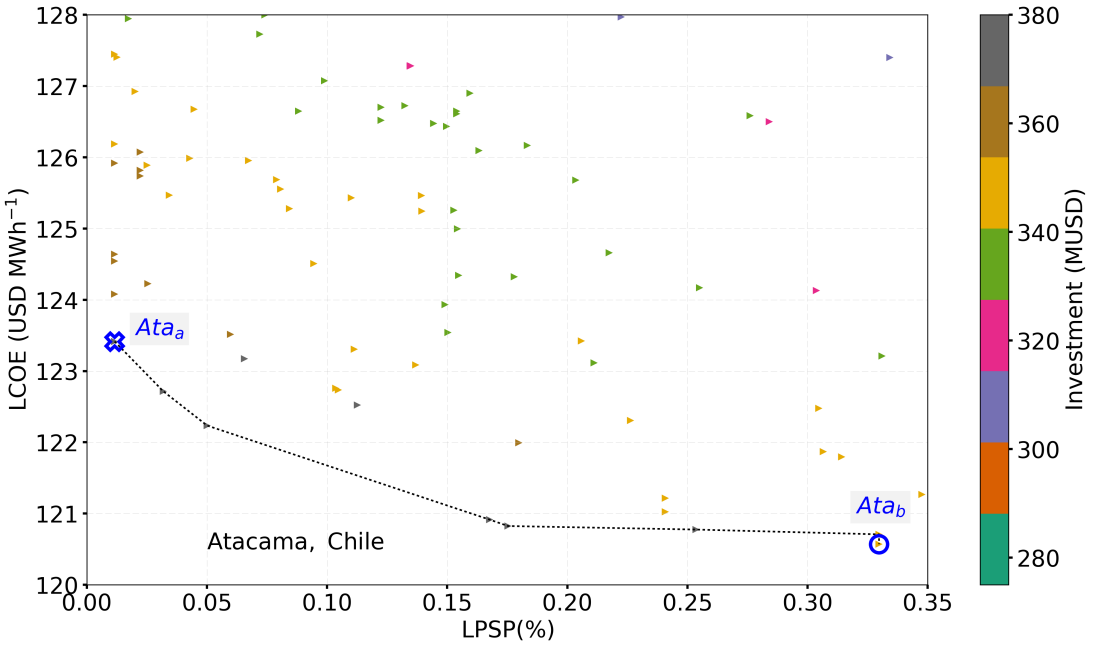

Figure 7.9: Pareto optimal solutions of the design optimisation for a hybrid solar power plant with TCES in the Atacama Desert

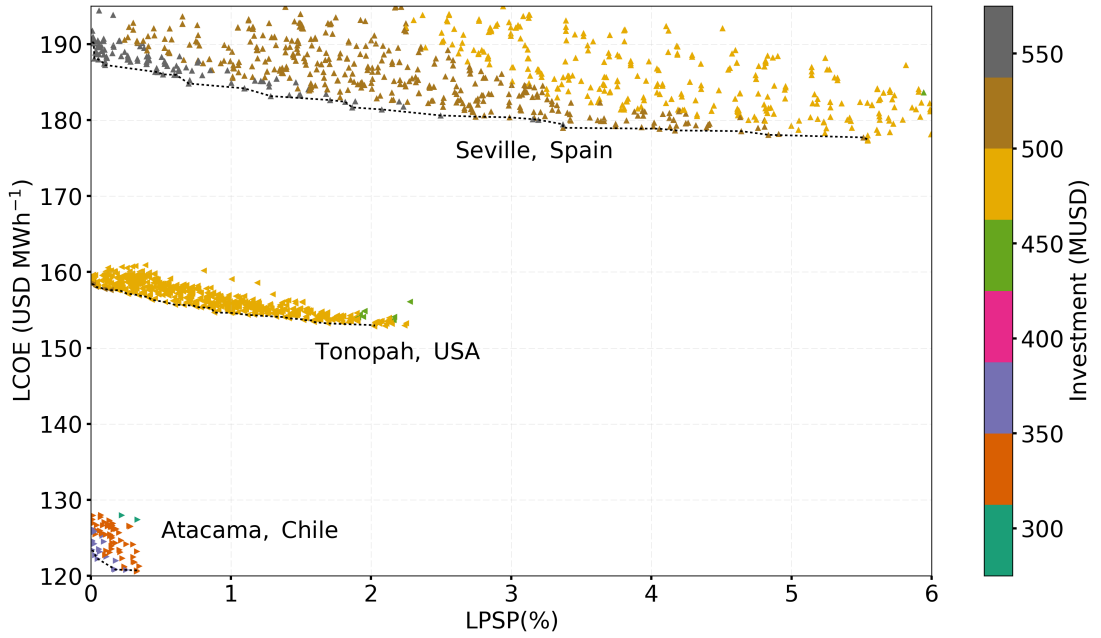

Figure 7.10: Pareto optimal solutions of the design optimisation for a hybrid solar power plant with TCES in Seville, Tonopah, and Atacama Desert

7.4.1 Comparison between optimised designs

Figures 7.7, 7.8, and 7.9, illustrate the result of the design optimisation in Seville, Tonopah, and the Atacama Desert, respectively. Besides, these figures are merged in Figure 7.10 to facilitate the comparison of the techno-economic performances of optimised power plants. Moreover, Table 7.3 and Figure 7.11 summarise the economic performance and cost breakdown of highly dispatchable designs, i.e. $LPSP \rightarrow 0$ (points Sev_a, Ton_a, and Ata_a in Figures 7.7, 7.8, and 7.9 respectively).

The breakdown analysis of the LCOE illustrated in Figure 7.11 shown the weights of the CSP-CaL and the PV plant in the total LCOE. For instance, the LCOE of a highly dispatchable hybrid solar power plant in Seville (Sev_a) can be divided in approximately 100 USD·MWh^{-1} corresponding to the CSP-CaL plus 42 USD·MWh^{-1} for the PV. Additionally, 32 USD·MWh^{-1} correspond to indirect costs (e.g. land cost, taxes) and finally, around 10 USD·MWh^{-1} of the LCOE is related to operational and maintenance costs. Then, by focusing on the CSP-CaL, the most significant expenses correspond to the solar field and tower (25 USD·MWh^{-1}), and the power plant (60 USD·MWh^{-1}). Here the power plant is composed of compressors, turbines, heat exchanger, and other elements of the CaL process. The breakdown analysis is essential in the development of initiatives to enable cost reductions of solar power plants by focusing on the most relevant elements.

As explained previously, all non-dominated solutions (Pareto optimal) represent optimised designs. To compare a highly dispatchable power plant with a more affordable power plant

Table 7.3: Economic performance of dispatchable hybrid solar power plants with CaL TCES

Location	LCOE USD·MWh^{-1}	Investment MUSD	LPSP %
Seville	188	566	0.02
Tonopah	158.5	504	0.01
Atacama	123.4	377	0.01

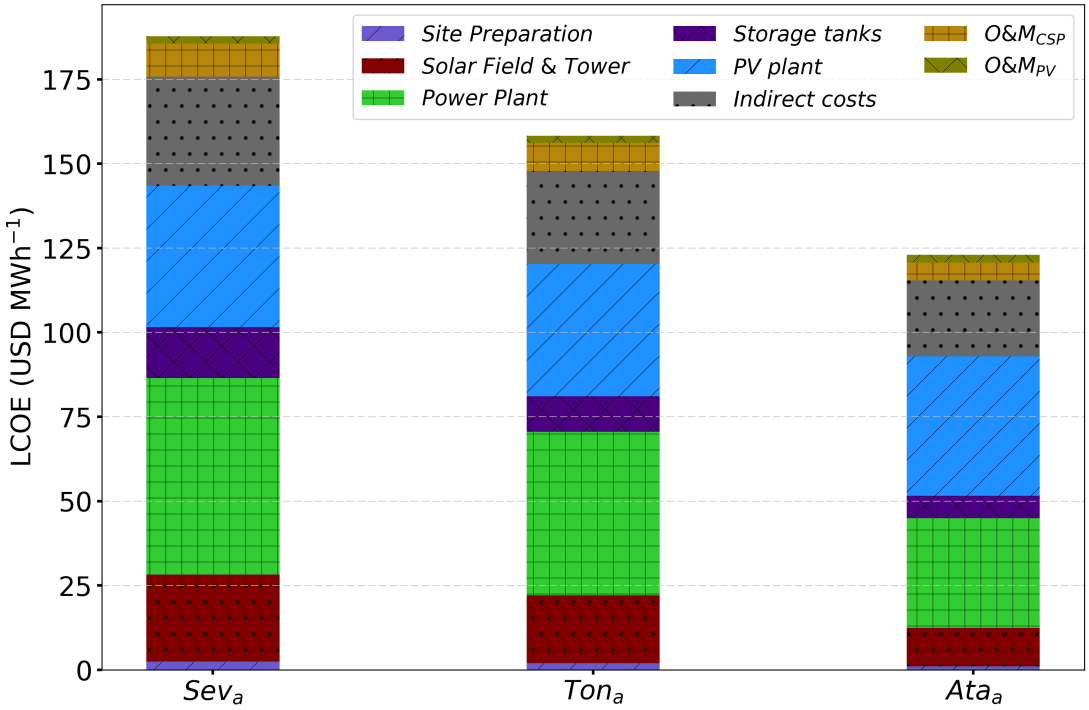

Figure 7.11: LCOE breakdown for a dispatchable hybrid power plant in Seville, Tonopah and the Atacama Desert

(low LCOE), two extreme points are chosen, marked with a or b as subscript (e.g. Sev_a, Sev_b) in Figures 7.7, 7.8, and 7.9. Then, the characteristics of these 6 points (2 points per location and three locations) are illustrated in Figure 7.12. The first section of the diagram corresponds to the objectives and the second section to the variables. Here, the data is scaled regarding minimum and maximum values of each data set shown. For instance, the LCOE of Ton_b can be estimated as: $LCOE_{Ton_b} \approx (188.1 - 120.6) \cdot 0.5 + 120.6 \approx 154$ USD·MWh^{-1}. The figure shows the large difference in the economic performance of both designs in the Atacama Desert compared with Tonopah and Seville.

Then, it is possible to check the capacity and the range in size between both designs in each location. For instance, the high value in the area of the PV plant for all designs (39.5 ha to 41 ha), which is linked to the commitment and maximum dispatch (transmission constraints), demonstrates the benefits of hybridising dispatchable CSP with affordable PV. The ranges in the

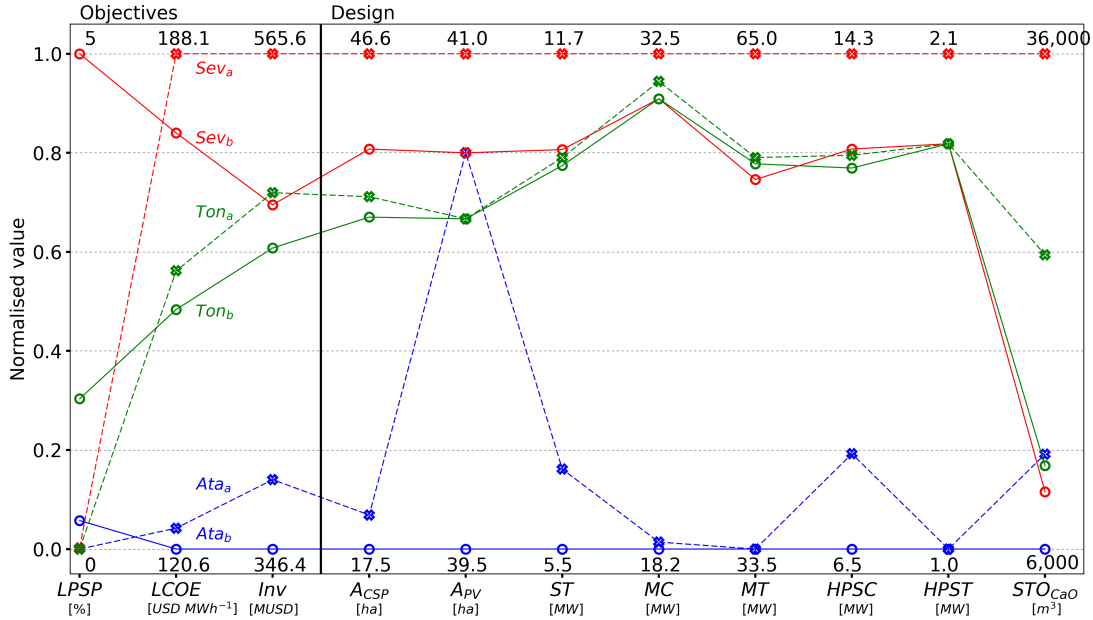

Figure 7.12: Key performance indicators of selected optimal designs in Seville, Tonopah, and Atacama Desert

area of heliostats and the capacities of each turbine and compressor reveal the requirements to design dispatchable power plants. Moreover, the diagram shows a positive correlation between the capacity of each turbine and compressor in the TCES system with the size of the CSP plant. Finally, the three points with the lowest LCOE in each location show a similar capacity of storage. The analysis suggests that there is a relationship between the optimised level of storage for these plants and the net capacity of the Brayton cycle. These interdependences are studied in Section 7.4.3.

Table 7.4 shows key performance indicators (KPI) of each power plant. These values are calculated by optimising the annual operation of each design under its respective solar irradiation data. The following KPI were exposed in Chapter 3 to evaluate and compare each design: (i) E^{net}: net energy dispatched; (ii) $E^{commitment}$: net energy to cover the commitment; (iii) E^{excess}: electricity dispatched when exceeding the commitment (in this model, the maximum power that can be dispatched is 5 times the commitment); (iv) $E^{curtailed}$: thermal energy available in the CSP that has to be curtailed; (v) $\bar{P}^{net}$: average power dispatched; (vi) P^{max}_{CSP}: maximum power dispatched by the CSP-TCES plant; (vii) CF_{CSP}: capacity factor of the CSP plant referred to the Brayton cycle (Figure 7.3); (viii) η_{CaL}: efficiency related to the thermal energy available in the calciner ; (ix) $\eta_{CSP,PB}$: efficiency considering the solar irradiation in the solar field of the CSP plant to electricity; (x) P^{max}_{hybrid} maximum power dispatched by the hybrid power plant; (xi) O&M costs: operational and maintenance costs.

These results show that a hybrid solar power plant integrated with CaL has the potential to provide dispatchable power at a cost competitive with current commercial systems. Besides,

Table 7.4: Operational key performance indicators of selected optimal designs in Seville, Tonopah, and Atacama Desert (Figures 7.7, 7.8, and 7.9)

KPI	unit	Sev_b	Sev_a	Ton_b	Ton_a	Ata_b	Ata_a
$LCOE$	USD·MWh^{-1}	177.3	188.1	153.2	158.6	120.5	123.5
$LPSP$	%	5.6	0.0	1.7	0.0	0.3	0.0
Invest.	MUSD	498	566	479	504	346	377
E^{net}	GWh·year^{-1}	256	276	288	292	264	279
$E^{commitment}$	GWh·year^{-1}	111.7	118.2	116.3	118.2	117.9	118.2
E^{excess}	GWh·year^{-1}	146.1	157.6	171.8	173.6	145.8	160.6
$E^{curtailed}$	GWh$_{th}$·year^{-1}	1.2	2.4	1	2.5	0.5	0.3
$\bar{P}^{net}$	MW	29.4	31.5	32.9	33.3	30.1	31.8
P_{CSP}^{max}	MW	29.1	33.2	29.7	29.9	17.2	17.1
CF_{CSP}	%	53.5	53.8	55.3	56.8	64.5	73.1
η_{CaL}	%	32.5	32.5	32.5	32.5	32.2	32.3
$\eta_{CSP,PB}$	%	13.8	13.8	13.1	13.0	13.8	13.8
P_{hybrid}^{max}	MW	67.5	67.5	67.5	67.5	67.5	67.5
O&M	MUSD·year^{-1}	3.0	3.3	3.0	3.1	2.1	2.1

the values obtained are aligned with those reported in Chapter 3 for Atacama. That study concluded that high dispatchability (LPSP $\approx 1\%$) is achieved with an LCOE closer to 122 USD·MWh^{-1}. However, the excellent results obtained with the integration of calcium-looping as TCES process are reached by using natural, widely available and environmentally friendly raw materials (limestone) instead of the use of molten salts or batteries. The results explore the integration level of each technology under different conditions, supporting the development of renewable and dispatchable power plants.

To complete the analysis, time-series results to show the power production for the three power plants with lowest LPSP are shown in Figures 7.13, 7.14, and 7.15. These diagrams clarify the potential of the linear programming models developed to achieve the best operational strategy of the combined hybrid solar power plants and thermochemical energy storage system. As can be seen in the figures, the results illustrate the power production from the hybrid power plant, i.e. photovoltaic + concentrating solar power plant with energy storage system, for the three configurations in each location. The diagrams show the high amount of electricity dispatched during summer, where high level of solar irradiation is available, and where the dispatch is constrained by the transmission capacity. On the other hand, a low power is dispatched during cloudy days in winter.

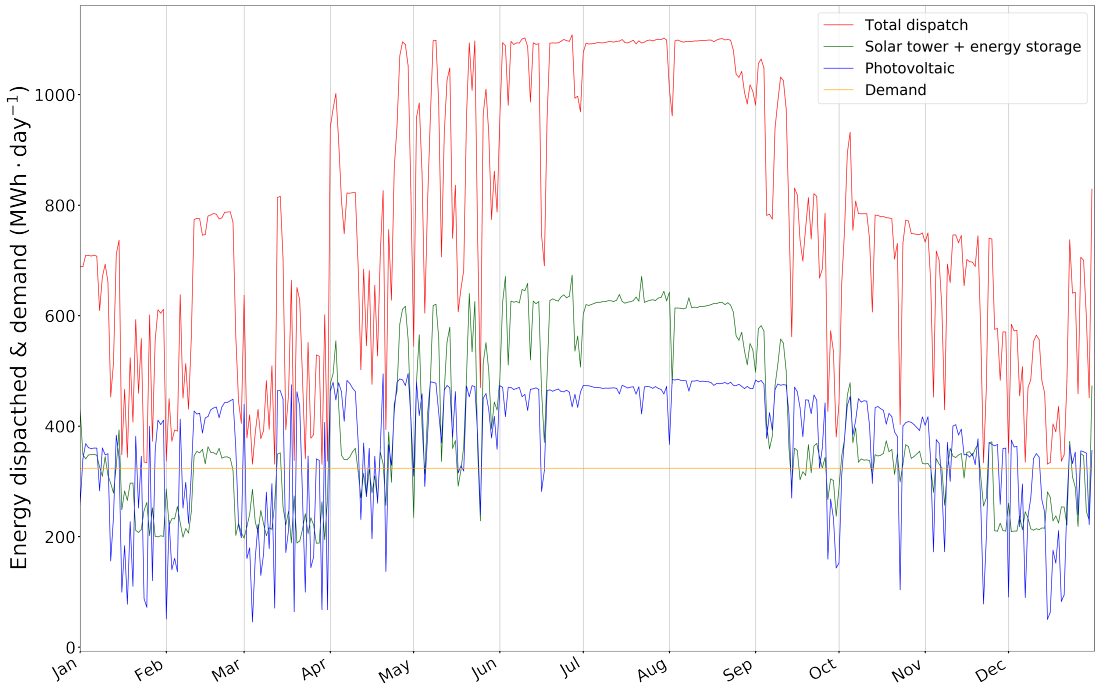

Figure 7.13: Time-series power dispatch for an optimised hybrid solar plant in Seville, configuration Sev$_a$

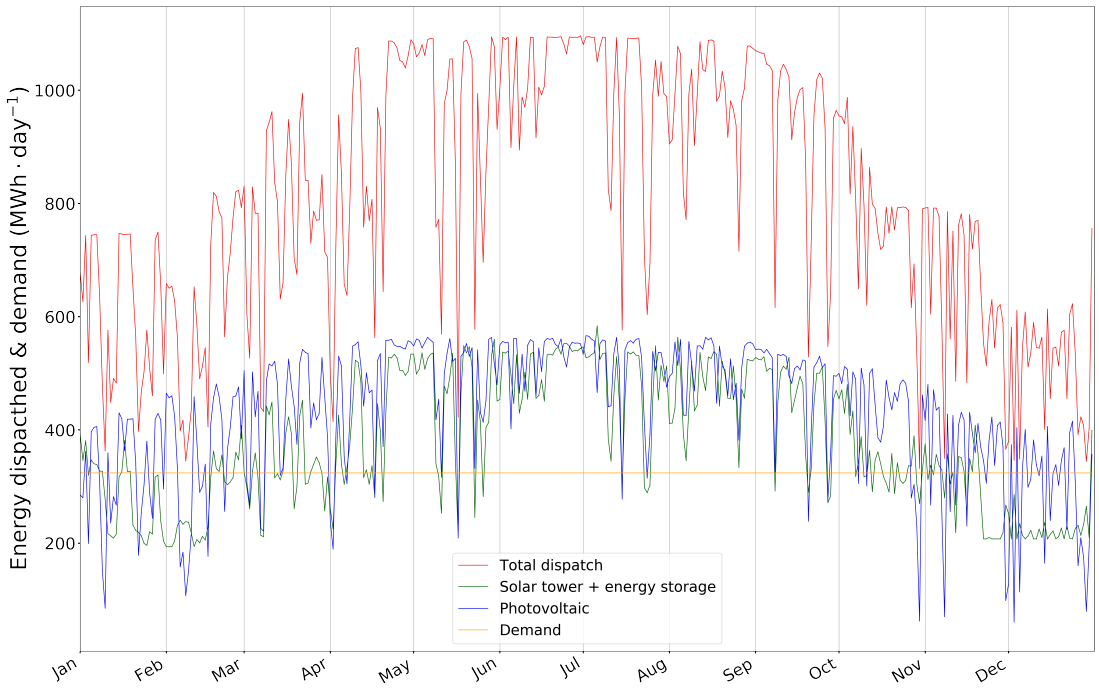

Figure 7.14: Time-series power dispatch for an optimised hybrid solar plant in Tonopah, configuration Ton$_a$

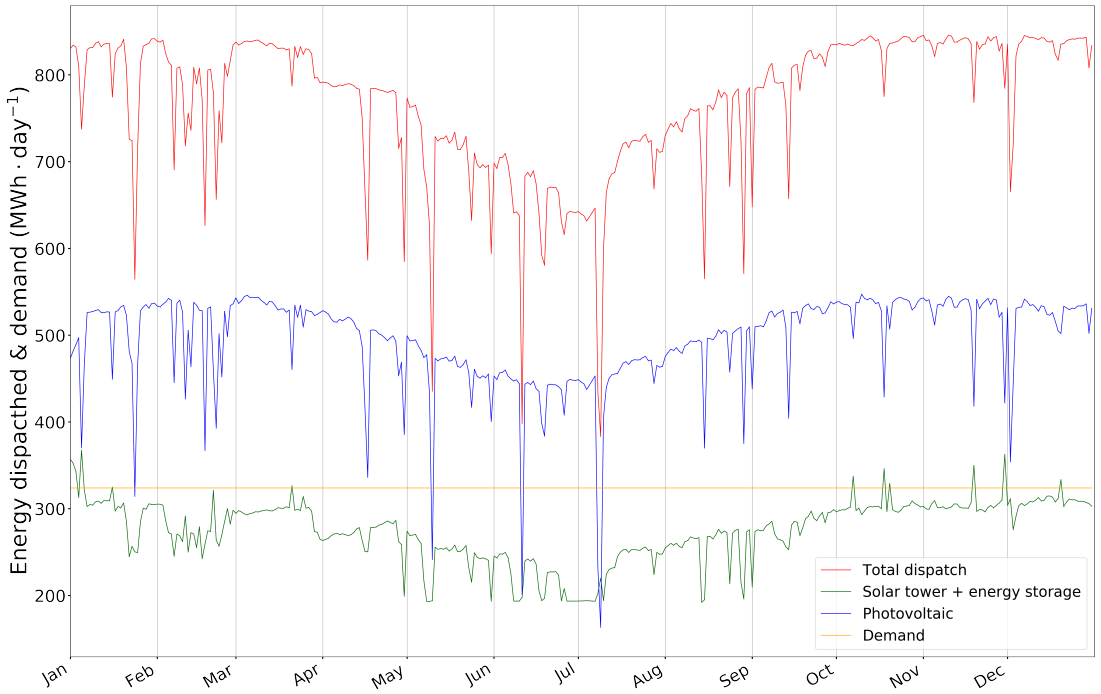

Figure 7.15: Time-series power dispatch for an optimised hybrid solar plant in Atacama, configuration Ata$_a$

7.4.2 Correlations and design ranges

Correlations between the objectives and main variables are shown in Figures 7.16, 7.17, and 7.18 for the three locations, to understand the features of optimised power plants in different areas. Furthermore, the minimum and maximum values of each variable reached in optimised power plants shown in Figures 7.7, 7.8, and 7.9 are summarised in Table 7.5.

Table 7.5: Ranges of the design optimisation variables in optimal designs for Seville, Tonopah, and Atacama Desert (Figure 7.10)

Variable	unit	Seville	Tonopah	Atacama
A^{CSP}	$10^4\ m^2$	[33,47]	[35,39]	[17,22]
P^{ST}	MW	[9,14.5]	[8.5,10.5]	[5,8]
P^{MC}	MW	[31,44]	[34,40]	[16,44]
P^{MT}	MW	[55,67]	[58,62]	[30,66]
P^{HPSC}	MW	[17,20]	[16,20]	[7,20]
P^{HPST}	MW	[4,6]	[2.5,5]	[2,8]
STO^{CO_2}	$10^3\ m^3$	[1.3,5.7]	[1.5,3.7]	[1,2.3]
STO^{CaO}	$10^3\ m^3$	[8.3,37]	[10.8,24]	[6,15]
STO^{Solids}	$10^3\ m^3$	[8.4,38]	[11,24.5]	[6.1,15.2]
A^{PV}	$10^4\ m^2$	[38,41]	[39,41]	[29,41]

First, according to Figures 7.16 and 7.17, there are significant negative correlations between LPSP and investment, and between LPSP and LCOE. These numbers suggest that, in Seville

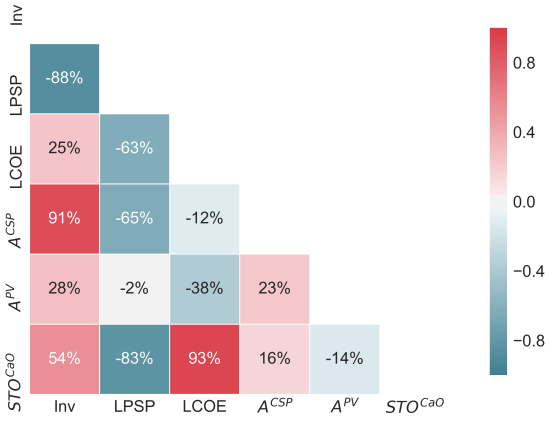

Figure 7.16: Correlation matrix for optimal designs in Seville, Spain

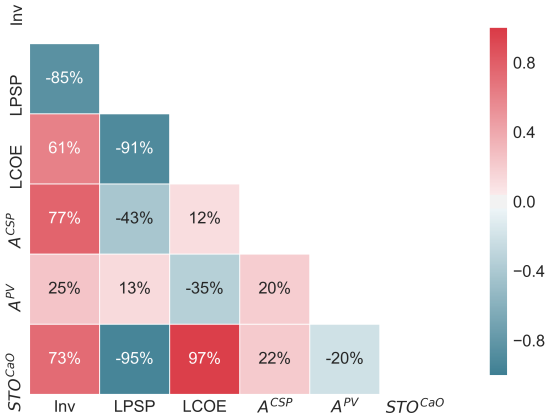

Figure 7.17: Correlation matrix for optimal designs in Tonopah, Nevada, USA

and Tonopah, high dispatchability can be reached in power plants with large CSP plants integrated with a large TCES system (see Table 7.5). Moreover, from the low correlation between investment and A^{PV}, significant positive correlation between investment and A^{CSP}, and negative correlation between LPSP and A^{CSP}, together with the ranges shown in Table 7.5 it can be inferred that, in Seville and Tonopah, a large PV is always required to keep a low LCOE, and extra capacity in CSP is required to give dispatchability.

On the contrary, in the Atacama Desert there is a high negative correlation between LCOE and investment, and between LCOE and A^{PV}, as well as a significant positive correlation between investment and A^{PV}, and low correlation between investment and A^{CSP}. These numbers suggest that a smaller CSP-TCES plant is required to accomplish the commitment (see Table 7.5), and additional investment in PV results in a considerable reduction in LCOE.

As expected, in the three locations exists a significant negative correlation between LPSP and the capacity of the TCES system (STO^{CaO}), highlighting the importance of the energy storage in increasing the dispatchability of the power plant.

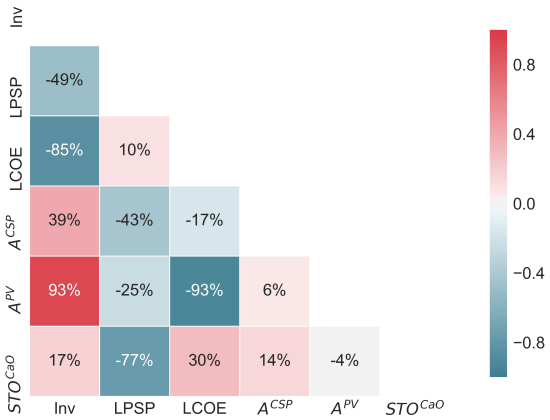

Figure 7.18: Correlation matrix for optimal designs in the Atacama Desert, Chile

7.4.3 Design guidelines based on resource and dispatchability

In this section the results are analysed to develop guidelines to use as a starting point for the optimal design of a hybrid solar plant with TCES. These guidelines are based on the solar irradiation of the three locations under study, that covers a range of different solar resources. First, a large PV will decrease the LCOE in every situation; hence, the optimal design starts by selecting the largest PV area considering the available land and the maximum power that can be dispatched as constraints. Then, it is possible to estimate the area of the CSP by evaluating the following equation:

$$A^{CSP} \approx \frac{P^{commitment} \cdot (24 - h_s) \cdot (1 - LPSP)}{h_s \cdot DNI_{average} \cdot \eta_{CSP,DNI}} \tag{7.5}$$

where h_s correspond to the number of sunshine hours, and the LPSP is the flexibility allowed. After that, as can be seen in Figure 7.12, there are clear relations between the capacities of compressors and turbines with the heliostat field area. In this context, the capacity of the steam turbine of the Rankine cycle, that is directly connected to the CSP plant can be estimated with the thermal power of the CSP plant, through the following equation:

$$P^{ST} \approx A^{CSP} \cdot DNI_{average} \cdot \eta_{CSP,th} \cdot \eta_{SSRC} \tag{7.6}$$

where $\eta_{CSP,th} \approx 0.36$ and $\eta_{SSRC} \approx 0.268$. Then, the following relations can be inferred from the optimised designs presented in Figure 7.12:

$$P^{MC} \approx 3 \cdot P^{ST} \tag{7.7}$$

$$P^{MT} \approx 1.8 \cdot P^{MC} \tag{7.8}$$

$$P^{HPSC} \approx 0.4 \cdot P^{MC} \tag{7.9}$$

$$P^{HPST} \approx 0.15 \cdot P^{HPSC} \tag{7.10}$$

Finally, the capacity of the energy storage system depends on the relationship between the storage hours and the capacity of the components. Using a specific power generation previously reported i.e. $\xi_i \approx 0.053$ MWh·ton$^{-1}_{CaO}$, the capacity of the CaO storage tank (STO^{CaO}, in ton_{CaO}) for each location (points Sev_b, Ton_b, Ata_b in Figures 7.7, 7.8, and 7.9 respectively) can be estimated by the maximum power dispatched from the Brayton cycle (i.e. $P^{Brayton\ cycle} = P^{MT} - P^{MC}$), according to the following equation:

$$STO^{CaO}(ton_{CaO}) \approx \frac{(24 - h_s) \cdot P^{Brayton\ cycle}}{\xi_i} \tag{7.11}$$

Then, considering a $\rho_{CaO} \approx 3370$kg·m^3, and values of porosity and packing density of solids equals to 0.5 and 0.6 respectively (Valverde *et al.*, 2015), allows to evaluate the capacity of the storage of CaO in units of volume (m^3). Finally, the capacity of the storage tank of solids and CO_2 can be estimated by:

$$STO^{Solids}(m^3) \approx 1.02 \cdot STO^{CaO}(m^3) \tag{7.12}$$

$$STO^{CO_2}(m^3) \approx 0.155 \cdot STO^{CaO}(m^3) \tag{7.13}$$

7.4.4 Sensitivity analysis

A sensitivity analysis was performed for power plants defined as Sev$_a$, Ton$_a$, and Ata$_a$ in Figures 7.7, 7.8, and 7.9, to determine the influence of key input parameters on the LCOE of dispatchable hybrid power plants. The following parameters, and its original values, were selected for the analysis:

$$\eta^{Receiver} = 0.85 \tag{7.14}$$

$$\zeta^{Reactors} = 1 \tag{7.15}$$

$$r = 7\% \tag{7.16}$$

where $\zeta^{Reactors}$ is a multiplier used to vary the investment cost of the reactors, i.e. calciner and carbonator; $\eta^{Receiver}$ is the efficiency of the receiver in the solar tower, where the calciner is located; and r is the annual interest rate. A summary of the sensitivity analysis results is shown in Figure 7.19.

First, the effect of a higher receiver efficiency does not produce a large decrease in the LCOE, because this technical parameter influences both, the LPSP and the LCOE, and these power plants are optimised considering the base value ($\eta^{Receiver} = 0.85$). For instance, in the case that the efficiency is 0.94, the solar field could be reduced, keeping a similar LPSP but reducing the

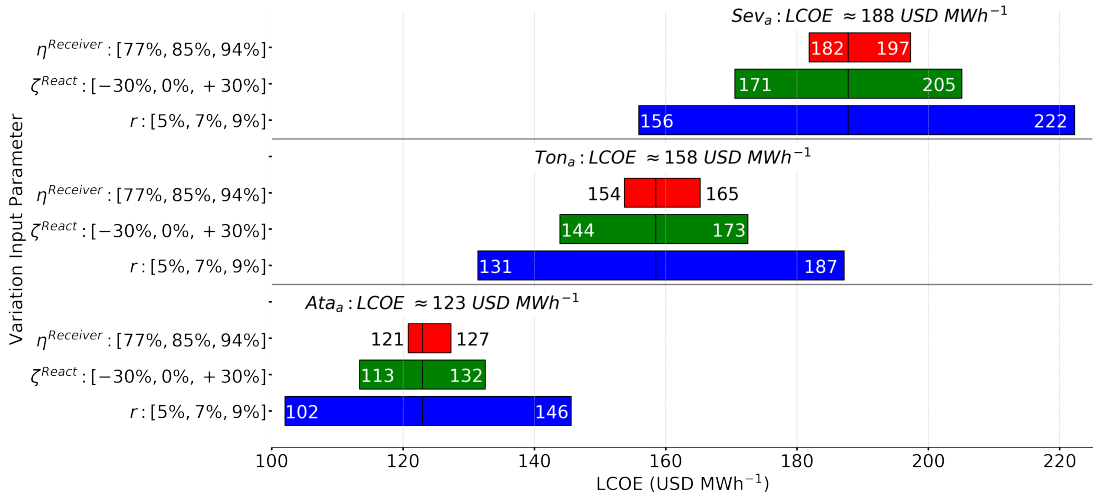

Figure 7.19: Sensitivity analysis for the LCOE by varying technical and financial parameters

LCOE. Hence, for an optimal design of the power plant, a new optimisation will be required when a key technical input parameters is modified. For instance, for a high receiver efficiency ($\eta^{Receiver} = 0.94$) and a 30% decrease in heliostats area in Atacama, the LCOE reduces to 115 USD·MWh^{-1} (< 121 USD·MWh^{-1}), while maintaining the same LPSP. Hence, a further reduction can be achieved by increasing the efficiency of the receiver and modifying the capacity of some components.

In addition, it can be observed that changes in the investment cost of the reactors and the interest rate have a significant impact on the LCOE. Remarkably, all simulated cases in Atacama (Ata), even in the worst scenarios proposed in the sensitivity analysis, show promising results in terms of LCOE and dispatchability.

7.5 Conclusions

Hybrid CSP-PV plants integrated with thermochemical energy storage are promising candidates to provide dispatchable and affordable clean energy but require sophisticated design tools to achieve this. This chapter presents the two-stage multi-objective optimisation framework to simultaneously optimise the design and operation of a hybrid solar power plant (CSP and PV) integrated with calcium-looping (CaL) as thermochemical energy storage (TCES) system. The optimisation results were used to develop general design guidelines for hybrid solar power plants with TCES systems.

This framework provides key information in the decision-making process for the design of reliable and affordable power plants, going beyond the often used manual design process. In addition, the one-year hourly operational optimisation stage which takes the seasonal variations in solar resource into account provides more suitable designs compared to studies which

use only a short time horizon or typical periods. The optimisation provides key performance indicators such as affordability, dispatchability, average power supplied, capacity factor, and efficiencies, to compare the performance of different designs and different locations.

The optimisation framework was applied to three locations with different levels of solar irradiation, i.e. Seville, Spain; Tonopah, Nevada, USA; and the Atacama Desert, Chile, to illustrate the opportunities in the integration of clean technologies under different conditions. The design and techno-economic performance of the optimised plants for each location are clearly defined by the average values and variability of the solar irradiation. Of the three locations, the Atacama Desert has the highest potential, achieving an LCOE of 123 USD·MWh^{-1} for a highly dispatchable power plant. This shows the impact of the stability and level of solar irradiation on the design of dispatchable power plants. It also highlights the significant potential of hybrid solar power plants with efficient energy storage systems to provide cost-competitive, dispatchable and clean energy.

The results show that the integration of CaL as TCES system increases the dispatchability of CSP plants with capacity factors as high as 73%, and that the hybridisation with PV plants is essential to achieve competitive energy costs. The results emphasize the potential of the integration of different technologies in the design of affordable and dispatchable renewable power plants to support the transition to a sustainable energy system. While it is clearly shown that multi-objective optimisation is required to achieve an optimal design, this contribution provides general information to understand the interactions and synergies between different technologies, and the opportunities in the development of solar power plants to support the transition to a sustainable energy system.

The optimal designs for the three locations were used to develop guidelines for the optimal design of affordable and dispatchable hybrid solar power plants with CaL as TCES for any location. The guidelines provide an affordable hybrid solar power plant with TCES design based on the solar resource and the required level of dispatchability. While it is only an approximation to the most optimal design, it is an ideal starting point for manual design optimisation in a process simulator such as Ansys. Thus, it can support the design of more affordable and dispatchable hybrid solar power plants which are required for the transition to a low carbon energy system.

Chapter 8

Conclusions

This research developed modelling and optimisation tools to optimise the design and operation of hybrid solar power plants with energy storage and to provide guidelines for the optimal development of sustainable energy systems under different conditions and requirements.

A review of previous studies on the modelling and optimisation of energy systems with energy storage was performed to investigate knowledge gaps. The following objectives were identified and pursued throughout the thesis:

1. To develop a multi-objective optimisation model for the operation of hybrid solar power plants with energy storage, taking into account the daily and seasonal variability of the solar resource.
2. To develop a two-stage multi-objective optimisation framework to simultaneously optimise the design and operation of a hybrid solar power plant integrated with energy storage.
3. To investigate the importance of multi-objective optimisation in exploiting synergies by the integration of dispatchable concentrating solar power systems with energy storage and low-cost photovoltaic technology.
4. To explore the role of the integration of different technologies in improving the performance of hybrid solar power plants, e.g. sensible heat thermal energy storage (two-tanks molten salts), thermochemical energy storage (calcium-looping), electrical energy storage (batteries)
5. To explore characteristics of dispatchable hybrid solar power plants under different solar conditions and operational requirements.
6. To examine flexibility approaches in increasing the performance of sustainable technologies to support the transition to an affordable and clean energy system
7. To develop guidelines for the optimal design of hybrid solar power plants based on the solar resource and required dispatchability.

These objectives have been analysed, developed and achieved in the studies reported in Chapters 3, 4, 5, 6 and 7 of this thesis. Summaries of these achievements are given in the following paragraphs.

8.1 Two-stage design and operational optimisation framework

The first two objectives were achieved by the framework developed in Chapter 3. Here the simulation of the operation of a hybrid solar power plant with energy storage was developed by mass and energy balances, considering each component as well as the interactions between different subsystems. The operational optimisation model, written in Python and using Pyomo, considers variables, constraints, and objectives. Here, financial and technical parameters as well as time-steps are defined as input parameters. Hence, the model can handle different configuration and requirements. Multi-objective linear programming methods were developed to evaluate the daily and seasonal behaviour of the system under variable resource. These methods, ε-constraint and linear scalarisation were evaluated. Then, due to the faster performance of the linear scalarisation compared to the ε-constraint method, an automated linear scalarisation method was developed.

The design optimisation routine was developed using genetic algorithms. Here, to simultaneously optimise the design and operation of the hybrid solar power plant with energy storage, the multi-objective operational optimisation is nested in the fitness evaluation routine of the genetic algorithm, and the objectives of both stages are linked in order to exploit synergies of technology integration. The rest of the objectives were accomplished in all different case studies analysed in Chapters 4, 5, 6, and 7, described below.

8.2 Improvement of a hybrid solar power plant with thermal energy storage

The first case study, developed in Chapter 4, focused on the application of the two-stage optimisation framework for the optimal design of a hybrid solar power plant (CSP-PV) integrated with a two-tank molten salt technology (sensible heat thermal energy storage system). Here the automated linear scalarisation method was analysed and used to develop guidelines to future applications. The framework was applied to analyse and improve the design of a power plant under construction in Northern Chile. The results showed the importance of energy storage to improve the dispatchability of solar technologies. Nevertheless, its appropriate design is essential to provide affordability. Besides, the benefit of the trade-off between technical and financial performance, achieved by the multi-objective optimisation was demonstrated. The analysis showed the importance to define direct links between the design and operational optimisation objectives to exploit synergies of technology integration.

8.3 Technology integration analysis and optimal design of dispatchable power plants

Different technologies were integrated and evaluated in Chapter 5. These case studies, located in Northern Chile, were analysed by configurations covering off-grid and grid-connected power plants, which have different requirements and constraints in the operation. Throughout this evaluation, a long-term cost analysis was addressed, concluding that due to the extreme reduction expected in the cost of batteries, in the long term, solar PV integrated with electrical energy storage could be the most competitive technology to provide affordable and dispatchable energy storage. Then, in order to increase the dispatchability of CSP, the integration of a fossil backup unit was studied. The results showed that, due to the high level of irradiation in the Atacama Desert (during summer and winter), the stable demand profile required, and the high costs of diesel in Northern Chile, small fossil backup units are enough to increase the performance of hybrid solar power plants. After that, an economic feasibility analysis was carried out to study the heat supply for low-temperature mining processes from the heat rejection from the Rankine cycle of the CSP plant. In this case, the results showed that the use of waste heat from CSP is highly recommended. Nevertheless, the technical feasibility of the project needs to be addressed considering the location of both, the solar power plant and the mining process where the heat is required. Finally, in order to reduce the variability of the natural resource, a wind power station was integrated into the CSP-PV plant, showing that the integration of different renewable technologies improves the performance of sustainable technologies.

8.4 Operational optimisation of a hybrid solar power plant with TCES

In Chapter 6, the operation of a concentrated solar power plant integrated with a calcium-looping process as a thermochemical energy storage system was analysed and optimised. Different designs and the hybridisation with a photovoltaic system were evaluated. Besides, the framework enables long-term studies for the optimisation of the operation of solar power plants with thermochemical energy storage and their integration into energy systems. The results summarise key indicators obtained by optimising the operation of a power plant located in Seville, Spain. The findings of this study indicate that the use of a thermochemical energy storage system in concentrated solar power plants increases the dispatchability, and by hybridising with a photovoltaic system, it can become cost-competitive. However, the significant differences in the solar irradiation in Seville between summer and winter could have a negative effect on the power system during summer by dispatching a large amount of power during the day.

8.5 Design optimisation of dispatchable hybrid solar power plants with TCES

In Chapter 7, the two-stage multi-objective optimisation framework was applied for the optimal design of hybrid CSP-PV plants with calcium-looping TCES with respect to competing technical and financial performances. While the design optimisation stage evaluates ten design variables and three objectives, the second stage, finds the best one-year hourly operational strategy for each design. The application of the framework provided a systematic methodology and guidelines for the design of dispatchable power plants which takes the yearly operation into account and goes beyond a manual design process. To analyse potential locations for further deployment of solar plants with TCES, the following locations which cover a range of different profiles were evaluated: Seville, Spain; Tonopah, Nevada, United States; and the Atacama Desert, Chile. The optimisation results were used to develop guidelines for the optimal design of dispatchable hybrid solar power plants with TCES based on the given solar resource and required dispatchability. These guidelines provide an initial design for affordable and dispatchable hybrid solar power plants and can enable their widespread development.

8.6 Final discussion

Hybrid CSP-PV plants integrated with energy storage are promising candidates to provide dispatchable and affordable clean energy but require sophisticated design tools to achieve this. In this research, a two-stage multi-objective optimisation framework to simultaneously optimise the design and operation of a hybrid solar power plant (CSP and PV) integrated with energy storage systems was developed. Different energy storage systems were integrated into a hybrid solar power plant. Molten-salt sensible thermal energy storage, calcium-looping thermochemical energy storage, and electrical batteries were implemented into solar power plants to study the improved performance of solar technologies. In addition, grid-connected and off-grid power plants were analysed. The optimisation results were used to develop general design guidelines for hybrid solar power plants with energy systems.

The framework developed provides essential information in the decision-making process for the design of reliable and affordable power plants, going beyond the often used manual design process. Besides, the one-year hourly operational optimisation stage which takes the seasonal variations in solar resource into account provides more suitable designs compared to studies which use only a short time horizon or typical periods. The optimisation provides key performance indicators such as affordability, dispatchability, average power supplied, capacity factor, and efficiencies, to compare the performance of different designs and different locations.

The optimisation framework was applied to different locations with different levels of solar irradiation, i.e. Seville, Spain; Tonopah, Nevada, USA; and the Atacama Desert, Chile, to

illustrate the opportunities in the integration of clean technologies under different conditions. The design and techno-economic performance of the optimised plants for each location are clearly defined by the average values and variability of the solar irradiation. Of the three locations, the Atacama Desert has the highest potential, achieving an LCOE close to 120 USD·MWh^{-1} for a highly dispatchable power plant integrated with thermal energy storage (two-tanks molten salts or calcium-looping). The results showed the impact of the stability and level of solar irradiation on the design of dispatchable power plants. It also highlights the significant potential of hybrid solar power plants with efficient energy storage systems to provide cost-competitive, dispatchable and clean energy.

The results confirm that the integration of an energy storage system increases the dispatchability of CSP plants with capacity factors higher than 70%, and that the hybridisation with PV plants is essential to achieve competitive energy costs. The results emphasise the potential of the integration of different technologies in the design of affordable and dispatchable renewable power plants to support the transition to a sustainable energy system. While it is clearly shown that multi-objective optimisation is required to achieve an optimal design, this contribution provides general information to understand the interactions and synergies between the integration of different technologies, and the opportunities in the development of solar power plants to support the transition to a sustainable energy system.

The optimal designs analysed in each case study were used to develop guidelines for the optimal design of affordable and dispatchable hybrid solar power plants with energy storage for any location. The guidelines provide an affordable hybrid solar power plant with energy storage design based on the solar resource and the required level of dispatchability. While it is only an approximation to the most optimal design, it is an ideal starting point for manual design optimisation. Thus, it can support the design of more affordable and dispatchable hybrid solar power plants which are required for the transition to a low carbon energy system.

Additionally, the model developed can be applied to other locations under different input parameters and demand profiles. For example, the cost competitiveness of the power plant would be increased if the demand is higher in summer and lower in winter, which would be the case for locations with high cooling demand in summer. In contrast, other places like the Atacama Desert whose demand is driven by the intensive mining industry need an almost constant supply of electricity throughout the year. Finally, the model can easily be extended to evaluate different energy conversion and storage technologies to design hybrid power plants with energy storage. Thus, the optimisation framework can provide valuable information for the integration of different technologies to support the affordable and sustainable transition to a clean energy system.

8.7 Recommendations for further work

The work presented in this research can be extended in several ways. Different options with high potential impacts are discussed in the following sections.

8.7.1 Multiple years and resolution

The case studies presented in this thesis consider a typical meteorological year (TMY) for the operational optimisation stage. As previously explained, the TMY represents the long term solar resource of the location under consideration. Hence, the operational optimisation of a power plant under the TMY does not show the performance of a particular year. Then, in order to be able to evaluate worst-case scenarios of the performance of hybrid solar power plants, the operational optimisation considering multiple years is suggested.

Besides, the TMY considered in this research has hourly resolution. However, by analysing a TMY with shorter resolution (e.g. 30 or 15 minutes), a more detailed operational strategy can be examined. In this case, the integration of other variables like ramp rates could be useful to give more applied results. Despite that the current model handles any time frame and resolution, the evaluation of a more extensive data set will require a more extended evaluation time.

In addition, other facts such as different weather datasets or weather forecasts considering different conditions in the Atacama Desert can be evaluated. The purpose to evaluate different designs under similar weather characteristics was done in order to make a comparison between designs under similar conditions. Nevertheless, it is possible to evaluate extreme conditions, such us the estimation of failure probabilities using Monte-Carlo methods to construct a probabilistic view of the performance of the system; consider ramp rates and power transients according to control schemes; analyse the technical performance of the power plant under climate change scenarios, among others.

8.7.2 Analysis of variable demand

In order to estimate the dispatchability of the power plants analysed in the case studies, this research considered two options: (i) a fixed commitment; (ii) a commitment equal to the power demand of a copper mine. In both cases, the commitment is not related with the profile of the solar resource. Future work will explore the analysis of a variable demand. For example, the cost competitiveness of a hybrid solar power plant would be increased if the demand is higher in summer and lower in winter, which would be the case for locations with high cooling demand in summer (e.g. Seville). In contrast, other places like the Atacama Desert whose demand is driven by the intensive mining industry need an almost constant supply of electricity throughout the year.

8.7.3 Demand side management

In order to increase the overall efficiency of a renewable power plant with energy storage, several studies recommend the integration of demand side management (DSM) strategies. In this case, demand respond mechanisms focus on changing the profile of the consumer power requirement by reducing or shifting it to maximise the use of the renewable energy resource. Here, the configuration is essential to define the problem appropriately. For instance, if DSM techniques are applied in an off-grid power plant that supplies energy to a copper mine, the analysis of the power consumption of each process is essential to define the power supply to operations that can be reduced or delayed, as well as the time that the delay could be performed.

8.7.4 Multi-mode operation

The case studies presented in this research consider the levelised cost of electricity as a metric to evaluate the financial performance of the power plant. Nevertheless, the ability of CSP with TES to adapt the power output could be analysed to increase the financial performance of the power plant. Hence, the participation in electricity markets, considering electricity prices and other income schemes in the optimisation in order to exploit this feature will need to be undertaken. For instance, the model can consider variable electricity price as well as other incomes by providing reserve services to optimise the financial performance of the power plant.

8.7.5 Data clustering

As mentioned in Chapter 5, the computation time taken by the two-stage optimisation was around 40 hours. Then, the implementation of a data cluster technique, in order to evaluate a shorter number of time-steps in the operational optimisation stage, become interesting. Here, a decrease in the number of evaluations required in the operational optimisation routine allows a drop in the computational time needed to achieve the desired results. Research into solving this problem is already in progress. The data clustering framework developed is detailed in Appendix A. Besides, the information displayed in Appendix A presents the results of the application of the data clustering process in the configuration studied in Section 5.4, i.e. the integration of a hybrid solar power plant with a wind farm.

8.7.6 Seasonal energy storage

The integration of thermochemical energy storage into hybrid solar power plants present attractive characteristicts and possibilities to be analysed in future studies. Figure 8.1 illustrates further independent studies intended to be undertaken. These topics are investigated in this and the following sections.

Thermochemical energy storage has the potential for high energy storage density and no storage losses, besides the initial loss of the sensible heat. Hence, further investigation of calcium-

looping as seasonal energy storage system is proposed. In this case, heaters will be required in order to recover the sensible heat lost and to allow the carbonation process to take place. Here, the volume of the storage system will be crucial to evaluate the economic feasibility of the configuration.

8.7.7 Use of power curtailment from renewable power plants

The reduction of curtailments from wind and solar PV plants is key to improve the revenue of renewable power plants (Bird *et al.*, 2014). Curtailment occurs typically due to constrains in the power transmission sector or excess generation. The fluctuation of the renewable resource in some areas results in high variability of the power supply to the network. Then, renewable energy curtailment is an essential mechanism to protect the electrical grid. Future work will explore the technical and economic feasibility to use the power curtailment from wind or solar power plants by converting electricity into heat and use it as a heat injection in the calciner of the calcium-looping system.

8.7.8 Operational parameters of the calcium-looping

In this research, to linearise the variables of the calcium-looping operation, the temperatures were fixed according to published investigations. Nevertheless, in order to get a broad operational strategy and general guidelines for the design of thermochemical energy storage systems, further work considering non-linear models or the evaluation of other operational conditions need to be done. In this context, temperatures and pressures in each process can be defined as optimisation variables (instead of input parameters).

8.7.9 Other reversible chemical reactions

In addition, further studies will need to be performed to analyse other reversible chemical reactions suitable to be used as thermochemical energy storage systems. For instance, the reversible hydration/dehydration reaction of calcium oxide: $Ca(OH)_2 \rightleftarrows CaO{+}H_2O$, with $\Delta\hat{H}_r^{\circ} = 104$ kJ·mol^{-1} (Salas *et al.*, 2018; Pardo *et al.*, 2014).

8.7.10 Calcium-looping as a CO_2 capture system

The current model can be modified to perform the analysis of a CO_2 capture system based on calcium-looping. In this case, the flue gas from a fossil-fuelled combustion process is compressed and conducted to the carbonator, where the CO_2 presented reacts with the CaO from the storage tank, forming $CaCO_3$. Then, while the flue gas (without CO_2) is driven to a turbine and then sent to the atmosphere, the $CaCO_3$ is stored in the storage tank. After that, the calcination process splits the $CaCO_3$ into CO_2 and CaO. Finally, the CO_2 can be compressed and stored for future transport, utilisation or permanent storage. In this work,

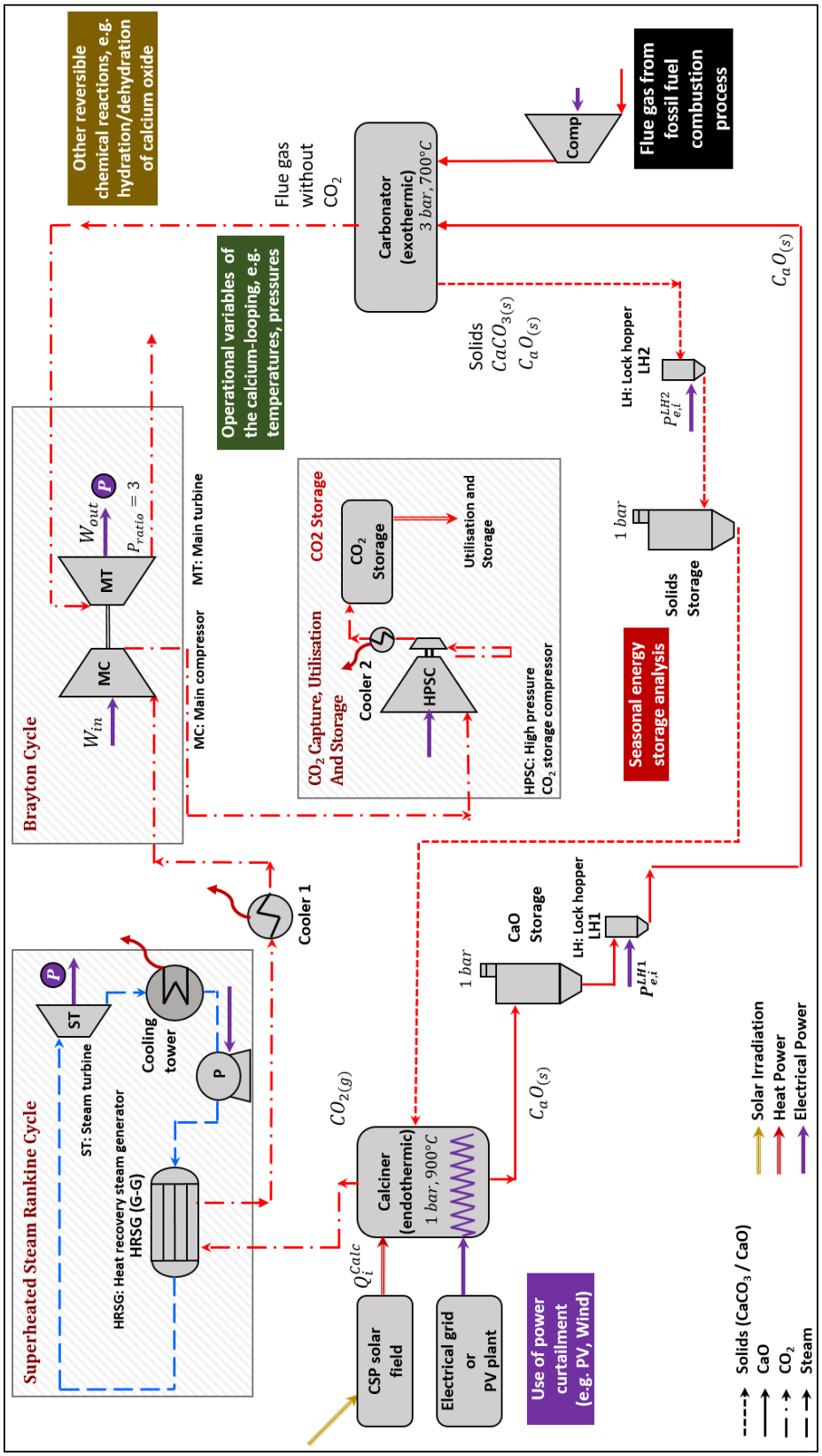

Figure 8.1: Recommendations for further work

further investigation needs to be undertaken to evaluate and define the reaction properties and kinetics of the carbonation of the CO_2-rich flue gas and CaO.

Appendix A

Data clustering

A.1 Introduction

This section focuses on the implementation of a data cluster technique in order to evaluate a shorter number of time-steps in the operational optimisation stage. This reduction of the total number of evaluations allows a drop in the computational time required to achieve the desired results of the design optimisation routine.

The purpose of data clustering is to find groups in data (Kaufman and Rousseeuw, 2005). Here, a cluster is defined as a group of data points that have similar features. Hence, a basic process for data clustering applied for the problems studied in this thesis, is to find a suitable number of clusters, and the data points that belong to each clusters.

The silhouette analysis, introduced by Rousseeuw (1987), is a process that helps in the definition of an optimal number of clusters for a given sample. The silhouette analysis measures the distance between each data point with the neighbouring clusters, and calculate a numerical value in the range [-1, 1]. A value close to 1 denotes that the point is distant from the neighbouring clusters; therefore, the observations are very well clustered. Then, a value close to 0 indicates that the point lies on the boundary between two clusters. Finally, a negative value shows that the data point was probably assigned in the wrong cluster.

Then, to optimise the location of the centroids in each cluster, the k-means algorithm will be employed. The k-means algorithm, proposed by Macqueen (1967), starts by selecting a random position of one centroid for each cluster. Then it assigns every data point to the closest cluster by minimising the sum of the squared distance between each point and a centroid. Then, the algorithm iterates by re-locating the centroids in the centre of mass, i.e. the location where the weighted relative position of all points in the cluster sums zero. Then, all data points are assigned to the new centroids, and a new re-location of the centroids is performed. This algorithm iterates until the location of the centroids do not change.

Hence, while the k-means algorithm optimises the location of the centroids for a given number of clusters, the silhouette analysis helps in the definition of an optimal number of clusters for a given sample. Furthermore, the simultaneous combination of both techniques are applied in

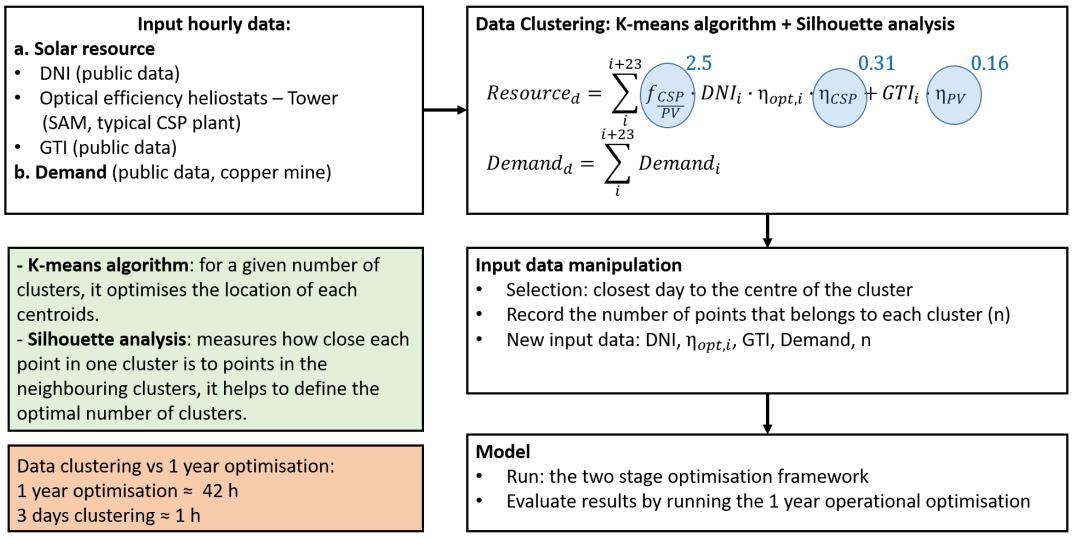

Figure A.1: Data clustering. Framework

this study, that gives us a powerful tool to optimise both, the number of clusters and the position of the centroids that represent the complete data set.

A.2 Implementation

Figure A.1 shows the framework developed for this study. First, the solar resource and the demand are used as input in the analysis. For a fixed design, the solar resource will determine the maximum power supplied by the power plant, and then the LCOE. On the other hand, the power commitment will provide the necessary information to select the best strategy to operate, considering the opportunity to store energy when there is a benefit in the future. Then, the data clustering analysis is performed by employing the k-means algorithm and Silhouette analysis.

In order to apply these tools, the variables need to be grouped and normalised. For instance, equation A.1 shows the grouping process of the solar resource for one day. This equation considers the estimation of the fraction between the CSP and the PV solar field, here a factor of 2.5 was considered (obtained from the analysis of the previous results presented in Chapter 5). Then, all variables that vary in each time step are considered: direct normal irradiation, global tilted irradiation, and the solar-to-electrical efficiency of the CSP and PV plants.

$$Resource_d = \sum_{i}^{i+23} f_{\frac{CSP}{PV}} \cdot DNI_i \cdot \eta_{opt,i} \cdot \eta_{CSP} + GTI_i \cdot \eta_{PV} \tag{A.1}$$

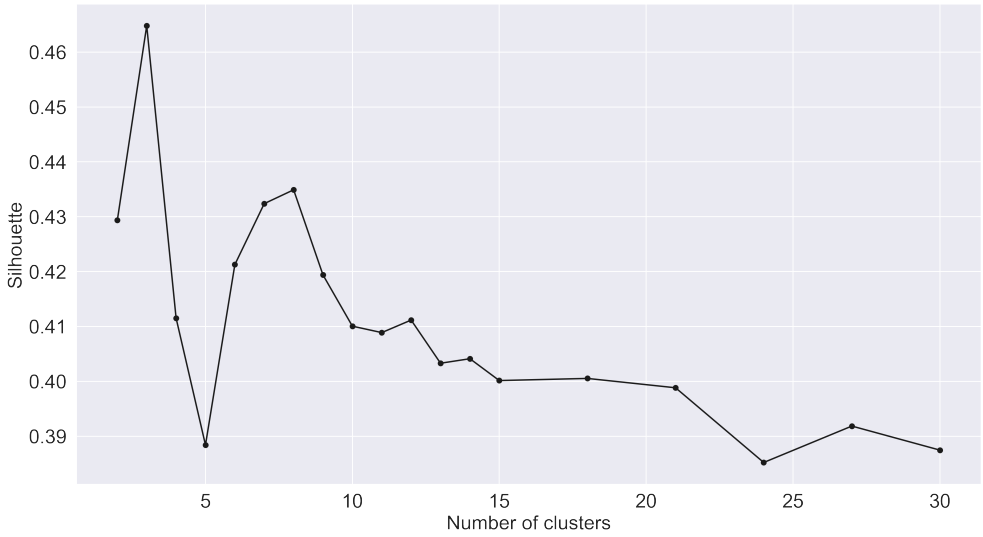

Figure A.2: Data clustering. Silhouette analysis

$$Demand_d = \sum_{i}^{i+23} Demand_i \tag{A.2}$$

Here, the data clustering analysis was applied for the optimal design of a power plant that supplies energy to El Abra copper mine, as studied in Section 5.5. The silhouette analysis was conducted, and an optimal number of 3 or 8 clusters was suggested, as shown in Figure A.2. Then, in order to be able to cover more details and interactions between the different technologies in the operational optimisation routine, a number of 8 clusters was selected. After that, the optimal location of each centroid is achieved by the k-means algorithm and shown in Figure A.3. This figure displays the normalised total demand per day in the x-axis, the normalised solar resource in the y-axis, and each point in the diagram correspond to a single day defined by both variables. Then, the big red dots correspond to the optimised location of the centroids obtained by the k-means algorithm. Next, the number that is shown bellow each centroid corresponds to the total number of samples (n) that belongs to that cluster. Finally, the closest day to the centroid is identified in the diagram and used as a representative day as a centroid in the clustering process.

When this process is finished, i.e. the number of clusters, the number of samples in each cluster, and the representative day of each centroid are known, the two-stage multi-objective optimisation framework is evaluated with this clustering data as input. For instance, instead of optimising for 8760 hours, this data clustering process allows optimising for eight days (192 hours) and multiplying each day for the number of samples (n), in order to have an approximation of the Pareto optimal solutions.

Then, a final stage is performed by optimising the annual operation of all non-dominated set of solutions obtained from the two-stage optimisation with data clustering. This step allows us

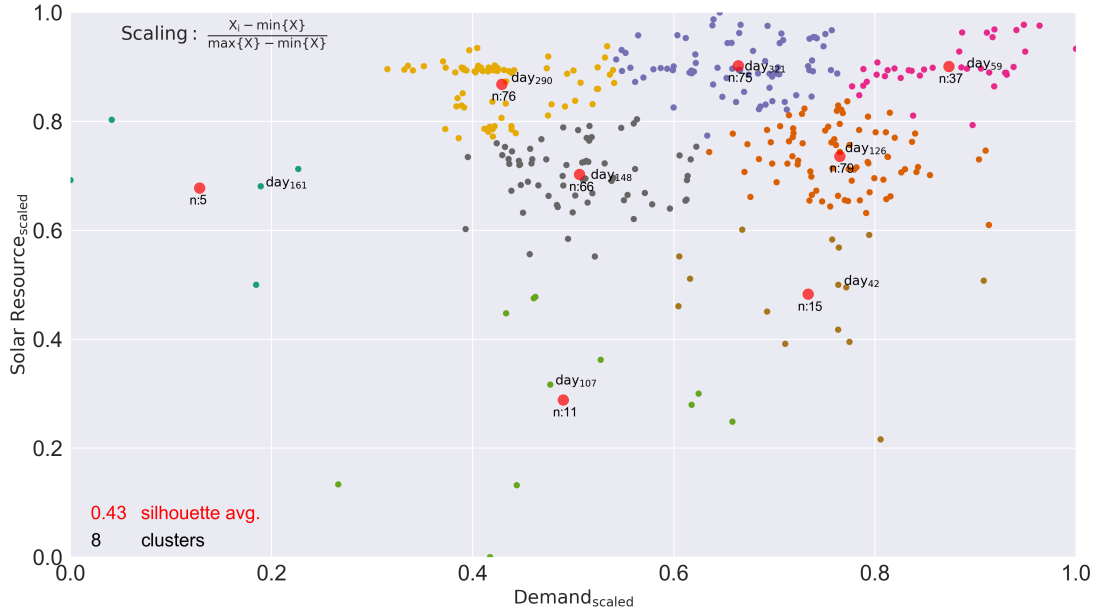

Figure A.3: Data clustering. k-means Algorithm

to improve the expected performance of the optimal designs achieved with the data clustering process. Besides, by optimising its one-year hourly operation, it is possible to compare these designs with the optimal designs resulted in the two-stage optimisation framework presented in the main chapters of this thesis.

A.3 Results and discussion

In order to be able to have an accurate comparison in the application of data clustering in the optimal design of sustainable power plants, the process was evaluated with different time scales. Here, days, weeks and fortnights were considered and grouped as defined in equations A.1 and A.2, with a proper definition of the summation process. By the silhouette analysis, it was determined that eight days, four weeks, and three fortnights are an appropriated number of clusters for each case.

Figure A.4 shows the three clustering process explained previously (8 hours, 4 weeks, and 3 fortnights) and the optimal designs achieved by the one-year annual optimisation. First, with a continuous black line, the results of the two-stage optimisation considering one-year hourly operation (8760 time-steps) are presented. This process required 42 hours to be computed. Then, with different colours and lines, the figure illustrates the results of the two-stage optimisation framework with data clustering. These processes are computed in 1 h, 3 h, and 4 h, respectively.

These results demonstrate that the use of data clustering considerably decreased the computational time. Nevertheless, despite that the optimal solutions are not the same, the diagram

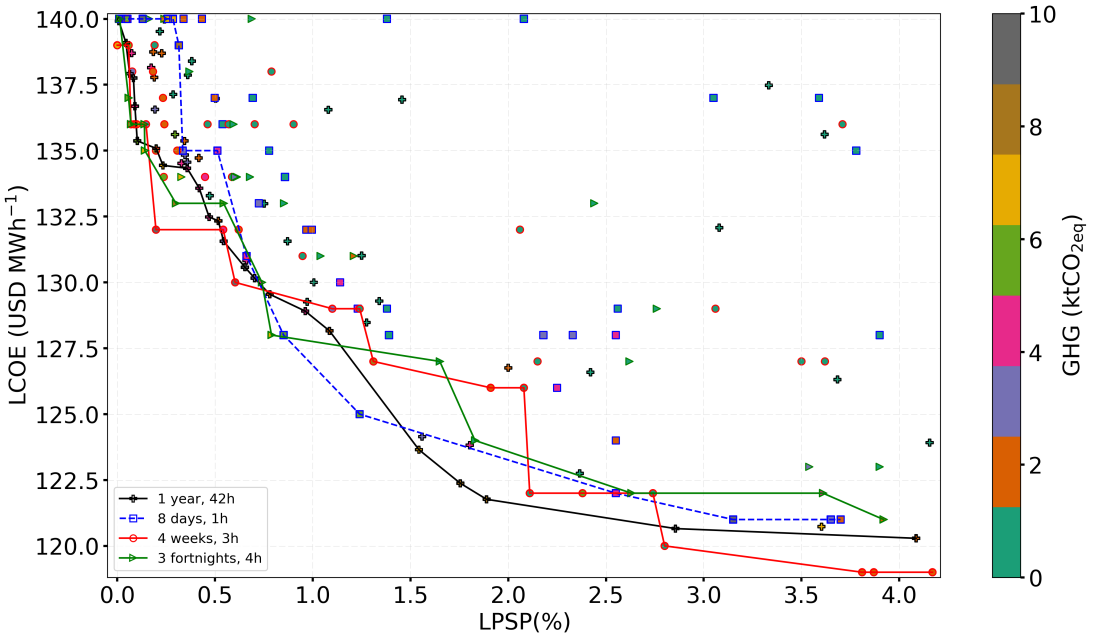

Figure A.4: Data clustering. Design optimisation results of a hybrid solar power plant with a wind power station

shows that the three time scales considered in the data clustering process reach solutions that are relatively close to the best approximation by considering one year in the operational optimisation stage. Consequently, these results highlight the potential of data clustering techniques as an excellent tool to reduce the computational requirements to achieve comparable results in the optimal design of dispatchable and affordable renewable power plants. In this context, the use of a data clustering technique could give a first approximation for optimal designs of a hybrid power plant with energy storage when the computational time could be a constraint.

Bibliography

Abbas, A., Huff, G., Currier, A. B., Kaun, B. C., Rastler, D. M., Chen, S. B., Bradshaw, D. T., and Gauntlett, W. D. DOE/EPRI 2013 electricity storage handbook in collaboration with NRECA. Technical Report July, Sandia National Laboratories, 2013.

Abengoa Solar. Abengoa: About Atacama-1, 2016. URL `http://www.abengoa.com/web/en/novedades/atacama-1/acerca/factsheet/`.

Alovisio, A., Chacartegui, R., Ortiz, C., Valverde, J. M., and Verda, V. Optimizing the CSP-Calcium Looping integration for Thermochemical Energy Storage. *Energy Conversion and Management*, 136:85–98, mar 2017. ISSN 01968904. doi: 10.1016/j.enconman.2016.12.093.

Amusat, O. O., Shearing, P. R., and Fraga, E. S. Optimal integrated energy systems design incorporating variable renewable energy sources. *Computers & Chemical Engineering*, 95:21–37, 2016. ISSN 00981354. doi: 10.1016/j.compchemeng.2016.08.007.

Amusat, O. O., Shearing, P. R., and Fraga, E. S. On the design of complex energy systems: Accounting for renewables variability in systems sizing. *Computers and Chemical Engineering*, 103:103–115, 2017. ISSN 00981354. doi: 10.1016/j.compchemeng.2017.03.010.

Amy, C., Seyf, H. R., Steiner, M. A., Friedman, D. J., and Henry, A. Thermal energy grid storage using multi-junction photovoltaics. *Energy Environ. Sci.*, 12(1):334–343, 2019. ISSN 17545706. doi: 10.1039/c8ee02341g.

Balghouthi, M., Trabelsi, S. E., Amara, M. B., Ali, A. B. H., and Guizani, A. Potential of concentrating solar power (CSP) technology in Tunisia and the possibility of interconnection with Europe. *Renewable and Sustainable Energy Reviews*, 56:1227–1248, 2016. ISSN 18790690. doi: 10.1016/j.rser.2015.12.052.

Bayon, A., Bader, R., Jafarian, M., Fedunik-Hofman, L., Sun, Y., Hinkley, J., Miller, S., and Lipiński, W. Techno-economic assessment of solid–gas thermochemical energy storage systems for solar thermal power applications. *Energy*, 149:473–484, apr 2018. ISSN 03605442. doi: 10.1016/j.energy.2017.11.084.

Bird, L., Cochran, J., Wang, X., Bird, L., Cochran, J., and Wang, X. Wind and Solar Energy Curtailment : Experience and Practices in the United States (NREL Technical Report/TP-6A20-60983). Technical Report NREL Technical Report/TP-6A20-60983,, 2014.

Bravo, R. and Friedrich, D. Two-stage optimisation of hybrid solar power plants. *Solar Energy*, 164:187–199, apr 2018. ISSN 0038092X. doi: 10.1016/j.solener.2018.01.078. URL `http://linkinghub.elsevier.com/retrieve/pii/S0038092X18300999`.

Bravo, R., Ortiz, C., Chacartegui, R., and Friedrich, D. Hybrid solar power plant with thermochemical energy storage: a multi-objective operational optimisation. *Energy Conversion and Management*, 205:112421, feb 2019. ISSN 01968904. doi: 10.1016/j.enconman.2019.112421.

Bravo, R., Ortiz, C., Chacartegui, R., and Friedrich, D. Multi-objective optimisation and guidelines for the design of dispatchable hybrid solar power plants with thermochemical energy storage. *Applied Energy*, 282:116257, 2021. doi: 10.1016/j.apenergy.2020.116257. URL `https://doi.org/10.1016/j.apenergy.2020.116257`.

Bui, M., Adjiman, C. S., Bardow, A., Anthony, E. J., Boston, A., Brown, S., Fennell, P. S., Fuss, S., Galindo, A., Hackett, L. A., Hallett, J. P., Herzog, H. J., Jackson, G., Kemper, J., Krevor, S., Maitland, G. C., Matuszewski, M., Metcalfe, I. S., Petit, C., Puxty, G., Reimer, J., Reiner, D. M., Rubin, E. S., Scott, S. A., Shah, N., Smit, B., Trusler, J. P., Webley, P., Wilcox, J., and Mac Dowell, N. Carbon capture and storage (CCS): The way forward. *Energy Environ. Sci.*, 11(5):1062–1176, 2018. ISSN 17545706. doi: 10.1039/c7ee02342a.

Cabeza, L., Martorell, I., Miró, L., Fernández, A., and Barreneche, C. *Introduction to thermal energy storage (TES) systems*. Woodhead Publishing Limited, 2015. ISBN 9781782420880. doi: 10.1533/9781782420965.1. URL `http://dx.doi.org/10.1533/9781782420965.1`.

Cáceres, G., Anrique, N., Girard, A., Degrève, J., Baeyens, J., and Zhang, H. L. Performance of molten salt solar power towers in Chile. *Journal of Renewable and Sustainable Energy*, 5 (5), 2013. ISSN 19417012. doi: 10.1063/1.4826883.

Carlson, M. D., Middleton, B. M., and Ho, C. K. Techno-economic comparison of solar-driven SCO2 brayton cycles using component cost models baselined with vendor data and estimates. In *ASME 2017 11th International Conference on Energy Sustainability, ES 2017, collocated with the ASME 2017 Power Conference Joint with ICOPE 2017, the ASME 2017 15th International Conference on Fuel Cell Science, Engineering and Technology, and the ASME 201*, 2017. ISBN 9780791857595. doi: 10.1115/ES2017-3590.

Carnegie Mellon University. Managing Variable Energy Resources to Increase Renewable Electricity's Contribution to the Grid P O L I C Y M A K E R G U I D E. Technical report, Carnegie Mellon University, 2013. URL `https://www.cmu.edu/epp/policy-briefs/briefs/Managing-variable-energy-resources.pdf`.

CDEC-SING. Annual Report and Operational Statistics 2015. Technical report, CDEC-SING, 2015.

Cengel, Y. A. and Boles, M. A. *Thermodyamics an engineering approach*, volume 1. McGraw-Hill Education, New York, New York, eighth edi edition, 2015. ISBN 0073107689. doi: 10.1017/CBO9781107415324.004.

Cerro Dominador. Cerro Dominador, 2019. URL `https://cerrodominador.com/en/proyectos-en/`.

Chacartegui, R., Alovisio, A., Ortiz, C., Valverde, J. M., Verda, V., and Becerra, J. A. Thermochemical energy storage of concentrated solar power by integration of the calcium looping process and a CO 2 power cycle. *Applied Energy*, 173:589–605, jul 2016. ISSN 03062619. doi: 10.1016/j.apenergy.2016.04.053.

Cherowbrier, J. • Euro to U.S. dollar exchange rate 1999-2018 | Statista, 2019. URL `https://www.statista.com`.

Chilean Center for Economic Load Dispatch. Northern Interconnected System. *http://cdec2.cdec-sing.cl*, 2016. URL `http://cdec2.cdec-sing.cl`.

Comisión Chilena del Cobre. Yearbook: Copper and other Mineral Statistics 1996-2015. Technical report, Comision Chilena del Cobre, 2016.

Cordero, R. R., Damiani, A., Seckmeyer, G., Jorquera, J., Caballero, M., Rowe, P., Ferrer, J., Mubarak, R., Carrasco, J., Rondanelli, R., Matus, M., and Laroze, D. The Solar Spectrum in the Atacama Desert. *Scientific Reports*, 6:22457, 2016. ISSN 2045-2322. doi: 10.1038/srep22457.

Criado, Y. A., Arias, B., and Abanades, J. C. Calcium looping CO2 capture system for back-up power plants. *Energy Environ. Sci.*, 10(9):1994–2004, 2017. ISSN 17545706. doi: 10.1039/c7ee01505d.

Denholm, P. and Hand, M. Grid flexibility and storage required to achieve very high penetration of variable renewable electricity. *Energy Policy*, 39(3):1817–1830, 2011. ISSN 03014215. doi: 10.1016/j.enpol.2011.01.019.

Denholm, P., Jorgenson, J., Miller, M., Zhou, E., Denholm, P., Jorgenson, J., Miller, M., and Zhou, E. Methods for Analyzing the Economic Value of Concentrating Solar Power with Thermal Energy Storage Methods for Analyzing the Economic Value of Concentrating Solar Power with Thermal Energy Storage. (July), 2015a.

Denholm, P., Jorgenson, J., Miller, M., Zhou, E., and Wang, C. Methods for Analyzing the Economic Value of Concentrating Solar Power with Thermal Energy Storage Methods for Analyzing the Economic Value of Concentrating Solar Power with Thermal Energy Storage. Technical Report July, National Renewable Energy Laboratory, 2015b.

Dick, E. *Fundamentals of Turbomachines*, volume 109. Springer, Dordrecht, 2015. doi: 10.1007/978-94-017-9627-9.

Dincer, I., Rosen, M. A., and Ahmadi, P. *Optimization of energy systems*. Wiley, jan 2017. ISBN 9781118894484. doi: 10.1002/9781118894484.

Dinter, F. and Möller, L. A review of Andasol 3 and perspective for parabolic trough CSP plants in South Africa. In *AIP Conference Proceedings*, volume 1734, page 100005, 2016. ISBN 9780735413863. doi: 10.1063/1.4949193. URL `https://doi.org/10.1063/1.4949193`.

Duffie, J. A. and Beckman, W. A. *Solar Thermal Power Systems*. Elsevier Inc., 2013. ISBN 9781118671603. doi: 10.1002/9781118671603.ch17. URL `http://dx.doi.org/10.1002/9781118671603.ch17`.

Energía Abierta. Capacidad instalada – Energía Abierta | Comisión Nacional de Energía, 2019. URL `http://energiaabierta.cl/visualizaciones/capacidad-instalada/`.

European Commission, J. R. C. JRC Photovoltaic Geographical Information System (PVGIS) - European Commission, 2017. URL `https://re.jrc.ec.europa.eu`.

Everett, R., Boyle, G., Peake, S., and Ramage, J. *Energy Systems and Sustainability: Power for a Sustainable Future (2nd ed.)*. Oxford University Press in association with the Open University, Oxford, second edi edition, 2012. ISBN 978-0-19-959374-3.

Fazlollahi, S., Mandel, P., Becker, G., and Maréchal, F. Methods for multi-objective investment and operating optimization of complex energy systems. *Energy*, 45(1):12–22, 2012. ISSN 03605442. doi: 10.1016/j.energy.2012.02.046.

Fernández, A. G., Gomez-Vidal, J., Oró, E., Kruizenga, A., Solé, A., and Cabeza, L. F. Mainstreaming commercial CSP systems: A technology review, sep 2019a. ISSN 18790682.

Fernández, R., Ortiz, C., Chacartegui, R., Valverde, J. M., and Becerra, J. A. Dispatchability of solar photovoltaics from thermochemical energy storage. *Energy Conversion and Management*, 191:237–246, jul 2019b. ISSN 01968904. doi: 10.1016/j.enconman.2019.03.074.

Festa, P. A brief introduction to exact, approximation, and heuristic algorithms for solving hard combinatorial optimization problems. In *International Conference on Transparent Optical Networks*. IEEE Computer Society, 2014. ISBN 9781479956005. doi: 10.1109/ICTON.2014.6876285.

Fortin, F.-A., Marc-André Gardner, U., Parizeau, M., and Gagné, C. DEAP: Evolutionary Algorithms Made Easy. *Journal of Machine Learning Research*, 13:1–5, 2012.

Frangopoulos, C. A., Von Spakovsky, M. R., and Sciubba, E. A brief review of methods for the design and synthesis optimization of energy systems. *International Journal of Applied Thermodynamics*, 5(4):151–160, 2002. ISSN 13019724. doi: 10.5541/ijot.97.

Fraunhofer ISE. Current and Future Cost of Photovoltaics. Long-term Scenarios for Market Development, System Prices and LCOE of Utility-Scale PV Systems. *Agora Energiewende*, 1(February):82, 2015. doi: 059/01-S-2015/EN. URL `www.agora-energiewende.de`.

Gebreslassie, B. H., Guillén Gosálbez, G., Jiménez, L., and Boer, D. Design of environmentally conscious absorption cooling systems via multi-objective optimization and life cycle assessment. *Applied Energy*, 86(9):1712–1722, 2009. ISSN 03062619. doi: 10.1016/j.apenergy.2008.11.019.

Gil, A., Medrano, M., Martorell, I., Lázaro, A., Dolado, P., Zalba, B., and Cabeza, L. F. State of the art on high temperature thermal energy storage for power generation. Part 1-Concepts, materials and modellization. *Renewable and Sustainable Energy Reviews*, 14(1):31–55, jan 2010. ISSN 13640321. doi: 10.1016/j.rser.2009.07.035.

Grageda, M., Escudero, M., Alavia, W., Ushak, S., and Fthenakis, V. Review and multi-criteria assessment of solar energy projects in Chile. *Renewable and Sustainable Energy Reviews*, 59:583–596, 2016. ISSN 18790690. doi: 10.1016/j.rser.2015.12.149.

Green, A., Diep, C., Dunn, R., and Dent, J. High Capacity Factor CSP-PV Hybrid Systems. In *Energy Procedia*, volume 69, pages 2049–2059, may 2015. doi: 10.1016/j.egypro.2015.03.218.

Gür, T. M. Review of electrical energy storage technologies, materials and systems: Challenges and prospects for large-scale grid storage. *Energy Environ. Sci.*, 11(10):2696–2767, 2018. ISSN 17545706. doi: 10.1039/c8ee01419a.

Gurobi Optimization, L. Gurobi Optimizer Reference Manual, 2019. URL `http://www.gurobi.com`.

Hanak, D. P., Anthony, E. J., and Manovic, V. A review of developments in pilot-plant testing and modelling of calcium looping process for CO2 capture from power generation systems. *Energy Environ. Sci.*, 8(8):2199–2249, 2015. ISSN 17545706. doi: 10.1039/c5ee01228g. URL `www.rsc.org/ees`.

Hart, W. E., Watson, J. P., and Woodruff, D. L. Pyomo: Modeling and solving mathematical programs in Python. *Mathematical Programming Computation*, 3(3):219–260, sep 2011. ISSN 18672949. doi: 10.1007/s12532-011-0026-8.

Hart, W. E., Laird, C. D., Watson, J.-P., Woodruff, D. L., Hackebeil, G. A., Nicholson, B. L., and Siirola, J. D. *Pyomo — Optimization Modeling in Python*, volume 67 of *Springer Optimization and Its Applications*. Springer International Publishing, Cham, 2017. ISBN 978-3-319-58819-3. doi: 10.1007/978-3-319-58821-6.

Health and Safety Executive. Specifications for high-strength seamless steel gas cylinders in a modified chromium molybdenum steel. Technical Report HSSS-2, Health and Safety Executive, 1992.

Houston, J. Variability of precipitation in the Atacama Desert: Its causes and hydrological impact. *International Journal of Climatology*, 26(15):2181–2198, dec 2006. ISSN 08998418. doi: 10.1002/joc.1359.

IEA. Technology Roadmap: Energy Storage - 2014 edition. Technical report, International Energy Agency, 2014a. URL `www.iea.org`.

IEA. Tracking Clean Energy Progress 2017. *International Energy Agency, Organisationf for Economic Co-operation and Development*, 2017. doi: 10.1787/energy_tech-2014-en.

IEA. *World Energy Outlook 2019*. IEA, Paris, 2019a. URL `https://www.iea.org/reports/world-energy-outlook-2019`.

IEA. Data & Statistics - IEA, 2019b.

IEA. Technology Roadmap: Solar Thermal Electricity. *International Energy Agency, Organisation for Economic Co-operation and Development*, 2014b. doi: 10.1007/SpringerReference_7300.

IEA, NEA, and OECD. Projected Costs of Generating Electricity 2015. *International Energy Agency, Nuclear Energy Agency, Organisationf for Economic Co-operation and Development*, 2015. ISSN 16602110. doi: 10.1787/cost_electricity-2015-en.

IEA, I. E. A. World Energy Outlook 2019 – Analysis - IEA. Technical report, IEA, 2019c. URL `https://www.iea.org/reports/world-energy-outlook-2019`.

IEC. Electrical Energy Storage - White Paper. Technical report, IEC, 2011.

Independent Group of Scientists appointed by the Secretary-General. Global Sustainable Development Report 2019: The Future is Now – Science for Achieving Sustainable Development. Technical report, United Nations, 2019.

International Renewable Energy Agency, T. Utility-scale Batteries. Technical report, International Renewable Energy Agency, 2019. URL `www.irena.org`.

IRENA. Renewable Capacity Statistics 2018. Technical report, International Renewable Energy Agency, 2018.

Jaccard, M. *Sustainable fossil fuels: The unusual suspect in the quest for clean and enduring energy*. Cambridge University Press, jan 2006. ISBN 9780511754104. doi: 10.1017/CBO9780511754104.

Jaffe, R. L. and Washington, T. *The physics of energy*. Cambridge University Press, Cambridge, United Kingdom ; New York, NY, 2018. ISBN 9781107016651. doi: 10.1017/9781139061292.

Jenkins, J. D., Luke, M., and Thernstrom, S. Getting to Zero Carbon Emissions in the Electric Power Sector. *Joule*, 2(12):2498–2510, dec 2018. ISSN 25424351. doi: 10.1016/j.joule.2018.11.013.

Joint Research Centre. *ETRI 2014 - Energy Technology Reference Indicator projections for 2010-2050*. European Connission, 2014. ISBN 9789279444036. doi: 10.2790/057687.

Jonemann, M. Advanced Thermal Storage System with Novel Molten Salt: December 8, 2011 - April 30, 2013. Technical report, National Renewable Energy Laboratory, 2013.

Kalogirou, S. A. Optimization of solar systems using artificial neural-networks and genetic algorithms. *Applied Energy*, 77(4):383–405, apr 2004. ISSN 03062619. doi: 10.1016/S0306-2619(03)00153-3.

Kalogirou, S. A. *Chapter three - Solar Energy Collectors*. Elsevier Inc., 2009. ISBN 978-0-12-374501-9. doi: http://dx.doi.org/10.1016/B978-0-12-374501-9.00003-0.

Kaufman, L. and Rousseeuw, P. J. *Finding Groups in Data: An Introduction to Cluster Analysis*, volume 180 of *Wiley Series in Probability and Statistics*. John Wiley & Sons, Inc., Hoboken, NJ, USA, mar 2005. ISBN 9780470316801. doi: 10.1002/9780470316801.

Knoll, C., Müller, D., Artner, W., Welch, J. M., Eitenberger, E., Friedbacher, G., Werner, A., Weinberger, P., and Harasek, M. Magnesium oxide from natural magnesite samples as thermochemical energy storage material. In *Energy Procedia*, volume 158, pages 4861–4869. Elsevier Ltd, 2019. doi: 10.1016/j.egypro.2019.01.707.

Kyaw, K., Kubota, M., Vvatanabe, F., Matsuda, H., and Hasatani, M. Study of carbonation of CaO for high temperature thermal energy storage. *Journal of Chemical Engineering of Japan*, 31(2):281–284, 1998. ISSN 00219592. doi: 10.1252/jcej.31.281.

Liu, M., Steven Tay, N. H., Bell, S., Belusko, M., Jacob, R., Will, G., Saman, W., and Bruno, F. Review on concentrating solar power plants and new developments in high temperature thermal energy storage technologies. *Renewable and Sustainable Energy Reviews*, 53:1411–1432, jan 2016. ISSN 18790690. doi: 10.1016/j.rser.2015.09.026.

Lund, H., Østergaard, P. A., Connolly, D., Ridjan, I., Mathiesen, B. V., Hvelplund, F., Thellufsen, J. Z., and Sorknses, P. Energy storage and smart energy systems. *International Journal of Sustainable Energy Planning and Management*, 11:3–14, oct 2016. ISSN 22462929. doi: 10.5278/ijsepm.2016.11.2.

Macqueen, J. Some methods for classification and analysis. In *Proceedings of the Fifth Berkeley Symposium on Mathematical Statistics and Probability, Volume 1: Statistics*, volume 233, pages 281–297, 1967. URL `http://projecteuclid.org/bsmsp`.

Maximov, S. A., Harrison, G. P., and Friedrich, D. Long term impact of grid level energy storage on renewable energy penetration and emissions in the chilean electric system. *Energies*, 12(6):1070, mar 2019. ISSN 19961073. doi: 10.3390/en12061070.

Meier, A., Gremaud, N., and Steinfeld, A. Economic evaluation of the industrial solar production of lime. *Energy Conversion and Management*, 46(6):905–926, apr 2005. ISSN 01968904. doi: 10.1016/j.enconman.2004.06.005.

Michalski, S., Hanak, D. P., and Manovic, V. Techno-economic feasibility assessment of calcium looping combustion using commercial technology appraisal tools. *Journal of Cleaner Production*, 219:540–551, may 2019. ISSN 09596526. doi: 10.1016/j.jclepro.2019.02.049.

Mining Council Chile. Consejo Minero, Reporte Anual 2015. *http://www.consejominero.cl*, page 54, 2015.

Ministerio de Energia and Universidad de Chile. Explorador Solar, 2016. URL `http://www.minenergia.cl/exploradorsolar/`.

Ministry of Energy - Chilean Government. Indicadores Ambientales del Sector Energía, 2017. URL `http://www.minenergia.cl/indicadoresambientales/`.

Ministry of Energy - University of Chile. Explorador Solar Chile - Department of Geophysics, 2016. URL `http://www.minenergia.cl/exploradorsolar/`.

Mohan, G., Venkataraman, M. B., and Coventry, J. Sensible energy storage options for concentrating solar power plants operating above 600 °C. *Renewable and Sustainable Energy Reviews*, 107:319–337, jun 2019. ISSN 18790690. doi: 10.1016/j.rser.2019.01.062.

Müller, B., Arlt, W., and Wasserscheid, P. A new concept for the global distribution of solar energy: Energy carrying compounds. *Energy Environ. Sci.*, 4(10):4322–4331, 2011. ISSN 17545692. doi: 10.1039/c1ee01595h.

Nguyen, A.-T., Reiter, S., and Rigo, P. A review on simulation-based optimization methods applied to building performance analysis. *Applied Energy*, 113:1043–1058, 2014. ISSN 03062619. doi: 10.1016/j.apenergy.2013.08.061.

Northey, S., Haque, N., and Mudd, G. Using sustainability reporting to assess the environmental footprint of copper mining. *Journal of Cleaner Production*, 40:118–128, 2013. ISSN 09596526. doi: 10.1016/j.jclepro.2012.09.027.

NREL. Concentrating Solar Power Projects, 2017. URL https://www.nrel.gov/csp/solarpaces/.

NREL. System Advisor Model (SAM), 2018. URL https://sam.nrel.gov/.

Obermeier, J., Sakellariou, K. G., Tsongidis, N. I., Baciu, D., Charalambopoulou, G., Steriotis, T., Müller, K., Karagiannakis, G., Konstandopoulos, A. G., Stubos, A., and Arlt, W. Material development and assessment of an energy storage concept based on the CaO-looping process. *Solar Energy*, 150:298–309, 2017. ISSN 0038092X. doi: 10.1016/j.solener.2017.04.058.

Ortiz, C., Chacartegui, R., Valverde, J. M., Alovisio, A., and Becerra, J. A. Power cycles integration in concentrated solar power plants with energy storage based on calcium looping. *Energy Conversion and Management*, 149:815–829, oct 2017. ISSN 01968904. doi: 10.1016/j.enconman.2017.03.029.

Ortiz, C., Romano, M. C., Valverde, J. M., Binotti, M., and Chacartegui, R. Process integration of Calcium-Looping thermochemical energy storage system in concentrating solar power plants. *Energy*, 155:535–551, jul 2018a. ISSN 03605442. doi: 10.1016/j.energy.2018.04.180.

Ortiz, C., Valverde, J. M., Chacartegui, R., and Perez-Maqueda, L. A. Carbonation of Limestone Derived CaO for Thermochemical Energy Storage: From Kinetics to Process Integration in Concentrating Solar Plants. *ACS Sustainable Chemistry and Engineering*, 6 (5):6404–6417, may 2018b. ISSN 21680485. doi: 10.1021/acssuschemeng.8b00199.

Ortiz, C., Valverde, J. M., Chacartegui, R., and Perez-Maqueda, L. A. Carbonation of Limestone Derived CaO for Thermochemical Energy Storage: From Kinetics to Process Integration in Concentrating Solar Plants. *ACS Sustainable Chemistry and Engineering*, 6 (5):6404–6417, 2018c. ISSN 21680485. doi: 10.1021/acssuschemeng.8b00199.

Ortiz, C., Valverde, J., Chacartegui, R., Perez-Maqueda, L., and Giménez, P. The Calcium-Looping (CaCO3/CaO) process for thermochemical energy storage in Concentrating Solar Power plants. *Renewable and Sustainable Energy Reviews*, 113:109252, oct 2019a. ISSN 13640321. doi: 10.1016/j.rser.2019.109252.

Ortiz, C., Binotti, M., Romano, M. C., Valverde, J. M., and Chacartegui, R. Off-design model of concentrating solar power plant with thermochemical energy storage based on calcium-looping. In *AIP Conference Proceedings*, volume 2126, page 210006. AIP Publishing LLC, jul 2019b. doi: 10.1063/1.5117755.

Pachauri, R. K., Meyer, L., Hallegatte France, S., Bank, W., Hegerl, G., Brinkman, S., van Kesteren, L., Leprince-Ringuet, N., and van Boxmeer, F. AR5 Synthesis Report: Climate Change 2014 — IPCC. Technical report, IPCC, 2014. URL https://www.ipcc.ch/report/ar5/syr/http://www.ipcc.ch.

Pan, C. A. and Dinter, F. Combination of PV and central receiver CSP plants for base load power generation in South Africa. *Solar Energy*, 146:379–388, 2017. ISSN 0038092X. doi: 10.1016/j.solener.2017.02.052.

Pardo, P., Deydier, A., Anxionnaz-Minvielle, Z., Rougé, S., Cabassud, M., and Cognet, P. A review on high temperature thermochemical heat energy storage. *Renewable and Sustainable Energy Reviews*, 32:591–610, apr 2014. ISSN 13640321. doi: 10.1016/j.rser.2013.12.014.

Parrado, C., Girard, A., Simon, F., and Fuentealba, E. 2050 LCOE (Levelized Cost of Energy) projection for a hybrid PV (photovoltaic)-CSP (concentrated solar power) plant in the Atacama Desert, Chile. *Energy*, 94:422–430, 2016a. ISSN 03605442. doi: 10.1016/j.energy.2015.11.015.

Parrado, C., Marzo, A., Fuentealba, E., and Fernandez, A. G. 2050 LCOE improvement using new molten salts for thermal energy storage in CSP plants. *Renewable and Sustainable Energy Reviews*, 57:505–514, 2016b. ISSN 18790690. doi: 10.1016/j.rser.2015.12.148.

Pehl, M., Arvesen, A., Humpenöder, F., Popp, A., Hertwich, E. G., and Luderer, G. Understanding future emissions from low-carbon power systems by integration of life-cycle assessment and integrated energy modelling. *Nature Energy*, 2(12):939–945, 2017. ISSN 20587546. doi: 10.1038/s41560-017-0032-9.

Peiró, G., Gasia, J., Miró, L., Prieto, C., and Cabeza, L. F. Influence of the heat transfer fluid in a CSP plant molten salts charging process. *Renewable Energy*, 113:148–158, dec 2017. ISSN 18790682. doi: 10.1016/j.renene.2017.05.083.

Peng, X., Root, T. W., and Maravelias, C. T. Storing solar energy with chemistry: The role of thermochemical storage in concentrating solar power. *Green Chemistry*, 19(10):2427–2438, 2017. ISSN 14639270. doi: 10.1039/c7gc00023e.

Perry, R. H., Green, D. W., and Maloney, J. O. *Perry's Chemical engineers' handbook*. McGraw-Hill, New York ; London, seventh ed edition, 1997. ISBN 0070498415.

Petrollese, M. and Cocco, D. Optimal design of a hybrid CSP-PV plant for achieving the full dispatchability of solar energy power plants. *Solar Energy*, 137:477–489, 2016. ISSN 0038092X. doi: 10.1016/j.solener.2016.08.027.

Powell, K. M., Rashid, K., Ellingwood, K., Tuttle, J., and Iverson, B. D. Hybrid concentrated solar thermal power systems: A review. *Renewable and Sustainable Energy Reviews*, 80: 215–237, 2017. ISSN 13640321. doi: 10.1016/j.rser.2017.05.067.

Prieto, C. and Cabeza, L. F. Thermal energy storage (TES) with phase change materials (PCM) in solar power plants (CSP). Concept and plant performance. *Applied Energy*, 254, nov 2019. ISSN 03062619. doi: 10.1016/j.apenergy.2019.113646.

Python Software Foundation. Python 3.5.3, 2017. URL `https://www.python.org/`.

Quiñones, G., Felbol, C., Valenzuela, C., Cardemil, J. M., and Escobar, R. A. Analyzing the potential for solar thermal energy utilization in the Chilean copper mining industry. *Solar Energy*, 197:292–310, feb 2020. ISSN 0038092X. doi: 10.1016/j.solener.2020.01.009.

Renaldi, R. and Friedrich, D. Multiple time grids in operational optimisation of energy systems with short- and long-term thermal energy storage. *Energy*, 133:784–795, 2017. ISSN 03605442. doi: 10.1016/j.energy.2017.05.120.

Rousseeuw, P. J. Silhouettes: A graphical aid to the interpretation and validation of cluster analysis. *Journal of Computational and Applied Mathematics*, 20(C):53–65, nov 1987. ISSN 03770427. doi: 10.1016/0377-0427(87)90125-7.

Salas, D., Tapachès, E., Mazet, N., and Aussel, D. Economical optimization of thermochemical storage in concentrated solar power plants via pre-scenarios. *Energy Conversion and Management*, 174:932–954, oct 2018. ISSN 01968904. doi: 10.1016/j.enconman.2018.08.079.

Sampaio, P. G. V. and González, M. O. A. Photovoltaic solar energy: Conceptual framework. *Renewable and Sustainable Energy Reviews*, 74:590–601, 2017. ISSN 18790690. doi: 10.1016/j.rser.2017.02.081.

Sánchez Jiménez, P. E., Perejón, A., Benítez Guerrero, M., Valverde, J. M., Ortiz, C., and Pérez Maqueda, L. A. High-performance and low-cost macroporous calcium oxide based materials for thermochemical energy storage in concentrated solar power plants. *Applied Energy*, pages 543–552, feb 2019. ISSN 03062619. doi: 10.1016/j.apenergy.2018.10.131.

Schmidt, O., Hawkes, A., Gambhir, A., and Staffell, I. The future cost of electrical energy storage based on experience rates. *Nature Energy*, 6:17110, 2017. ISSN 2058-7546. doi: 10.1038/nenergy.2017.110.

Sengupta, M., Habte, A., Kurtz, S., Dobos, A., Wilbert, S., Lorenz, E., Stoffel, T., Renné, D., Gueymard, C., Myers, D., Wilcox, S., Blanc, P., and Perez, R. Best Practices Handbook for the Collection and Use of Solar Resource Data for Solar Energy Applications. Technical report, National Renewable Energy Laboratory, 2015.

Servicio de Evaluación Ambiental. Sistema de Evaluación de Impacto Ambiental e-seia, 2014. URL `http://seia.sea.gob.cl`.

Short, W., Packey, D. J., and Holt, T. A manual for the economic evaluation of energy efficiency and renewable energy technologies. Technical Report March, National Renewable Energy Laboratory, 1995.

Siemens. Onshore Wind Turbine SG 2.1-114, 2018. URL https://www.siemensgamesa.com/en-int/products-and-services/onshore/wind-turbine-sg-2-1-114.

Sinsel, S. R., Riemke, R. L., and Hoffmann, V. H. Challenges and solution technologies for the integration of variable renewable energy sources—a review. *Renewable Energy*, 145: 2271–2285, jan 2020. ISSN 18790682. doi: 10.1016/j.renene.2019.06.147.

Solar Energy Technologies office. Linear Concentrator System Basics for Concentrating Solar Power | Department of Energy, 2013. URL https://www.energy.gov/eere/solar/articles/linear-concentrator-system-basics-concentrating-solar-power.

Solar Reserve LLC. Crescent Dunes, 2012. URL http://www.solarreserve.com/en/global-projects/csp/crescent-dunes.

SolarPACES. Concentrating Solar Power Projects, 2018. URL https://solarpaces.nrel.gov/https://solarpaces.nrel.gov/by-technology.

Srilakshmi, G., Suresh, N., Thirumalai, N., and Ramaswamy, M. Preliminary design of heliostat field and performance analysis of solar tower plants with thermal storage and hybridisation. *Sustainable Energy Technologies and Assessments*, 19:102–113, 2017. ISSN 22131388. doi: 10.1016/j.seta.2016.12.005.

Starke, A., Cardemil, J. M., Escobar, R., and Colle, S. Assessing the performance of hybrid CSP+PV plants in northern Chile. In *AIP Conference Proceedings*, volume 1734, 2016. ISBN 9780735413863. doi: 10.1063/1.4949230.

Starke, A. R., Cardemil, J. M., Escobar, R., and Colle, S. Multi-objective optimization of hybrid CSP+PV system using genetic algorithm. *Energy*, 147:490–503, 2018. ISSN 03605442. doi: 10.1016/j.energy.2017.12.116.

Ströhle, S., Haselbacher, A., Jovanovic, Z. R., and Steinfeld, A. The effect of the gas-solid contacting pattern in a high-temperature thermochemical energy storage on the performance of a concentrated solar power plant. *Energy Environ. Sci.*, 9(4):1375–1389, 2016. ISSN 17545706. doi: 10.1039/c5ee03204k.

Tezer, T., Yaman, R., and Yaman, G. Evaluation of approaches used for optimization of stand-alone hybrid renewable energy systems. *Renewable and Sustainable Energy Reviews*, 73: 840–853, jun 2017. ISSN 1364-0321. doi: 10.1016/J.RSER.2017.01.118.

The World Bank. *Source: Global Solar Atlas 2.0, Solar resource data: Solargis.* Solargis, 2019. URL https://solargis.com/.

U.S. Energy Information Administration. Electricity data browser - Rockport, 2020. URL https://www.eia.gov/electricity/.

Ushak, S. and Grageda, M. *Using molten salts and other liquid sensible storage media in thermal energy storage (TES) systems*. Woodhead Publishing Limited, 2015. ISBN 9781782420965. doi: http://dx.doi.org/10.1533/9781782420965.1.49.

Valverde, J. M., Sanchez-Jimenez, P. E., and Perez-Maqueda, L. A. Limestone Calcination Nearby Equilibrium: Kinetics, CaO Crystal Structure, Sintering and Reactivity. *The Journal of Physical Chemistry*, 2015. doi: 10.1021/jp508745u.

Webley, P. Analysing Energy Systems, 2014.

Worley Parsons. Electricity Generation Technology Cost Assessment Appendices. Technical Report July, CSIRO, 2012.

Zini, G. Energy Storage as a Value Proposition. In *Green Electrical Energy Storage: Science and Finance for Total Fossil Fuel Substitution*. McGraw Hill Professional, Access Engineering, 2016.

Zurita, A., Mata-Torres, C., Valenzuela, C., Felbol, C., Cardemil, J. M., Guzmán, A. M., and Escobar, R. A. Techno-economic evaluation of a hybrid CSP + PV plant integrated with thermal energy storage and a large-scale battery energy storage system for base generation. *Solar Energy*, 173:1262–1277, oct 2018. ISSN 0038092X. doi: 10.1016/j.solener.2018.08.061.